Illuminating the functions of understudied proteins using novel covalent and chemical genetic approaches

A dissertation presented

by

Zainab Murtaza Doctor

to

The Division of Medical Sciences

in partial fulfillment of the requirements

for the degree of

Doctor of Philosophy

in the subject of

Biological Chemistry and Molecular Pharmacology

Harvard University

Cambridge, Massachusetts

March 2019

Advisor: Dr. Nathanael S. Gray Zainab Murtaza Doctor

Illuminating the functions of understudied proteins using novel covalent and chemical genetic approaches

Abstract

Small molecule inhibitors can modulate biological systems by disrupting the activities of proteins, and thus can be used both as therapies and as tools to interrogate protein function. While many small molecules reversibly interact with their targets, covalent inhibitors irreversibly react with nucleophilic moieties, such as cysteine thiols in or around active sites. Though historically covalent inhibitors were avoided due to toxicity concerns from off-target modifications, advances in design have led to renewed interest in this class of small molecules, several of which have been FDA-approved. Irreversible inhibitors have several advantages, including enhanced selectivity by targeting uniquely positioned cysteines and improved potency, making them useful tools for evaluating the functions of poorly annotated proteins. Here, I paired the development of novel covalent inhibitors with complementary chemical genetic approaches to investigate several understudied proteins and putative cancer targets.

Cyclin-dependent kinase 14 (CDK14) is an understudied CDK for which no selective inhibitors exist. Through several iterations of medicinal chemistry, we developed a covalent CDK14 inhibitor with pan-TAIRE family selectivity. In parallel, we employed genetic and chemical genetic approaches to assess the consequences of disrupting CDK14 activity. We determined that CDK14 coordinates Wnt signaling in mitosis, and characterized its impact on cell cycle, the phospho-proteome and epithelial-mesenchymal transition.

Next, we developed CITe-Id, a chemoproteomic approach for assessing site-level selectivity of covalent inhibitors. We used CITe-Id to profile the covalent CDK7/12/13 inhibitor THZ1 and identified previously unknown off-targets, including a novel targetable cysteine on the understudied Protein Kinase N3 (PKN3). We leveraged CITe-Id to develop a THZ1 analog selective for PKN3 and used this probe to identify candidate substrates of PKN3.

Finally, we developed a highly selective, cell-penetrant and potent covalent inhibitor of the proline isomerase PIN1. Using this inhibitor, along with a complementary chemical-induced targeted degradation strategy (dTAG), we discovered that PIN1 inhibition impairs pancreatic cancer growth and characterized the transcriptional effect of PIN1 inhibition.

In sum, we developed novel covalent inhibitors and complementary chemical genetic tools and leveraged them to investigate the understudied proteins CDK14, PKN3 and PIN1. We anticipate that these tools will be useful in future studies of these targets.

Table of Contents

Acknowledgements

First, I would like to thank my advisor, Nathanael. Your continuous support and guidance are what got me through graduate school. It has truly been a privilege working with you these past few years. Your ability to rapidly evaluate science and the state of a project is remarkable, from specific experiments to an overall view of the field.

Thank you to the members of the Gray lab, who made it enjoyable to come to work every day even when it didn't feel like I was making any progress. Your encouragement and advice, both experimental and in life, were always appreciated. During the years of grad school, I spend more cumulative weekly hours with you all than anyone else in my life, and I feel lucky that I got to work and learn alongside such talented scientists and kind people.

The BBS program and the community that came with it was one of the best parts of graduate school. Kate, Maria, Danny and Anne in the BBS office made every transition straightforward and seamless. Thanks for sharing your wisdom learned from the years of watching students go through this program, for always putting students' needs first, and for constantly making me feel supported, even if I was only in the office for five minutes a month.

I would like to thank the members of my dissertation advisory committee (DAC), Steve Buratowski, Karen Cichowski, and Tom Roberts for their helpful feedback and project guidance over the course of my graduate career. Finally, I would like to thank my dissertation defense committee, Sara Buhrlage, Michael Eck and Michael Yaffe, for carrying out this examination. A special thank you to Steve for being my exam chair, for advising me throughout my graduate career and for being on every committee I have needed since my PQE.

Finally, I would like to thank my family. To my sister, for keeping me calm when I stress, and for being my best friend and biggest cheerleader. You're irreplaceable, and I'm so lucky to have you. And to my parents – your unconditional love ensured that we grew up in a warm and caring environment. Thank you for being the constant living example of the importance of hard work. I remember you both saying that your own education is what got you to America, and to where you are in life today. I often think back to your insistence on the importance of curiosity, filling long car rides with riddles and puzzles to teach us how to think logically and critically, and making me do elementary school math homework replacing the numbers with xs and ys to solve for all similar problems rather than the single instance. You always made our education the top priority, not for the sake of getting into the next good school, but for the way that it would shape us as a person.

Chapter 1: Introduction

Overview

I will begin the first chapter with a background on understudied protein kinases and the opportunities they present to expand the target space of therapeutics, as well as the concept of the druggable genome. I will describe pharmacological strategies to interrogate protein function from a historical perspective, as well as opportunities provided by more recent strategies including common chemical biology and chemical genetic approaches. I will particularly focus on the use of covalent inhibitors and the advantages (and disadvantages) offered over traditional reversible small molecule inhibitors. I will next describe in detail the use of inhibitors in the context of the cyclin-dependent kinase family, which in some cases were used as tools to understand function while others were developed as cancer therapies through concerted effort. This lays the groundwork for our subsequent work described here on the development of covalent inhibitors of CDK14, PKN3 and PIN1 in an effort to elucidate their function. The experimental approaches used here also provide the opportunity to validate these proteins as cancer targets, as all three have been previously reported to play roles in cell growth or cell cycle regulation, cell migration and metastasis.

The second chapter describes the development of a CDK14 covalent inhibitor, derivatized from the clinical pan-CDK inhibitor AT7519. AT7519 was prioritized from a series of CDK-directed scaffolds due to its superior cellular binding to CDK14. Aided by docking studies, AT7519 was derivatized to favor covalent engagement of cysteine 218 on CDK14 in an effort to achieve selectivity. Detailed structure-activity relationships were determined through several iterative rounds of medicinal chemistry, paired with antiproliferation and CDK14 binding data for all

compounds. This effort led to the development of FMF-04-159-2, used in subsequent studies to investigate CDK14.

The third chapter focuses on the development and characterization of FMF-04-159-2 as a covalent CDK14 inhibitor with pan-TAIRE kinase family kinome-wide selectivity. This compound emerged from the medicinal chemistry effort described in chapter two as a promising tool compound to interrogate CDK14. To our knowledge, it is the first tool compound that specifically targets CDK14 covalently and possesses a TAIRE kinase-biased selectivity profile. This compound and its reversible analog were used to characterize the cellular consequences of covalent CDK14 inhibition, including an unbiased investigation using phospho-proteomics. To reduce confounding off-target activity, washout conditions were used to deconvolute CDK14-specific effects. This investigation suggested that CDK14 plays a supporting role in cell cycle regulation, particularly mitotic progression, and identified putative CDK14 substrates. Together these results represent an important step forward in understanding the cellular consequences of inhibiting CDK14 kinase activity.

The fourth chapter summarizes the use of genetic and chemical genetic approaches to disrupt CDK14 kinase activity, in order to complement studies performed with FMF-04-159-2 discussed in the previous chapter. The use of CRISPR/Cas9-mediated knockout, rescue with or overexpression of CDK14 wild type, kinase-dead or cyclin binding-deficient variants, and chemical-induced targeted protein degradation using the degradation tag (dTAG) system (Nabet et al., 2018) were valuable orthogonal methods to perturb CDK14 activity in addition to the development of a chemical inhibitor. These allowed us to better-understand the roles of CDK14

in cell growth, cell cycle progression, Wnt signaling and epithelial-mesenchymal transition (EMT), and to continue to parse the CDK14-specific effects of FMF-04-159-2.

The fifth chapter describes the development of CITe-Id, a novel chemoproteomic approach that we developed to profile the selectivity of covalent inhibitors proteome-wide and directly quantify dose-dependent binding at cysteine-thiols across the proteome. CITe-Id analysis of our covalent CDK7/12/13 inhibitor THZ1 identified dose-dependent covalent modification of several unexpected kinases, including a previously unannotated cysteine, Cys840 on the understudied kinase PKN3. These data streamlined our development of the THZ1 analog JZ128 as a selective covalent PKN3 inhibitor. Using JZ128 as a probe compound, we then identified novel potential PKN3 substrates, thus offering an initial molecular view of PKN3 cellular activity.

The sixth chapter reports on rationally designed peptide inhibitors that covalently target cysteine 113, a highly conserved cysteine located in the Peptidyl-prolyl isomerase NIMA-interacting 1 (PIN1) active site. The use of a covalent inhibitor allowed for dramatically improved potency and selectivity compared to previous PIN1 inhibitors. This series of inhibitors was optimized for potency, selectivity, and cell permeability to result in BJP-06-005-3, a versatile tool compound with which to probe PIN1 biology and interrogate its role in cancer. We describe the extensive characterization of this compound, including CITe-Id profiling to assess its proteome-wide selectivity. In parallel to inhibitor development, we employed genetic and chemical genetic strategies to assess the consequences of PIN1 loss in human PDAC cell lines, including the dTAG system (Nabet et al., 2018). We demonstrated that PIN1 cooperates with mutant KRAS to promote tumorigenesis in PDAC, and that PIN1 inhibition impairs proliferation at extended timepoints in PDAC cell lines. Using the combination of pharmacological, genetic and chemical

genetic strategies, we described the role of PIN1 in PDAC and were able to assess its value as a cancer target.

I will conclude with a discussion of the research described above in the context of the use of pharmacological and chemical genetic strategies to investigate the protein function. The use of several complementary strategies including development of novel covalent inhibitors strengthened the conviction of insights gained into the functions of CDK14, PKN3 and PIN1. We present several novel chemical tools that were developed in the course of these studies, which aided in initial interrogation of the cellular roles of these targets, and even in the identification of putative substrates and downstream targets. Several challenges still remain with respect the investigating kinases and proteins whose functions are not well-understood, and indeed questions still remain around the roles of CDK14, PKN3 and PIN1.

Covalent inhibitors allowed us to achieve selectivity for the CDK family protein CDK14, improve compound potency to access PIN1 in cellular contexts, and inspired us to develop novel methods for assessing the selectivity of covalent inhibitors, allowing us to quickly develop a selective PKN3 inhibitor by accessing a novel cysteine. This work highlights the importance of using multiple complementary approaches to further our understanding of poorly annotated proteins or proteins with multiple conflicting roles reported. We anticipate that the pharmacological, genetic and chemical tools presented in this study will be useful to further elucidate cellular functions of these targets and their roles in signaling and cancer biology and represent a general strategy for thorough validation of potential cancer targets.

Understudied Kinases of the Human Kinome

Protein kinases are a large family of consisting of over 500 highly conserved enzymes. The eukaryotic kinases consist of 478 of these, which are more highly related than the additional 40 atypical protein kinases which are sequence-divergent from the rest but still possess kinase activity (Duong-Ly & Peterson, 2013; Manning, Whyte, Martinez, Hunter, & Sudarsanam, 2002). The human eukaryotic protein kinases are sub-classified into seven sub-families based on further structural similarity are commonly represented as a kinome tree (Figure 1-1) (Manning et al., 2002). The dendrogram shows the sequence similarity, and the distance along the branches between two kinases is proportional to the divergence between their sequences. Seven primary families are shown, each as a major branch. The genome also contains many nonfunctional copies of kinase genes that are not expressed or encode truncated proteins, called pseudo-kinases. These pseudo-kinases possess some of the conserved structural kinase features, but their activity or function has not been described (Manning et al., 2002).

Kinases function to transfer the gamma phosphate group from adenosine triphosphate (ATP) to their target molecules. These target molecules are mostly other proteins, though there are roughly 20 lipid kinases described in addition to the protein kinases (Fruman, Meyers, & Cantley, 1998). The ATP phosphate is transferred primarily to tyrosine, serine and threonine residues on the target protein. Tyrosine kinases are more structurally distinct and belong to their own sub-family, separated from the other serine/threonine kinases.

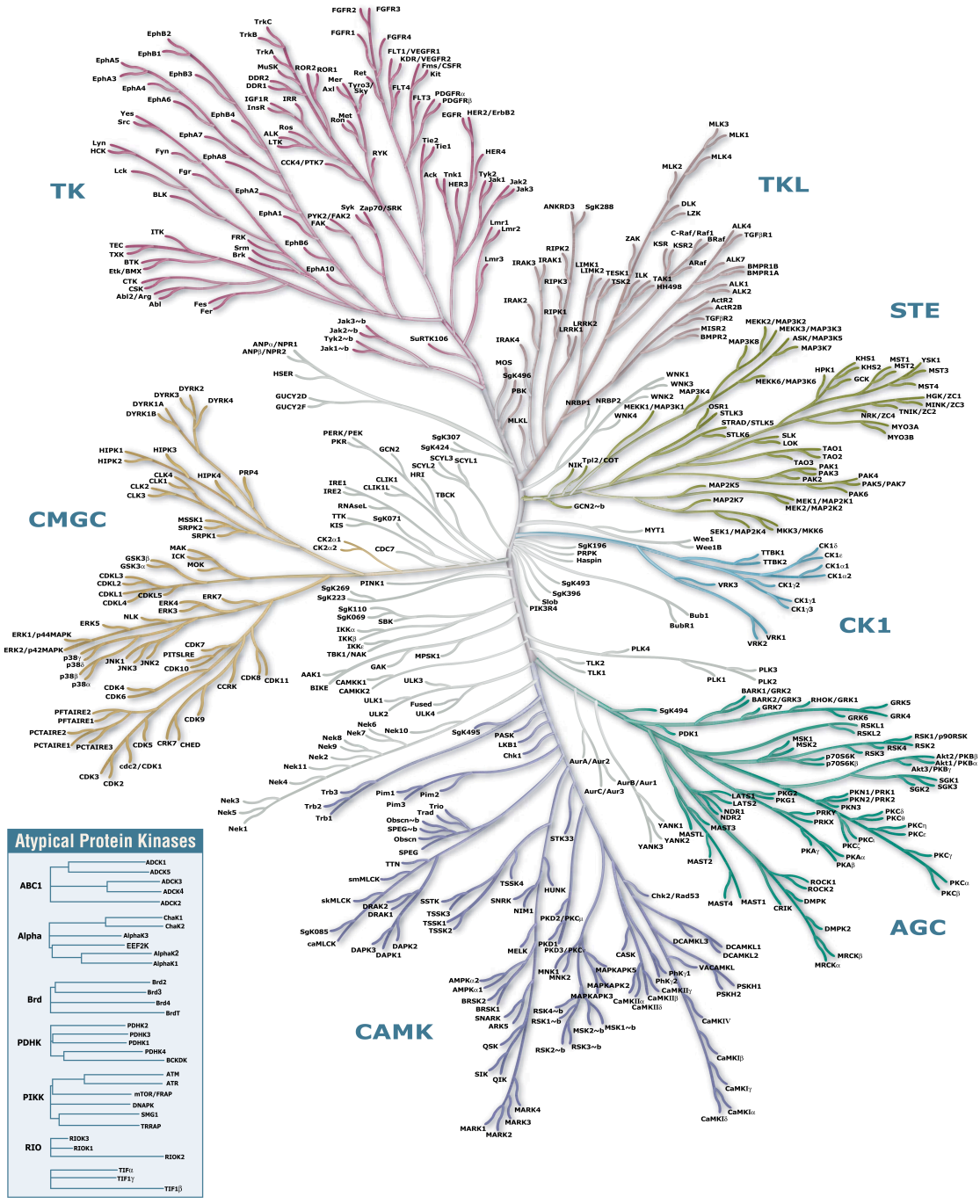

Figure 1-1. Kinome tree, mapped by sequence similarity (Manning et al., 2002), generated for print by Cell Signaling Technology.

The conserved kinase structure typically consists of an N and C lobe on either side of the catalytic core of the protein, also known as the hinge region, where ATP-binding occurs (Figure 1-2) (Johnson, Lowe, Noble, & Owen, 1998; Manning et al., 2002). ATP interacts through hydrogen bonding between adenosine and the kinase hinge region. All kinases possess a conserved activation loop responsible for regulating their kinase activity, marked by the DFG motif at the start and APE motif at the end (J. Zhang, Yang, & Gray, 2009). The conformation of the activation loop determines if the kinase is catalytically active. The active state is termed "DFG-in" since the aspartic acid residue orients towards ATP, and this conformation is stabilized by phosphorylation at several sites on the activation loop. This phosphorylation can be deposited by other kinases, providing a mechanism for regulatory kinase signaling cascades, or can be deposited by the kinase itself in *cis* through intramolecular autophosphorylation of in *trans* by another molecule of the same kinase (Kumar, Gururaj, & Barnes, 2006; Oliver, Knapp, & Pearl, 2007; White, Shoelson, Keutmann, & Kahn, 1988).

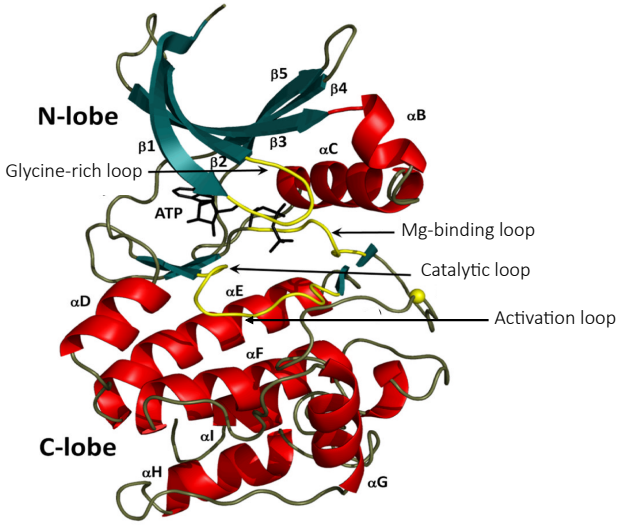

Figure 1-2. Structure of the conserved protein kinase core, showing mapping of conserved protein kinase motifs onto structure of protein kinase A (PKA) (adapted from (Taylor & Kornev, 2011).

Phosphorylation by kinases direct the activity, localization and overall function of many proteins, and coordinate the activity of numerous cellular processes and complex functions, placing kinases at the crux of signal transduction and regulation. Due to their crucial cellular roles, it is unsurprising that these enzymes are frequently mutated and subsequently dysregulated in disease, and as a result, kinases are among the most common drug targets (Ferguson & Gray, 2018). Kinase inhibitors have been extensively developed for clinical use, with great benefit. These inhibitors, and their targets, will be discussed in detail in the following sections. This has led to the extensive study of kinases such as EGFR, BRAF, ALK and PI3KCA in order to understand the function of the endogenous enzymes and of the dysregulated enzymes in cancer (Lemmon & Schlessinger, 2010; J. Zhang et al., 2009).

However, the functions of about one-third of kinases are unknown or poorly annotated. This subset of kinases is understudied and have received little or no attention (based on literature or grants publicly submitted) because foundational data on their biochemical and biological functions is not available (L. C. Huang et al., 2018). Though not specific to kinases, one analysis found that 75% of published research focuses on only 10% of known mammalian proteins (Edwards et al., 2011). Despite this, the understudied or “dark” kinases are among the most heavily mutated or overexpressed kinases in cancer (Cerami et al., 2012; Gao et al., 2013). Of note, these kinases are often the targets of multi-targeting kinase inhibitors, even those that are already clinically approved, as will be discussed next. It is thus critical to devote efforts to understanding the functions of these understudied kinases.

The Druggable Genome

The subset of genes which express proteins considered targetable using small molecules is termed the druggable genome. Biological systems contain four types of macromolecules which can be perturbed using small molecules: proteins, polysaccharides, lipids and nucleic acids; however, challenges around toxicity, specificity and potency for the other macromolecules have made proteins the most common and successful drug targets (Hopkins & Groom, 2002). Genomic information on protein family sequence similarity in combination with prior known drug targets suggest that at least 3000 proteins can be drugged (Hopkins & Groom, 2002).

Intervention using other therapeutic modalities such as nucleic-acid therapeutics and biologics may broaden the classification of druggable proteins. Recent developments in the use of hetero-bifunctional small molecules to induce targeted degradation through the E3-ubiquitin ligase machinery further expand the potential of druggable proteins (Lai & Crews, 2017). However, small molecules made up an overwhelming 86% of FDA-approved drugs and 63% of clinical trials as of 2014, easily making them the dominant class of therapeutics (Rask-Andersen, Masuram, & Schioth, 2014).

Kinases are one of the major protein families targeted by drugs. Inhibition of protein kinases using both small molecules and antibodies constitutes one of the great success stories in pharmaceutical development of the past two decades, especially in the field of oncology (Cohen, 2002; J. Zhang et al., 2009). Both serine/threonine kinases and receptor tyrosine kinases are commonly targeted (Ferguson & Gray, 2018). G-coupled protein receptors (GPCRs) are also common drug targets due to their surface accessibility for ligand binding and key roles in

signaling. According to one estimate, they make up an estimated 19% of the drug-targeted genome with over 50 unique GPCRs targeted (Rask-Andersen et al., 2014).

Nearly 600 proteins are currently the targets of clinical drugs, including small molecules and biologics (Santos et al., 2017). The concept of druggability for a protein typically rests upon the presence of ligand binding sites or domains of a protein, which either may not be known or may not exist (Surade & Blundell, 2012). The fact that proteins undergo alternate splicing and post-translational modifications, and that individual proteins combine in biological contexts in ways that could lead to more opportunities for therapeutics has given rise to the concept of the druggable proteome (Kubinyi, 2003).

Importantly, not all druggable proteins are necessarily good drug targets; their impact on human diseases dictates whether they are suitable for pharmaceutical drug development. Thus, using approved drugs and clinical trials to estimate targeted members of the druggable genome only represents one aspect of drugging proteins. The estimate of proteins targeted by small molecules is further confused by the fact that the complete profile of targets that a drug is able to bind to is often unknown, even in the case of FDA-approved drugs (Davis et al., 2011). Due to the conserved structural features of the ATP binding site of kinases and the clinical success of ATP-competitive inhibitors, the kinase family as a whole is considered druggable, despite the fact that nearly one third of the kinase family is considered understudied (L. C. Huang et al., 2018).

Several unexplored therapeutic opportunities exist around understudied potentially druggable proteins (Edwards et al., 2011; Oprea et al., 2018). To this end, in 2014 the NIH initiated a concerted effort to illuminate the druggable genome with specific focus on understudied proteins that represent unexplored druggable opportunities, which in its pilot

phase has already been successful (Rodgers et al., 2018). Beyond therapeutic benefit, small molecules serve as powerful tools to illuminate the functions of understudied proteins, as will be discussed next.

Pharmacological strategies to assess protein function

Small molecules are powerful tools to interrogate protein function. Cell-permeable inhibitors that are selective for individual protein targets allow for direct investigation of the cellular function of proteins in the relevant contexts. Such molecules hold several advantages over genetic strategies for the disruption of protein activity. Drug-like inhibitors act quickly and reversibly, and do not allow the cell to compensate for the missing protein activity.

Genetic strategies have historically been extremely valuable in parsing protein function. However, these strategies still have disadvantages. Nucleic acid-based approaches such as siRNA and shRNA to induce target knockdown suffer from off-target effects, and can lead to phenotypic effects being incorrectly attributed to the desired target protein (Jackson et al., 2003; Milstein, Nguyen, Meyers, & de Fougerolles, 2013; Rao, Vorhies, Senzer, & Nemunaitis, 2009). With the development of CRISPR/Cas9-mediated editing, the facility and specificity of gene editing or genetic deletions has improved. Off-target editing is still a concern for CRISPR, and these genetic changes are irreversible, both on- and off-target (M. Chen et al., 2019). Additionally, the time required to isolate cells with the desired genetic change allows cells time to compensate for the altered protein activity. The use of temperature-sensitive mutants in genetically tractable systems such as yeast allows for selective disruption of essential genes but is complicated by systemic heat shock responses (Jarolim et al., 2013).

The use of small molecule inhibitors to investigate function specifically for proteins of interest will be discussed extensively in the following section. Beyond specific inhibitors, small molecules are broadly useful in other applications. In particular, the use of small molecules in combination with genetic modifications overcomes one of the major challenges associated with using small molecules – selectivity for the desired target. This approach is broadly termed chemical genetics.

One of the earliest applications of chemical genetics was engineering analog-sensitive alleles of target kinases to make them selectively susceptible to a bulky ATP analog (A. C. Bishop et al., 2000). Mutation of an amino acid residue with a bulky solvent-exposed side chain within the active site to a smaller residue creates a novel pocket, or 'hole', within the protein. This change must be rationally engineered. In order to do so, this mutation should not impact activity and the pocket cannot be present in wild type protein kinases. Using a bulky ATP analog with a 'bump' that takes advantage of the newly-created pocket in the active site results in selective inhibition of the desired target (A. C. Bishop et al., 2000). It is important that these compounds should not inhibit any wild type kinases. Several such analogs such as 1-NM-PP1 have already been reported (A. C. Bishop et al., 2000; Lera & Burkard, 2012). Alternatively, a paired cell line expressing the wild type un-edited kinase can be used to control for off-target effects. This 'bump-hole' strategy was first successfully used for Src kinase (Anthony C. Bishop et al., 1999; Y. Liu, Shah, Yang, Witucki, & Shokat, 1998). It has since been a valuable approach, particularly for investigating mitotic kinases whose study is complicated by multiple functions and substrates, the large number of phosphorylation events that occur in coordinating mitosis, and the short time window in which mitotic events occur (Larochelle et al., 2007; Lera & Burkard, 2012). This

chemical genetic approach can also be used in combination with SILAC mass spectrometry to identify putative substrates of the target kinase (Lera & Burkard, 2012).

More recently, a chemical genetic strategy to induce targeted protein degradation was reported, known as dTAG (Nabet et al., 2018). A previous success of the bump-hole strategy was the development of AP1867, a molecule highly selective for the FK506-binding protein 12 (FKBP12) F36V mutant compared to the FKBP12 wild type protein (Clackson et al., 1998). Conjugating ortho-AP1867 to an iMiD analog using a linker resulted in hetero-bifunctional dTAG molecules. The target protein is engineered by fusing FKBP12 F36V to the protein of interest. This is performed by exogenous expression of the fusion protein, followed by CRISPR-mediated knockout of the endogenous protein – alternatively, this can be achieved using CRISPR to knock-in FKBP12 F36V at the endogenous locus (Nabet et al., 2018). Treatment with the dTAG molecule recruits cereblon to FKBP12 F36V, inducing ubiquitination and subsequent cereblon-dependent degradation of the fusion protein (Nabet et al., 2018). This leaves the activity of the target under complete chemical control of the dTAG molecule, without loss of the protein prior to dTAG treatment. It is critical to validate that the fusion protein retains activity comparable to that of the endogenous protein. This approach has been successfully used for kinases, transcription factors and bromodomain-containing proteins to date (Erb et al., 2017; H. T. Huang et al., 2017; Nabet et al., 2018).

A cellular perturbation strategy has a number of desirable qualities. Ideally, perturbation techniques should be specific, robust, conditional, efficient, reversible, tunable and rapid (Rakhit, Navarro, & Wandless, 2014). Small molecule approaches such as inhibition or targeted degradation fit many of these requirements, though they are limited by specificity and the ability

to access the desired target. Chemical genetic approaches such as those described here overcome these limitations but can require time and extensive genetic engineering. Together these two approaches can form a complementary strategy for interrogating challenging targets.

The use of inhibitors as chemical probes to interrogate protein function

Small molecules inhibitors have tremendous value as chemical probes that can be used to interrogate protein function. Several characteristics of inhibitors are important to consider when qualifying them as useful chemical probes for studying biology. These factors include potency, selectivity, chemistry and their use in the appropriate context (Blagg & Workman, 2017; Workman & Collins, 2010). In terms of chemistry, compounds should have defined stability, be sufficiently soluble, have spectroscopically defined chemical structure and demonstrated permeability for the relevant biological system. It is important that compound's biochemical and cellular potency as well as its pharmacokinetic properties are appropriate for the experimental system being assessed. Probes should have a defined selectivity profile for the characterized target, and ideally be paired with an inactive analog or other chemotypes with similar activity or distinct chemical structure. Complementing pharmacological studies with genetic methods and consideration of the cellular context of the target being studied are also important to consider (Workman & Collins, 2010). Taken together, these criteria for an optimal chemical probe are one step towards ensuring that biological conclusions are appropriately drawn from the phenotypes studied using chemical probes. High-quality chemical probes have the potential to inform the tractability and translatability for a prospective target (Garbaccio & Parmee, 2016).

Traditionally, many proteins are studied and extensively validated as promising therapeutic candidates before inhibitors are developed. Compounds targeting key oncogenic drivers such as EGFR, PIK3CA and BRAF were developed after initial understanding of their roles in signaling pathways and their dysregulation in oncogenic events, all of which are now targets of FDA-approved drugs (Bhullar et al., 2018). After v-Src, protein kinase C (PKC) was one of the first kinases to be associated with oncogenesis, as PKC hyperactivation was shown to correlate with tumor formation (Castagna et al., 1982). Soon after, the antifungal compound staurosporine, which had not previously been shown to inhibit any kinases, was shown to inhibit PKC (Ward & O'Brian, 1992). Staurosporine was later used as a parent compound to produce additional PKC analogs, though staurosporine is now known to be multi-targeting and have poor kinase selectivity (Bhullar et al., 2018; Davis et al., 2011). A series of naphthalene sulphonamides were reported as the first protein kinase inhibitors, and were demonstrated to inhibit PKC (Hidaka, Inagaki, Kawamoto, & Sasaki, 2002). These served as a basis for developing future kinase inhibitors.

In some cases, the development of inhibitors is synchronous with the understanding of target biology. Histone deacetylase (HDAC) inhibitors have both been isolated from natural products and synthesized. HDACs are a family of proteins that play important roles in chromatin remodeling by deacetylating histones tails and are associated with gene expression silencing programs. HDACs also have non-histone targets such as transcription factors and proteins involved in the regulation of cell proliferation, migration and death (Marks & Dokmanovic, 2005). Trichostatin A was a natural product isolated as an antifungal, which was later found to inhibit mammalian HDAC activity and induce erythroleukemic cell differentiation (Yoshida, Kijima, Akita,

& Beppu, 1990; Yoshida, Nomura, & Beppu, 1987). The small molecule hexamethylene bisacetamide (HMBA) was found to induce growth arrest and differentiation in transformed cells and also to selectively alter the expression of specific genes (Marks & Rifkind, 1978; Richon, Ramsay, Rifkind, & Marks, 1989). Although the mechanism was not known, structure activity relationship of HMBA analogs and the differentiation phenotypes suggested that the cellular effects were due to specific target binding (Marks & Breslow, 2007). These results prompted the initiation of HMBA clinical trials, but acute myeloid leukemia patients only experienced partial remission (Andreeff et al., 1992).

Vorinostat (also known as suberanilohydroxamic acid, or SAHA) received FDA approval as anti-cancer agents for the treatment of cutaneous T-cell lymphoma in 2006. Vorinostat has since undergone trials for other indications, but early trial results in solid tumors have been disappointing (H.-J. J. Kim & Bae, 2011). SAHA was synthesized as part of a series of analogs of HMBA, and was optimized for its ability to induce cell differentiation; observation of the structural similarity between SAHA and trichostatin A led to the demonstration of HDACs as the target of SAHA (Marks & Breslow, 2007). Concurrent with the development of vorinostat, a pan-HDAC family inhibitor, biological studies including generating individual HDAC protein knockout mice, aided in furthering understanding of HDAC activity in gene control and tissue-specific developmental programs (H.-J. J. Kim & Bae, 2011). The development and use of HDAC inhibitors helped to establish the function of HDACs in connecting gene expression control with cell differentiation.

Small molecules often help elucidate protein function and even aid in discovery. FKBP proteins are so named due to their ability to bind the immunosuppressant drug FK506. FK506

was the first compound found to cause chemical-induced dimerization, bringing FKBP into proximity with calcineurin (J. Liu et al., 1991). Another immunosuppressant well-studied drug, rapamycin, was critical in identifying and elucidating the function of mammalian target of rapamycin (mTOR) (J. Li, Kim, & Blenis, 2014). Rapamycin represents the most thoroughly studied chemical dimerizer (Rakhit et al., 2014). It was first identified as an antifungal metabolite, and quickly found to possess immunosuppressive properties (Schreiber, 1991). Investigation into its mechanism of action led to the identification of the protein mTOR (Laplante & Sabatini, 2012; Loewith & Hall, 2011). Rapamycin binds FKBP12, resulting in a complex which allosterically inhibits the mTOR complex. The use of rapamycin has led to extensive subsequent study of the roles of mTOR in integrating environmental signals to regulate metabolic signaling, cell growth and (when dysregulated) in cancer (J. Li et al., 2014). These advances have motivated researchers to develop selective chemical probes as a strategy for uncovering protein function.

The advantages (and disadvantages) of covalent inhibitors

Covalent inhibitors irreversibly react with nucleophilic side chains of residues in or around the protein active site. These residues include lysine, aspartic acid and others, but the thiol side chains of cysteines are most commonly targeted (Shannon & Weerapana, 2015). While some covalent compounds readily react with solution-accessible nucleophiles, others react after non-covalent binding first occurs based on proper compound trajectory towards the target cysteine (Potashman & Duggan, 2009). The binding mode depends on the reactivity of the covalent warhead, which is critical not only for formation of the expected covalent interaction but also for determination of toxicity based on either on-target of off-target effects (Z. Zhao &

Bourne, 2018). Several electrophiles have been used as covalent warheads, the most common of which is acrylamide (Z. Zhao & Bourne, 2018).

The majority of clinical and preclinical kinase inhibitors are ATP-competitive, non-covalent inhibitors that achieve selectivity by taking advantage of unique structural features of the protein (Q. Liu et al., 2013). Due to the high sequence conservation of the ATP active site, it is difficult to achieve selectivity for active site inhibitors. Covalent inhibitors offer an additional feature of the active site which can be taken advantage of – the position of the cysteine within the kinase active site. The positions within the active site of targetable cysteines across the kinome have been previously mapped (Q. Liu et al., 2013; J. Zhang et al., 2009). These cysteines include positions within the glycine-rich P-loop, the DFG region, gatekeeper, the kinase hinge region and even remote cysteines away from the active site, as in the case of CDK7/12/13 (Kwiatkowski et al., 2014; Q. Liu et al., 2013; J. Zhang et al., 2009).

A common strategy for developing covalent inhibitors is to use structure-guided design to elaborate upon existing non-covalent inhibitors for the desired target to access a known cysteine (Chaikuad, Koch, Laufer, & Knapp, 2018; Potashman & Duggan, 2009). Reversible interactions stabilize covalent inhibitors in the target active site and are important for compound potency (Schwartz et al., 2014). Selecting a reversible inhibitor with a favorable selectivity profile that allows installation of an electrophile with the correct trajectory to engage the nucleophilic cysteine is thus key to the success of this design approach (Chaikuad et al., 2018). This requirement can also result in improved selectivity over other kinases, as cysteines at alternate positions near the active site should not be engaged (Q. Liu et al., 2013; J. Zhang et al., 2009). For

kinases with cysteines positioned similarly to that of the desired target, off-target activity should be carefully monitored during compound development.

One of the first clinical successes for covalent inhibitors was targeting EGFR cysteine 797, an oncogenic highly activated form of EGFR. The first covalent EGFR inhibitor was published in 1998, and afatinib was the first covalent inhibitor to receive approval in 2013 (Dungo & Keating, 2013; Fry et al., 1998). As of 2018, three of the four FDA-approved covalent kinase inhibitors target EGFR – the other is ibrutinib, which covalently targets BTK (Z. Zhao & Bourne, 2018). The scope of kinases initially thought to be targetable through covalent inhibition has expanded from the initial 11 EGFR-related kinases to over 190 kinases (Leproult, Barluenga, Moras, Wurtz, & Winssinger, 2011; Q. Liu et al., 2013). Further opportunities for achieving selectivity using covalent inhibitors exist, allowing access to previously undruggable proteins. For example, the oncogenic mutant KRAS G12C yields a cysteine which does not exist on the wild type protein, allowing opportunities for selectively targeting the mutant form (Zeng et al., 2017).

Despite recent clinical successes for irreversible drugs, potential toxicities mediated by unpredictable modification of off-target cysteines represents a major obstacle for expansion of covalent drug development (Ferguson & Gray, 2018). This concern is despite the fact that increased potency and effect windows should require lower doses, resulting in fewer side effects (Chaikuad et al., 2018). For inhibitors that are obligately covalent, it is possible to mutate the reactive target cysteine to a serine or alanine and re-introduce the mutant kinase to the experimental system of interest to assess the rescue of inhibitor-induced effects (Kwiatkowski et al., 2014; Q. Liu et al., 2013). Characterizing target-dependent effects using inhibitor-resistant mutants is one method of evaluating selectivity and potential toxicities, and this method of doing

so is unique to covalent inhibitors (Kwiatkowski et al., 2014; Q. Liu et al., 2013). Conversely, this points to another disadvantage of covalent inhibitors – acquired resistance through loss of the target cysteine (Ferguson & Gray, 2018). The ability to completely characterize the selectivity of covalent inhibitors and monitor covalent off-target modifications would be a valuable advance for covalent drug development.

In this thesis I employed the above-described chemical and genetic approaches to elucidate the functions of three distinct understudied proteins: CDK14, PKN3 and PIN1. The following sections describe the background and motivation for interrogating these targets.

The cyclin dependent kinase (CDK) family and CDK inhibitors

Cyclin dependent kinases (CDKs) are a family of serine/threonine kinases that are conserved across many eukaryotic species. To date, twenty CDK family members have been identified based on conserved structural features. The conserved catalytic core consists of the ATP-binding pocket, the activating loop and cyclin binding domain, typically consisting of an amino acid sequence close to 'PSTAIRE' (Lim & Kaldis, 2013). CDKs play critical roles in a variety of essential cellular functions, including cell cycle progression, RNA Polymerase II (RNAPII)-based transcription, activation of specific transcriptional programs such as Wnt and NFκB signaling, epigenetic regulation, DNA damage repair and more.

Binding of a cyclin partner is required for CDK activation and control of enzymatic activity (Morgan, 1997). The cyclin family is diverse, and proteins are classified as cyclins only by possession of a cyclin box that is capable of mediating binding to a CDK (Gopinathan, Ratnacaram, & Kaldis, 2011). Regulation of synthesis and proteasomal degradation of cyclins

allows for temporal control of CDK activity, particularly during specific cell cycle phases (Ang & Harper, 2004; Evans, Rosenthal, Youngblom, Distel, & Hunt, 1983; Glotzer, 1995; Murray, Solomon, & Kirschner, 1989; Reed, 2006; Skaar & Pagano, 2009).

However, CDK-independent functions for cyclins have recently been identified. For example, cyclin D1 was associated with more than 900 promoter regions by chromatin immunoprecipitation (Coqueret, 2002). Cyclin Y possesses an N-terminal myristoylation at Glycine2, which allows the protein to localize to the plasma membrane. This in turn allows cyclin Y to recruit its CDK binding partners to the plasma membrane as well (Davidson et al., 2009; Jiang, Gao, Yang, Zhu, & Chen, 2009; T. Yang & Chen, 2001). Cell cycle cyclins such as the D-type cyclins also play roles in transcription independently of their CDK partners through regulation of numerous transcription factors (Hydbring, Malumbres, & Sicinski, 2016).

Traditionally, CDKs1-6 were considered the classical cell cycle CDKs for their roles in regulating cell cycle transition, while the transcriptional CDKs, CDKs7-13, are responsible for coordinating transcription (Figure 1-3). Cell cycle CDKs also play a role in regulation of DNA repair, as CDK1/2 phosphorylate BRCA2 and other upstream regulators of homologous recombination, reducing DNA damage repair through Rad51 (Hydbring et al., 2016). This event is important for proper timing of mitotic onset and appears to be required for normal chromosome segregation. As mentioned previously, CDKs are conserved across species; yeast possess a single CDK, most homologous to human CDK1 - Cdc28 for *S. cerevisiae* and Cdc2 in *S. pombe*. These yeast CDKs play critical roles in DNA damage repair, as inhibition of Cdc28 prevents recruitment of the homologous recombination repair machinery to the site of damage and increases incidence of non-homologous end joining (Ira et al., 2004).

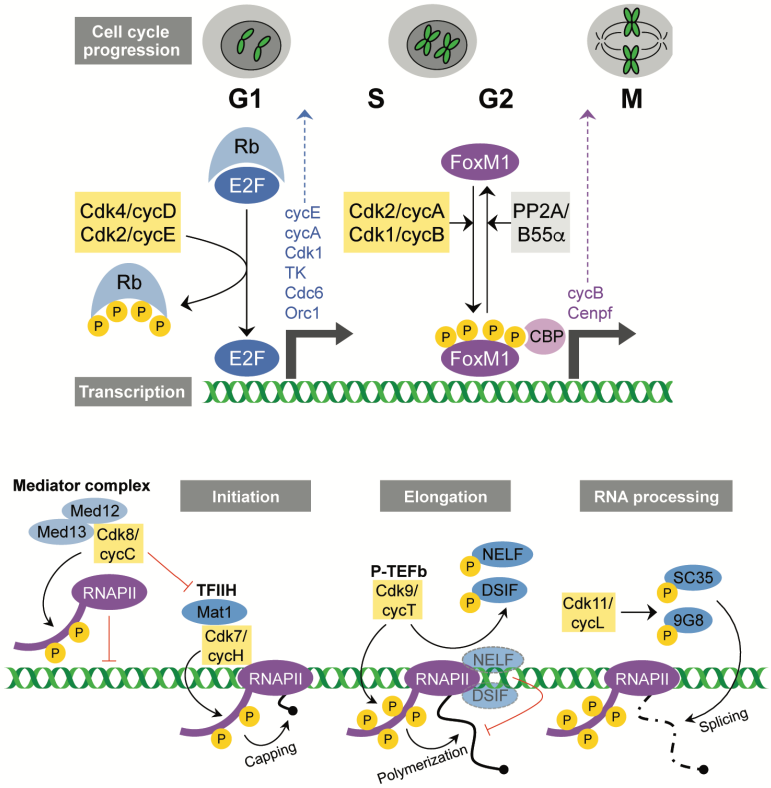

Figure 1-3. Diagram of functions of cell cycle (top) and transcription (bottom) CDKs (Lim & Kaldis, 2013).

The cell cycle and transcriptional groups of CDKs were once considered distinct; however, this is no longer the case. CDK7 is responsible for RNAPII elongation through phosphorylation of Serine2, but also possesses CDK-activating kinase (CAK) activity, phosphorylating activating sites on cell cycle kinases like CDK1 at Threonine161 (Lim & Kaldis, 2013). Additionally, stem cell differentiation requires a decrease in the rate of cell cycle progression, suggesting a role for cell cycle regulation to connect with cell fate-determining transcriptional programs. CDK activity is required for Neurogenin2 phosphorylation in neuronal stem cells, preventing binding to DNA and subsequently expression of neurogenic genes (Ali et al., 2011). In myoblasts, phosphorylation of the transcription factor Myoblast determination protein 1 (MyoD) is CDK-dependent and promotes its degradation, contributing to maintenance of the proliferative state

(Song, Wang, Goebl, & Harrington, 1998). CDK1 was also reported to pair with Oct4 to maintain stemness in embryonic stem cells (L. Li et al., 2012).

Kinase-independent functions of CDKs have also been identified. CDK10 binds directly to the transcription factor ETS Proto-Oncogene 2 (Ets2), preventing its activation and subsequently suppressing MAPK signaling; the kinase-inactive CDK10 is still able to similarly effect Ets2 (Kasten & Giordano, 2001). In addition to the kinase-dependent role of CDK6 in cell cycle regulation, which it shares with the closely-related CDK4, CDK6 plays a role in inducing transcription of proinflammatory genes during the G1 phase of the cell cycle. CDK6 does not possess any identified DNA-binding domains, and as such it associates directly with transcription factors from the NFκB, STAT and AP-1 families directly to induce gene expression at specific promoters, resulting in the production of inflammatory mediators (Kollmann et al., 2013). c-Jun is required for VEGF-A induction, while STAT3 is required for $p16^{INK4A}$ induction. CDK6 also mediates NFκB recruitment to its target genes, and although CDK6 is able to phosphorylate the p65 subunit of NFκB, the kinase-inactive CDK6 is also able to mediate NFκB recruitment to target genes (Schmitz & Kracht, 2016). The mechanism of this interplay is not well-understood.

CDK inhibitors and their use in cancer treatment

Much of the work to characterize and understand the function of the classical cell cycle CDKs came from genetic studies that preceded the development of inhibitors. Given that unchecked proliferation and dysregulation of the cell cycle is a common feature of cancer, it is unsurprising that CDKs and cyclins, which are critical components of cell cycle machinery, are frequently mutated or overexpressed in cancer (Asghar, Witkiewicz, Turner, & Knudsen, 2015).

CDK inhibitors have been in development for over twenty years (Asghar et al., 2015). Structurally, these inhibitors encompassed several heteroaromatic scaffolds including flavonoid, purine, indenopyrazole, aminopyrimidine, aminothiazole, indirubin, and paullone derivatives (Whittaker, Mallinger, Workman, & Clarke, 2017). The first generation of CDK inhibitors, such as flavopiridol and roscovitine, were pan-CDK targeting (Fischer & Lane, 2000). Flavopiridol, for example, inhibits CDK1, CDK2, CDK4, CDK6, CDK7 and CDK9. Regardless of their multi-targeting nature, as knowledge of CDK biology evolved in conjunction with the development of these compounds, they proved to be useful tools for understanding CDK function in different disease contexts. Over 60 clinical trials have been conducted using flavopiridol for various cancer types, but despite good *in vitro* activity, *in vivo* efficacy in trials was limited overall (Asghar et al., 2015). Second generation CDK inhibitors were developed to improve upon the potency and specificity of the first generation. These included compounds such as dinaciclib, which also inhibits several CDKs - CDK1, CDK2, CDK4, CDK5, CDK6, CDK7 and CDK9 (Opoku-Temeng, Dayal, Hernandez, Naganna, & Sintim, 2018). Dinaciclib is currently in clinical trials both as a single agent and in combination regimens for a number of cancer types. In initial phase III trial results for dinaciclib, most patients experienced severe adverse events in addition to incomplete response (Morales & Giordano, 2016).

Due to homology within the CDK family, it is difficult to develop active-site inhibitors of CDKs which are selective for specific CDKs. There have been few exceptions; the first is the development of covalent inhibitors targeting transcriptional CDKs, which to date have primarily been used as tool compounds. THZ1 was reported as a covalent inhibitor of CDK7, which was later found to have off-target activity towards CDK12, but otherwise good selectivity over the

other CDKs (Kwiatkowski et al., 2014). A selective covalent inhibitor of CDK12, THZ-5-31 was later developed which did not retain any CDK7 activity (T. Zhang et al., 2016). These compounds have been powerful tools to further our understanding of these transcriptional CDKs. The development of these selective inhibitors was facilitated by covalent targeting of unique cysteines within the target CDK active site.

Recent studies also demonstrated that conjugation of a small molecule to an E3 ubiquitin ligase-recruiting moiety may be an additional strategy to achieve selectivity. SNS-032, which binds multiple CDKs, was conjugated to a thalidomide derivative to yield THAL-SNS-032, which selectively degrades CDK9 without disrupting the other targets of SNS-032 (Olson et al., 2018). A recently developed novel ATP-competitive selective CDK9 inhibitor, NVP-2, was also characterized, and the cellular effects of THAL-SNS-032 were more similar to NVP-2 than its parent SNS-032 (Olson et al., 2018).

The transcriptional CDKs have been identified as promising cancer targets, particularly in leukemias, which exhibit transcriptional addiction (Galbraith, Bender, & Espinosa, 2019; Kwiatkowski et al., 2014). Later work suggested that the effects seen with first generation pan-CDK inhibitors were likely due to inhibition of CDK7 or CDK9 and impaired transcription (Whittaker et al., 2017). Compounds like SNS-032 and dinaciclib which were originally thought to be CDK9-specific do in fact retain activity towards other CDKs. The therapeutic value of the selective covalent CDK inhibitors has yet to be clinically evaluated. Despite their promising *in vitro* activity, the clinical use of inhibitors that target multiple CDKs has been limited by adverse events. The best indication for clinical activity of multi-CDK inhibitors has been in hematological malignancies (Whittaker et al., 2017).

The other exception to multi-targeting CDK inhibitors is the development of selective CDK4/CDK6 inhibitors. CDK4/6 inhibitors like palbociclib, abemaciclib and ribociclib have been the most successful of the CDK inhibitors in the clinic. Palbociclib was first reported in 2004, but it wasn't until 2009 that promising activity in luminal breast cancer lines was demonstrated (Finn et al., 2009). Palbociclib is now approved for the treatment of hormone receptor (HR)-positive, human epidermal growth factor receptor 2 (HER2)-negative advanced or metastatic breast cancer in combination with endocrine therapy. Since then, ribociclib and abemaciclib have both been approved for the same indication, and abemaciclib has been investigated in a Phase I trials in NSCLC, glioblastoma, breast cancer, melanoma or colorectal cancer with promising results (Patnaik et al., 2016).

Biomarkers for response to CDK4/6 inhibition have been identified, such as phospho-RB levels (Patnaik et al., 2016). In particular, cancers in which CDK4/6 is coupled to G1/S checkpoint control and exerts downstream effects through the Retinoblastoma protein (RB) pathway are particularly susceptible to CDK4/6 inhibition, while amplification of genes like cyclin E or the E2F transcription factors can limit therapeutic benefit (Knudsen & Witkiewicz, 2017). Several combination treatments for CDK4/6 inhibitors, including co-treatment with PI3K inhibitors, MEK inhibitors and BRAF inhibitors, have shown preclinical promise and are now under clinical investigation (Kwong et al., 2012; M. S. Lee et al., 2016; Vora et al., 2014).

The extensive development of small molecule CDK inhibitors, albeit with varying selectivity, has provided a wealth of chemical tools with which to investigate CDK biology and begin to validate CDKs as therapeutic targets. The use of small molecule inhibitors recently revealed additional roles for CDKs in innate immunity and inflammatory signaling. A screen for

potentiators of Interleukin-10 identified a small molecule that was highly selective for CDK8 and its paralog CDK19 (also known as CDC2L6) (Johannessen et al., 2017). Selective inhibitors of CDK8/19 have recently been identified, including the natural product cortistatin A, the small molecule inhibitor CCT251545 and the small molecule BRD6989, though their clinical use is limited (Johannessen et al., 2017; Pelish et al., 2015; Xi et al., 2019). Small molecule inhibition with R547 or siRNA silencing of multiple CDKs blocked the activating phosphorylation of STAT1 and STAT3, resulting in reduced transcription of IFN-stimulated genes and subsequent antiviral response upon DNA challenge (Cingöz & Goff, 2018). Promising preclinical results have demonstrated the CDK4/6 inhibition in combination with anti-PD-1 immunotherapy agents dramatically potentiate the effect of immunotherapy by induction of innate immune signaling and T-cell activation, occurring through previously unrecognized CDK4/6 functions (J. Deng et al., 2018; Goel et al., 2017).

The poorly annotated CDKs

The remaining higher number CDKs, CDKs14-20 are mostly uncharacterized. CDK19 is a paralog of CDK8, and CDK19-specific roles have yet to be identified. CDK20 (also known as CCRK) was recently characterized as a CDK family protein due to conserved structural features and is most similar to CDK7 and its CAK function (Wohlbold et al., 2006). However, depletion of CDK20 did not impair CDK2 activation in the manner that CDK7 depletion did (Wohlbold et al., 2006). CDK20 has some cell cycle activity, and CDK20 silencing was also shown to impair lung cancer cell proliferation and impact cell cycle through interaction with the ubiquitin ligase KEAP1, though it does not cause cell cycle arrest at a specific point (Q. Wang et al., 2017; Wohlbold et al., 2006). The TAIRE kinases, CDKs14-18, make up the rest of the CDK family, and are so-named due to the

amino acid sequence of the cyclin binding domain. CDK16 is overexpressed or over-active in a number of cancer types (Mikolcevic, Rainer, & Geley, 2012; Phadke et al., 2018; Yanagi & Matsuzawa, 2015). Little else is known about the TAIRE kinases CDK15, CDK16, CDK17 and CDK18, all of which bind cyclin Y. The functions of CDK14 will be discussed in detail in the following section.

CDK14 is implicated in Wnt signaling and its connection to the cell cycle

CDK14, also known as PFTK1 or PFTAIRE1, does not clearly fall into either category of known CDK functions, cell cycle regulation or transcription. Despite containing two predicted nuclear localization sequences, it has only been found in the cytoplasm (T. Yang & Chen, 2001). Three cyclins have been implicated in binding to or enhancing the activity of CDK14: cyclin Y, D3, and B. Cyclin Y, identified as a novel cyclin by yeast two-hybrid screening for CDK14 binders, is the most widely accepted cyclin partner for CDK14 (Jiang et al., 2009). Cyclin Y has a single cyclin fold and is N-terminally myristoylated, allowing it to localize to the plasma membrane and to recruit CDK14 to the plasma membrane (Davidson et al., 2009; Jiang et al., 2009; T. Yang & Chen, 2001). Functionally, exogenous overexpression of Cyclin Y has been shown to enhance phosphorylation of CDK14 downstream targets (Davidson et al., 2009; S. Li et al., 2014; T. Sun, Co, & Wong, 2014). Additionally, cyclin Y itself is a substrate of CDK14, and CDK14-dependent phosphorylation leads to its ubiquitination and degradation, resulting in a negative feedback loop downregulating cyclin Y-mediated CDK14 activation (S. Li et al., 2014). Cyclin D3 and cyclin B have also been identified as alternate partners for CDK14 (X. Gu et al., 2015; Shu et al., 2007). The functional implications of these two other cyclins binding to CDK14 have not been studied or

further validated, and it is unclear how these alternate cyclin partners reconcile with the role of Cyclin Y.

While the best-known role for CDK family members is in regulating cell cycle, the role of CDK14 in the cell cycle regulation is unclear. Levels of CDK14 remained constant throughout the cell cycle in U2OS cells, while HEK293 cells exhibit cycling levels of CDK14, peaking in mitosis (Davidson et al., 2009; Shu et al., 2007). Overexpression of CDK14 promoted G1 to S phase transition in U2OS cells, while knockdown stalled SH-SY5Y cells in G1 (Shu et al., 2007). In invasive gastric cancer cells, overexpression resulted in an increased proportion of cells in S phase and fewer in G0/G1, while siRNA knockdown had the opposite effect (L. Yang et al., 2015). In liver cancer cells, CDK14 overexpression led to a reduction in Wee1, an inhibitor of entry into mitosis through inhibition of CDK1 (Pang et al., 2007). These data suggest that CDK14 may be involved in promoting the G1/S transition, despite not being classified as a cell cycle CDK.

CDK14 modulates Wnt signaling. The LRP6 trans-membrane canonical Wnt signaling co-receptor is a kinase target of CDK14 (Davidson et al., 2009). CDK14 phosphorylates LRP6 at Ser1490 in a mitosis-dependent Wnt-independent manner, priming it for a second phosphorylation by CK1γ in response to Wnt ligand stimulation, leading to full activation of Wnt/β-catenin signaling and, ultimately, increased cell survival (Davidson et al., 2009). CDK14 and Cyclin Y expression peak during M phase in HEK293 cells, as does Ser1490 LRP6, suggesting that Wnt receptor activation is under cell cycle control through CDK14 (Davidson et al., 2009). This was also observed in *Drosophila* cells and *Xenopus* eggs during development (Davidson et al., 2009). The consequence of this priming phosphorylation in mitosis is not completely understood. This phenotype is consistent with the idea that Wnt signaling plays broader cellular

roles beyond transcriptional regulation (Davidson & Niehrs, 2010; Niehrs & Acebron, 2012; Niehrs & Shen, 2010). Cell cycle-dependent activation of LRP6 could be a mechanism to enhance signaling in proliferative contexts, for example during development or in stem cells, which would be consistent with the surprising observation of CDK14-mediated LRP6 phosphorylation in *Xenopus* eggs (Davidson & Niehrs, 2010; Davidson et al., 2009).

Overactivation or dysregulation of Wnt signaling is prevalent in cancer (Polakis, 2012; Y. Wang, 2009). The Wnt signaling pathway is evolutionarily conserved across metazoans and plays key roles in cell migration and other processes during development. The canonical Wnt/β-catenin cascade has long been implicated in cancer; recently dysregulation of the non-canonical planar cell polarity pathway has been implicated in tumor metastasis (Y. Wang, 2009). The non-canonical pathway specific ligand Wnt5a and signal transducer Frizzled10 were separately shown to promote metastasis through activation of the signaling cascade (Y. Wang, 2009). Downstream effectors of the non-canonical (β-catenin independent) Wnt pathways include RhoA and Rac1 GTPases, which lead to rearrangement of actin cytoskeletal filaments and subsequent modulation of cell adhesion, motility and movement in development (Schlessinger, Hall, & Tolwinski, 2009). Though the mechanism is not completely understood, a role for over-activation of non-canonical Wnt signaling in cancer cell motility is thus not surprising.

CDK14 has also been implicated in activating non-canonical Wnt signaling when overexpressed in cancer cell lines. Overexpression of CDK14 in gastric cancer and hepatocellular carcinoma leads to increases in Naked1 and Dishevelled2 (Dvl2) protein levels, which both act downstream of receptor activation in non-canonical Wnt signaling (T. Sun et al., 2014; L. Yang et al., 2015). Naked1 inhibits the canonical Wnt/β-catenin pathway by binding to Dishevelled (Dvl),

directing activity towards the non-canonical Wnt pathway. Dvl proteins transduce the Wnt signal downstream by binding the cytoplasmic tail of the Frizzled receptor; Dvl acts in canonical Wnt while Dvl2 acts in non-canonical Wnt pathways. GTP-associated RhoA, Rac1 and Cdc42 were increased upon CDK14 transfection in two liver cancer cell lines, indicating activation of actin polymerization downstream (T. Sun et al., 2014). In the cases where non-canonical Wnt signal is activated by increasing CDK14 protein expression in cancer cell lines, canonical Wnt signaling is unaffected, with one exception in breast cancer cells (X. Gu et al., 2015). The downstream outcome of non-canonical Wnt signaling is actin polymerization, a driver of cell motility.

Two actin binding and remodeling proteins, transgelin2 and caldesmon, were altered in response to CDK14 modulation in hepatocellular carcinoma cells (Leung, Ching, Chan, et al., 2011; Leung, Ching, & Wong, 2011). CDK14 knockdown led toreduced phosphorylation of these two actin-binding proteins. This resulted in transgelin2 binding to actin, resulting in actin destabilization, and displacement of caldesmon from actin, leading to reduced actin stress fiber formation. These data suggest transgelin2 and caldesmon phosphorylation, which dictate their actin binding properties, occurs downstream of CDK14. However, there is no evidence of direct interaction or phosphorylation by CDK14.

CDK14 protein expression is high in several cancers compared to paired normal tissue and higher in advanced grade and more invasive cancers (Fan et al., 2015; X. Gu et al., 2015; Leung, Ching, Chan, et al., 2011; Pang et al., 2007; L. Yang et al., 2015; W. Zhang et al., 2016). Exogenous overexpression or inherently high expression of CDK14 in a number of cancer cell lines results in increased cell invasion and migration, while siRNA knockdown decreases it; furthermore, high CDK14 expression correlates with worse patient prognosis in a variety of

cancers in which motility has been studied: gastric cancer, glioma, ovarian and breast cancer (Fan et al., 2015; X. Gu et al., 2015; Pang et al., 2007; L. Yang et al., 2015; W. Zhang et al., 2016; Zheng, Zhou, & He, 2015). To date, these effects have been observed in breast cancer, hepatocellular carcinoma, gastric cancer, ovarian cancer, pancreatic cancer and glioma.

Several studies have recently reported increases in CDK14 expression through decreased long non-coding RNA (lncRNA) or micro-RNA (miRNA) expression in ovarian cancer, glioma, NSCLC, pancreatic cancer, osteosarcoma and hepatocellular carcinoma cell lines (Dai et al., 2018; Du, Zhang, Tan, & Xu, 2017; Z. Gu et al., 2018; Ji et al., 2017; Jin, Jin, Wu, Xu, & Li, 2018; J. Li, Shao, & Feng, 2019; Q. Li et al., 2018; Y. Sun et al., 2019; Tu et al., 2019; B. Wang et al., 2017; Yan, Qiu, Sun, & Li, 2018; J. Yang, Zhu, Jin, & Song, 2018; Zheng, Hu, & Zhou, 2019). No two studies reported the same miRNAs and lncRNAs, even those in the same cancer types. They all proposed similar mechanisms and showed that modulating levels of the miRNA or lncRNA led to effects on cell migration and proliferation consistent with a negative regulator of a driver of cell migration. None of the studies verified the specificity of the miRNA's effect on CDK14, and some studies failed to directly connect activity at the miRNA level to CDK14.

Elevated levels of CDK14 have been reported in several types of cancer, unrelated to cell motility effects. CDK14 levels were increased in chronic lymphocytic leukemia cells compared to normal B cell lymphocytes (McCarthy et al., 2015), and CDK14 was amplified as a result of spontaneous genomic changes in a mouse model of colorectal cancer (Y. Zhou et al., 2014). Moreover, CDK14 has been implicated in actually promoting tumorigenesis and/or pathogenesis. For instance, CDK14 was identified as a potential driver of a subtype of renal cell carcinoma (Anderson et al., 2015), and high levels of CDK14 correlate with chemotherapy

resistance in oesophageal squamous cell carcinoma patients (Miyagaki et al., 2012). Given these observations of the varied importance of CDK14 in cancer, further understanding of its role in normal and transformed cells is essential.

The role of the kinase activity of CDK14 in promoting cell migration, a process central to the transition from early to advanced stage cancer, has not been addressed by prior studies. Previous work on CDK14 has used siRNA knockdown or exogenous overexpression to modulate CDK14 protein levels and study its role. As a result, it is unclear whether these processes require CDK14 as a kinase or as a scaffolding protein, functioning in some indirect role. CDK14's various hypothesized cellular functions have not previously been connected by study in a unified system. Deeper unbiased study of the pathways in which CDK14 functions is needed to understand the role it plays in cancer biology and the consequence of disrupting its kinase activity by pharmacologic inhibition or chemical biology approaches.

PKN3 is a poorly annotated kinase reported to play a role in cell migration

Protein kinase N3 (PKN3) is an understudied kinase. It is a member of the protein kinase C family, characterized by high sequence homology in the C-terminal domain of the protein, and is one of three PKN isoforms – PKN1, PKN2 and PKN3 (Manning et al., 2002). While PKN1 and PKN2 are widely expressed in normal human adult tissue, PKN3 is barely detectable in normal tissues but is up-regulated in cancerous tissues, including prostate cancer (Leenders et al., 2004; Oishi, Mukai, Shibata, Takahashi, & Ona, 1999).

PKN3 plays a role in cancer metastasis, but little to no role in tumor growth. Early studies demonstrated that PKN3 was the first serine/threonine protein kinase shown to bind to the small

GTPase Rho, which regulates its activity (Hideyuki Mukai, 2003). PKN3 preferentially binds RhoC, and its catalytic activity is increased *in vitro* in the presence of RhoC (Unsal-Kacmaz et al., 2012). This regulatory pathway suggested that PKN3 may be involved in the same processes as Rho. The Rho GTPases play important roles in actin cytoskeleton reorganization, cell migration and cell-cell adhesion (Lawson & Ridley, 2018).

PKN3 is important for cell morphology and motility. Knockdown of PKN3 in human endothelial cells (HUVEC) resulted in unusual cell morphology and movement, consistent with the observed irregular actin organization (Mopert, Loffler, Roder, Kaufmann, & Santel, 2012). PKN3 also plays a role in adherens junction dynamics, as knockdown caused uneven distribution of adhesion molecules like VE-cadherin (Mopert et al., 2012). Upon stimulation with the pro-inflammatory cytokine TNF-α, cells with PKN3 knockdown have reduced adhesion at intracellular adherens junctions and show lower cell surface expression of the adhesion molecule ICAM-1, a critical step in responding to pro-inflammatory signals (Mopert et al., 2012). It was later demonstrated that PKN3 knockdown in HUVEC leads to glycosylation defects of cell-surface glycoproteins, including common adhesion molecules such as ICAM-1, integrin β1 and integrin α5 (H. Mukai et al., 2016). These effects on adhesion molecules, though not fully understood from a mechanistic standpoint, are consistent with a role for PKN3 in migration and metastasis.

From a screen for regulators of malignant growth in activated phosphoinositide 3-kinase (PI3K) signaling settings, expression of PKN3 at the RNA level was found to be induced by PI3K activation (Leenders et al., 2004). That expression was essential for PI3K-induced growth in Matrigel (Kleinman & Martin, 2005) for PC-3 prostate cancer cells, and while PKN1 expression was also induced by PI3K signaling activation, knockdown of PKN1 and PKN2 did not impair

growth in these conditions while knockdown of PKN3 did (Leenders et al., 2004). Transformation of human mammary epithelial cells by Ras G12V was impaired by PKN3 knockdown, while PKN3 expression was increased in a PI3K-dependent manner in transformed cells compared to untransformed cells (Leenders et al., 2004). PKN3 overexpression also promotes growth in Matrigel for triple negative breast cancer cell lines, and this phenotype is dependent on RhoC (Unsal-Kacmaz et al., 2012).

PKN3 knockout mice develop normally, but have defects in angiogenesis and micro-vessel sprouting (H. Mukai et al., 2016). Furthermore, these mice also show reduced lung metastases upon tail vein injection of melanoma cells compared to wild type mice (H. Mukai et al., 2016). In prostate cancer cell transplant models into nude mice, PKN3 knockdown by dox-inducible shRNA in the transplanted cells significantly impaired metastasis formation, though had minimal effect on tumor growth (Leenders et al., 2004). Furthermore, liposomal formulation of siRNA targeting PKN3, known as Atu027, showed efficacy in orthotopic mouse models for prostate and pancreatic cancers, causing significant inhibition of lymph node metastasis formation and mild impairment of tumor growth (Aleku et al., 2008). The tumor vasculature in treated animals showed reduction in lymph vessel density but no significant changes in microvascular density (Aleku et al., 2008). The mechanism underlying PKN3's effects on angiogenesis are not known.

Taken together, these data suggest that PKN3 promotes metastasis in preclinical models of breast cancer, prostate cancer and pancreatic cancer to date. PKN3 also plays critical roles in regulating cell migration and adhesion as well as proper maturation of cell surface glycoproteins and adhesion molecules. However, further study is required to further clarify the role of PKN3

kinase activity and to identify putative substrates and specific signaling pathways in which PKN3 is involved in in an unbiased manner.

PIN1 regulates the cell cycle and various cellular processes through proline isomerization

The proline isomerase PIN1 regulates the function and stability of specific proteins by catalyzing the cis-trans isomerization of peptidyl-prolyl bonds that follow phosphorylated serine or threonine residues (pSer/Thr-Pro motifs). Proteins with prolyl isomerase activity include the cyclophilins, FK506-binding proteins (FKBPs), and parvulins. PIN1 is a member of the parvulin family, and is unique amongst known proline isomerases due to its substrate specificity for prolines following a phosphorylated serine or threonine residue (X. Z. Zhou & Lu, 2016).

Proline-directed protein phosphorylation serves an essential role in cell signaling networks and is often dysregulated in cancer. Proline-directed phosphorylation at Ser/Thr-Pro motifs is carried out by numerous Pro-directed kinases, including CDKs, MAPKs, and ERKs (Z. Lu & Hunter, 2014). Since the majority of Pro-directed kinases (and phosphatases) are trans- or cis-specific, the pSer/Thr-Pro motif acts as a logic gate that is dependent upon PIN1 function (K. P. Lu & Zhou, 2007; E. S. Yeh & Means, 2007; X. Z. Zhou & Lu, 2016). By controlling the conformation of proline, PIN1 regulates the activity of numerous protein targets, simultaneously activating as many as 43 oncogenes and inactivating at least 20 tumor suppressors (Cheng & Tse, 2018; K. P. Lu, Finn, Lee, & Nicholson, 2007; K. P. Lu & Zhou, 2007; E. S. Yeh & Means, 2007). Furthermore, proline isomerization by PIN1 also controls protein stability, subcellular localization, protein-protein interactions and DNA binding affinity of transcription factors, thereby impacting numerous cellular programs (K. P. Lu et al., 2007; X. Z. Zhou & Lu, 2016).

From its initial discovery, it was evident that PIN1 plays a role in cell cycle regulation. PIN1 was discovered for its interaction with the fungal mitotic-regulatory protein kinase Never In Mitosis (NIMA) (K. P. Lu, Hanes, & Hunter, 1996). PIN1 overexpression delays mitosis entry and causes arrest in G2, and was shown to specifically interact with a subset of mitotic proteins (Yaffe et al., 1997). PIN1 also tunes the function of several cell cycle regulators, making it reportedly essential to normal cell cycle progression (Cheng & Tse, 2018). Furthermore, *PIN1*-null mice have no obvious defects for over half of their lifespan, and ultimately resemble cyclin D1 knockout phenotypes (Liou et al., 2002). However, the PIN1 ortholog Ess1 in yeast is essential (Hanes, 2014). In yeast, Ess1 plays a driving role in regulating transcription, as it binds the phosphorylated form of the RNA Pol II CTD, and has been shown to play an important role in multiple stages of transcription (Verdecia, Bowman, Lu, Hunter, & Noel, 2000; X. Wu, Wilcox, & G., 2000). PIN1 and proline isomerization has also been proposed to be an important part of the RNA Pol II CTD code (Buratowski, 2003).

The roles of PIN1 in cancer

PIN1 also exerts effects on specific transcriptional program by acting on specific transcription factors. PIN1 activates at least 43 oncogenes, such as β-catenin (A. Ryo, Nakamura, Wulf, Liou, & Lu, 2001), cyclin D1 (G. M. Wulf et al., 2001), NFκB (A. Ryo et al., 2003), c-Jun (G. M. Wulf et al., 2001), and Notch1 (Rustighi et al., 2009), and inactivates or destabilizes as many as 20 tumor suppressors, including Fbw7 (Min et al., 2012) and Smad (Sheng et al., 2010). PIN1 has also been shown to regulate the stability of Myc protein as well as its DNA binding (Farrell et al., 2013; E. Yeh et al., 2004). Myc is tightly regulated, PIN1, can isomerize proline 63 to facilitate removal of the PIN1-stabilizing phosphorylation at serine 62, causing Myc to be targeted for

degradation by the ubiquitin-proteasome system through the E3 ubiquitin ligase SCF^{Fbw7} (E. Yeh et al., 2004). PIN1 positively regulates Myc recruitment and binding to promoters and subsequent transcription of specific genes, binding only the phospho-Ser62 form of Myc (Farrell et al., 2013).

PIN1 itself is commonly overexpressed in human cancers, including breast cancer and pancreatic ductal adenocarcinoma (PDAC). This overexpression or activation occurs through several mechanisms, including: transcriptional activation by E2F/RB (Campaner et al., 2017), dephosphorylation at the PIN1 inhibitory site Ser71 due to loss of Death associated protein kinase 1 (DAPK1) (T. H. Lee et al., 2011), and phosphorylation of PIN1 at Ser65 by Polo-like kinase 1 (PLK1) (Eckerdt et al., 2005).

While PIN1 is dispensable for viability in mice (Liou et al., 2002), it is required for activated Ras to induce tumorigenesis, suggesting a role for PIN1 inhibitors in Ras-driven tumors, such as pancreatic ductal adenocarcinoma (PDAC) (G. Wulf, Garg, Liou, Iglehart, & Lu, 2004). In mice, transgenic overexpression of MMTV-PIN1 results in chromosome duplication and mis-segregation, aneuploidy, and tumor development (Suizu, Ryo, Wulf, Lim, & Lu, 2006). Conversely, PIN1 ablation in mice prevents tumorigenesis – for example, preventing MMTV-HER2 or -Ras from transforming mammary epithelial cells and inducing mouse mammary gland carcinoma (Akihide Ryo et al., 2002; G. Wulf et al., 2004). Overexpression of PIN1 has been implicated in HER2-positive, estrogen receptor (ER)-positive, and triple-negative breast cancer (TNBC) (Lam et al., 2008; Rajbhandari et al., 2014; Wei et al., 2015).

PIN1 has also been reported to play a role in epithelial-mesenchymal transition (EMT). PIN1 reduction by genetic approaches results in decreased expression of Notch1 and Notch1-

intracellular domain (N1-ICD), increased Fbxw7α, and subsequently decreased mesenchymal markers and increased expression of epithelial markers (Rustighi et al., 2009; Rustighi et al., 2014). PIN1 destabilizes Fbxw7α and stabilizes N1-ICD, thereby activating Notch1 signaling, which promotes EMT (Espinoza & Miele, 2013).

Existing PIN1 inhibitors are not reliable cellular probes

Reported roles of PIN1 in promoting cancer cell growth and signaling are conflicting. The use of poorly characterized inhibitors as PIN1 probes has contributed to this. The other major PPIase families, the cyclophilins and FKBPs, are inhibited by the immunosuppressant drugs, Cyclosporin A and FK506. These inhibitors are excellent tool compounds that have aided the study of these enzymes and the characterization of their biological phenotypes (Hunter, 1998; Schreiber, 1991). However, potent and selective inhibitors targeting PIN1 have yet to be developed. Existing non-selective and/or cell-impenetrate PIN1 inhibitors have been identified via prolyl isomerase activity assays, binding-based screens, or structure-based design (Guo et al., 2014; Hennig et al., 1998; Wildemann et al., 2006; S. Zhao & Etzkorn, 2007). These compounds include the natural product, juglone, synthetic small molecules, and peptidic substrate mimetics (Dong et al., 2010; Hennig et al., 1998; Y. Zhang et al., 2007; S. Zhao & Etzkorn, 2007).

The developed compounds lack the requisite specificity, potency, and/or cell permeability to accurately probe PIN1 functions. Juglone was one of the first molecules reported to inhibit the parvulin family of peptidyl-prolyl isomerases (Hennig et al., 1998). Its specificity for PIN1 has not been demonstrated, yet it has been used as a tool to study PIN1-dependent biology. A potent peptide-mimetic PIN1 inhibitor, pTIDE, has been reported; however, it is not cell-penetrant (Y. Zhang et al., 2007). To identify cell-penetrant compounds and improve upon

pTIDE, fluorescence polarization screens were performed, which revealed that all-*trans* retinoic acid (ATRA) competes for pTIDE binding to active PIN1 (Wei et al., 2015). ATRA was considered one of the first targeted therapies, used for the treatment of acute promyelotic leukemia, though the target itself was initially unknown. ATRA inhibits and induces degradation of active PIN1 in cells, which leads to degradation of the fusion oncogene PML-RARα (Wei et al., 2015). Complete profiling of ATRA has not been performed, and thus the non-PIN1-related cellular effects of ATRA are unclear.

A recent review concluded that there are no PIN1 inhibitors that can reliably be used in cellular assays (Moore & Potter, 2013). The use of multi-targeted inhibitors to elucidate function has led to confusing pharmacology around PIN1. A selective, cell-penetrant PIN1 inhibitor would not only enable interrogation of the therapeutic value of targeting PIN1 in cancer, but also would address a critical need for small molecule probes with which to study PIN1 biology.

Drivers of Cell Cycle Dysregulation and Metastasis in Cancer

Cell cycle regulation (and dysregulation) and epithelial-mesenchymal transition (EMT) are both immensely complex processes requiring the activity of numerous proteins. CDK14, PKN3 and PIN1 have all been implicated in promoting cell migration and metastasis in cancer through previous study. CDK14 and PIN1 have also been reported to play a role in cell cycle regulation, and more importantly dysregulation in cancer. In order to frame the study of these proteins and their function in cancer, it is important to understand the known drivers of these processes.

Uncontrolled cell proliferation is a hallmark of cancer and is often promoted by loss of cell cycle checkpoint regulation (Hanahan & Weinberg, 2000). Cells can temporarily arrest at cell

cycle checkpoints in order to allow for damage repair to prevent propagation of incorrect genomic information, or activate pathways leading to programmed cell death if the damage is too great to repair (Paulovich, Toczyski, & Hartwell, 1997). Components of the cell cycle machinery are subject to genomic alterations, point mutations, or epigenetic modifications in human cancers. Amplification, genetic rearrangements and/or overexpression of cyclin or CDK genes have been observed in numerous tumor types, and the cyclin D1 is the second most frequently amplified locus across all human cancers (Hydbring et al., 2016). Retinoblastoma protein (RB) is a tumor suppressor whose phosphorylation state orchestrates the progression of G1-S phase transition. RB itself is frequently lost in tumors, and regulators of RB such as CDK4 and CDK6 as well as cyclin D1 and cyclin E are frequently amplified (Zheng & Lee, 2001). RB is now recognized to have several roles beyond the cell cycle in regulating cellular processes, including cell adhesion (Engel, Cress, & Santiago-Cardona, 2015).

Many oncogenes have been shown to promote cell proliferation by affecting a variety of signaling pathways that impinge on the regulation cell cycle phase transition. Genetic alterations of cell cycle checkpoint signaling molecules are also common in human tumors. For example, disruption of the tumor suppressor p53 is the most common genetic lesion in cancer (Stewart & Pietenpol, 2001). P53 plays critical roles in cell cycle regulation and in coordination cellular response to stress-inducing signals such as DNA damage and hypoxia, and is considered a master cell regulator (Zilfou & Lowe, 2009). Mutations in components of pathways associated with response to DNA damage are also observed in cancers, along with alteration of mitotic spindle checkpoints (Stewart, Westfall, & Pietenpol, 2003).

EMT is the process through which an epithelial cell interacts with its basal membrane to induce a series of biochemical changes, resulting in the adoption of a mesenchymal phenotype and ultimately detachment from the basal membrane, which allows for enhanced migration capacity, invasiveness, elevated resistance to apoptosis, and increased production of extra-cellular matrix (ECM) components (Kalluri & Neilson, 2003). EMT occurs primarily in three distinct contexts: tissue regeneration or wound healing and fibrosis, differentiation in development, and in cancer progression and metastasis (Kalluri & Weinberg, 2009). In cancer, EMT is the initial step towards metastasis and malignancy (Thiery, 2002).

EMT-inducing signals are thought to originate tumor-associated stroma, and include HGF, EGF, PDGF, and TGF-β. Signaling induced by these (and other) factors are responsible for the activating a series of EMT-inducing transcription factors, notably Snail, Slug, zinc finger E-box binding homeobox 1 (ZEB1) and Twist (Kalluri & Weinberg, 2009). These transcription factors work together to implement the cell state transition through by inducing a number of intracellular signaling networks and cell surface proteins, primarily integrin families (Tse & Kalluri, 2007). These factors include but are not limited to signaling molecules such as ERK, MAPK, PI3K, Akt, Smad, β-catenin, lymphoid enhancer binding factor (LEF) and Ras (Tse & Kalluri, 2007). Also critical to EMT is disruption of cell-cell adherens junctions and cell-ECM adhesion, which is facilitated by integrins (Kalluri & Weinberg, 2009; J. Yang & Weinberg, 2008).

Loss of E-cadherin is considered one of the hallmarks of EMT and is thought to be responsible for suppressing migratory potential (Hanahan & Weinberg, 2011). In addition to loss of E-cadherin, induced expression of Vimentin, N-cadherin are well-validated indicators of EMT and invasive potential (Rustighi et al., 2014). Altered distribution of specific transcription factors

are also observed during EMT. While cytoplasmic β-catenin correlates with the preservation of epithelial features of cancer cells, during mesenchymal transition, β-catenin moves to the nucleus, where it becomes part of T-cell factor (Tcf) -LEF complexes and participates in initiating transcriptional programs (K. Kim, Lu, & Hay, 2002). Expression of the Snail and Slug transcription factors impact EMT in a number of ways, including suppressing E-cadherin and facilitating β-catenin-dependent induction of TGF-β (Medici, Hay, & Olsen, 2008). This is just one example of many of the cross-talk that occurs between the different factors responsible for orchestrating EMT.

Given the complexities of both of these processes, it is important to understand the roles that other proteins beyond the canonical drivers may play. CDK14 and PKN3 are both understudied kinases, implicated in different aspects of these processes – PKN3 in adherens junctions and CDK14 in promoting EMT by altered expression of EMT markers. CDK14 is also responsible for a priming LRP6 phosphorylation of mitosis-dependent Wnt signaling, suggesting a potential connection between CDK14's reported cell cycle role and EMT role. PIN1 has been reported to regulate many of the known transcription factors and signaling molecules associated with EMT, though it is difficult to get a sense of the systematic effects of PIN1 disruption (Cheng & Tse, 2018). Studies of PIN1 and its role in these processes have been further confused by the use of poorly characterized compounds as 'selective' PIN1 inhibitors (Moore & Potter, 2013). Leveraging covalent inhibitors and chemical biology approaches offers an opportunity to investigate the roles of CDK14, PKN3 and PIN1 in cell cycle dysregulation, EMT and beyond to better understand the cellular functions of these enzymes and their implications for cancer.

Chapter 2: Synthesis and structure activity analysis of a series of 4-amino-1*H*-pyrazoles as covalent inhibitors of CDK14

Author Contributions

Zainab M. Doctor designed and carried out all biological experiments pertaining to compound studies. Fleur M. Ferguson, a postdoctoral fellow in the Gray lab, designed and synthesized all analogs shown here. Scott Ficarro performed compound labeling mass spectrometry studies. Taebo Sim and Nam Doo Kim carried out compound docking studies to guide synthesis efforts. Nathanael S. Gray conceived of and held overall responsibility for the study.

Introduction

The TAIRE family of kinases are an understudied branch of the CDK kinase family that have been implicated in a number of cancers. CDK14 is a member of the understudied TAIRE subfamily of cyclin-dependent kinases (Fedorov, Muller, & Knapp, 2010; Fleuren, Zhang, Wu, & Daly, 2016; Malumbres, 2014). CDK14 overexpression has been reported in numerous cancers including colorectal cancer (Zhu, Liu, Liu, Wang, & Zhu, 2016), ovarian cancer (W. Zhang et al., 2016) and gastric cancer (L. Yang et al., 2015). However, selective tool compounds to interrogate the pharmacological consequences of CDK14 inhibition have not previously been described.

We set out to develop and characterize a covalent CDK14 inhibitor with a selectivity profile conducive to its use as a tool compound to further investigate CDK14 biology. Using the non-covalent compound AT7519 as a starting scaffold, we synthesized 102 4-amino-1*H*-pyrazole analogs for CDK14 and assessed their biochemical and cellular potency, measured by effects on HCT116 proliferation. We show cellular engagement of CDK14 by lead molecules and demonstrate their covalent nature by MS/MS studies. Through characterization of this series of compounds, we describe the structure activity relationships (SAR). This data is of interest, as 4-amino-1*H*-pyrazole is a widely used kinase inhibitor scaffold (Dimova & Bajorath, 2017). This SAR analysis may aid in the development of future improved CDK14 inhibitors, and in addition provides insight into how CDK14 activity can be removed from 4-amino-1*H*-pyrazole analogs targeted towards other kinases. This work culminated in identification of FMF-04-159-2, a potent, covalent CDK14 inhibitor with a TAIRE kinase biased selectivity profile, which will be discussed in the following chapter.

Identifying a lead CDK-directed chemical scaffold

To begin this effort of developing a covalent inhibitor of CDK14, we first turned to a set of existing CDK-directed compounds. Most of these compounds were generated as analogs in the course of previous efforts in the Gray lab to develop inhibitors of CDK7 and CDK12 (Kwiatkowski et al., 2014; T. Zhang et al., 2016). Also included were published CDK-directed compounds, some of which are approved for use in the clinical treatment of cancer (Asghar et al., 2015). We adapted a FRET-based binding assay originally developed by Invitrogen to screen this set of compounds (Figure 2-1). Briefly, the assay consists of a GST-tagged protein (here, CDK14 and Cyclin Y), a Europium (Eu)-labelled anti-GST antibody, and an ATP-mimetic tracer conjugated to a fluorophore. If the candidate inhibitor binds the target protein, the ATP-mimetic is no longer able to bind, results in low FRET signal due to lack of fluorescence transfer from Europium.

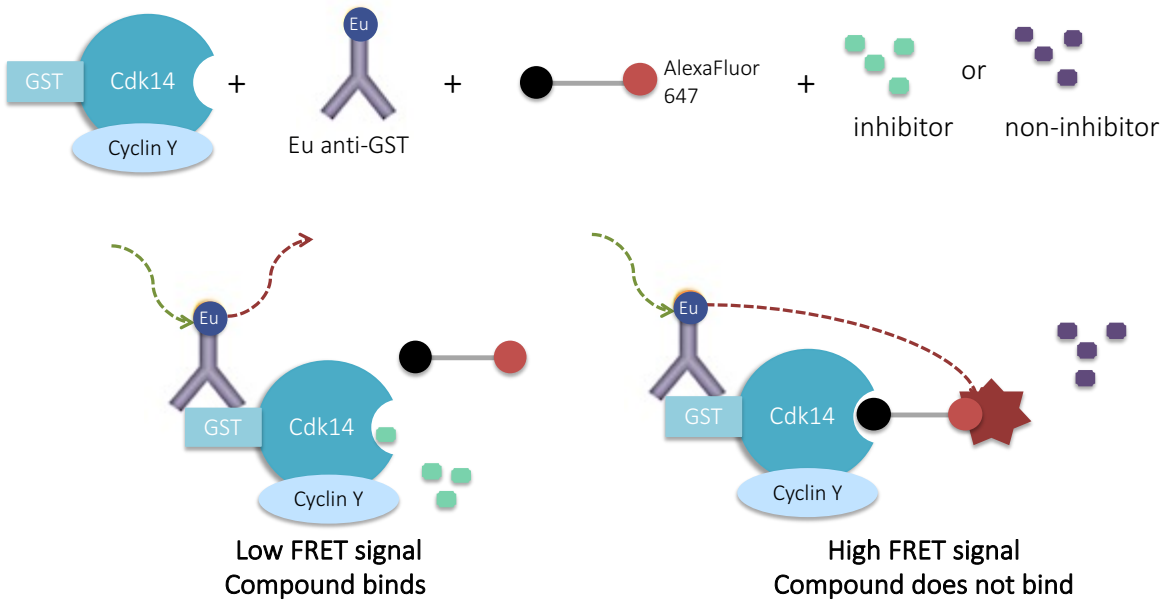

Figure 2-1. Schematic diagram of FRET-based Lantha binding assay used to assess compound binding to CDK14.

For screening, the broad-spectrum kinase inhibitor staurosporine (Patricelli et al., 2011) was used as a positive control inhibitor and DMSO as a negative control. Only a few of the THZ- and MFH- analogs shown, which were synthesized for CDK7- and CDK12-selective inhibitor development, showed any binding to CDK14, and none of the compounds showed binding comparable to staurosporine at the lower concentration tested. Of the set of compounds screened, the known CDK inhibitors AT7519, flavopiridol and dinaciclib were the only compounds that showed binding to CDK14 equivalent (or slightly better) than staurosporine at both concentrations, 250nM and 1μM (Figure 2-2). AT7519, originally published as a CDK2 inhibitor (Squires et al., 2009; Wyatt et al., 2008), was selected for further development due to documented SAR studies and its favorable selectivity profile.

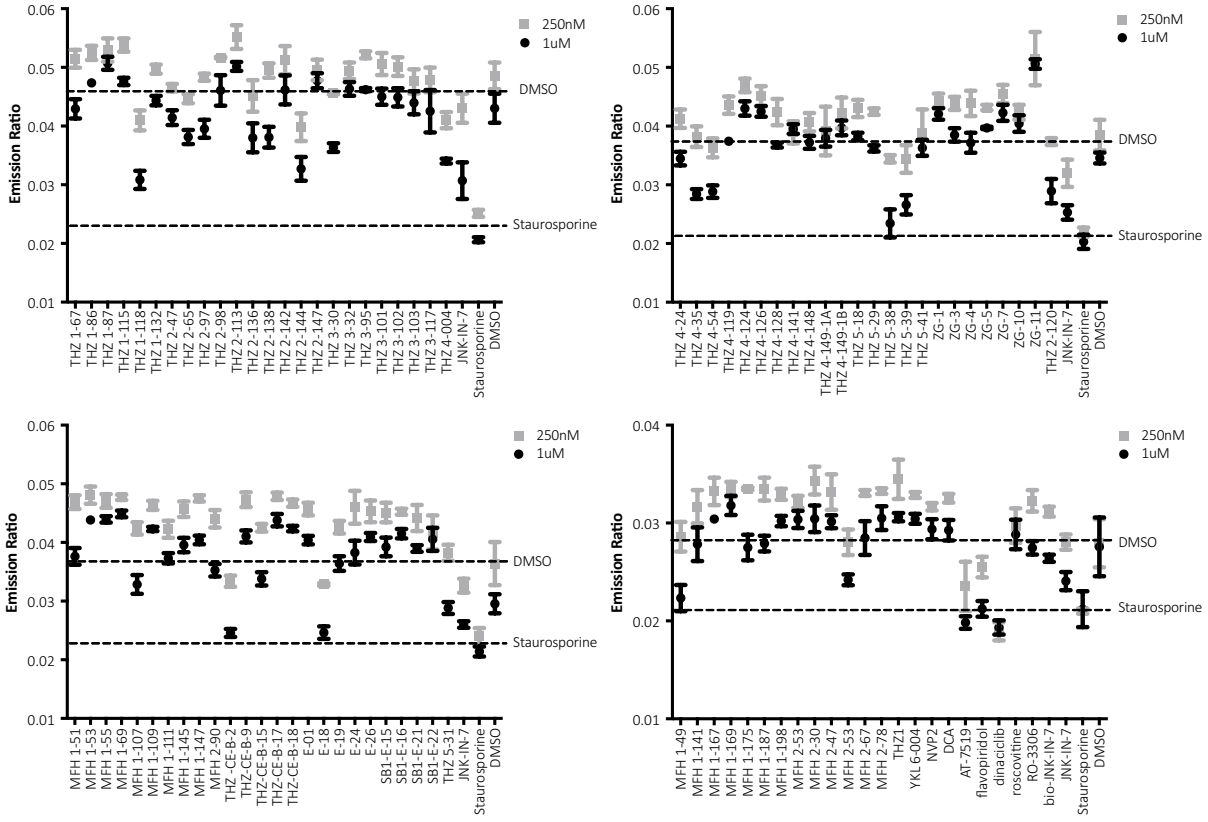

Figure 2-2. Lantha screening results against CDK14/Cyclin Y for binding of the set of CDK-directed compounds.

Structure-Activity Relationships around the development of a CDK14 inhibitor from the AT7519 scaffold

As previously reported, AT7519 is a potent inhibitor cell proliferation (Wyatt et al., 2008). CDK14 contains a uniquely placed cysteine, C218, located at the beginning of the αD helix, proximal to the ATP pocket (Chaikuad et al., 2018; J. Zhang et al., 2009). In order to improve the potency and selectivity of AT7519 towards CDK14, we sought to design a covalent inhibitor. Examination of the co-crystal structure of CDK2 in complex with AT7519 (PDB: 2VU3) revealed that the 4-aminopiperidine is oriented towards the αD helix in CDK2 (Wyatt et al., 2008). Assuming a conserved binding mode, this substituent (R1) should provide a suitable vector for targeting CDK14 C218. Therefore analogs containing varied R1 substituents incorporating acrylamide and (*E*)-4-(dimethylamino)but-2-enamide warheads were synthesized according to Scheme 1. Initially, molecules containing a single saturated or unsaturated ring were synthesized (Table 2-1). These analogs lost significant potency relative to AT7519, potentially due to the loss of a hydrogen bonding interaction with the piperidine NH seen in CDK2 (PDB:2VU3), which was not compensated for by covalent inhibition.

JNK3 contains a cysteine in an equivalent region of the kinase to CDK14. Examination of the structure of JNK3 in complex with JNK-IN-7 indicated that a longer distance between the hinge binding motif and the acrylamide is required in order to successfully form a covalent bond (T. Zhang et al., 2012). Therefore analogs were prepared containing two linked cyclic aliphatic or aromatic rings decorated with acrylamide or (*E*)-4-(dimethylamino)but-2-enamide warheads (Table 2-2, Table 2-3). Docking studies into a CDK14 homology model built from the X-ray structure of CDK12 (4NST) predicted that a range of linked two ring systems, with 1,4-

regiochemistry in ring 1 and a 1,3- regiochemistry in ring 2 would best allow for C218 covalent engagement.

Table 2-1. Single ring R_1 analogs of AT7519. A) CDK14 IC_{50}s were measured using a LanthaScreen binding assay. IC_{50}s were calculated as the average of three replicates, the 95% CI of the IC_{50} is reported in parentheses. B) Antiproliferative activity against the HCT116 cell line was measured using a CellTiter-Glo assay. IC_{50}s were calculated as the average of three replicates, the 95% CI of the IC_{50} is reported in parentheses.

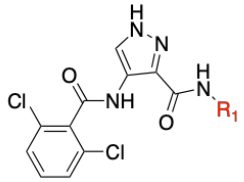

Compound Name	R_2	R_3	IC_{50} CDK14 (nM)	IC_{50} HCT116 (nM)	Compound Name	R_2	R_3	IC_{50} CDK14 (nM)	IC_{50} HCT116 (nM)	Compound Name	R_2	R_3	IC_{50} CDK14 (nM)	IC_{50} HCT116 (nM)
AT7519		-	19.8 ± 2.8	132 ± 33	FMF-03-184-1		H	479 ± 102	737 ± 200	FMF-03-188-2	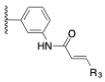	CH_2NMe_2	88 ± 13	723 ± 352
FMF-03-177-1	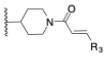	H	401 ± 60	341 ± 97	FMF-03-184-2		CH_2NMe_2	977 ± 421	1341 ± 412	FMF-05-064-1	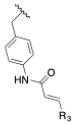	H	> 1000	117 ± 41
FMF-03-177-2	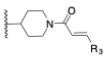	CH_2NMe_2	208 ± 40	1053 ± 309	FMF-03-182-1		H	> 1000	17 ± 6	FMF-05-064-2	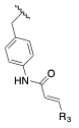	CH_2NMe_2	108 ± 53	4700 ± 130
FMF-03-183-1		H	569 ± 121	39 ± 10	FMF-03-182-2		CH_2NMe_2	82 ± 10	395 ± 102	FMF-05-067-1	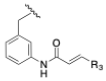	H	ND	8500 ± 3700
FMF-03-183-2		CH_2NMe_2	148 ± 66	157 ± 38	FMF-03-188-1	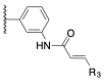	H	> 1000	169 ± 55	FMF-05-067-2	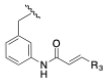	CH_2NMe_2	183 ± 49	> 10000

SiRNA mediated CDK14 knockdown does not cause significant proliferation defects in the HCT116 cell line, unlike knockdown of other CDK kinases (McDonald et al., 2017). A selective CDK14 inhibitor is consequently also expected to have mild to insignificant effects on HCT116 cell growth. Therefore, we used potency in a CellTiter-Glo (Promega) proliferation assay as a first pass approximation of compound selectivity for CDK14 when prioritizing molecules for progress through further rounds of characterization (Figure 2-3).

Table 2-2. Extended R_1 analogs of AT7519. A) CDK14 IC_{50}s were measured using a LanthaScreen binding assay. IC_{50}s were calculated as the average of three replicates, the 95% CI of the IC_{50} is reported in parentheses. B) Antiproliferative activity against the HCT116 cell line was measured using a CellTiter-Glo assay. IC_{50}s were calculated as the average of three replicates, the 95% CI of the IC_{50} is reported in parentheses. –R is used to denote reversible control compounds (without an alkene group).

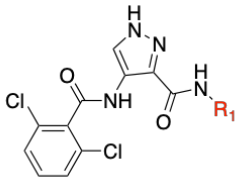

Compound Name	R_2	R_3	IC_{50} CDK14 (nM)	IC_{50} HCT116 (nM)	Compound Name	R_2	R_3	IC_{50} CDK14 (nM)	IC_{50} HCT116 (nM)	Compound Name	R_2	R_3	IC_{50} CDK14 (nM)	IC_{50} HCT116 (nM)
AT7519		-	19.8 ± 2.8	132 ± 33	FMF-04-056-2	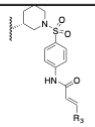	CH_2NMe_2	ND	> 10000	FMF-05-074-1	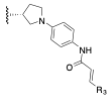	H	> 1000	2900 ± 940
FMF-03-186-1	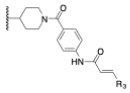	H	126 ± 21	42 ± 11	FMF-04-057-1	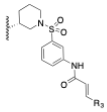	H	836 ± 321	> 10000	FMF-05-074-2	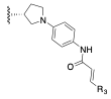	CH_2NMe_2	117 ± 28	> 10000
FMF-03-187-1	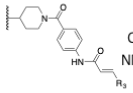	CH_2NMe_2	83 ± 11	404 ± 111	FMF-04-057-2	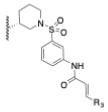	CH_2NMe_2	> 1000	> 10000	FMF-05-086-1	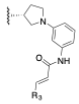	H	> 1000	826 ± 420
FMF-03-196-1	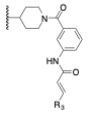	H	45 ± 4	32 ± 10	FMF-04-012-1	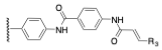	H	169 ± 28	8.3 ± 3.1	FMF-05-086-2	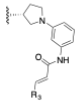	CH_2NMe_2	218 ± 59	> 10000
FMF-03-196-2	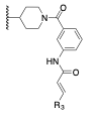	CH_2NMe_2	77 ± 12	485 ± 126	FMF-04-012-2	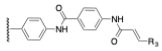	CH_2NMe_2	68 ± 10	14 ± 4	FMF-05-075-1	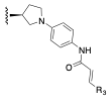	H	267 ± 156	64 ± 15
FMF-04-058-1	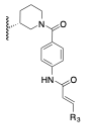	H	ND	726 ± 510	FMF-03-205-1	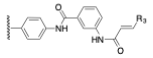	H	> 1000	6.3 ± 3.2	FMF-05-075-2	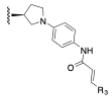	CH_2NMe_2	738 ± 289	714 ± 179
FMF-04-058-2	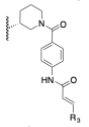	CH_2NMe_2	> 1000	> 10000	FMF-03-206-1	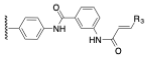	CH_2NMe_2	17 ± 3	38 ± 12	FMF-05-087-1	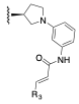	H	> 1000	22 ± 6
FMF-04-059-1	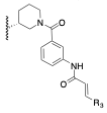	H	> 1000	> 10000	FMF-04-085-1	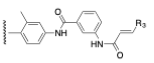	H	> 1000	ND	FMF-05-087-2	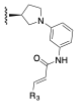	CH_2NMe_2	> 1000	124 ± 33
FMF-04-059-2	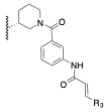	CH_2NMe_2	> 1000	> 10000	FMF-04-085-2	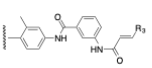	CH_2NMe_2	> 1000	320 ± 94	FMF-05-066-1	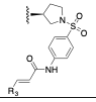	H	> 1000	3000 ± 670

Table 2-3. Additional extended R_1 analogs of AT7519. A) CDK14 IC_{50}s were measured using a LanthaScreen binding assay. IC_{50}s were calculated as the average of three replicates, the 95% CI of the IC_{50} is reported in parentheses. B) Antiproliferative activity against the HCT116 cell line was measured using a CellTiter-Glo assay. IC_{50}s were calculated as the average of three replicates, the 95% CI of the IC_{50} is reported in parentheses. –R is used to denote reversible control compounds (without an alkene group).

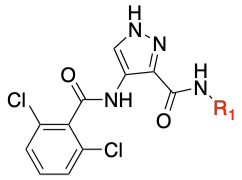

Compound Name	R_2	R_3	IC_{50} CDK14 (nM)	IC_{50} HCT116 (nM)	Compound Name	R_2	R_3	IC_{50} CDK14 (nM)	IC_{50} HCT116 (nM)	Compound Name	R_2	R_3	IC_{50} CDK14 (nM)	IC_{50} HCT116 (nM)
FMF-03-199-1	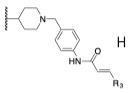	H	10 ± 3	< 1	FMF-03-203-1	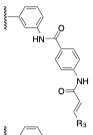	H	ND	6.0 ± 1.5	FMF-05-065-1	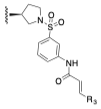	H	> 1000	467 ± 134
FMF-03-199-2	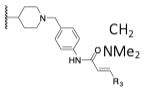	CH_2NMe_2	14 ± 3	2.6 ± 0.9	FMF-03-204-1	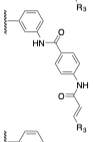	CH_2NMe_2	72 ± 12	24 ± 6	FMF-05-084-2		CH_2NMe_2	41 ± 18	> 10000
FMF-03-200-1	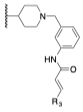	H	< 1	< 1	FMF-04-011-1	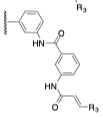	H	308 ± 63	31 ± 12	FMF-05-068-1	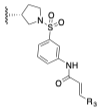	H	450 ± 315	6150 ± 2240
FMF-03-200-2	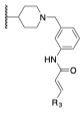	CH_2NMe_2	< 1	2.2 ± 0.9	FMF-04-196-1	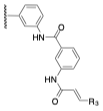	CH_2NMe_2	34 ± 12	367 ± 152	FMF-05-068-2	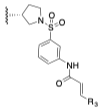	CH_2NMe_2	308 ± 72	> 10000
FMF-03-197-1	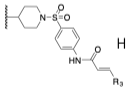	H	62 ± 8	31 ± 10	FMF-05-073-1	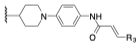	H	154 ± 24	30 ± 10	FMF-05-072-1	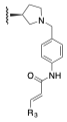	H	257 ± 55	< 1
FMF-03-197-2	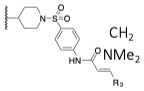	CH_2NMe_2	2.6 ± 0.8	23 ± 6	FMF-05-073-2	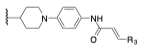	CH_2NMe_2	45 ± 16	541 ± 134	FMF-05-071-1	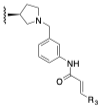	H	282 ± 120	< 1
FMF-03-198-1	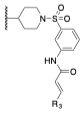	H	< 1	< 1	FMF-05-085-1		H	ND	93 ± 29	FMF-05-070-1	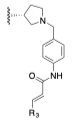	H	572 ± 178	31 ± 8
FMF-03-198-2	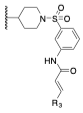	CH_2NMe_2	1.8 ± 0.7	5.1 ± 1.4	FMF-05-085-2		CH_2NMe_2	27 ± 7	427 ± 102	FMF-05-069-1	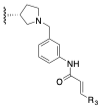	H	151 ± 72	27 ± 8
FMF-04-056-1	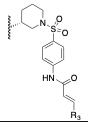	H	> 1000	> 10000	FMF-04-060-1 [FMF-03-198-R]	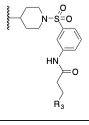	H	11 ± 2	76 ± 11	FMF-04-172-2 [FMF-03-200-R]	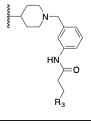	H	82 ± 29	123 ± 38

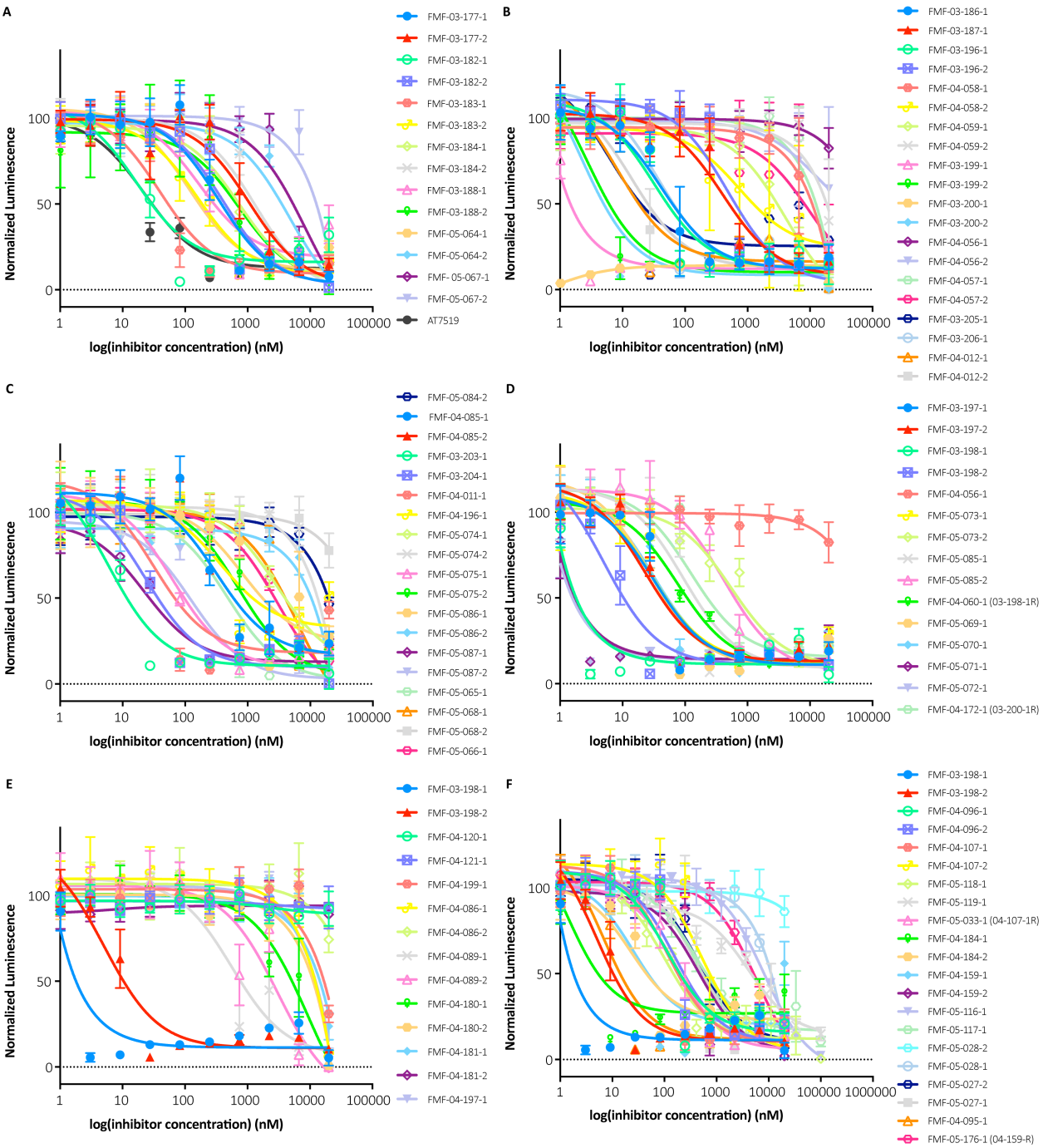

Figure 2-3. HCT116 antiproliferation curves for compound analogs shown in SAR tables. (A) Single ring R1 analogs shown in Table 2-1. (B-D) Extended R1 analogs shown in Table 2-2 and Table 2-3. (E) FMF-03-198 analogs with a modified heterocyclic core. (F) FMF-03-198 analogs with varied R_2 substituents.

Molecules containing a piperidine linked to an aminobenzamide at R_1 displayed reduced potency for CDK14 relative to AT7519. 1,4 aminopiperidine regiochemistry at R_1 is strongly preferred at, with 1,3 aminopiperidine regiochemistry not well tolerated this position.

Preference for a 1,3 aminobenzamide regiochemistry of the second ring was observed. with the most potent analog, FMF-03-196-1, combining these two regiochemistries, in line with computational docking results. Whilst FMF-03-196-1 is less potent against CDK14 than AT7519, it also displays reduced toxicity, indicating a potential concurrent reduction in off-target potency.

Replacing the aminobenzamide with an aminobenzylamine (compounds FMF-03-199-1 to FMF-03-200-2) dramatically increased potency against CDK14. Again, a strong preference for a 1,4 aminopiperidine regiochemistry and a 1,3 aminobenzylamine regiochemistry was observed. The most potent analogs, FMF-03-200-1 and FMF-03-200-2, inhibited CDK14 with IC_{50}s below 1 nM in the LanthaScreen biochemical assay. FMF-03-200-2 was chosen for follow-up studies due to its lower toxicity in the CellTiter-Glo assay, relative to FMF-03-200-1. Both compounds show increased toxicity relative to AT7519, indicating off-target activity. Compounds containing an aminobenzylsulfonamide followed similar trends to the aminobenzamide series. FMF-03-198-2 is highly potent against CDK14, and also displays increased toxicity against HCT116 cells.

Inspired by the acrylamide bearing substituent in JNK-IN-7, amide linked biphenyls were introduced to R1 (T. Zhang et al., 2012). Although these compounds displayed reduced affinity, they also exhibited the same regiochemical preferences. Interestingly in this series, the *E*)-4-(dimethylamino)but-2-enamide warhead was preferred to the acrylamide warhead. FMF-03-206-1 was the most potent of this subseries against CDK14, but also had increased toxicity relative to AT7519. In an attempt to improve selectivity in a manner analogous to JNK-IN-8, compounds were synthesized with ortho-methylation of the 1,4-diaminoaniline in ring 1 (FMF-04-085-1 and FMF-04-085-2). Unfortunately, this methylation was not tolerated by CDK14.

Substitution of the ring 1 piperidine group for a pyrrolidine resulted in compounds with a less favorable CDK14:HCT116 potency profile, with the exception of FMF-05-084-2, which was taken forward for validation. Removal of the linking atoms between rings 1 and 2 to afforded 3(piperidine-1-yl)anilines FMF-05-073-1, -2, and FMF-05-085-1,-2. This series maintained acceptable CDK14 potency and the dimethylamino-substituted analogs FMF-05-073-2 and FMF-05-085-2 had low HCT116 toxicity. FMF-05-085-2 was chosen for follow up.

Finally, the propyl amide analogs of the most potent molecules were synthesized to examine the effects of removal of the covalent warhead. FMF-04-060-1 [FMF-03-198-R] was ~ 10-fold less potent against CDK14 compared to FMF-03-198-1 and -2, and displayed similar toxicity against HCT116 cells to FMF-03-198-2. FMF-04-172-2 [FMF-03-200-R] was significantly less potent against both CDK14 and HCT116 cells than FMF-03-200-1 and -2. This indicated that the covalent binding component improved binding towards CDK14, but also towards off-targets that alter cell proliferation.

To verify that the 6 lead compounds and two reversible control compounds identified in Table 2-3 were able to engage CDK14 in cells we performed a pull-down experiment. Cells were treated for 4 h with compounds at various doses, and then lysed and treated with biotinylated JNK-IN-7 (T. Zhang et al., 2012), followed by streptavidin coated beads. CDK14 capture was assayed by western blot. (Table 2-4, Figure 2-3).

Table 2-4. Cellular target engagement of lead compounds in pull-down assay.

Compound Name	IC_{50} CDK14 (nM)	Compound Name	IC_{50} CDK14 (nM)
FMF-03-196-1	1000	FMF-03-206-1	1000
FMF-03-200-2	500	FMF-03-198-2	50
FMF-04-172-2 [FMF-03-200-R]	> 1000	FMF-04-060-1 [FMF-03-198-R]	> 1000
FMF-05-085-2	1000	FMF-05-084-2	> 1000

Of these compounds, FMF-03-198-2 was able to potently block CDK14 pulldown at 50 nM, and FMF-03-200-2, FMF-03-206-1 and FMF-03-196-1 also showed effects at 500 – 1000 nM concentrations (Table 2-8,Figure 2-3). FMF-05-84-2 and FMF-05-085-2 were not active, or weakly active in the cellular assay (Table 2-8,Figure 2-3). The reversible control molecules also showed no activity in this assay, indicating a dependency on covalent bond formation for activity in cells. Covalent bond formation by FMF-03-198-2 and FMF-03-200-2 was verified by incubating compounds with purified, recombinant CDK14 followed by MS/MS analysis. Both compounds achieved complete labeling of CDK14 when incubated for 3 hours at room temperature, at a 10:1 molar ratio of compound to CDK14/Cyclin Y protein. Digest experiments followed by MS analysis showed that C218 was exclusively labeled.

Figure 2-4. Western blots corresponding to cellular target engagement experiments for lead compounds shown throughout SAR tables.

Figure 2-4 (Continued).

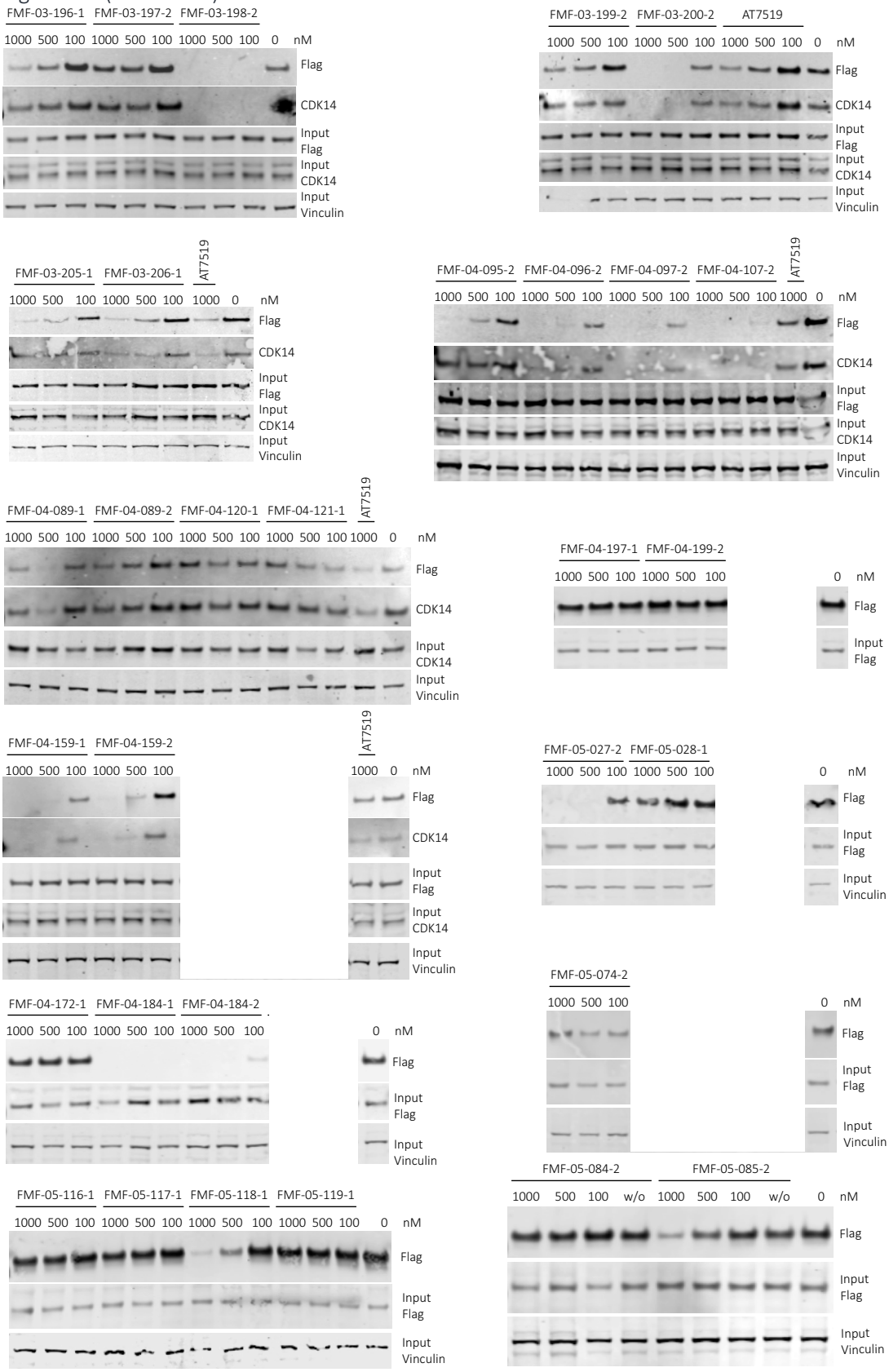

To evaluate the cellular targets of FMF-03-198-2 and FMF-03-200-2 more broadly, we performed KiNativ profiling at 1 μM compound concentration (Figure 2-3, Table 2-5) (Patricelli et al., 2011). This revealed that whilst both compounds were potent against CDK14, they also inhibited a large number of other kinases. As hinge binding is a common feature of Type I kinase inhibitors, analogs of FMF-03-198-2 with altered hinge binding motifs predicted to reduce hydrogen bonding interactions were synthesized, in an attempt to increase the selectivity for CDK14 by reducing the reversible binding affinity while maintaining the ability to bind covalently. Unfortunately, none of these analogs were active above a 500 nM IC50 cutoff in the CDK14 binding assay (Table 2-6). Therefore, the 2,6-dichlorobenzamide substituent (R2) was varied in an effort to improve selectivity (Table 2-7). In the co-crystal structure of AT7519 in complex with CDK2, the 2,6-benzamide group fills a small hydrophobic pocket, and prior studies have demonstrated that CDK2 binding activity can be tuned by altering its substituents, by introducing steric clashes with the back pocket (Wyatt et al., 2008). Substitution of the 2,6-dichloro for the more polar 2,6-difluoro (FMF-04-096-1, -2) yielded modest reduction in toxicity and maintained potent CDK14 inhibition. The bulkier 2-chloro, 6-methoxy substitution yielded a further reduction in toxicity, whilst maintaining potency for CDK14 (FMF-04-107-1, -2). The reversible propyl amide FMF-05-033-1 [FMF-04-107-R] maintained comparable potency towards CDK14 and comparable potency against HCT116 cells as FMF-04-107-1, indicating this effect was primarily driven by changes in the reversible binding profile of the compounds. However, further increase in the bulk of the 6-substituent to an ethoxy group afforded a more toxic compound (FMF-04-118-1), indicative of a narrow SAR window at the 6-position.

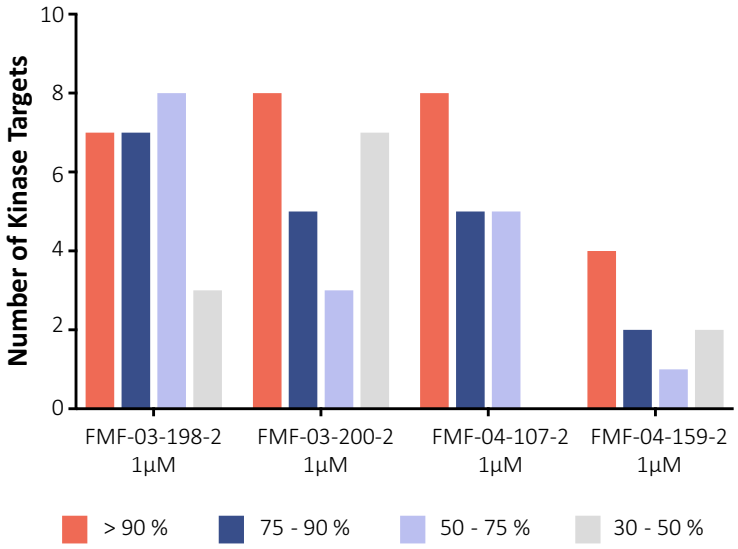

Figure 2-5. KiNativ profiling results of lead compounds at 1µM compound concentration.

Table 2-5. Summary of KiNativ profiling results of lead compounds at 1µM compound concentration.

Compound name	No. of kinases inhibited				CDK14	No. targets
	> 90% I	75 - 90 % I	50 - 75 % I	35 - 50 % I	> 90 %	Total
FMF-03-198-2 (1 µM)	7	7	8	3	Y	25
FMF-03-200-2 (1 µM)	8	5	3	7	Y	23
FMF-04-107-2 (1 µM)	8	5	5	0	N	18
FMF-04-159-2 (1 µM)	4	2	1	2	Y	9

2,6- dimethoxy substitution (FMF-05-119-1), 2,4,6- methoxy substitution (FMF-05-028-1) and 2,4,6- chloro substitution (FMF-04-159-2) patterns resulted in reduced CDK14 potency, but also dramatically reduced HCT116 toxicity. Addition of a methoxy group to the 3-posiiton of FMF-03-198-2 to afford FMF-04-184-2 didn't significantly affect CDK14 binding or toxicity. Finally, the un-substituted compound FMF-05-027-2 exhibited potent CDK14 inhibition and reduced HCT116 toxicity. The active compounds from this series were taken forward for cellular

target engagement studies (Table 2-8,Figure 2-3). Of these, only FMF-04-107-2 and FMF-04-159-2 were able to completely inhibit CDK14 pulldown at concentrations below 1 µM.

FMF-04-159-2 and FMF-04-107-2 were both evaluated using the KiNativ platform for cellular selectivity at concentrations of 1 µM and compared to the profiles of FMF-03-198-2 and FMF-03-200-2. FMF-04-107-2 demonstrated a comparable number of targets compared to FMF-03-198-2 and FMF-03-200-2, despite its reduced cytotoxicity. However, FMF-04-159-2 showed a favorable profile, with a dramatically reduced number of targets.

Table 2-6. FMF-03-198 analogs with a modified heterocyclic core. A) CDK14 IC_{50}s were measured using a LanthaScreen binding assay. IC_{50}s were calculated as the average of three replicates, the 95% CI of the IC_{50} is reported in parentheses. B) Antiproliferative activity against the HCT116 cell line was measured using a CellTiter-Glo assay. IC_{50}s were calculated as the average of three replicates, the 95% CI of the IC_{50} is reported in parentheses.

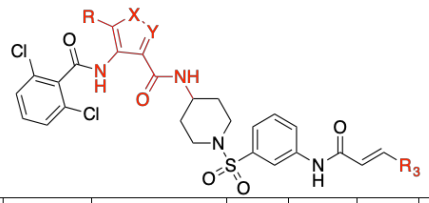

Compound Name	Scaffold	R_3	IC_{50} CDK14 (nM)	IC_{50} HCT116 (nM)	Compound Name	Scaffold	R_3	IC_{50} CDK14 (nM)	IC_{50} HCT116 (nM)	Compound Name	Scaffold	R_3	IC_{50} CDK14 (nM)	IC_{50} HCT116 (nM)
FMF-03-198-1		H	< 1	< 1	FMF-04-089-1		H	> 1000	563	FMF-04-180-1		H	> 1000	9200 ± 3000
FMF-03-198-2		CH_2NMe_2	1.8 ± 0.7	5.1 ± 1.4	FMF-04-089-2		CH_2NMe_2	> 1000	3045	FMF-04-180-2		CH_2NMe_2	> 1000	> 10000
FMF-04-120-1		H	> 1000	> 10000	FMF-04-086-1		H	> 1000	> 10000	FMF-04-181-1		H	> 1000	> 10000
FMF-04-121-1		CH_2NMe_2	487 ± 249	> 10000	FMF-04-086-2		CH_2NMe_2	> 1000	> 10000	FMF-04-181-2		CH_2NMe_2	> 1000	> 10000
FMF-04-199-1		CH_2NMe_2	> 1000	> 10000	FMF-04-197-1	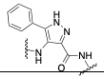	CH_2NMe_2	> 1000	> 10000					

Table 2-7. FMF-03-198 analogs with varied R_2 substituents. A) CDK14 IC_{50}s were measured using a LanthaScreen binding assay. IC_{50}s were calculated as the average of three replicates, the 95% CI of the IC_{50} is reported in parentheses. B) Antiproliferative activity against the HCT116 cell line was measured using a CellTiter-Glo assay. IC_{50}s were calculated as the average of three replicates, the 95% CI of the IC_{50} is reported in parentheses. –R is used to denote reversible control compounds (without an alkene group).

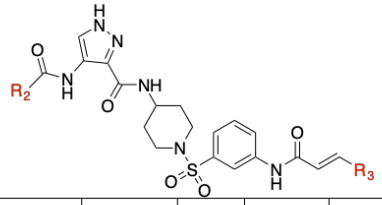

Compound Name	R_2	R_3	IC_{50} CDK14 (nM)	IC_{50} HCT116 (nM)	Compound Name	R_2	R_3	IC_{50} CDK14 (nM)	IC_{50} HCT116 (nM)	Compound Name	R_2	R_3	IC_{50} CDK14 (nM)	IC_{50} HCT116 (nM)
FMF-03-198-1		H	< 1	< 1	FMF-04-097-1		H	1.6 ± 2.5	9 ± 3	FMF-04-095-1		H	ND	7 ± 2
FMF-03-198-2		CH_2NMe_2	1.8 ± 0.7	5.1 ± 1.4	FMF-04-097-2		CH_2NMe_2	ND	174 ± 49	FMF-04-095-2		CH_2NMe_2	ND	90 ± 22
FMF-04-096-1		H	> 1000	114 ± 41	**FMF-05-119-1**		CH_2NMe_2	50 ± 33	4100 ± 1200	**FMF-05-028-1**		H	48 ± 33	> 10000
FMF-04-096-2		CH_2NMe_2	3.4 ± 2.7	157 ± 48	FMF-04-184-1		H	0.4 ± 1.5	1.4 ± 1.2	FMF-05-028-2		CH_2NMe_2	221 ± 91	> 10000
FMF-04-107-1		H	2.2 ± 5.3	115 ± 37	FMF-04-184-2		CH_2NMe_2	6.4 ± 6.6	23 ± 8	FMF-05-027-1		H	315 ± 182	382 ± 156
FMF-04-107-2		CH_2NMe_2	3.0 ± 2.8	524 ± 165	FMF-04-159-1		H	49 ± 11	25 ± 13	**FMF-05-027-2**		CH_2NMe_2	3 ± 20	440 ± 112
FMF-05-118-1		CH_2NMe_2	ND	102 ± 34	**FMF-04-159-2**		CH_2NMe_2	88 ± 10	1140 ± 190	FMF-05-116-1		CH_2NMe_2	332 ± 126	8200 ± 990
FMF-05-033-1 (FMF-04-107-R)		H	0.8 ± 1.8	173 ± 33	FMF-05-176-2 (FMF-04-159-R)		CH_2NMe_2	139 ± 10	5900 ± 1200	FMF-05-117-1		CH_2NMe_2	14 ± 5	395 ± 131

Of the 6 targets inhibited at > 75% by FMF-04-159-2, four were TAIRE kinases (CDK14, CDK16, CDK17, CDK18). These kinases have been reported to display functional redundancy, and thus the pan-TAIRE activity of FMF-04-159-2 may aid interrogation of the biology of these understudied kinases (Davidson et al., 2009). The other targets of FMF-04-159-2 were CDK2 and

CDK10. Use of washout conditions is therefore recommended when using FMF-04-159-2 to probe the pharmacological consequences of CDK14 inhibition.

Table 2-8. Cellular target engagement of additional lead compounds in pull-down assay.

Compound Name	IC_{50} CDK14 (nM)	Compound Name	IC_{50} CDK14 (nM)
FMF-04-107-2	50	FMF-05-119-1	> 1000
FMF-04-159-1	500	FMF-05-028-1	> 1000
FMF-05-27-2	1000	FMF-05-176-2	> 1000

Conclusions on the development of a CDK14 inhibitor as a tool compound

Selective inhibitors can serve as useful tools to interrogate biology. The inhibitors described here represent novel chemical tools, which can provide insight into structure-activity relationships for TAIRE kinases. As with all chemical tools, it is important to be aware of the specificity and limitations of multi-targeted compounds. Through several iterations of medicinal chemistry, we have refined the target profile of AT7519 compounds derivatized to favor covalent engagement of CDK14. Future work is required to remove activity against these targets to develop CDK14 / TAIRE kinase probes. FMF-04-159-2 represents a significant advance towards developing chemical probes for the TAIRE kinase family as the first targeted covalent CDK14 inhibitor. Further characterization of FMF-04-159-2, a covalent CDK14 inhibitor with pan-TAIRE selectivity, offers an opportunity to interrogate the role of CDK14 in cell cycle, proliferation and signaling, as will be described next.

Chapter 3: Discovery of covalent CDK14 inhibitors with pan-TAIRE family specificity

Author Contributions

Zainab M. Doctor designed and carried out all biological experiments pertaining to compound studies, and performed relevant data analysis. Fleur M. Ferguson, a postdoctoral fellow in the Gray lab, designed and synthesized all compounds. Scott B. Ficarro performed compound labeling mass spectrometry studies. Chris M. Browne performed mass spectrometry substrate validation experiments based on the phospho-proteomics results. Taebo Sim and Nam Doo Kim performed compound docking studies to guide synthesis efforts. Jared L. Johnson and Tomer M. Yaron performed phospho-array experiments and peptide motif analysis. Marian Kalocsay and Matthew J. Berberich conducted proteomics and phosphoproteomics experiments. Nathanael S. Gray conceived of and held overall responsibility for the study.

Introduction

Cyclin-dependent kinases (CDKs) are a family of serine/threonine kinases whose activity depends on interaction with their cyclin binding partners. The CDKs have classically been categorized into three sub-families: CDKs which regulate progression through cell cycle (CDKs 1-7), CDKs which regulate various aspects of transcription (CDK7-13 and 19), and the TAIRE CDKs (CDKs 14-18) named for their common "TAIRE" sequence motif which is essential for binding to the G2/M cyclins, Cyclin Y and Cyclin Y-like 1 (Jiang et al., 2009; Malumbres, 2014; Mikolcevic et al., 2012). Due to their critical role in regulating important cellular processes, cell cycle and transcriptional CDKs have been well studied, and many small molecules have been developed to inhibit their kinase activity, with some obtaining FDA approval for various oncology indications (Ferguson & Gray, 2018; P. Wu, Nielsen, & Clausen, 2015).

In contrast, the TAIRE subfamily of CDKs (CDK14-18) are a sub-family of understudied CDKs without clearly described biological functions (Malumbres, 2014). Despite this, two members of the TAIRE subfamily, CDK14 and CDK16 have been implicated as potential therapeutic targets in a number of different cancers, including colorectal cancer. CDK14 (also annotated as PFTAIRE1 and PFTK) is overexpressed in human colorectal cancer patients, relative to surrounding normal colorectal lesions, and is associated with poor prognosis (W. Zhang et al., 2016). CDK14 is also spontaneously amplified in a chimeric-mouse colon cancer model driven by mutant p53 and β-catenin (Y. Zhou et al., 2014). Knockdown of CDK16 reportedly causes mild inhibition of HCT116 colorectal cancer cell growth (Yanagi et al., 2016).

The only reported substrate of the CDK14-Cyclin Y complex is LRP6, a transmembrane receptor protein involved in the canonical Wnt pathway. CDK14-Cyclin Y phosphorylates S1490

of LRP6 during the G2/M transition in a Wnt-independent manner. This primes LRP6 for Wnt-induced phosphorylation at PPP(S/T)P motifs by GSK3 and CK1, leading to stabilization of cytoplasmic β-catenin and activation of the canonical Wnt signaling pathway (Davidson et al., 2009; MacDonald & He, 2012; X. Wang, Jia, Fei, Song, & Li, 2016). Deregulation of Wnt signaling via loss of the Wnt pathway negative regulator APC is a hallmark of colorectal cancer (Novellasdemunt, Antas, & Li, 2015). However, the functional consequences of S1490 phosphorylation and its relevance to cells in mitosis is not fully understood (Davidson & Niehrs, 2010). Interestingly, in human HEK293 cells, ablation of LRP6 S1490 phosphorylation occurred upon RNAi-mediated knockdown of Cyclin Y and Cyclin Y-like 1. However, CDK14 knockdown showed no effect, suggesting that functional redundancy may exist among the human TAIRE kinases and providing rationale for the development of pan-TAIRE inhibitors as research tools and potential clinical leads (Davidson et al., 2009).

In a recent study, a systemic, mass-spectrometry (MS)-based chemical proteomic profiling method (the kinobeads platform) was used to profile the targets of 243 diverse clinical kinase inhibitors in cell lysates. Although CDK14 was not detected in this kinome panel, 12% of the profiled inhibitors showed binding to either CDK16 or CDK17 (select Kd data plotted, Figure 3-1A), indicating that TAIRE-kinases are frequently inhibited by clinically-relevant molecules (Klaeger et al., 2016). However, despite their proven druggability, and association with colorectal cancer, the consequences of TAIRE kinase inhibition are poorly understood. Thus, further insight into their functions is essential to determining the underlying mechanism of action for these drugs and drug candidates. Improved understanding of the roles of TAIRE kinases in signal

transduction and cellular physiology in healthy and diseased cells will also enable better rational design of drug target profiles.

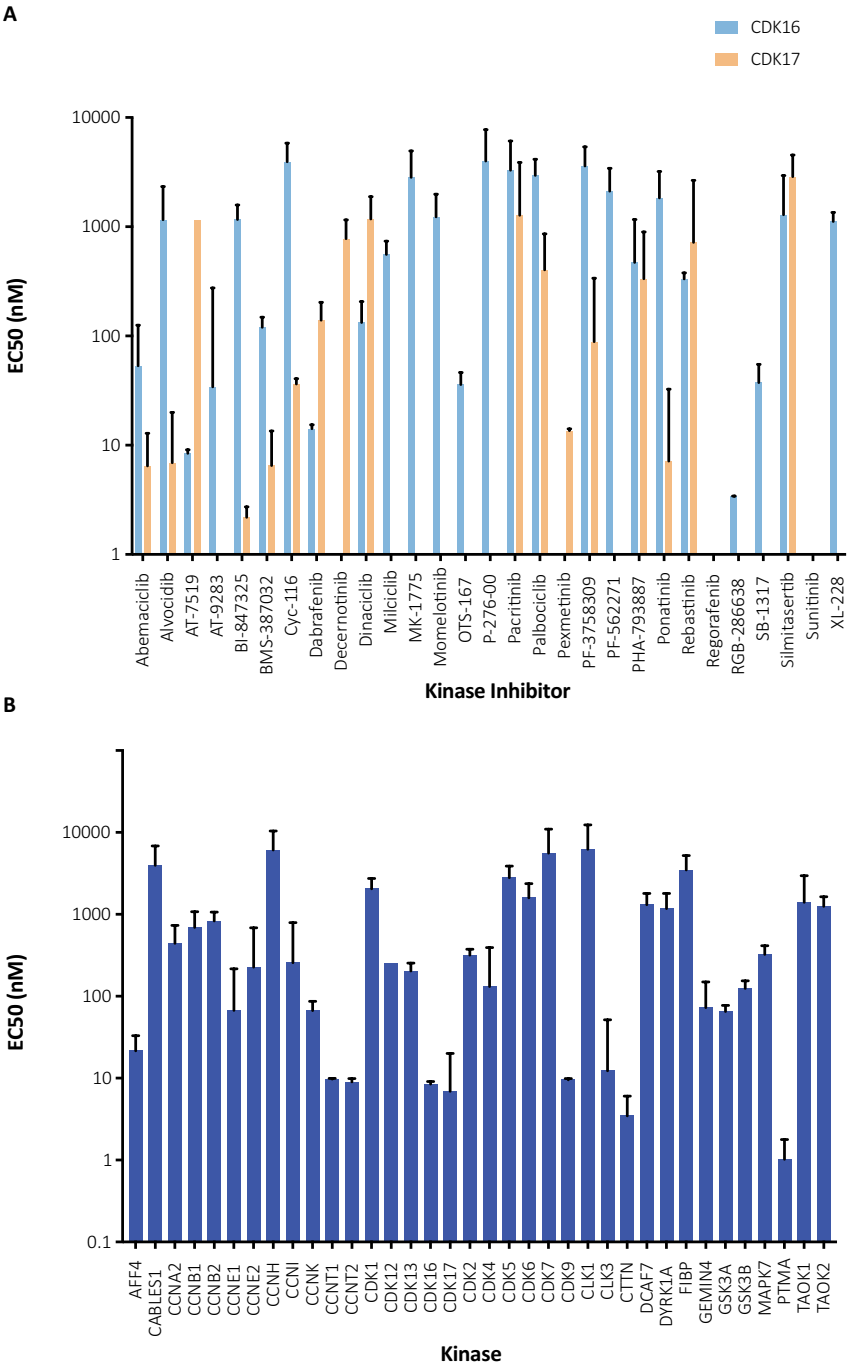

Figure 3-1. Target characterization of clinical kinase inhibitors. (A) Clinical kinase drugs that inhibit CDK16 and/or CDK17 in cells, analyzed from published data (Klaeger et al., 2017). (B) Kinase targets of AT7519, assessed by kinobeads, analyzed from published data (Klaeger et al., 2017).

To begin to address this need, we have developed a series of covalent CDK14 inhibitors with pan-TAIRE family specificity and characterized the pharmacological effects of the lead tool compound in the human colorectal cancer cell line HCT116. Additionally, we have employed the lead tool compound in combination with peptide array profiling and phospho-proteomics to characterize the acute cellular effects of pan-TAIRE kinase inhibition and identify signaling pathways involving CDK14.

Identification of Cys218 of CDK14 as an off-target of JNK-IN-7

In order to identify chemical starting points for the development of TAIRE-kinase family inhibitors, we implemented a combined screening and structure-guided drug design approach. The CDK family contains 20 members and the ATP-binding sites are highly conserved, which makes finding selective CDK inhibitors challenging. From our comprehensive analysis of cysteine residue locations in kinases, we noted that CDK14 possesses Cys218 in the "hinge 7" position. Based on sequence and structure alignments, a cysteine is present in this position in only 3 other kinases (JNK1, JNK2, JNK3) (Q. Liu et al., 2013). In particular, we noticed that Cys218 is only present in CDK14 amongst all CDKs, thereby affording the opportunity to use this residue as a means to achieve selectivity for CDK14 within the CDK family. Since only a small fraction of the kinases that possess a cysteine near the ATP-binding pocket have been experimentally demonstrated to be labeled by a suitable covalent ligand, we queried our chemical proteomics database generated using the KiNativ methodology (Patricelli et al., 2011) for compounds that exhibited CDK14 binding. Our proteomic data revealed that JNK-IN-7 (T. Zhang et al., 2012), a previously reported covalent pan-JNK inhibitor, also engages CDK14 (Figure 3-2).

JNK and CDK14 are categorized into different kinase sub-families (JNK and CDK respectively) and CDK14 and JNK3 have a 28.6% overall sequence homology. Therefore, we first validated this unexpected result and demonstrated that the CDK14:JNK-IN-7 interaction is specific and covalent. We used an established pull-down assay protocol (T. Zhang et al., 2016) to confirm that biotinylated JNK-IN-7 can engage CDK14 in lysates derived from HEK293 cells, and that this interaction was competed out in a dose dependent manner by pre-treatment of the cells before lysis with JNK-IN-7 (Figure 3-2D). We next incubated recombinant CDK14 with JNK-IN-7 and observed the covalent addition of a single inhibitor molecule to the protein by LC-MS (Figure 3-2E). Pull-down of WT CDK14 but not C218S CDK14 from lysate, using biotin-JNK-IN-7, confirmed that Cys218 is the residue that is covalently engaged (Figure 3-2F). To provide molecular rationale for JNK-IN-7 covalently targeting CDK14, we examined the structural alignment of JNK3 bound to JNK-IN-7 (PDB:3V6S) (T. Zhang et al., 2012) and a homology model of CDK14 built using the structure of CDK12 (PDB: 5ACB) (Bosken et al., 2014). This analysis pointed to the presence of a conserved cysteine in α-D loop of both proteins, and further supported Cys218 as the site of modification in CDK14 (Figure 3-2G). This cysteine is not present in other CDKs, explaining this compound's selectivity for CDK14 over the rest of the CDK family. Taken together, these results demonstrate that suitable acrylamide-modified heterocycles can efficiently label Cys218 of CDK14. However, as the phenylamino pyrimidine hinge-binding motif present in JNK-IN-7 is a generic kinase-inhibitor scaffold, we sought to identify more CDK selective ATP-site binders to help improve non-covalent potency and selectivity for the CDK-family versus other kinases.

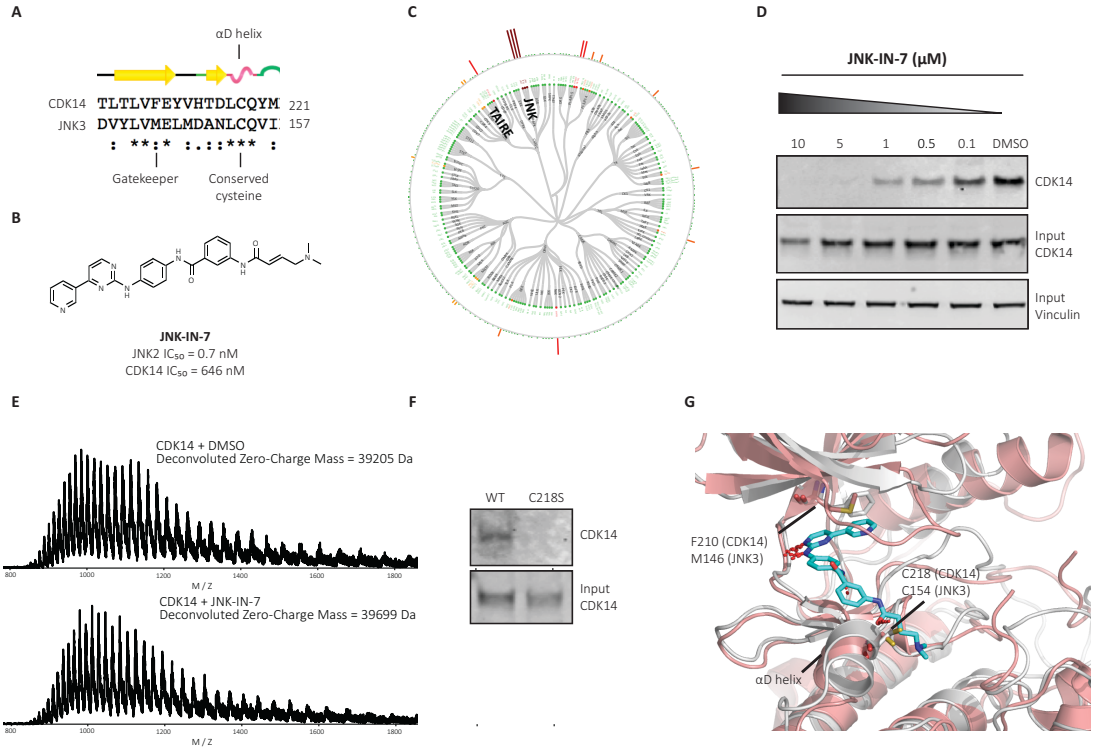

Figure 3-2. CDK14 is a covalent target of JNK-IN-7. (A) Sequence alignment of α-D loop of JNK3 and CDK14. (B) Chemical structure and biochemical potency of JNK-IN-7. (C) KiNativ profiling of JNK-IN-7 cellular selectivity at 1 μM. (D) Biotinylated JNK-IN-7 can pull down CDK14 from treated cell lysates. JNK-IN-7 shows dose dependent competition with biotin-JNK-IN-7. (E) Intact mass spectrum of recombinant CDK14 protein incubated with JNK-IN-7, resulting in mass shift compared to DMSO. (F) Biotin-JNK-IN-7 can pull down WT CDK14-flag, but not C218S CDK14-flag from HEK293 lysates, demonstrating that covalent bond formation occurs with the native protein. (G) Overlay of the crystal structure of JNK3 with the homology model of CDK14, showing spatial proximity of targeted cysteine residues.

Identification of AT7519 as a potent TAIRE-kinase inhibitor

To identify a CDK directed scaffold that could serve as a starting point for covalent inhibitor design, we screened a library of commercial and in-house kinase inhibitors using an in vitro CDK14 LanthaScreen binding assay (Invitrogen), followed by hit validation in a 33P-ATP CDK14 kinase assay (Reaction Biology). Finally, compounds that inhibited CDK14 in both biochemical assays were tested in a cellular target engagement assay. In this assay we determined whether pre-treatment of HEK293 cells with the compound of interest could block

CDK14 pull-down by biotinylated JNK-IN-7 (Figure 3-3A,C). This screening cascade identified AT7519, a pan-CMCG kinase family inhibitor originally developed to target CDK1/2, as a remarkably potent reversible CDK14 inhibitor, with a biochemical IC50 of 19.8 ± 2.7 nM (Table 3-1) (Wyatt et al., 2008).

Table 3-1 Biochemical IC_{50} data and cellular target engagement by pulldown for lead compounds discussed in this article against TAIRE kinases CDK14, CDK16, CDK17 and CDK18, and off-target CDK2. IC_{50}s are reported as the average of triplicate (CDK14) or duplicate (CDK16-18) replicates ± the standard error of the mean (SEM). Cellular target engagement of CDK14 by pulldown assay. Lowest concentration at which complete inhibition of CDK14 pulldown is achieved is reported.

Compound Name	IC_{50} CDK14 Lanthascreen (nM)	IC_{50} CDK14 NanoBRET (nM)	IC50 CDK14 Pulldown (nM)	IC_{50} CDK14 ^{33}P kinase assay (nM)	IC_{50} CDK16 binding by Lanthascreen (nM)	IC_{50} CDK2 Z'LYTE kinase assay (nM)	IC_{50} CDK2 NanoBRET (nM)	IC_{50} HCT116 Proliferation (nM)
AT7519	19.8 ± 2.7	77.7 ± 5.9	> 1000	11 ± 1.4	3.9 ± 0.7	28 ± 3	969 ± 160	132 ± 33
FMF-03-198-2	1.7 ± 0.7	143 ± 30.8	50	44 ± 4.5	0.9 ± 0.9	1.0 ± 0.7	113 ± 62.1	5.1 ± 1.4
FMF-04-159-2	88.0 ± 9.6	39.6 ± 2.8	500	352 ± 40	10.1 ± 1	8.2 ± 0.8	256 ± 26	1144 ± 190
FMF-04-159-R	139.1 ± 10.4	563 ± 145	> 1000	367 ± 135	5.9 ± 2	4.9 ± 0.5	493 ± 81	5869 ± 1191

To broadly assess the kinase targets of AT7519 in live cells, we performed KiNativ profiling in HCT116 cells treated with 1 μM compound for 4 h. Consistent with our previous data, we found that AT7519 potently inhibited CDK14, and also had strong activity against other TAIRE kinases, including CDK16, CDK17, and CDK18, as well as other CMCG family kinases, such as CDK9, GSK-α, and GSK-β (Figure 3-4). Surprisingly, poor engagement was observed for CDK1/CDK2, and the overall selectivity profile therefore identified fewer targets than have previously been reported, potentially reflecting differences in the methodologies used, or a false negative in our data. Aside from this, the detected targets from KiNativ were largely consistent with a recent report evaluating the cellular targets of AT7519 in mixed cell lysates using the kinobeads platform (Klaeger et al., 2016). In that study, AT7519 was found to be highly potent against CDK9, CDK16 and CDK17, and also had activity against CDK1, CDK2, CDK4, CDK12, GSKα, GSKβ and other CMCG kinases (Figure 3-1B, Table 3-2).

Table 3-2. Complete KiNativ profiling data for AT7519, FMF-03-198-2 and FMF-04-159-2. Reported values represent percent inhibition relative to un-treated control. All experiments were performed at 1 μM for 4 h in HCT116 cells. Repeated kinase names indicate different sites of modification identified.

Kinase	AT7519	FMF-03-198-2	FMF-04-159-2
ABL, ARG	-2.4	16	-0.1
ABL, ARG	8.4	8.5	19.5
ACK	-10	17.5	1.7
ACK	0.7	-1.1	9.5
AKT1	-9.9	-5.1	-16.9
ALK2, ALK4, ALK7, BMPR1B, TGFbR1	12.2	13.1	11.7
AMPKa1, AMPKa2	9	14.8	7.5
AMPKa1, AMPKa2	-9.1	3.8	-11.2
ANKRD3	4.4	2.1	7.9
ARAF	-39.9	-54.1	-7.1
ATR	-23.9	3.6	-7.8
AurA	35.5	-3.9	30.7
AurA	30.4	-16.5	6.4
AurA, AurB, AurC	17.3	-7	25.4
AurB	16.1	17.7	25.6
BARK1	3.6	22.7	14.2
BRAF	0.1	3.3	11.4
CaMK1a	1.9	8.7	-31.4
CaMK1d	-1.8	6.7	-5.8
CaMK2a, CaMK2b, CaMK2d, CaMK2g	2.1	10	6.7
CaMK2a, CaMK2b, CaMK2d, CaMK2g	-0.4	-0.3	13.1
CaMK2d	2.8	11.6	-0.1
CaMK2g	17.8	27.7	4.7
CaMK4	-6.4	-5	1.4
CaMKK2	6.4	50.7	6.7
CaMKK2	-5.2	45.7	-2.5
CASK	51.8	51	7
CDC2	4.4	96.3	54.4
CDC2	6.3	-4.5	-21.7
CDK10	41.7	85.7	76.5
CDK11, CDK8	-24.3	19.5	-15.9
CDK11A	55.2	72.3	25.9
CDK12	5.5	82.2	13.9
CDK14	87.4	98.7	94
CDK14	76.9	97	96.6

Table 3-2 (Continued).

CDK16	84	84	>95
CDK16	84	84	>95
CDK16, CDK18	87.4	94	80.1
CDK17	96	96	94.2
CDK17, CDK18	90.3	96	81.3
CDK2	35.2	99.6	96.5
CDK2	37.7	88.7	95.1
CDK20	-3.1	44.8	6.7
CDK4	-0.9	84.4	21.6
CDK5	-9.1	95.4	44.9
CDK5	10.9	95.1	41.3
CDK6	6	86.4	3.4
CDK7	31.5	63	23.9
CDK7	11.3	50.1	12.1
CDK9	84.3	86	28.6
CDK9	-1.5	-0.7	-12.5
CHK1	11.4	12.2	16.8
CHK1	3.9	1.2	24.6
CHK2	-1.2	8.4	5.2
CHK2	-5.5	-5.3	15.1
CK1a	-21.6	1.7	9
CK1d, CK1e	-2.5	18.1	-0.5
CK1g1	13.3	28.9	24.3
CK1g2	3.2	19.3	16.5
CK1g3	11.5	24.9	19.2
CLK3	-7.3	40.5	15.7
CSK	15.1	18	10.8
CSK	7.9	8.8	8.5
DGKA	-7.7	-9.6	0.5
DGKH	-4.6	-4.3	-5.8
DNAPK	11.4	13.9	26.6
DNAPK	15	-8.6	16.2
eEF2K	8.8	9.8	-14.9
EGFR	2.2	9.3	9.6
EGFR	-5.3	-5.1	7.5
EGFR	-9.4	-6.5	-7.8
EphA1	10.2	17	27.3
EphA1	13.5	12.5	24.2

Table 3-2 (Continued).

EphA2	9.4	17.5	18.7
EphA2	8.9	15.2	3
EphA3, EphA4, EphA5	28.6	31.4	-1.4
EphB2	5.3	12.1	13.9
EphB4	13.9	25.6	20.8
Erk1	-2.7	-0.8	4.7
Erk2	-11	-4.4	4.1
Erk5	57.7	84.8	44.3
FAK	-14.7	23.1	-22.3
FAK	-9.1	13.1	-26.7
FAM20B	-13.9	1.7	3
FER	-4.2	7.7	18.4
FER	-1.3	4.2	-5.2
FRAP	-7.4	-6.3	-5.6
FRK	32.1	31	22.5
FYN, SRC, YES	7.6	23.4	18.3
GAK	-12.2	4.9	14.6
GCK	-3.3	8.2	-0.5
GCK	-16.5	-10.7	-27.7
GCN2 domain2	17.7	12.9	-10.5
GCN2 domain2	-3.2	-3.7	5.1
GSK3A	73.3	76.9	21.4
GSK3B	44	63.4	16.3
HER2/ErbB2	-48	-32.6	-21
HER2/ErbB2	-32.4	-38.6	-37.3
HER3/ErbB3	-21.7	-6.8	-9.8
HER3/ErbB3	-14.2	-12.2	22.2
IKKa	-8.7	-4.7	1.5
IKKb	-8.7	0.1	19.4
IKKe, TBK1	-7.1	18.2	-48.8
ILK	2.6	5.2	-14.3
ILK	-28.6	-6.2	-33.6
IRAK1	-7.2	1.2	-11.5
IRAK4	7.2	16.7	-3.2
IRAK4	-6.6	0.3	-24
IRE1	-5.3	11	17.3
ITPK1	-11.2	-6.7	-22.7
JAK1 domain1	8.5	17.9	-27.1

Table 3-2 (Continued).

JAK1 domain2	12.1	10.7	24.8
JAK1 domain2	6.5	6	25.1
JNK1, JNK2, JNK3	0.2	5.6	-13.3
KHS1	2.1	6.5	12.3
KHS1	2.3	0.8	8.3
KHS2	6.6	1.1	1.8
KHS2	4.2	0.1	3.6
KSR1	-8.6	-20	-44.9
KSR1, KSR2	5	2.6	-19.8
LATS1	9.8	22.8	-22
LATS1	14.3	16.9	-10
LATS2	12.7	46.3	-8.4
LATS2	30.8	44.5	29.3
LKB1	3.1	13	-3.8
LKB1	0.5	8.6	-15.7
LOK	12.6	12.9	9.4
LOK	-15.7	-1	-19.7
LYN	-0.6	19.5	-9.7
LYN	13.5	6.2	2.3
MAP2K1	-18.7	5.6	-44.6
MAP2K1, MAP2K2	3.2	9.4	13
MAP2K1, MAP2K2	-8.3	-3.9	-10.2
MAP2K3	-5.3	13.6	-3.9
MAP2K3	-14	5.1	-26.4
MAP2K3	-6.1	-4	1.5
MAP2K4	-6.1	12.5	11.9
MAP2K4	-4.4	3	20.9
MAP2K4	-0.3	-3.2	9.6
MAP2K5	-4.9	10.8	3.3
MAP2K5	5.2	4	13.4
MAP2K6	-12.7	-0.5	-1.4
MAP2K7	-3.2	-0.1	-8.9
MAP3K1	24	64.4	-0.8
MAP3K15, MAP3K5, MAP3K6	4.9	2.3	-7.3
MAP3K2	16.3	3.3	16.2
MAP3K2, MAP3K3	-2.5	-4.3	5.9
MAP3K3	14.1	0.4	-11.5
MAP3K4	-9	-23	-22.9

Table 3-2 (Continued).

MAP3K5	9.5	25.5	-18.9
MAP3K6	-12.2	-2.5	8.9
MAPKAPK2, MAPKAPK3	-23	-25.8	1.8
MAPKAPK3	4.8	17.4	-8.2
MARK1	1.6	17.4	8
MARK1, MARK2	9	15.1	4.2
MARK2	5	14.2	5.4
MARK2	-7.3	0.3	2.9
MARK2, MARK3	-8.5	17.7	5.8
MARK3	11.9	21.7	9.6
MARK3, MARK4	19.1	23.3	14.7
MARK4	3.3	22.4	0.8
MARK4	4	15.5	22
MAST1, MAST2	-20.5	18.3	2.1
MAST3	8.2	10.7	8.1
MASTL	7.2	13	9.1
MASTL	4.2	8.4	0.3
MELK	1.6	3.1	12.4
MET	-14.6	14.5	1.2
MET	3.5	-5.8	12.6
MET	-17.4	-7.8	4
MLK1	5.4	6.8	9.6
MLK3	-22	8.8	-3.2
MLK4	-5.4	3.6	-32.8
MLKL	-1	11.5	-13.1
MLKL	1.6	8.1	-7
MPSK1	1.3	8.5	-12.9
MPSK1	-0.7	6.5	-40.2
MRCKb	-5.4	7.5	-20
MSK1 domain1	24.4	19.2	-4
MSK2 domain1	-22.2	8.9	-32.4
MSK2 domain1	-4.4	-5.9	9
MST1	-0.1	5.3	12.3
MST1, MST2	-6	-4.8	-13.4
MST2	-6.1	-2.6	12.6
MST3	3.2	12.4	3.4
MST3	-20.6	11.1	-38.3
MST4	-10.7	-0.6	20.6

Table 3-2 (Continued).			
MST4, YSK1	9.2	9	-11.5
NDR1	-13.7	10.7	-13
NDR1	-1.5	4.2	-3.5
NDR1, NDR2	10.3	6.2	4.9
NDR2	-10.7	11.5	-3
NDR2	-2.5	-2	9.2
NEK1	1.6	14.9	-5.5
NEK3	5.9	10.7	-19.3
NEK4	-5.2	-0.3	-4.1
NEK6, NEK7	-15.9	2.3	10
NEK7	-3.1	7.8	-13.2
NEK8	-16.3	-5.7	4.8
NEK9	23.3	28	-8.2
NEK9	9	20.3	2.1
NEK9	-0.3	8	-7.1
NuaK2	50.2	53	4.4
OSR1	4.2	-1.7	18.8
p38a	12.7	24.9	-47.7
p38a	12.9	7.9	-26.1
p38b	-4.9	6.6	-38.8
p38d, p38g	-0.3	2.4	-41.6
p70S6K	-10	6.3	-38
p70S6Kb	-25.1	-8.9	-24.4
PAK2	-6.2	14.9	-20.3
PAN3	-17.4	8.1	-11.5
PAN3	-5.1	-2	3.7
PDK1	10.1	9.3	9.6
PEK	-29.7	-6.7	-48.1
PHKg2	-13.5	6.2	2.8
PI4KA, PI4KAP2	-10	18.9	-25.8
PI4KB	12.1	22.7	25.4
PI4KB	22.6	21.7	8.1
PIK3C3	5.7	30.5	-10.7
PIK3CB	18.8	23.1	1
PIK3CB	-6.9	8	-40.9
PIP4K2A	6.6	19.2	11
PIP4K2B	-1.3	-11.4	-14.3
PIP4K2C	-10	11.1	-30.5

Table 3-2 (Continued).

PIP4K2C	-15.7	6.7	-24.5
PIP5K3	-1.1	0	10.4
PKCi	-21	-4.5	-5.5
PKD1, PKD2	7.6	8.1	13.7
PKD2	8.1	9.1	8.4
PKN1	-5.5	3.2	4.5
PKN1	-20.2	-6	18.5
PKN2	15.5	12.4	27.3
PKR	15.1	12	0.9
PKR	-1.5	7.6	-3.4
PKR	-8.9	-0.5	-10.1
PLK1	-0.8	-17.8	-3
PLK1	-0.6	-19.5	15.5
PRP4	0.7	5.1	15
PRPK	24	32.6	24.3
RAF1	-40.5	-23.9	-35.6
ROCK1	-5.1	-2.2	5.1
ROCK1, ROCK2	-15	-3.2	-20.6
RON	2	1.5	-0.2
RON	-23.3	-14.2	-5.7
RSK1 domain1	10.9	18.5	-8.4
RSK1 domain1	-0.7	9.1	-31.5
RSK1 domain1, RSK2 domain1, RSK3 domain1	7.4	21.1	4.7
RSK1 domain2	0.4	14.4	6.7
RSK2 domain1	16.1	22.9	1.2
RSK2 domain2	9.8	15.8	5.1
RSKL1	-30.7	-12.5	-2
SGK3	-1	8.2	-2.8
SGK3	-4.8	-9.4	8.7
SLK	8.9	25	12.9
SLK	-9.7	4.7	-1.9
SMG1	-1.9	-6.4	18.4
SMG1	-14.2	-19.3	0.2
SNRK	25.6	17	16.2
SNRK	18.3	16.6	8
SRC	1.9	24.3	16
SRPK1	-11.1	-3.9	6.1
SRPK1, SRPK2	-18	-10.4	-7.6

Table 3-2 (Continued).

STK33	-23.9	-3.4	-20.9
STLK3	-36.8	-22.4	-6.8
STLK5	29.1	26.3	-41.7
STLK5	1.6	-0.5	14.1
STLK6	10.9	17.9	18.5
SYK	9.3	11.5	2.7
SYK	0.1	4.7	-4.4
TAK1	-3.3	11.2	-12.1
TAO1, TAO3	9.8	11.5	-7.6
TAO2	31.3	52.6	-1.6
TBK1	-3.5	19.4	-23.8
TLK1	13.4	7.2	0.9
TLK1	-9.3	-7.6	14.5
TLK2	12.6	12.4	10.1
TLK2	-6.3	-8.1	14.3
TNK1	1.3	2.4	17.5
ULK1	-9.8	-6.6	-23.3
ULK2	-3.3	9.1	-9
ULK3	-7.2	-0.1	14.6
ULK3	-11.9	-4.7	-10.1
Wnk1, Wnk2, Wnk3	1.6	4.7	-22.1
Wnk1, Wnk2, Wnk4	2.2	9.7	-18.4
YANK3	-1.3	5	12.7
ZAK	9.4	8.5	3.5
ZC1/HGK, ZC2/TNIK, ZC3/MINK	-6.9	-1.9	-8.4
ZC2/TNIK	8	22	-26.2

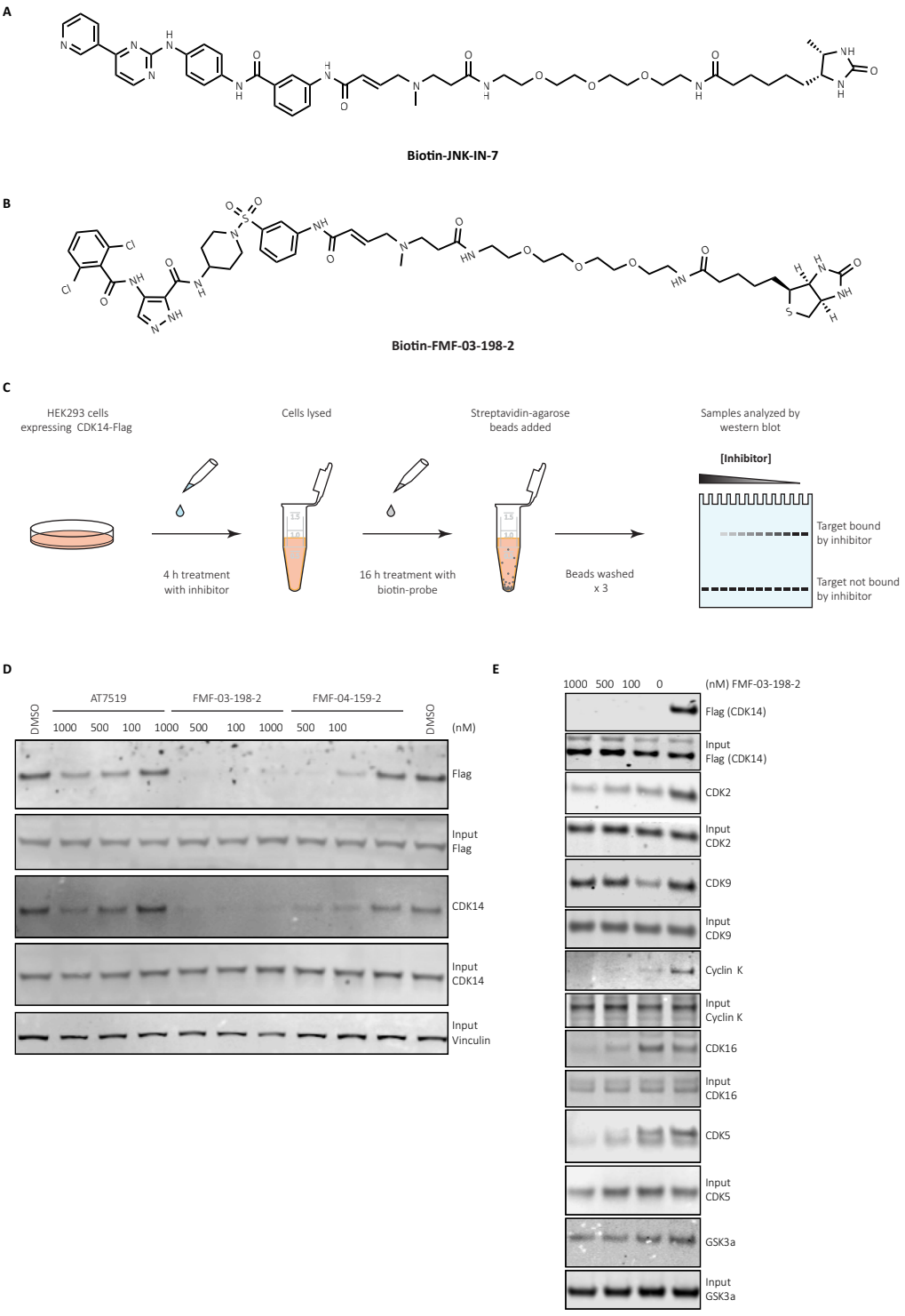

Figure 3-3. Pull down reagents, schematic, and experimental validation using biotin compounds, performed in the course of FMF compound characterization. (A) Chemical structure of desthiobiotin-PEG3-3-amidopropanamide-JNK-IN-7, dubbed Biotin-JNK-IN-7, used as a pull-down reagent. (B) Chemical structure of Biotin-FMF-03-198-2, used as a pull-down reagent. (C) Schematic depicting pull-down assay protocol. (D) Representative western blot data reported in Table 3-1 for cellular pulldown using Biotin-JNK-IN-7. (E) Pre-treatment of cells with FMF-03-198-2 results in dose-dependent competition of pull down of several CDKs and CMGC kinases using Biotin-FMF-03-198-2.

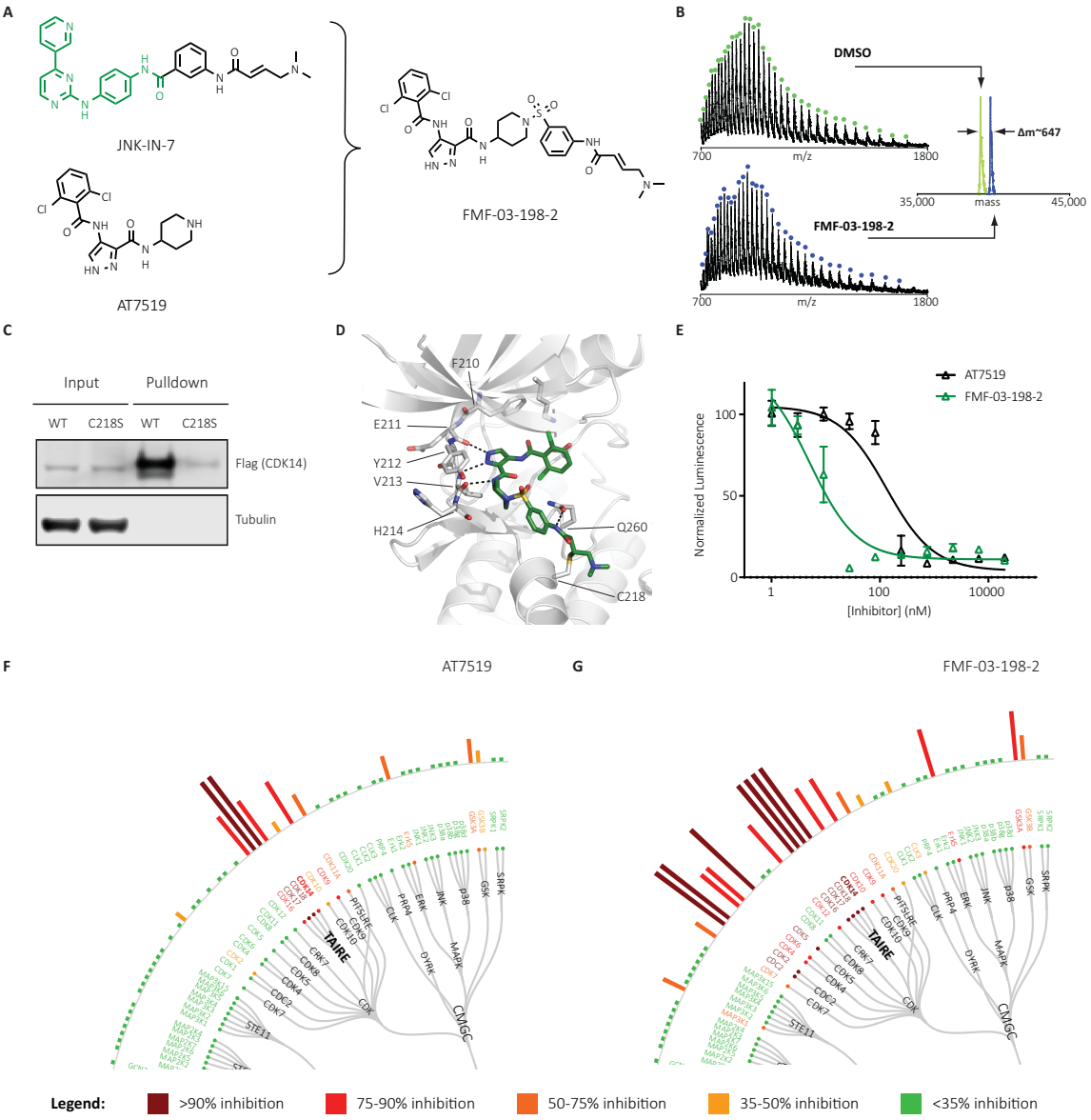

Figure 3-4. AT7519 analog FMF-03-198-2 is a pan-CMCG kinase inhibitor that targets CDK14 C218 covalently. (A) Chemical structures of AT7519 and FMF-03-198-2. (B) Intact MS analysis of recombinant CDK14 protein incubated with DMSO (top panel) or FMF-03-198-2 (bottom panel) demonstrating a mass shift corresponding to covalent addition of FMF-03-198-2 with 1:1 stoichiometry. (C) Biotin-FMF-03-198-2 can pull down WT CDK14-flag, but not C218S CDK14-flag from HEK293 lysates, demonstrating that covalent bond formation with the native protein occurs. (D) Covalent docking model of FMF-03-198-2 into a homology model of CDK14. The (1,4)-(1,3) regiochemistry is modeled to be uniquely permissive of covalent bond formation. CDK14 protein carbons shown grey, FMF-03-198-2 carbons shown green, hydrogen bonds depicted as black dotted lines. (E) Effects of AT7519 and FMF-03-198-2 on cell viability, using CellTiter-Glo. Data points are plotted as the average of three replicates ± standard error of the mean (SEM). (F) Live cell KiNativ profiling upon 4 h treatment with 1µM AT7519 or (G) FMF-03-198-2.

Developing covalent AT7519 analogs with CDK14 activity

Developing selective inhibitors of CMCG kinases is notoriously challenging, with the majority of reported CDK inhibitors possessing extensive poly-pharmacology (Klaeger et al., 2016). As targeting non-conserved cysteines within or near the ATP-binding pocket with a covalent warhead has been a useful strategy for improving selectivity against otherwise homologous kinases (Chaikuad et al., 2018), we focused our initial efforts on hybridizing the acrylamide warhead of JNK-IN-7 with the AT7519 scaffold.

Initially, we sought to generate a cell-penetrant, covalent CDK14 inhibitor based on the AT7519 scaffold as a proof-of principle compound, before optimizing for other properties. Through an extensive analoging campaign in which the piperidine of AT7519 was replaced with acrylamide bearing groups, varying in composition and regiochemistry, to be described in detail elsewhere, we identified the potent multi-targeted inhibitor FMF-03-198-2 (Figure 3-4A). FMF-03-198-2 incorporates the hinge-binding scaffold of AT7519 and the acrylamide orienting 1,3-aniline of JNK-IN-7. Covalent bond formation to CDK14 was confirmed by incubating FMF-03-198-2 with purified recombinant CDK14 protein followed by mass spectrometry analysis, which demonstrated an increase in mass corresponding to the molecular weight of FMF-03-198-2 (Figure 3-4B). To verify engagement of CDK14 in a cellular context, a biotinylated analog of FMF-03-198-2 (Figure S2B) was synthesized, and lysates from HEK293 cells expressing flag-tagged wildtype or C218S-CDK14 were subjected to a pull-down assay. As expected, CDK14-flag was successfully pulled down, but C218S-CDK14 was not, indicating that biotin-FMF-03-198-2 covalently labeled CDK14 at C218 in cell lysates, and that C218 was essential for compound binding activity (Figure 3-4C). Molecular modeling demonstrated that the 1,4 amino-piperidine,

1,3 aniline regiochemistry is exclusively permissive of covalent bond formation between CDK14 C218 and the acrylamide warhead (Figure 3-4D).

To test the effects of FMF-03-198-2 on cell proliferation, we treated HCT116 cells with a dose range of the compound and evaluated cell growth using CellTiter-Glo, which showed that FMF-03-198-2 was 26-fold more potent than AT7519 (IC50 = 5.1 ± 1.4 nM compared to 132 ± 33 nM) (Figure 3-4E). RNAi knockdown studies of CDK14 – CDK18 have demonstrated that these kinases are not essential for the 2D proliferation of colorectal cancer cell line cultures, including HCT116 cells (Table 3-3), unlike the other CMCG kinase targets of AT7519; for example, CDK1 depletion results in a profound effect on proliferation (Table 3-3) (McDonald et al., 2017). Therefore, the increased toxicity of FMF-03-198-2 against HCT116 cells was unlikely attributable to selective CDK14 inhibition, suggesting that this molecule potentially inhibited additional targets. Indeed, KiNativ profiling in HCT116 cells revealed that FMF-03-198-2 is a pan-CDK kinase inhibitor that also has potent activity against the CMCG kinases ERK5, GSK3α and GSK3β (Figure 3-4G). Accordingly, biotin-FMF-03-198-2 pulled down a number of CMCG kinases (including CDK2, CDK5, CDK9, CDK16 and GSK3α) from cell lysates, and when cells were pre-treated with FMF-03-198-2, dose-dependent competition was observed (Figure 3-3D,E).

Table 3-3. Dependence of cell proliferation on TAIRE kinases in HCT116 cells using RNAi. Data from Novartis Project DRIVE (McDonald et al., 2017). CDK1 data shown for reference. A significant dependency is defined by an ATARIS score of -3 or less.

Kinase	ATARIS score
CDK14	-0.36
CDK15	-0.625
CDK16	-0.605
CDK17	-1.871
CDK18	-1.129
CDK1	-3.143

While FMF-03-198-2 was not suitable as a selective probe for CDK14 and other TAIRE kinases, it confirmed that hybridization of the acrylamide warhead of JNK-IN-7 with AT7519 is a viable strategy for developing covalent CDK14 inhibitors targeting C218. Furthermore, its increased potency for TAIRE kinases (compared to AT7519), as well as its additional activity against a broad range of CMCG family kinases, enabled the use of biotin-FMF-03-198-2 as a tool for monitoring cellular target engagement for CDK14 and off-target kinases simultaneously. This ability to rapidly assess the cellular engagement of poorly characterized kinases, largely without reported downstream substrates, greatly aided our efforts to generate of more selective inhibitors. With the requisite tools in hand, we continued to optimize our pan-CMCG inhibitor to improve its selectivity.

Development and characterization of FMF-04-159-2 as a covalent CDK14 inhibitor with pan-TAIRE activity

To improve the selectivity profile of FMF-03-198-2, we subjected this compound to rounds of iterative medicinal chemistry, which resulted in development of FMF-04-159-2 (Figure 3-5A). Here, we built upon published SAR studies of AT7519 and related compounds which demonstrate that incorporation of a substituent at the 4-position of the benzamide ring reduces CDK2 and GSK-3β inhibition in biochemical assays, and reduces anti-proliferative activity against human cell lines (Urich et al., 2014; Wyatt et al., 2008). We demonstrated that FMF-04-159-2 could covalently label CDK14 by mass spectrometry analysis, and confirmed that C218 was the site of covalent attachment by chymotryptic digestion followed by nano-LC/MS analysis of the resulting peptides (Figure 3-5B, C). As a chemical control to distinguish between covalent and

reversible interactions, we synthesized the reversible dimethylbutanamide analog FMF-04-159-R (Figure 3-5A). The biochemical binding assay for CDK14 showed that FMF-04-159-2 and FMF-04-159-R have similar biochemical potencies (IC50 = 86 nM and 149 nM respectively, Figure 3-5D, Table 3-1), indicating that reversible binding activity is the primary driver of potency measured in this assay. The ^{33}P kinase assay highlighted the effects of covalent inhibition, as FMF-04-159-2 was ~10-fold more potent than FMF-04-159-R as an inhibitor of CDK14 kinase activity (Table 3-1).

Proliferation assays in HCT116 cells revealed that FMF-04-159-2 and FMF-04-159-R were less potent than AT7519 and FMF-03-198-2 (Figure 3-5E, Table 3-1). Additionally, we observed a 5-fold difference in HCT116 cell IC50 between the reversible and covalent inhibitor pair, which suggested that a mild anti-proliferative effect is due to covalent binding (Figure 3-5E). This suggested that FMF-04-159-2 has a much narrower target range when compared to the parental FMF-03-198-2, given that previous studies had reported only mild impairment of cell proliferation upon siRNA-mediated knockdown of CDK14 (McDonald et al., 2017).

To quantitatively assess cellular engagement of CDK14, we used the Promega NanoBRET live cell target engagement assay (Figure 3-5F, Table 3-4) (Perez-Riverol et al., 2019). Here, we found that CDK14 was potently engaged by FMF-04-159-2 (IC50 = 39.6 ± 2.8 nM), and this engagement was sustained after a 2 h compound washout (IC50 = 56.3 ± 6.0 nM), indicative of irreversible binding. In contrast, inhibition of CDK14 by FMF-04-159-R was 5-fold less potent (IC50 = 563 ± 145 nM) and was reduced by a further 7-fold after washout (IC50 = 3417 ± 1154 nM), suggesting that covalent bond formation enhances cellular inhibition of CDK14, a feature not detected in biochemical assays.

Figure 3-5. Characterization of FMF-04-159-2 as a covalent CDK14 inhibitor with TAIRE kinase selectivity. (A) Chemical structure of FMF-04-159-2 and reversible control compound FMF-04-159-R. (B) Intact MS analysis demonstrates stoichiometric labeling of recombinant CDK14 by FMF-04-159-2. (C) Chymotryptic digestion of FMF-04-159-2 labeled CDK14 demonstrates exclusive labeling of C218 by MS/MS. (D) Biochemical CDK14 binding curves generated using a LanthaScreen assay. Data points are plotted as the average of three replicates, ± the standard error of the mean (SEM). Curves fit using nonlinear regression curve fit in GraphPad Prism 7. (E) HCT116 cytotoxicity of compounds after 72 h treatment, assessed using CellTiter-Glo. Data points are plotted as the average of three replicates, ± the standard error of the mean (SEM). Curves fit using nonlinear regression curve fit in GraphPad Prism 7. (F) In-cell target engagement of CDK14 using the NanoBRET assay (Promega), with and without compound washout for 2 h following compound treatment for 4 h. Data points are plotted as the average of three biological replicates, ± the standard error of the mean (SEM). IC_{50} determined using nonlinear regression curve fit in GraphPad Prism 7. (G) Cellular kinome profiling of FMF-04-159-2 in HCT116 cells using the KiNativ platform at 1 μM. (H) Comparison of kinome-wide selectivity of AT7519, FMF-03-198-2 and FMF-04-159-2, assessed by KiNativ (1 μM 4 h treatment in HCT116 cells).

Figure 3-5 (Continued).

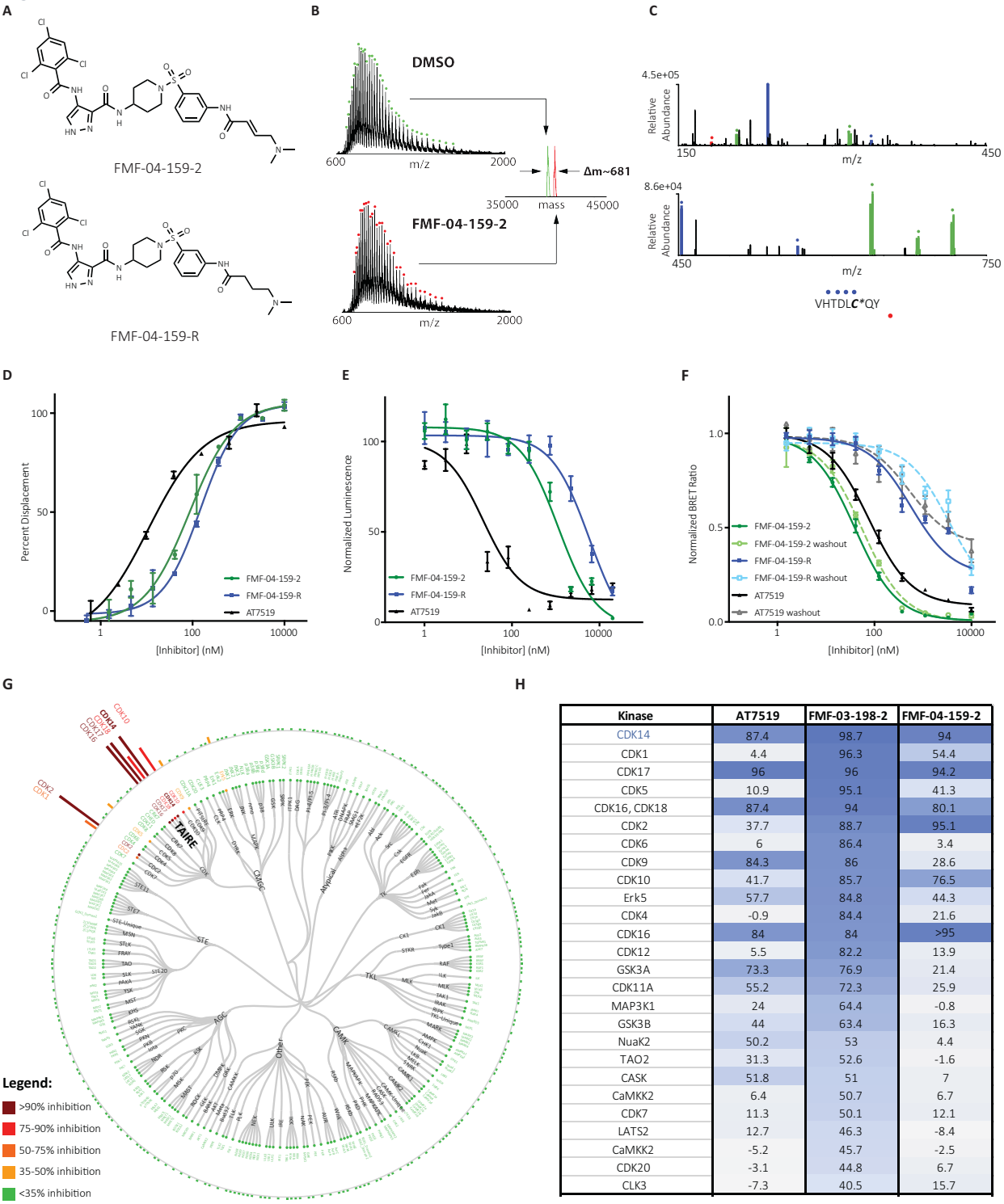

H

Kinase	AT7519	FMF-03-198-2	FMF-04-159-2
CDK14	87.4	98.7	94
CDK1	4.4	96.3	54.4
CDK17	96	96	94.2
CDK5	10.9	95.1	41.3
CDK16, CDK18	87.4	94	80.1
CDK2	37.7	88.7	95.1
CDK6	6	86.4	3.4
CDK9	84.3	86	28.6
CDK10	41.7	85.7	76.5
Erk5	57.7	84.8	44.3
CDK4	-0.9	84.4	21.6
CDK16	84	84	>95
CDK12	5.5	82.2	13.9
GSK3A	73.3	76.9	21.4
CDK11A	55.2	72.3	25.9
MAP3K1	24	64.4	-0.8
GSK3B	44	63.4	16.3
NuaK2	50.2	53	4.4
TAO2	31.3	52.6	-1.6
CASK	51.8	51	7
CaMKK2	6.4	50.7	6.7
CDK7	11.3	50.1	12.1
LATS2	12.7	46.3	-8.4
CaMKK2	-5.2	45.7	-2.5
CDK20	-3.1	44.8	6.7
CLK3	-7.3	40.5	15.7

Table 3-4. IC_{50} results for NanoBRET (Promega) CDK14 assay. IC_{50} comparing direct compound treatment for 6 h to compound treatment for 4 h following by washout for 2 h.

Compound	IC50 (nM)
FMF-04-159-2	39.6 ± 2.8
FMF-04-159-2 washout	56.3 ± 6.0
FMF-04-159-R	563 ± 145
FMF-04-159-R washout	3417 ± 1154
AT7519	77.7 ± 5.9
AT7519 washout	532 ± 160

To assess the cellular kinome-wide selectivity, we performed KiNativ profiling of HCT116 cells treated with 1 μM FMF-04-159-2 for 4 h, and found that it had an improved selectivity profile compared to FMF-03-198-2 (Figure 3-5G, H). FMF-04-159-2 potently inhibited the TAIRE kinases CDK14, CDK16, CDK17 and CDK18. Given reports of functional redundancy among the TAIRE kinases, this pan-TAIRE inhibition profile was deemed acceptable. Some residual off-target activity was detected against CDK2, and to a lesser extent CDK10.

To verify cellular engagement of the other TAIRE kinases and assess the extent of CDK2 activity, we turned to the NanoBRET assay in HCT116 cells (Perez-Riverol et al., 2019). CDK2 was inhibited by FMF-04-159-2 (IC50 = 256 ± 26 nM), and this activity was similar to that of FMF-04-159-R (IC50 = 493 ± 81 nM), consistent with the reversible nature of the interaction, as CDK2 has no equivalent cysteines in the ATP-binding site. At the 2 h timepoint (Figure 3-6, Table 3-5), FMF-04-159-2 shows nearly 20-fold weaker potency for CDK14 (IC50 = 803 ± 111 nM) than at 6 h (Figure 3-5F), suggesting the time dependence of covalent bond formation and increased potency for CDK14 with time. FMF-04-159-2 and its reversible counterpart also engaged the other TAIRE kinases (CDK15, CDK16, CDK17 and CDK18) with comparable potency to each other, indicative of reversible binding (Figure 3-6, Table 3-5).

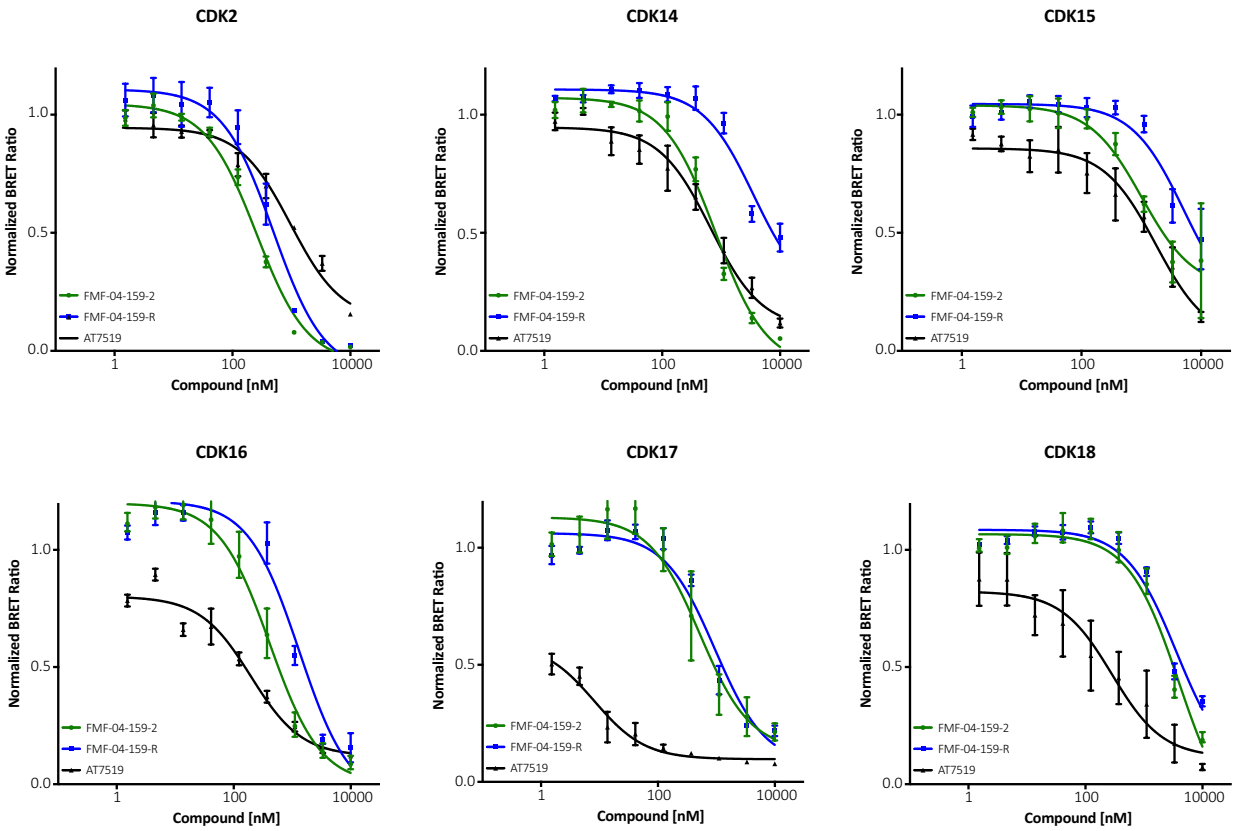

Figure 3-6. NanoBRET (Promega) live-cell target engagement. NanoBRET results in HCT116 cells of the indicated CDK targets for FMF-04-159-2, FMF-04-159-R and AT7519 2 h treatment.

Table 3-5. NanoBRET (Promega) live-cell target engagement IC50 values.

Compound	CDK2 IC50 (nM)	CDK14 IC50 (nM)	CDK15 IC50 (nM)	CDK16 IC50 (nM)	CDK17 IC50 (nM)	CDK18 IC50 (nM)
FMF-04-159-2	256± 26	803 ± 111	1014 ± 320	413 ± 67	521 ± 151	3977 ± 951
FMF-04-159-R	493 ± 81	3540 ± 988	5165 ± 2097	1315 ± 326	942 ± 210	3607 ± 918
AT7519	969 ± 160	661 ± 124	1748 ± 500	197 ± 41	8.2 ± 2.1	285 ± 110

To verify the concentration dependence of binding to the different CDK family kinases, we used the multi-targeted biotin-FMF-03-198-2 probe as bait in a competition pull-down assay (Figure 3-3B,C). Cells were treated with escalating concentrations of FMF-04-159-2 or FMF-04-159-R, followed by cell lysis and pull-down (Figure 3-7A). Complete engagement of CDK14 was observed at 500 nM FMF-04-159-2 and above, whereas FMF-04-159-R failed to block pull-down

at concentrations up to 1 μM, consistent with the NanoBRET assay. Engagement of CDK10 was observed at concentrations above 750 nM of FMF-04-159-2 and FMF-04-159-R, while CDK16 and CDK17 were inhibited at concentrations above 750 nM of FMF-04-159-2, but not by FMF-04-159-R, despite the reversible nature of their interactions with FMF-04-159-2. Only slight inhibition of CDK2 by FMF-04-159-2 and FMF-04-159-R was observed at concentrations above 500 nM in this assay. The pull-down assay was also utilized to investigate the effects of compound washout (Figure 3-7B). CDK14 engagement was sustained for up to 2 h after washout by 1 μM FMF-04-159-2, whereas CDK2, CDK10 and CDK17 were no longer inhibited at this time point after washout and CDK16 target engagement was almost fully removed.

Cumulatively these results suggest that FMF-04-159-2 is a potent, covalent inhibitor of CDK14 in cells, but will also engage non-covalently with CDK2, CDK10 and the TAIRE family kinases at micromolar concentrations, consistent with the reversible CDK binding conferred by the pyrazole amide tridentate hinge binding motif of AT7519. FMF-04-159-2 should only be used as a pharmacological probe of CDK14 when controlled for by compound washout experiments and by use of reversible control compound FMF-04-159-R. Our structured set of preliminary experiments in the HCT116 cell line established experimental conditions relevant to mapping cellular consequences of CDK14 inhibition, namely 1 μM treatment with FMF-04-159-R or FMF-04-159-2 with a 2 h washout control.

Figure 3-7. Characterization of the target engagement and cellular effects of FMF-04-159-2 and FMF-04-159-R in HCT116 cells. (A) Target engagement of FMF-04-159-2 and FMF-04-159-R with 4 h treatment at the indicated concentration, assessed using biotin-FMF-03-198-2 pull down, followed by immunoblotting. (B) Target engagement of FMF-04-159-2 and FMF-04-159-R, treated for 4 h at 1 μM before washout for the indicated time, assessed using biotin-FMF-03-198-2 pull down followed by immunoblotting. (C) Immunoblot for known phospho-substrates of targets of FMF-04-159-2 identified by KiNativ. HCT116 cells were treated for either 6h or 4 h followed by 2 h compound washout with the indicated inhibitors. (D) Double thymidine-synchronized HCT116 CDK14 knockout cells expressing WT or C218S CDK14 were released and allowed to progress through the cell cycle, subject to treatment with 1 μM FMF-04-159-2 or FMF-04-159-R for 4 h windows, followed by compound washout. Cells were collected at indicated times after release. (E) FACS PI cell cycle analysis of 24 h treatment of HCT116 CDK14 knockout cells expressing WT or C218S CDK14. Reported as mean ± standard error for percentage of cells in each cell cycle phase from n=3 biological replicates.

Figure 3-7 (Continued).

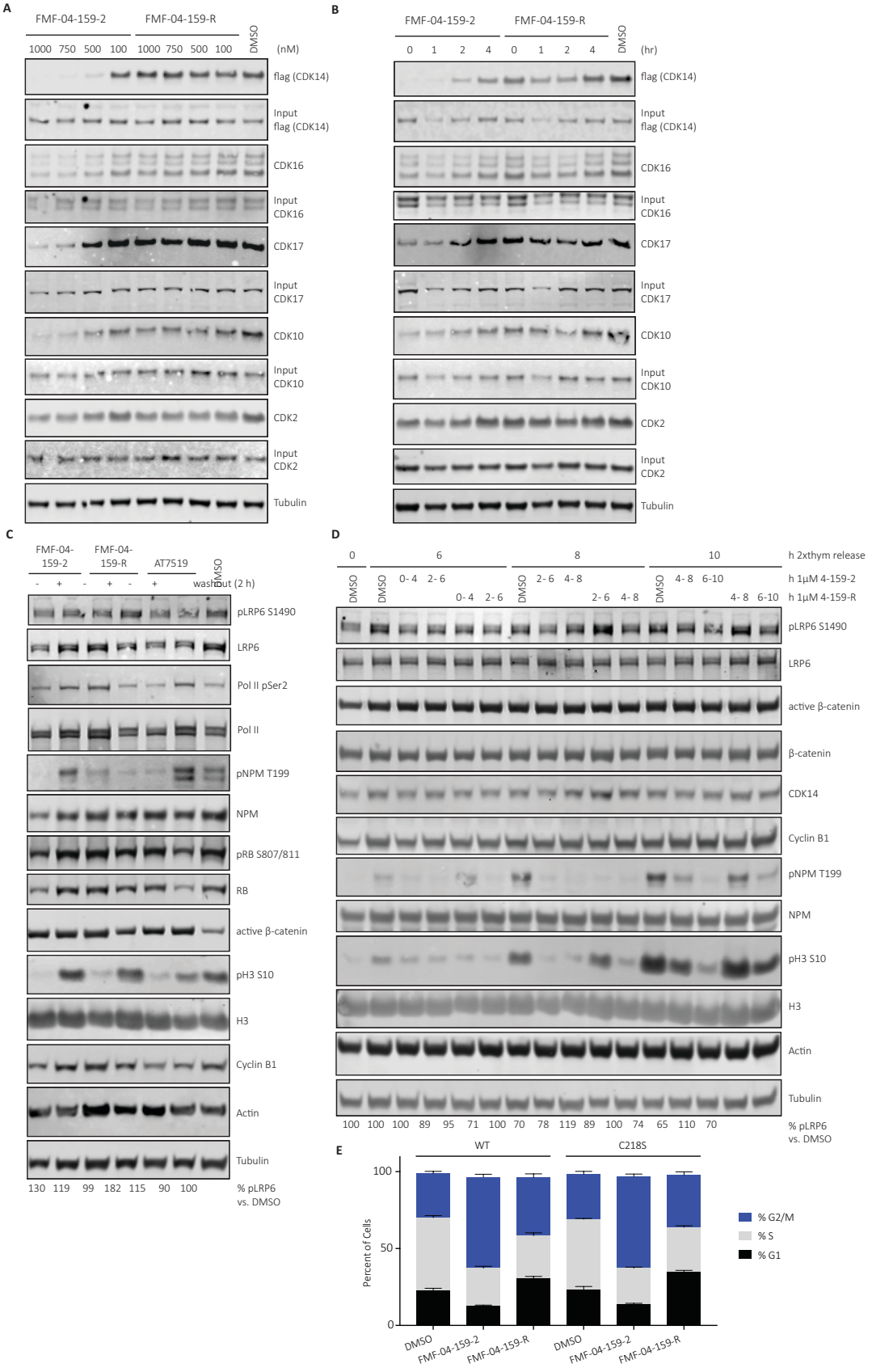

Mapping cellular consequences of CDK14 versus pan-TAIRE inhibition

LRP6 is basally phosphorylated by the *Drosophila* homolog of CDK14, L63, during mitosis specifically in a Wnt-independent manner, and is otherwise a substrate of GSK kinases (Davidson et al., 2009). Initially, we assessed LRP6 phosphorylation in unsynchronized HCT116 cells, where we did not observe substantial reduction of phosphorylated LRP6 S1490 levels, the only known substrate of CDK14 (Figure 3-7C). Given the cell cycle dependence of this CDK14-mediated phosphorylation, large changes in CDK14-dependent LRP6 phosphorylation are expected to be challenging to detect in unsynchronized cells, and this was confirmed by our initial observations (Figure 3-7C) (Davidson et al., 2009).

As we had found that FMF-04-159-2 had some activity against CDK2, we examined the phosphorylation status of reported CDK2 substrates in parallel (Lundberg & Weinberg, 1998). Interestingly, we did not observe major reductions in the levels of phosphorylated RB S807/811 after treatment with 1 μM FMF-04-159-2 and FMF-04-159-R, while a partial reduction was seen upon treatment with AT7519 at 1 μM, which was rescued by compound washout (Figure 3-7C). Inhibition of Nucleophosmin (NPM) T199 phosphorylation was observed at levels comparable to AT7519 upon treatment with either FMF-04-159-2 or FMF-04-159-R but was fully rescued upon compound washout for FMF-04-159-2, but not FMF-04-159-R (Figure 3-7C). This data corroborated that the experimental conditions identified by the competition cellular target engagement studies are suitable for examining the downstream effects of CDK14 inhibition.

CDK14-Cyclin Y expression peaks in mitosis, and this is the phase of the cell cycle in which CDK14 is reported to phosphorylate LRP6 at S1490 (Davidson & Niehrs, 2010; Mikolcevic et al., 2012; X. Wang et al., 2016). Thus, we examined LRP6 phosphorylation in the context of double

thymidine-synchronized cells, treated with FMF-04-159-2 or FMF-04-159-R in 4 h windows, harvested either with or without 2 h drug washout. In this setting, a partial reduction of pLRP6 (22 – 35 %) was seen during mitosis upon FMF-04-159-2 treatment, which was reached around 8 to 10 h after synchronization release, as reflected by peak expression of Cyclin B1 and pNPM T199, followed by increased expression of pH3 S10 (Figure 3-7D). This was only partially rescued when the reversible inhibitor FMF-04-159-R was used, consistent with the hypothesis that the multiple TAIRE kinases inhibited reversibly by FMF-04-159-R can also phosphorylate LRP6 in human cells (Davidson et al., 2009).

CDK14-Cyclin Y has also been reported to play a role in cell cycle progression in promoting the G1/S phase transition, although CDK14 expression peaks in mitosis (Pang et al., 2007; Shu et al., 2007; L. Yang et al., 2015). To assess cell cycle-related consequences of TAIRE kinase inhibition, CDK14 knockout HCT116 cells expressing either WT or C218S CDK14 were analyzed by FACS after treatment with FMF-04-159-2 or FMF-04-159-R (Figure 3-7E). Significant effects on cell cycle were observed, with increased numbers of cells in G2/M upon FMF-04-159-2 treatment (two-way ANOVA p_{adj} = .0001). Treatment with the reversible inhibitor FMF-04-159-R resulted in a more modest effect, resulting in increases in cells in G1 and G2/M and a reduction in S-phase cells. Similar effects were observed in both the WT and C218S CDK14-expressing cells, indicating that these effects were not solely due to covalent CDK14 inhibition.

Cell cycle data from HCT116 CDK14 CRISPR KO corroborates the observation that CDK14 covalent inhibition alone is not solely responsible for the observed cell cycle effects, as CDK14 KO cells did not show significant cell cycle differences at baseline compared to CDK14 WT or parental HCT116 cells (Figure 3-8A-C). Treatment with FMF-04-159-2 in the HCT116 CDK14 KO

cells results in a more modest G2/M accumulation, or partial rescue, compared to the WT cells (Figure 3-8D), suggesting that the non-CDK14 targets of FMF-04-159-2 are also contributing the observed cell cycle effects. Taken together, these data suggest that under the above-mentioned experimental conditions, CDK14 kinase activity does not play a driving role in regulating cell cycle progression in the HCT116 cell line. The reversible binding effects of FMF-04-159-2/-R, namely pan-TAIRE kinase inhibition and/or CDK2 inhibition, may be responsible for some of the observed G2/M arrest, suggesting possible functional redundancy in within the TAIRE family.

The effects on cell cycle upon FMF-04-159-2 treatment were also observed in additional cell lines of differing tissues of origin: PATU-8988T (pancreatic cancer), MDA-MD-231 (breast cancer) and HepG2 (liver cancer). The magnitude of G2/M accumulation varied between different cell types, though the effect overall was consistent with what was observed in the HCT116 cells (Figure 3-8E-G). We also investigated the phenotypic effects of treatment with FMF-04-159-2 and did not observe major effects on actin cytoskeleton in HCT116 cells (Figure 3-8H).

Figure 3-8. Cell cycle and phenotypic characterization of FMF-04-159-2. (A) Western blot analysis of HCT116 CDK14 knockout (KO) cell line (612) and CDK14 wild-type (WT) control. (B) Indel spectrum for both cell lines based on genomic DNA PCR, generated using the TIDE online software (Brinkman, Chen, Amendola, & van Steensel, 2014). (C) FACS PI analysis of parental HCT116 cells compared to HCT116 CDK14 KO and WT clonal cell lines. (D) FACS PI analysis of HCT116 CDK14 KO and WT cells, treated with DMSO or FMF-04-159-2 for 24 h. (E) FACS PI cell cycle analysis following 24 h treatment with DMSO or FMF-04-159-2 of HepG2 (F) of MDA-MD-231 and (G) of PATU-8988T cells. (H) HCT116 cells with CRISPR-mediated CDK14 knockout (KO) or wild-type (WT), treated with DMSO or FMF-04-159-2 for 24 h then stained with Phalloidin-488 and DAPI. Scale bar represents 50 microns. Images are representative of n=3 biological replicates.

Figure 3-8 (Continued).

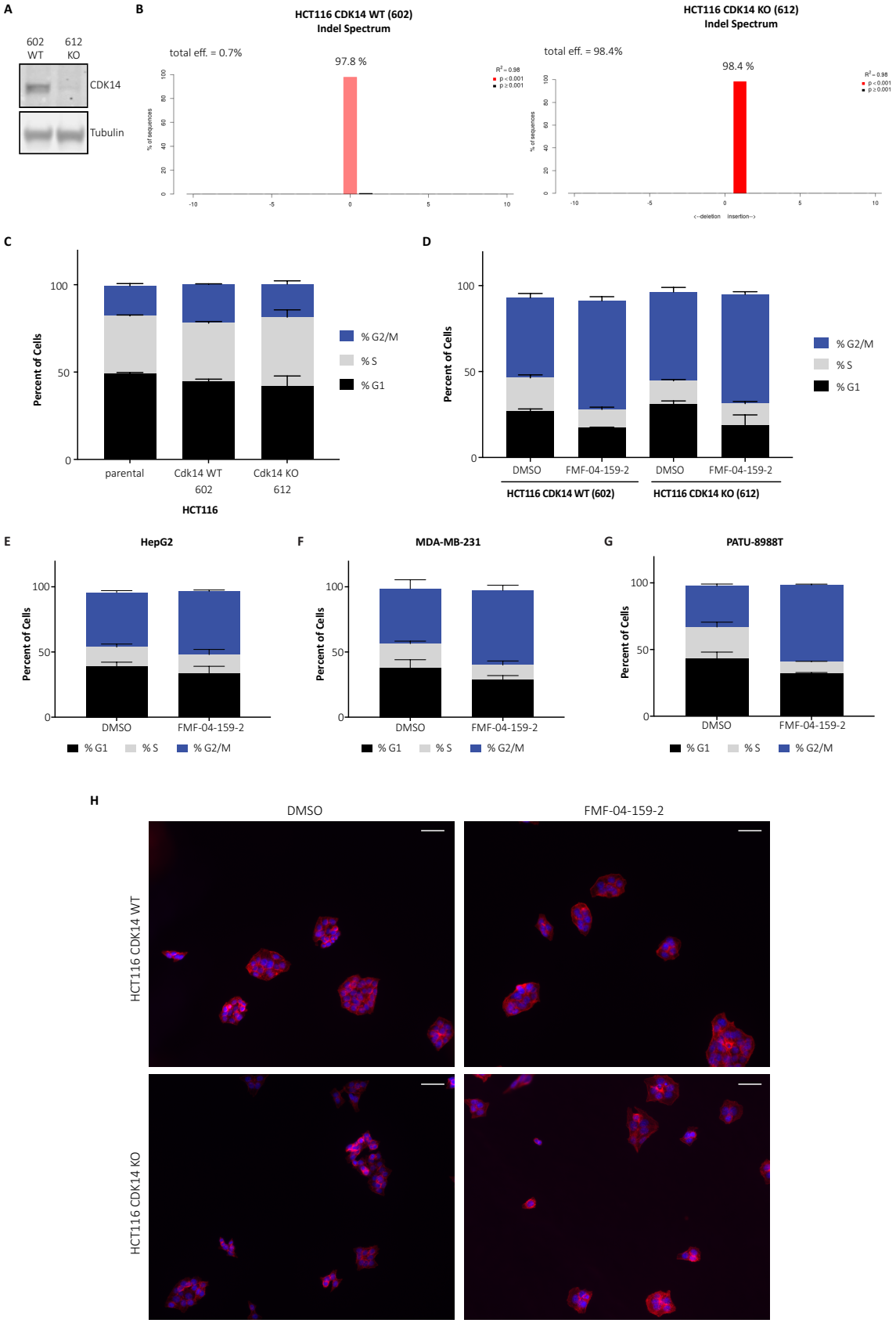

FMF-04-159-2 as a tool for determining CDK14 substrates and phenotypes

Having established conditions in which CDK14 inhibition is maximized while CDK2 inhibition is minimized (Figure 3-7), we sought to further characterize the immediate consequences of CDK14 inhibition versus pan-TAIRE kinase inhibition, as well as potentially identify substrates of CDK14 using FMF-04-159-2 as a chemical tool through dual proteomics and phospho-proteomics experiments.

For the dual proteomics and phospho-proteomics experiment, HCT116 cells were treated with FMF-04-159-2, with and without a 2 h washout step, before subjecting either total peptides or enriched phospho-peptides to tandem mass tag labeling (TMT) and quantitative LC-MS. Few significant changes in total protein levels were observed proteome-wide upon compound treatment (Figure 3-9A-B), consistent with the absence of reported direct transcriptional roles for the TAIRE kinases in the literature. Phospho-proteomics was conducted, and though direct treatment with FMF-04-159-2 resembled AT7519 treatment (Figure 3-9C-D, A), compound washout resulted in fewer significantly affected phospho-peptides (435 versus 1305 2-fold up- or down-regulated sites) (Figure 3-10A-D).

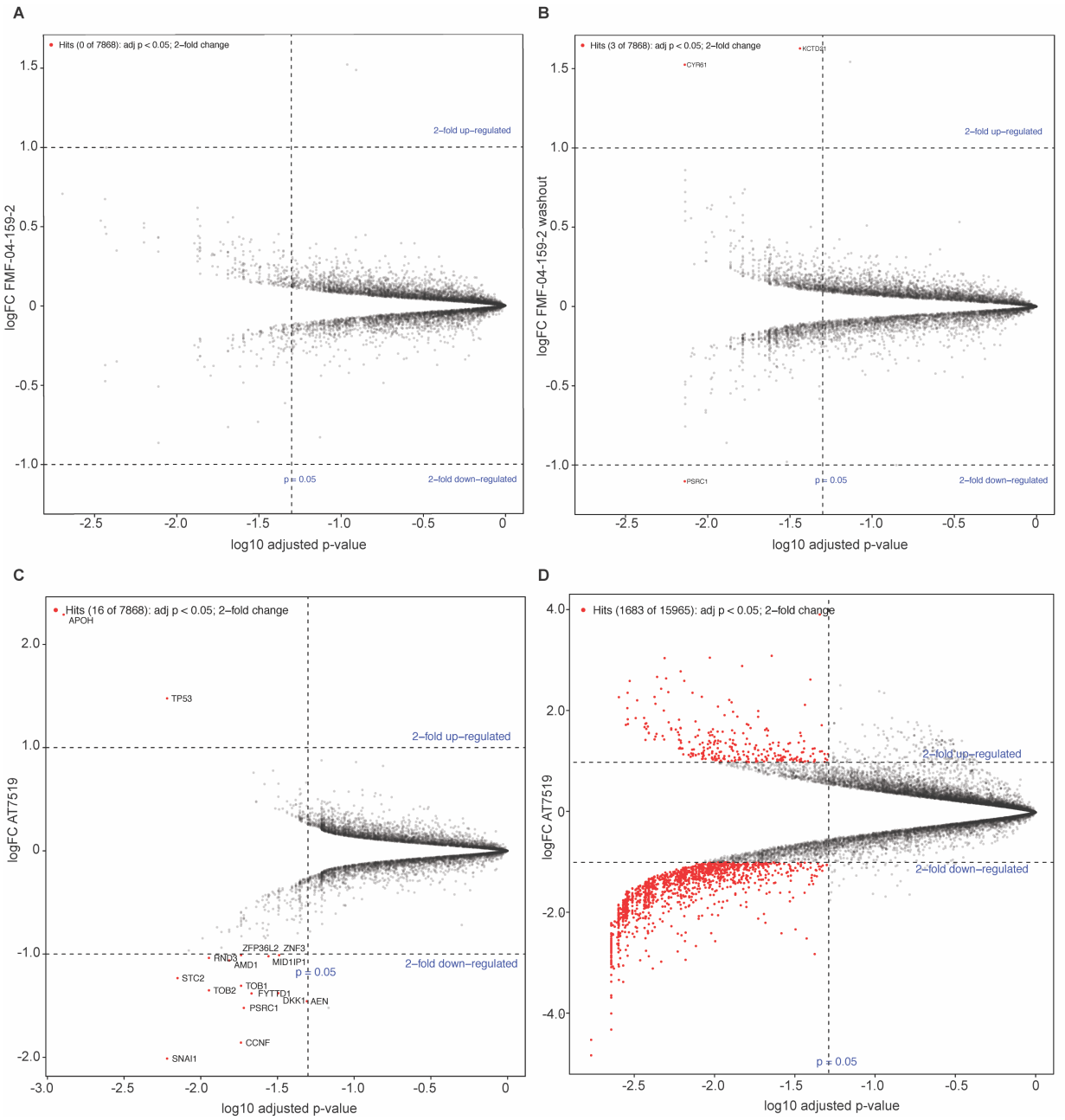

Figure 3-9. Proteomics and phospho-proteomics analysis for additional compounds and conditions. (A) Proteome-wide effect of FMF-04-159-2 4 h treatment of HCT116 cells. (B) Proteome-wide effect of FMF-04-159-2 4 h treatment of HCT116 cells followed by 2 h compound washout. (C) Proteome-wide effect of AT7519 4 h treatment of HCT116 cells. (D) Phospho-proteomics for AT7519 4 h treatment of HCT116 cells.

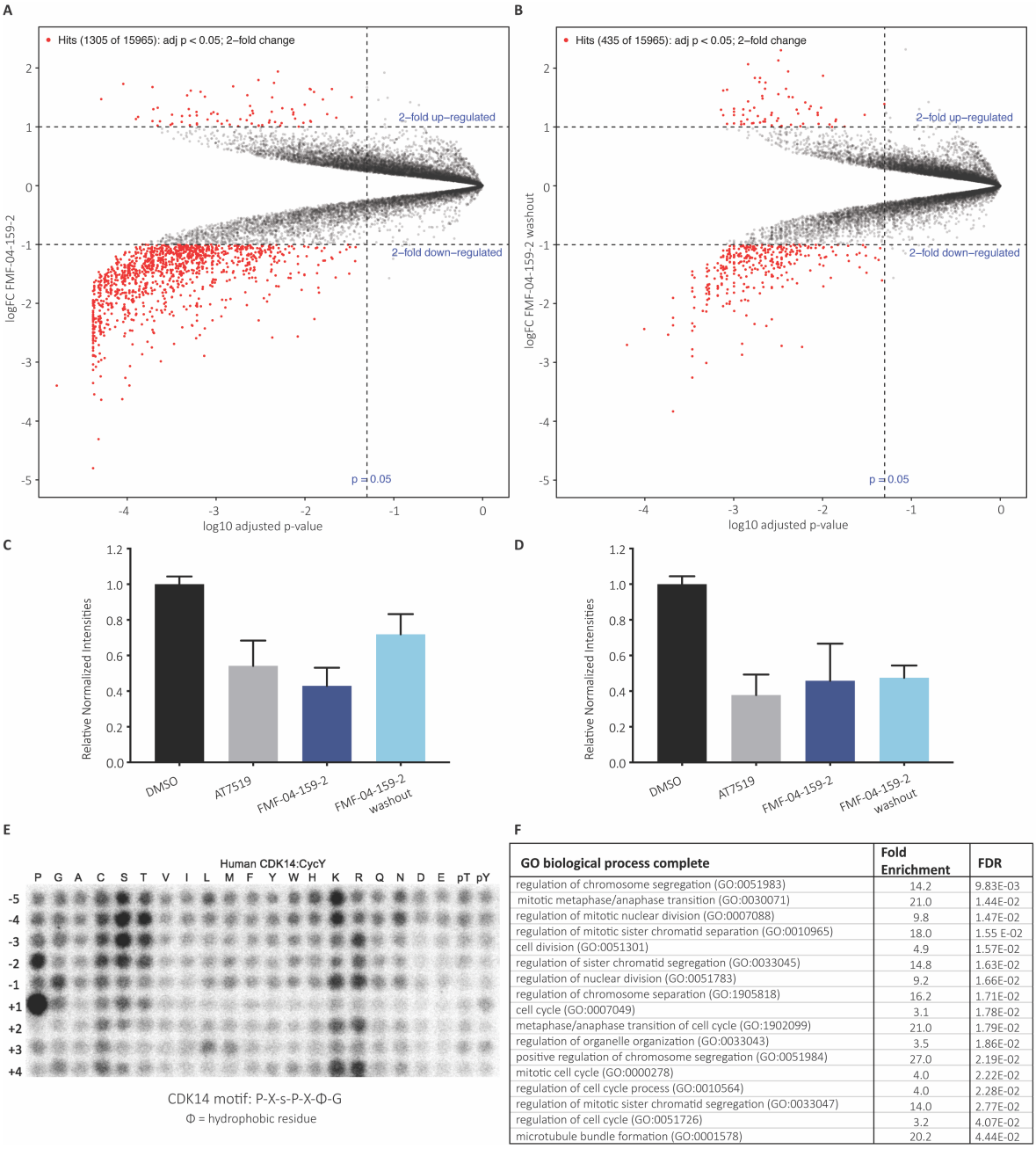

F

GO biological process complete	Fold Enrichment	FDR
regulation of chromosome segregation (GO:0051983)	14.2	9.83E-03
mitotic metaphase/anaphase transition (GO:0030071)	21.0	1.44E-02
regulation of mitotic nuclear division (GO:0007088)	9.8	1.47E-02
regulation of mitotic sister chromatid separation (GO:0010965)	18.0	1.55 E-02
cell division (GO:0051301)	4.9	1.57E-02
regulation of sister chromatid segregation (GO:0033045)	14.8	1.63E-02
regulation of nuclear division (GO:0051783)	9.2	1.66E-02
regulation of chromosome separation (GO:1905818)	16.2	1.71E-02
cell cycle (GO:0007049)	3.1	1.78E-02
metaphase/anaphase transition of cell cycle (GO:1902099)	21.0	1.79E-02
regulation of organelle organization (GO:0033043)	3.5	1.86E-02
positive regulation of chromosome segregation (GO:0051984)	27.0	2.19E-02
mitotic cell cycle (GO:0000278)	4.0	2.22E-02
regulation of cell cycle process (GO:0010564)	4.0	2.28E-02
regulation of mitotic sister chromatid segregation (GO:0033047)	14.0	2.77E-02
regulation of cell cycle (GO:0051726)	3.2	4.07E-02
microtubule bundle formation (GO:0001578)	20.2	4.44E-02

Figure 3-10. Cellular consequence of TAIRE kinase inhibition. (A) Volcano plot showing phospho-proteomics results for FMF-04-159-2 4hr treatment, analyzed using Bioconductor in R to assess fold change relative to DMSO. (B) Volcano plot showing phospho-proteomics results for FMF-04-159-2 4hr treatment followed by 2 h compound washout, analyzed using Bioconductor in R to assess fold change relative to DMSO. (C) Relative normalized TMT channel intensities for hits from FMF-04-159-2 direct treatment, reported as mean ± standard error. (D) Relative normalized TMT channel intensities for hits from FMF-04-159-2 washout condition with strong scores for CDK14 phosphorylation motif consensus, reported as mean ± standard error. (E) In vitro kinase assay results for phosphorylation of peptide library array by CDK14/Cyclin Y. (F) Top ten GO enrichment terms (Ashburner et al., 2000) for significantly downregulated phospho-peptides identified as hits from compound washout with strong scores for CDK14 phosphorylation motif consensus. FDR reported from Fisher's exact test.

To further triage the results of phosphoproteomic analysis, we conducted in vitro phospho-motif characterization of CDK14 using a peptide-scanning substrate array (Figure 3-10E). We identified P-X-s-P-X-Φ-G (Φ=hydrophobic) as the CDK14 phosphorylation motif. Reassuringly, this motif is in general agreement with the known substrate LRP6 S1490 (PP-s-PATE). We characterized another TAIRE kinase, CDK16, using the same peptide-scanning substrate array methodology, and established that this kinase has an identical consensus motif, with higher in vitro activity than CDK14 (Figure 3-11A). We observed the same consensus motif with CDK18, though with lower in vitro activity (Figure 3-11B). The identified TAIRE phospho-motif was distinct from the CDK2 motif, X-X-X-X-X-s-P-X-K-X, which was also shared by CDK3 (Figure 3-11C, D). This motif was used to score putative substrates based on phospho-peptide sequence matching to the predicted motif. Our peptide-scanning substrate array data provide not only a sequence motif to score putative substrates and bootstrap our phosphoproteomic analysis, but also further evidence for strong functional redundancy of the TAIRE kinases, given that CDK14, CDK16 and CDK18 likely regulate an overlapping pool of substrates based on the identical consensus phosphorylation motif.

All phospho-sites detected in the experiment were scored against the CDK14 phospho-motif, which identified 41 likely substrates from the set of 2-fold significantly down-regulated phospho-sites in the washout condition. Unfortunately, none of these high scoring substrates had available phospho-antibodies, antibodies or recombinant proteins commercially available to validate the identified putative substrates in a cellular context. Therefore, we synthesized four 15-mer peptides based on the protein sequences surrounding high scoring phospho-sites identified in washout proteomics. We also identified the sites on recombinant Rb protein that

are phosphorylated by CDK14, Rb S608 and Rb S780 (Figure 3-11E) and synthesized two 15-mer control peptides based on the sequences surrounding these residues to be used as positive controls. We incubated recombinant CDK14 protein, ATP, and the target peptide, and assessed serine/threonine phosphorylation by mass spectrometry. We found that both positive controls, as well as 3 of the 4 putative substrate peptides could be phosphorylated at the expected sites by CDK14/Cyclin Y in vitro (Figure 3-11F-J), with MS/MS spectra passing a 1% false discovery rate. In all five cases, phosphorylation was dramatically reduced by pre-treatment with FMF-04-159-2 (Figure 3-11). These data demonstrate that the putative substrate peptides identified by the phospho-proteomics experiment can indeed be phosphorylated by CDK14 in vitro. Further work is required to fully validate their parental proteins as bona fide CDK14 substrates in a cellular context.

The distribution of the 41 sites prioritized from the washout condition among reported cellular processes was calculated using gene ontology (GO) enrichment (Ashburner et al., 2000). This analysis showed strong enrichment for terms related to mitosis, cell cycle and cell division (Figure 3-10F). Though LRP6 itself was not detected, this further suggests that CDK14 plays a supporting, but not driving, role in mitosis, and that the covalent action of FMF-04-159-2 impairs mitotic cell cycle progression. Taken together, these results demonstrate the utility of FMF-04-159-2 as a tool compound to investigate CDK14 kinase biology and point to a role for CDK14 in mitosis and cell division. The weak anti-proliferative effects of FMF-04-159-2 indicate potential functional redundancy amongst the CDKs in driving mitosis and cell cycle progression.

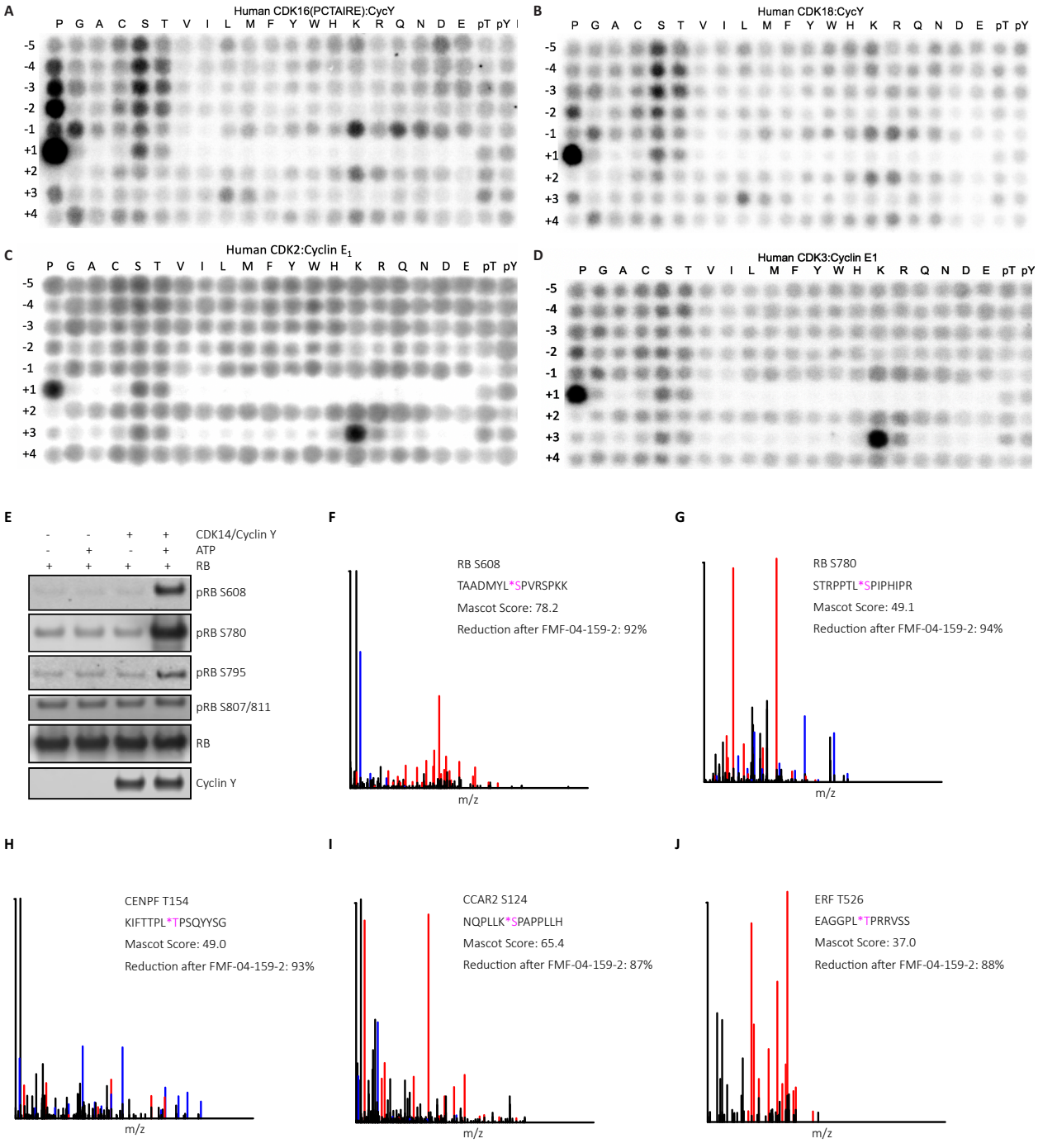

Figure 3-11. *In vitro* phospho-array kinase assay and phosphorylation of putative CDK14 substrates. *In vitro* kinase assay results for phosphorylation of peptide library array by (A) CDK16/Cyclin Y (B) CDK18/Cyclin Y (C) CDK2/Cyclin E1 and (D) CDK3/Cyclin E1. (E) *In vitro* kinase assay using CDK14/Cyclin Y with recombinant RB protein, followed by western blotting with phospho-specific RB antibodies. (F-I) MS/MS spectra of five indicated synthetic peptides phosphorylated in vitro by CDK14. Phosphorylated residue is indicated in pink. Singly charged, doubly charged, and phosphate neutral loss fragment ions are highlighted (y-type ions: red, b-type ions: blue). Included are Mascot search scores and the percentage of phospho-peptide precursor signal lost after CDK14 kinase was incubated with 1 µM FMF-4-129-2 for 1 h prior to in vitro phosphorylation reactions.

Discussion

Kinases, a large family of enzymes that catalyze the transfer of a phosphate from ATP to a specific substrate (Avendaño & Menéndez, 2008), are involved in almost every known signal transduction pathway in the cell. Understanding the kinases that regulate these pathways has led to the successful development of kinase inhibitors for diseases such as cancer, where cell growth is deregulated (Ferguson & Gray, 2018). To date, there are 38 FDA approved kinase inhibitors, making kinases one of the most productively targeted human gene families (P. Wu et al., 2015). It is well-recognized that the majority of approved kinase inhibitors have more than one kinase target, and this polypharmacology is postulated to confer an advantage over highly selective compounds in the context of heterogeneous and highly adaptive cancers (Davis et al., 2011; Klaeger et al., 2017). However, the poly-pharmacology of clinical kinase inhibitors is rarely rationally designed, and in some cases is the root of undesirable toxicity (Gujral, Peshkin, & Kirschner, 2014).

Research in academia and industry is heavily biased towards kinases with well-defined roles in cellular signaling (Fedorov et al., 2010). Consequently, the biological function of roughly 25% of kinases remains completely unknown, and roughly 50% of kinases are largely uncharacterized (Knapp et al., 2013). However, cancer driver mutations and the potential drug targets identified by genetic knockdown are distributed throughout the kinome, establishing a case for expanding the scope of current research efforts (Fedorov et al., 2010; McDonald et al., 2017; Tsherniak et al., 2017). An example of such a subfamily of kinases is the TAIRE CDKs, which include CDK14-18. Although genetic studies have implicated CDK14 and CDK16 as therapeutic

targets especially in the context of colorectal cancers (W. Zhang et al., 2016; Y. Zhou et al., 2014; Zhu et al., 2016), not much is known about their biological roles and substrate preferences.

The need for annotating the understudied branches of the kinome is broadly recognized, and is even a key component of the NIH "Illuminating the Druggable Genome" initiative (Fedorov et al., 2010; Fleuren et al., 2016; Rodgers et al., 2018). However, the absence of foundational data on the biochemical and biological functions of kinases of interest presents a huge challenge to small molecule chemical probe development. In the absence of characterized cellular inhibition phenotypes or substrates, innovative solutions must be found for establishing cellular target engagement. For example, in the course of this study, we developed a biotinylated probe, biotin-FMF-03-198-2, which acts to pull down CMCG family kinases from cell lysates. This assay using biotin-FMF-03-198-2 is broadly applicable to other kinase inhibitor projects and enables analysis of cellular target engagement by ATP-competitive small molecules for many kinases, including those that are understudied. We were able to use this tool to monitor the selectivity of synthesized compounds for CMGC kinases under various experimental conditions, eventually resulting in the development of FMF-04-159-2, that covalently targets CDK14 at C218 and possesses pan-TAIRE kinase biased selectivity profile.

Characterization of FMF-04-159-2 through pull-down assays and live cell target engagement using the NanoBRET platform verified sustained, covalent inhibition of CDK14, and reversible binding to the remaining TAIRE kinases CDKs 15-18. Reversible off-target activity against CDK2 was also measured. In the course of the development of FMF-04-159-2, compounds with increased selectivity for CDK14 and the TAIRE kinases showed reduced cytotoxic effects; FMF-04-159-2 was more than 200-fold less potent than FMF-03-198-2 in

HCT116 cell proliferation assays. The mild cytotoxicity of FMF-04-159-2 may be due to the residual off-target reversible CDK2 activity. This is in agreement with RNAi data in the publicly available PROJECT DRIVE database (McDonald et al., 2017). Taken together, these results suggest that selective CDK14 or pan-TAIRE inhibition is not a promising method for inhibiting colorectal cancer cell growth.

Analysis of known downstream substrates of the CDKs targeted by FMF-04-159-2 showed the expected effects of kinase inhibition. We were able to pharmacologically validate that LRP6 is a target of the human TAIRE-kinases in mitosis through compound treatment in synchronized cells, as evidenced by a maximal reduction of LRP6 pS1490 of 35%, as LRP6 is known to be phosphorylated by other kinases (Davidson & Niehrs, 2010). We did not observe a meaningful reduction in LRP6 S1490 phosphorylation in unsynchronized cells upon compound treatment, consistent with reported results.

Few direct substrates other than LRP6 have been identified and validated for CDK14. Development of FMF-04-159-2 as a covalent CDK14 inhibitor provided the opportunity to identify potential substrates, and better characterize the immediate cellular consequences of CDK14 kinase inhibition. The GO analysis terms derived from phospho-proteomics experiments performed on cells treated with FMF-04-159-2 were very similar to those produced by cells treated with AT7519. This could be due to the dominant effects of CDK2 inhibition but does not rule out the involvement of the pan-TAIRE kinase inhibition activity shared by both molecules impairing cell cycle progression, particularly in mitosis. Integrating kinase motif studies with significantly down-regulated phospho-sites in the compound washout condition allowed for identification of 41 additional putative CDK14 substrates. Pathway analysis of these putative

substrates suggested that CDK14 plays a role in mitotic cell cycle regulation and further supported CDK14's role in mitotic progression, in agreement with cell cycle analysis data. These phenotypes warrant further investigation.

Finally, the availability of a narrow-spectrum TAIRE family kinase tool compound enables study of this class of kinases upon acute inhibition, complementing previous genetic studies. As there is evidence that the TAIRE kinases have some redundancies, the ability to rapidly inhibit these kinases in concert may also aid in initial substrate and functional annotation.

Significance

CDK14 and other TAIRE cyclin dependent kinase family members (CDKs 15-18) are frequent drug off-targets, despite their biological functions remaining poorly understood. Here we describe the development of FMF-04-159-2, a tool compound that specifically targets CDK14 covalently. FMF-04-159-2 has a TAIRE-kinase biased reversible binding selectivity profile, with substantial off-target activity only detected against CDK2. In addition to validating LRP6 as a substrate of CDK14 in mitosis, unbiased investigation into the consequences of pan-TAIRE/CDK2 and covalent CDK14 inhibition through phospho-proteomics suggested that CDK14 plays a supporting role in cell cycle regulation. We characterize the cellular consequences of covalent CDK14 kinase inhibition, and describe characteristics of putative substrates of these kinases. When used in combination with FMF-04-159-R, or a compound washout control, FMF-04-159-2 is a valuable tool for further study of CDK14 kinase function.

Chapter 4: The effects of genetic modulation of CDK14 and its kinase activity on cell cycle, Wnt signaling and EMT

Author Contributions

Zainab M. Doctor designed and carried out all biological experiments pertaining to compound and target studies and performed relevant data analysis. Fleur M. Ferguson, a postdoctoral fellow in the Gray lab, provided experimental guidance. Nathanael S. Gray conceived of and held overall responsibility for the study.

Introduction

In order to complement the use of FMF-04-159-2 as a tool compound to interrogate CDK14 biology, several genetic and chemical biology approaches were used. These methods included: CRISPR/Cas9-mediated CDK14 knockout, rescue of knockout with wild type, kinase-dead, and cyclin-binding-deficient variants of CDK14, overexpression of these CDK14 protein variants, and acute chemical-induced targeted protein degradation of CDK14 using the dTAG system (Nabet et al., 2018). The use of these multiple orthogonal methods to perturb CDK14 activity in addition to the development of a chemical inhibitor allowed us to clarify and better-understand the roles of CDK14 in cell growth, cell cycle progression, Wnt signaling and epithelial-mesenchymal transition (EMT). Furthermore, it allowed us to begin to parse the CDK14-specific phenotypes observed with FMF-04-159-2 treatment and subsequent washout, given its non-covalent off-target activity against the other TAIRE kinases and CDK2.

Previous literature around CDK14 has used siRNA knockdown, with varying knockdown efficiency, to reduce levels of CDK14 in a number of different cancer types, including hepatocellular carcinoma, breast cancer, ovarian cancer and pancreatic cancer (X. Gu et al., 2015; Mao et al., 2017; Ou-Yang, Huang, & Sun, 2017; L. Yang et al., 2015; W. Zhang et al., 2016; Zheng et al., 2015). This knockdown resulted in modest impairment of cell growth and cell migration in several of these cancers. A growing body of recent literature also associates a handful of micro-RNAs with the regulation of CDK14 levels in cancer cell lines and demonstrate that blocking the micro-RNA results in CDK14 upregulation as well as increased cell growth and migration (Du et al., 2017; Ji et al., 2017; J. Li et al., 2019; Q. Li et al., 2018; Y. Sun et al., 2019; Tu

et al., 2019; B. Wang et al., 2017; Yan et al., 2018; J. Yang et al., 2018; Zheng et al., 2019). The specificity of this correlative observation was not further corroborated using CDK14 rescue.

Given the timescales of genetic perturbation using siRNA or shRNA for knockdown, or up-regulation by overexpression or indirectly using miRNA inhibitors, the specific substrates of CDK14 and the impact of acute CDK14 loss remain elusive. Furthermore, the role of CDK14's kinase activity, and not just its protein levels, in phenotypes related to cell growth, cell cycle, cell migration and Wnt signaling has not been investigated. The above-described genetic and chemical genetic experiments were carried out in a set of pancreatic cancer cell lines, which were genetically tractable and vary in their nature as more epithelial or more mesenchymal, making them an optimal system to interrogate CDK14 using the described approaches. Complementary studies were carried out in HCT116 cell as well to facilitate comparison to the effects of FMF-04-159-2.

Phenotypic effects of genetic modulation of CDK14 activity

We first characterized several pancreatic cell lines to determine their baseline expression of EMT and Wnt signaling markers (Figure 4-2). BxPC3 and PATU-8902 cells were more epithelial, showing string expression of E-cadherin. Mia-PaCa2 and PATU-8988T were more mesenchymal, showing complete E-cadherin loss, though interestingly no concurrent N-cadherin gain. Both cell lines were the only ones with TCF8/LEF expression. Mia-PaCa2 cells had the highest expression compared to all other cell lines of Vimentin and of the transcription factor Snail, which represses E-cadherin expression (Zeisberg & Neilson, 2009). BxPC3 cells showed a more intermediate phenotype, expressing both E-cadherin and N-cadherin, as well as ZO-1 and Slug at levels comparable to BxPC3 cells.

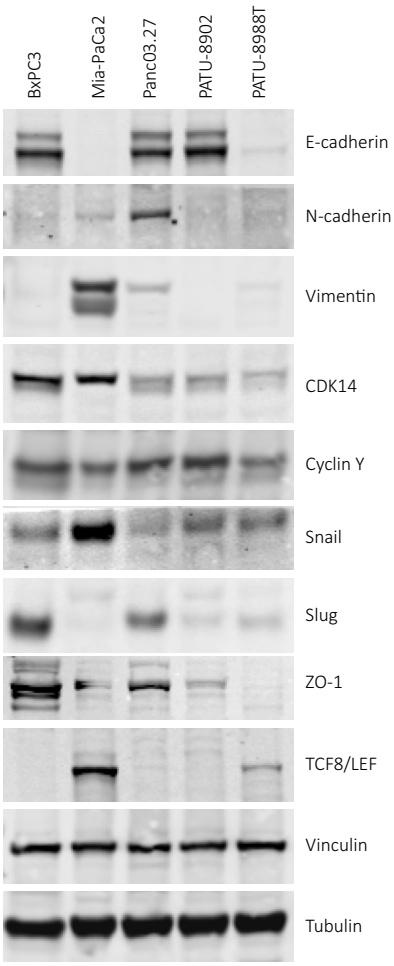

Figure 4-1. Western blot of a panel of pancreatic cancer cell lines, assessing basal expression of various EMT markers.

In this set of cell lines, CDK14 expression did not correlate with epithelial or mesenchymal cell status. In agreement with a previous publication on the expression of CDK14 in pancreatic cancer cells, the BxPC3 cell line expressed high levels of CDK14 (Zheng et al., 2015). Mia-PaCa2 cells also expressed higher levels of CDK14 compared to Panc03.27, PATU-8902 and PATU-8988T.

In order to test the hypothesis that CDK14 promotes cell migration, we overexpressed literature-reported CDK14 wild type, kinase dead and cyclin binding-deficient variants (Jiang et al., 2009; S. Li et al., 2014) in the more epithelial type pancreatic cancer cell lines. In PATU-8902

cells, overexpression of wild-type CDK14 showed lower levels of ZO-1, a tight junction protein, compared to expression of all non-active forms of CDK14 or the GFP control (Figure 4-2), suggesting that high levels of wild type CDK14 suppress ZO-1 expression. Slight effects on Claudin levels were observed, but did not seem to correlate with CDK14 kinase activity. In Panc03.27 cells, another pancreatic cancer cell line, similar effects were seen on ZO-1 with overexpression of WT but not mutant CDK14 (Figure 4-2). In this cell line, Vimentin levels were increased relative to the control GFP-expressing vector, but this increase did not appear to depend on CDK14 kinase activity or activation through cyclin binding.

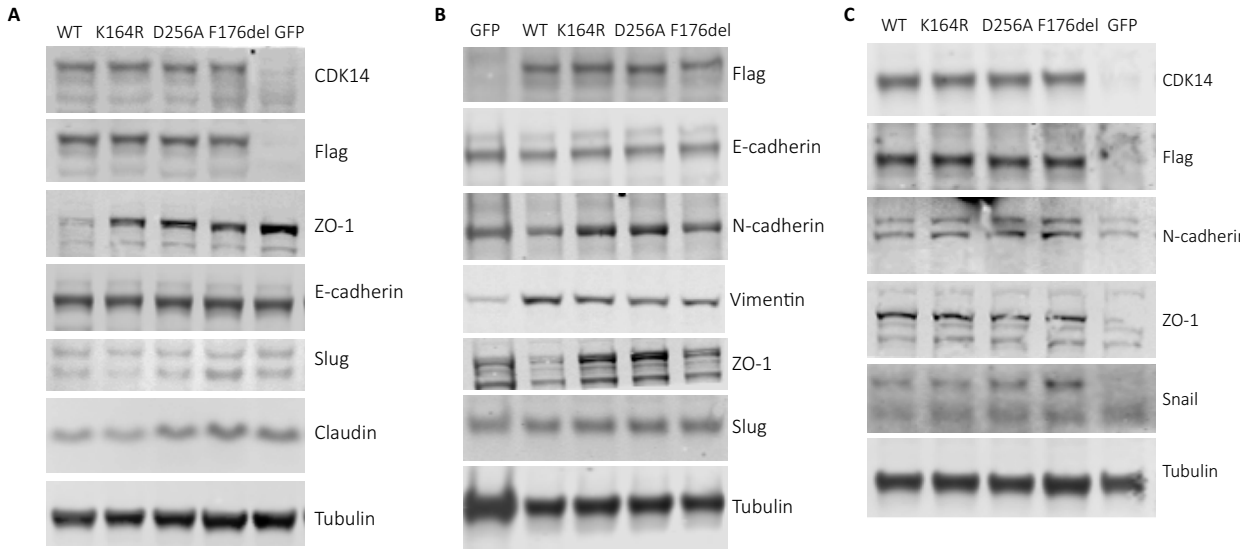

Figure 4-2. CDK14 variant overexpression in (A) PATU-8902 cells, (B) Panc03.27 cells and (C) BxPC3 cells.

These results suggest that the role of CDK14 in EMT may have components that depend both on its activity and on the protein itself. In BxPC3 cells, effects on EMT markers similarly did not seem to be dependent on CDK14 activity (Figure 4-2). Expression of any of the CDK14 protein variants resulted in increased ZO-1 compared to the GFP-only vector. Interestingly, N-cadherin was also very slightly increased. As N-cadherin expression is a pro-EMT marker, this effect agrees

with reported literature on CDK14 as promoting EMT but is not consistent with the increase in ZO-1. Further studies may be required to clarify the role of CDK14 in BxPC3 cells.

To further evaluate CDK14's role in pancreatic cancer contexts, we used CRISPR-Cas9 to create CDK14 clonal knockouts in PATU-8988T cells. Genomic DNA PCR showed disruption of the CDK14 sequence at the +1 position after the PAM sequence of the guide RNA, and also identified a control cell line with un-edited wild type CDK14 (Figure 4-3). There were no dramatic differences in growth over time between the CDK14 KO and WT cells under 2D conditions. However, there is a significant growth disadvantage by day 5 in the CDK14 KO cells compared to CDK14 WT in ultra-low attachment (ULA) growth conditions (Figure 4-3).

Growth in low attachment conditions is a measure reflective of cellular transformation, recently proposed as a replacement for soft agar assays (Rotem et al., 2015). To investigate the state of transformation at the molecular level, we assessed the basal expression of EMT markers. These two cell lines did not show significant difference in EMT markers except for a loss of Vimentin in the CDK14 knockout but was paired with a slight increase in N-cadherin in the knockout compared to wild type (Figure 4-3). There was no difference in ZO-1 expression as there was in the more epithelial pancreatic cancer cell lines.

Given CDK14's reported roles in Wnt signaling, we also examined the basal expression of phospho-LRP6 S1490 and active β-catenin. There appeared to be a slight increase in basal phospho-LRP6 S1490 levels in the PATU-8988T CDK14 KO cells compared to CDK14 WT (Figure 4-3). FACS propidium iodide analysis did not show dramatic differences in cell cycle phase distribution between the two clonal cell lines (Figure 4-3). To compare cell cycle progression in CDK14 KO versus WT cells, we assessed cell cycle markers after release from double thymidine

block. CDK14 WT PATU-8988T cells showed a clear peak in phospho-LRP6 S1490 in mitosis, while this phosphorylation did not fluctuate with cell cycle in the CDK14 KO PATU-8988T cells (Figure 4-3). These results agreed with previous literature that reports LRP6 as the substrate of CDK14 (Davidson et al., 2009), as well as characterized effects of FMF-04-159-2 in double thymidine-synchronized cells (Figure 3-7). Interestingly, basal levels of phospho-LRP6 in the CDK14 KO line were slightly higher than those in the WT cell line and were comparable to the peak phosphorylation during mitosis in the CDK14 WT line (Figure 4-3). The significance of this mitotic phosphorylation, or its potential compensation for CDK14 KO, is not well understood (Davidson & Niehrs, 2010).

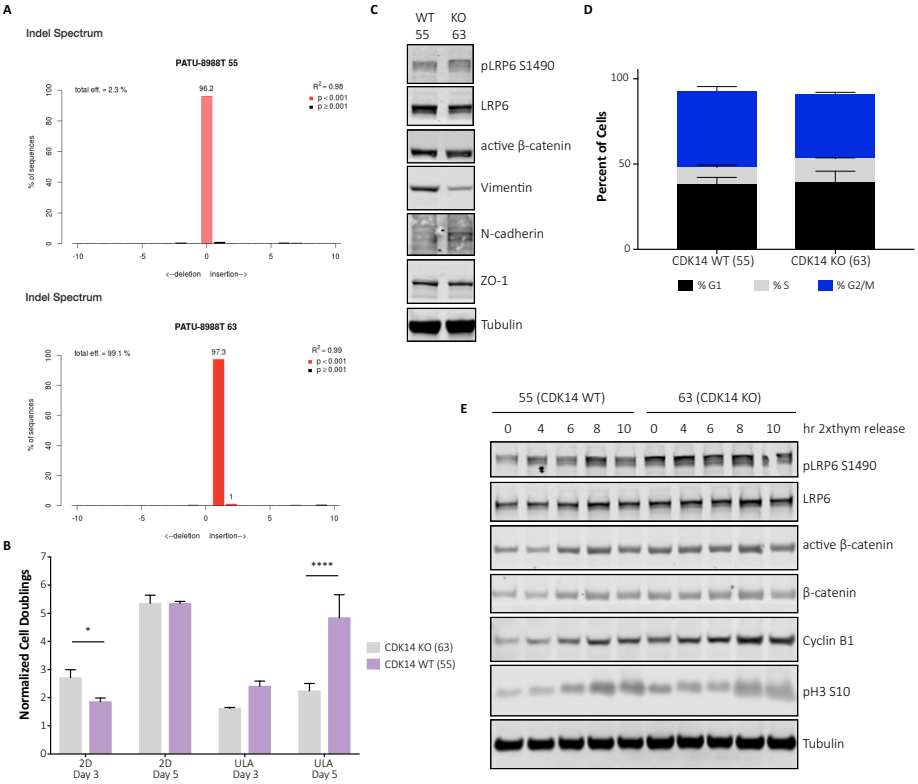

Figure 4-3. Phenotypic effects of CDK14 knockout in PATU-8988T cells. (A) TIDE analysis (Brinkman et al., 2014) following genomic DNA PCR of edited clonal cell lines. (B) Growth over time of PATU-8988T CDK14 WT and KO cell lines. Significance assessed by two-way ANOVA. (C) Western blot for basal differences in EMT markers and Wnt signaling in CDK14 WT and KO PATU-8988T cells. (D) FACS PI analysis of PATU-8988T CDK14 WT and KO cells. (E) Western blot of CDK14 WT and KO PATU-8988T cells at indicated timepoints after double thymidine block and release to monitor cell cycle progression.

To further understand the role of CDK14 kinase activity in EMT, wild-type and kinase-dead and cyclin-binding mutant variants of CDK14 were expressed to rescue CDK14 KO in the PATU-8988T line. The relative growth of these rescue cell lines was evaluated 72 hours after plating in 2D and ultra-low attachment (ULA) condition (Figure 4-3). Very modest growth defects were evident with the CDK14 inactive variants and the GFP control compared to the CDK14 WT rescue. In 2D growth conditions, effects of the CDK14 K164R rescue, the ATP-binding mutant, looked more similar to CDK14 WT than to GFP and the other inactive mutants, however none of these growth effects were statistically significant (Figure 4-3).

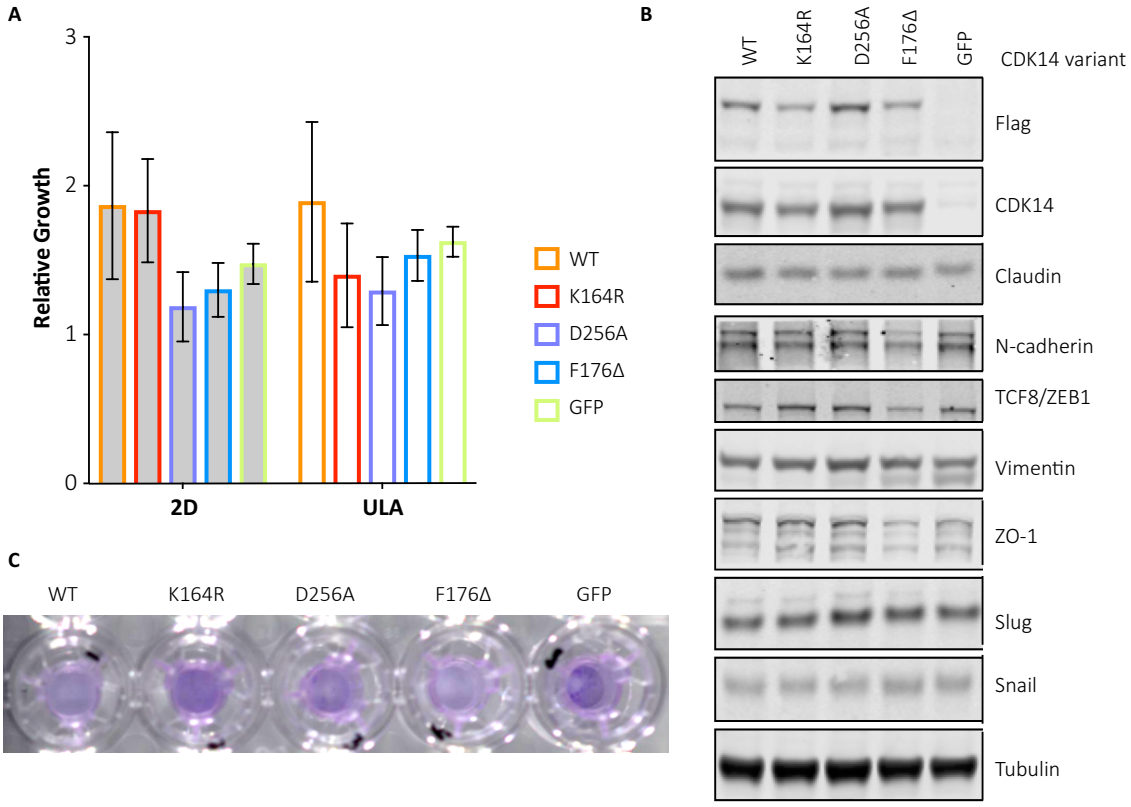

Figure 4-4. Effect of CDK14 variant rescues of CDK14 KO PATU-8988T cells on cell growth and EMT markers. (A) Relative growth in 2D and ultra-low attachment (ULA) conditions upon expression of CDK14. (B) Western blot for markers of Wnt signaling and EMT in these cell lines. (C) Trans-well migration assay of CDK14 KO PATU-8988T cells expressing CDK14 variants.

We next evaluated the effects of EMT markers in the PATU-8988T cell context in the CDK14 rescue cell lines using western blot analysis to evaluate EMT markers. There were no clear effects on EMT markers that were dependent on CDK14 activity. The CDK14 F176Δ cyclin-binding mutant expressed more epithelial cell markers, including lower ZO-1, more comparable to the GFP control than the WT and other variants. We also observed lower TCF8/ZEB1 and concordantly, lower N-cadherin, though E-cadherin was not increased to detectable levels (Figure 4-5).

The wild-type, ATP binding mutant and kinase-dead CDK14 variants showed comparable levels of EMT markers, which were higher than the CDK14 F176Δ cyclin-binding mutant rescue. Taken together, this data indicates that the cyclin-binding deficient CDK14 results in a more epithelial phenotype in the PATU-8988T cell lines. Since Cyclin Y is responsible for recruitment of CDK14 to the plasma membrane (Jiang et al., 2009), there may be a localization component to CDK14's role in EMT in the PATU-8988T cells. A phenotypic assay of EMT in the PATU-8988T CDK14 rescue lines did not further distinguish between more epithelial and more mesenchymal behavior as assessed by trans-well migration (Figure 4-5). CDK14 F176Δ shows weaker migration but looks more similar to WT than the ATP-binding, kinase-dead and GFP control rescues, however, crystal violet is a qualitative measure, so it is difficult to make quantitative comparisons between different rescue cell lines.

Evaluating the effect of CDK14 variant rescues in the PATU-8988T CDK14 KO cells showed that the cyclin binding mutant F176Δ has slightly lower basal levels of phospho-LRP6 S1490 and active β-catenin than the other variants, and is similar to the GFP control rescue (Figure 4-5). This is consistent with the requirement of Cyclin Y to recruit CDK14 from the cytoplasm to the

plasma membrane to phosphorylate the transmembrane LRP6 in a mitosis-dependent manner (Jiang et al., 2009; X. Wang et al., 2016). The most striking result is the decreased expression of Dvl2, the non-canonical Wnt marker, for the F176Δ CDK14 rescue compared to the wild-type and kinase-dead variants (Figure 4-5). CDK14 was previously reported to up-regulate non-canonical Wnt signaling, but not canonical Wnt signaling, in hepatocellular carcinoma cell lines, even without Cyclin Y co-expression (T. Sun et al., 2014). This data suggests a requirement for CDK14 binding to Cyclin Y in order to impact non-canonical Wnt signaling in pancreatic cell contexts, which contradicts the previous study.

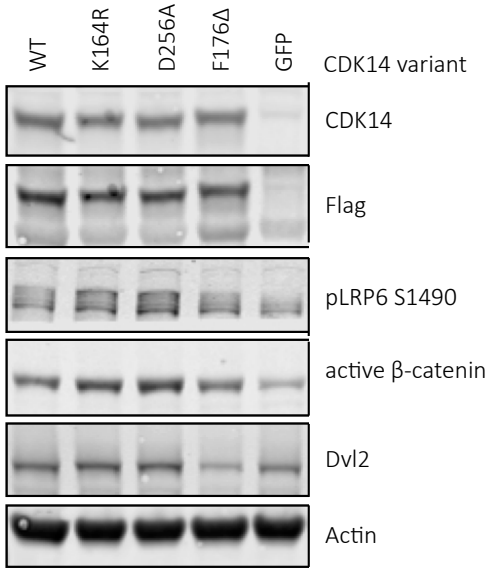

Figure 4-5. Effect of CDK14 variant rescues of CDK14 KO PATU-8988T cells on Wnt signaling markers, assessed by western blotting.

Since there is likely functional redundancy across the TAIRE kinases, as determined from characterization of FMF-04-159-2 described in the previous chapter, it is possible that other TAIRE kinases are able to compensate in the absence of active CDK14 and effect non-canonical Wnt signaling under certain contexts. However, in the absence of CDK14 binding to Cyclin Y,

there seems to be a dominant effect which prevents Dvl2 increase by other mechanisms. This is consistent with a reported role for CDK14 in regulating Cyclin Y levels through feedback (S. Li et al., 2014).

Rapid and specific degradation of CDK14 using the dTAG system

To specifically investigate the function of CDK14, we turned to dTAG system, a chemical genetic approach to induce acute and specific loss of CDK14 (Nabet et al., 2018). The CDK14 CRISPR lines are clonal, they require time to isolate and thus have the opportunity to adapt in culture between when the edit occurs, and different phenotypes are assessed. In the dTAG system, mutant FKBP12 ($FKBP12^{F36V}$) acts as a degradation tag and is fused to a protein of interest, here CDK14. The F36V mutation introduces a 'hole' in the FKBP12 binding site that accommodates a 'bump' on an $FKBP12^{F36V}$-specific binding ligand, AP1867, which does not effectively bind to wild-type FKBP12 (Clackson et al., 1998). Using a recently recognized strategy for the generation of small molecule degraders (Winter et al., 2015), we synthesized heterobifunctional molecules (dTAG molecules) by conjugating AP1867, the $FKBP12^{F36V}$ targeting compound, to thalidomide, which is a potent ligand for $CRL4^{CRBN}$. These molecules bring the $FKBP12^{F36V}$-fusion protein and $CRL4^{CRBN}$ into close proximity, thus inducing rapid ubiquitination and subsequent proteasomal degradation of the $FKBP12^{F36V}$-CDK14 fusion protein while sparing endogenous FKBP12 (Figure 4-6).

To maintain continuous expression of CDK14, the $FKBP12^{F36V}$-CDK14 fusion protein was first expressed in PATU-8988T cells before CRISPR/Cas9 was used to disrupt endogenous CDK14, and single cell clones were isolated. A silent mutation was first introduced to the CDK14 coding

sequence to disrupt the PAM sequence, making it insensitive to sgCDK14. CDK14 is rapidly degraded, as early as 15 minutes after dTAG treatment (Figure 4-6). We verified the mechanism of degradation, as pre-treatment with either end of the molecule (lenalidomide or AP1867) rescued dTAG-induced degradation (Figure 4-6). Pre-treatment with the proteasome inhibitor Carfilzomib or the neddylation inhibitor MLN4924 also resulted in rescue, indicating that degradation is neddylation- and proteasome-dependent.

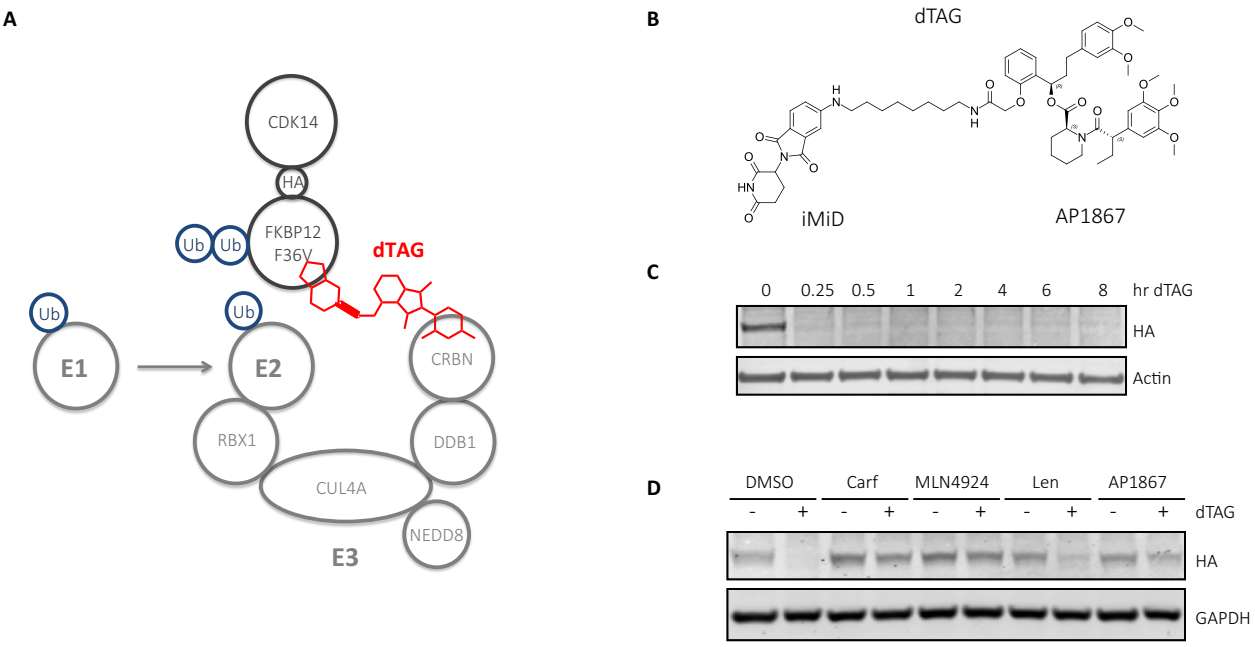

Figure 4-6. CDK14 dTAG in PATU-8988T cells. (A) Schematic of dTAG system applied to CDK14. (B) dTAG molecule used in CDK14 studies. (C) Western blot showing timecourse of CDK14 degradation at indicated timepoints after dTAG treatment. (D) Western blot showing effect of 2 h treatment with DMSO or dTAG after 2 h pre-treatment with indicated compound

We next evaluated the impact of acute CDK14 loss at longer timepoints. Treatment with dTAG did not result in a significant growth defect at 72 h, particularly when compared to treatment with either end of the molecule, AP1867 or lenalidomide (Figure 4-6). The slight decrease in growth seen at the highest concentration of compound, well above the

concentration needed to see degradation (dTAG was typically used at 250nM for these experiments, though complete degradation was also observed at lower concentrations). Degradation was sustained out to 72 h after a single dTAG treatment, as verified by western blot (Figure 4-7). Active β-catenin was reduced at the 48 hour and 72 h timepoints after dTAG treatment compared to the DMSO control.

There was variation in expression of some of the EMT markers based on cell density. Comparing DMSO to dTAG treatment, there was a decrease in Vimentin with dTAG treatment compared to DMSO at 24 h, consistent with CDK14 promoting EMT (Figure 4-7). There were no other significant effects on EMT markers upon dTAG treatment, and no dramatic changes at the later timepoints. This could be indicative of cells adapting to CDK14 loss, or more likely, cellular changes which occur as a result of increases in cell density in 2D culture. The effect on Vimentin recapitulated what was observed in the PATU-8988T CDK14 CRISRPR lines (Figure 4-3).

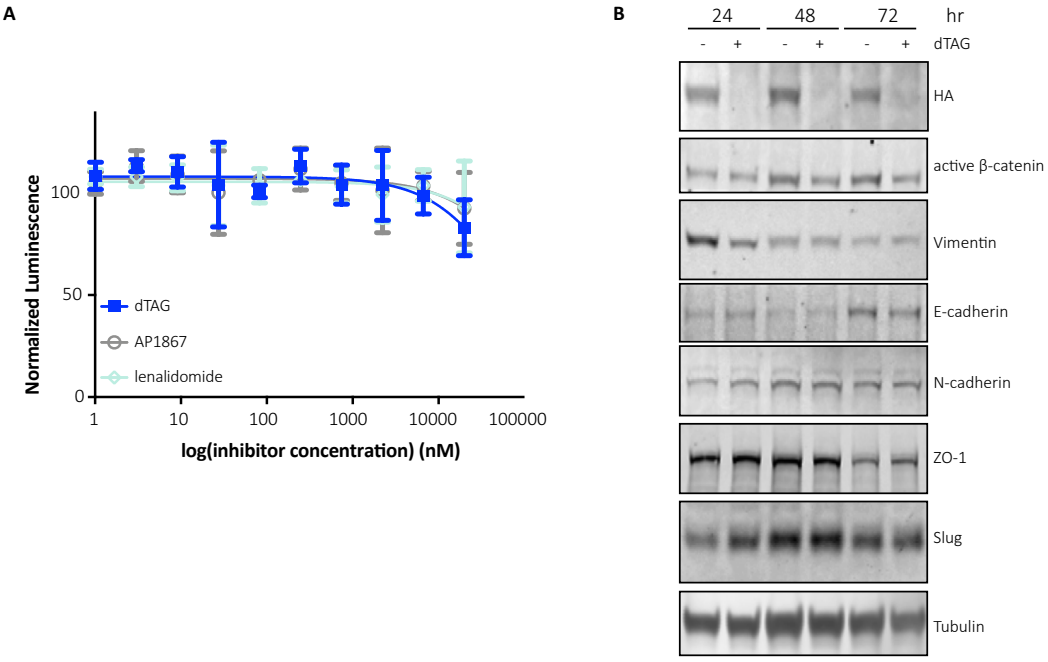

Figure 4-7. Long term effects of CDK14 loss using dTAG-CDK14 in PATU-8988T cells. (A) Antiproliferation assay in PATU-8988T CDK14 dTAG cell line, assessed 72 h after treatment with the indicated compound. (B) Western blot analysis of EMT markers after treatment with DMSO or dTAG for the indicated time.

Prominent cell cycle effects were not observed after 48 h treatment with DMSO or dTAG based on FACS PI analysis (Figure 4-7), consistent with what was observed in the CDK14 CRISPR lines. To investigate cell cycle more closely, we assessed the effect of dTAG treatment on cell cycle progression after release from double thymidine block using western blotting. The mitotic peak in LRP6 S1490 phosphorylation was observed around 10 hours, but with dTAG treatment this mitosis-dependent peak was abrogated (Figure 4-8). These results matched what was observed in the PATU-8988T CDK14 CIRSPR lines (Figure 4-3), lending further support to the fact that CDK14 is required for mitosis-dependent LRP6 S1490 phosphorylation. Basal levels of phospho-LRP6 with dTAG treatment were lower than those seen in the PATU-8988T CDK14 KO (63) cell line (Figure 4-3).

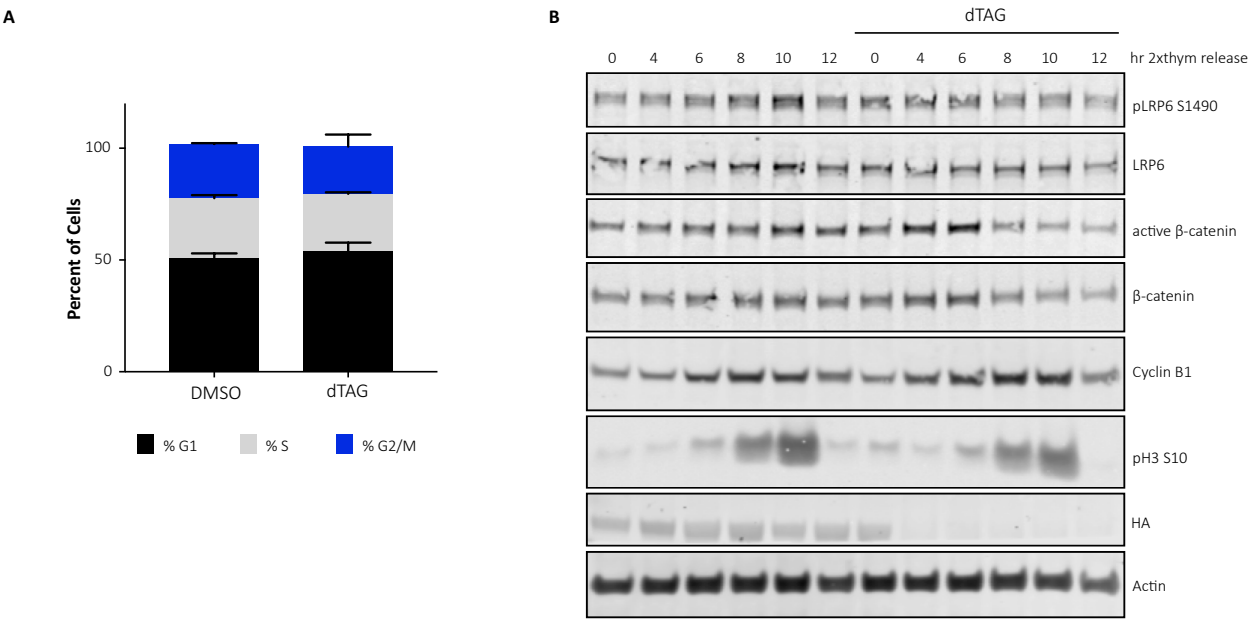

Figure 4-8. Cell cycle effects of CDK14 loss using dTAG-CDK14 in PATU-8988T cells (A) FACS PI analysis after 48 h treatment with DMSO or dTAG. (B) Western blot of CDK14 dTAG PATU-8988T cells at indicated timepoints after double thymidine block and release to monitor cell cycle progression, with or without dTAG treatment at the time of thymidine release.

To further characterize the effects of short term dTAG loss in an unbiased manner, we performed proteomics after 4 h treatment with dTAG. At this short timepoint, there were no significant proteome-wide effects in response to acute CDK14 loss (Figure 4-9). Given CDK14's reported roles in cell cycle and in LRP6 S1490 phosphorylation in mitosis, we also performed proteomics in double thymidine synchronized cells. Cell were treated with DMSO or dTAG at the time of release (thymidine washout) and harvested after 8 h. There were 26 proteins of the 8497 detected which were significantly up- or down-regulated (Figure 4-7, Table 4-1, Table 4-2).

There were no significantly enriched pathways in the set of up- and down-regulated genes as assessed by GO enrichment (Ashburner et al., 2000), likely due to the low number of proteins. Based on Reactome (Fabregat et al., 2018), targets such as CENPF, BIRC5 and GTSE1 are part of cell cycle checkpoints and G2-M transition and KIF20A in M-phase and cytokinesis. Down-regulated targets such as FASN are involved in fatty acid biosynthesis, while SLBP involved in mRNA processing and PLIN2 and ATAD2 in gene transcription. Further experiments are required to determine whether these changes are directly dependent on CDK14, and what their phenotypic consequence is, if any.

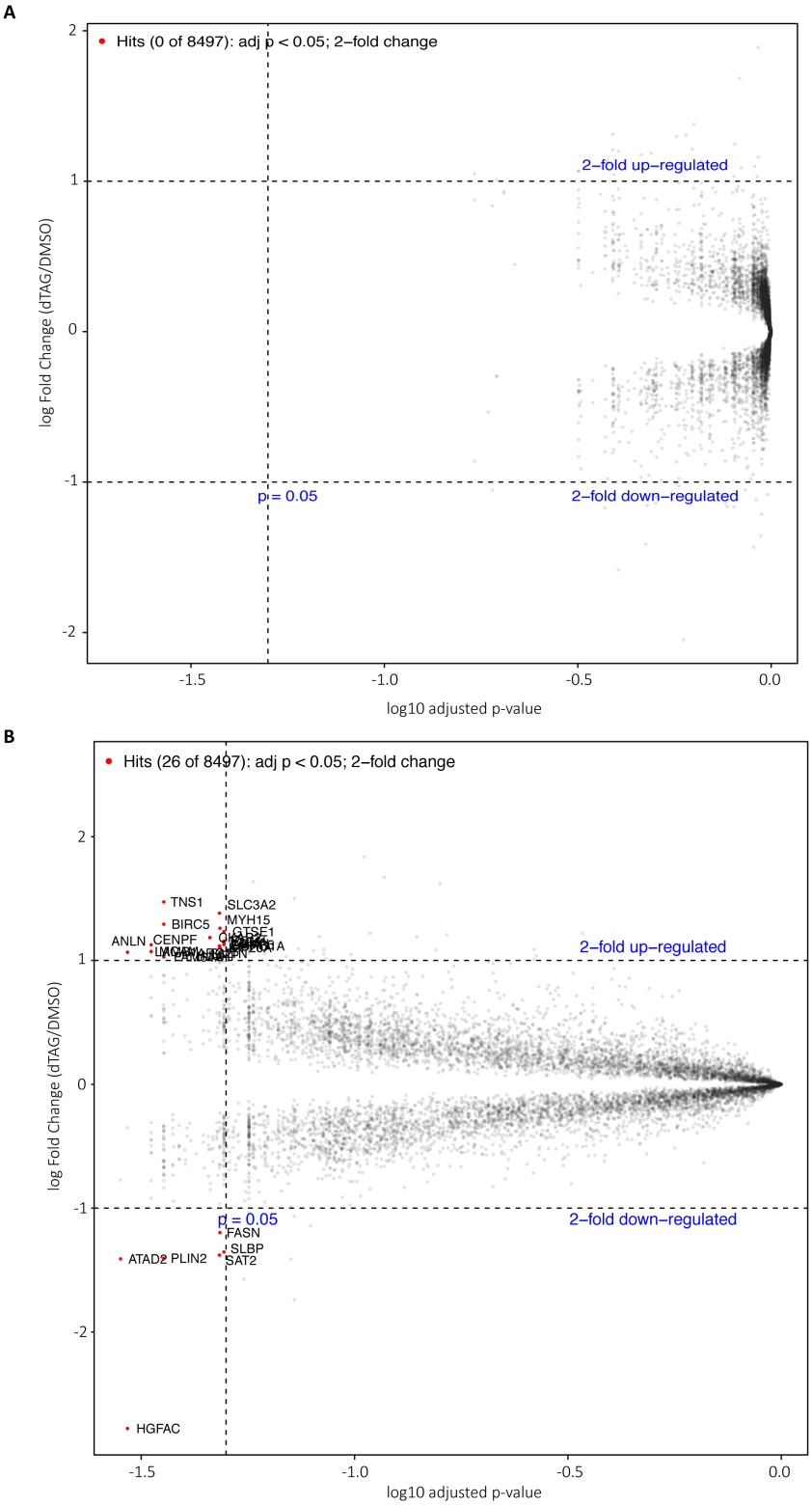

Figure 4-9. Proteomics in PATU-8988T CDK14 dTAG. (A) Proteome-wide effects of 4 h dTAG treatment. (B) Proteome-wide effects of dTAG treatment in double thymidine synchronized cells in mitosis (8 h after release).

Table 4-1. Up-regulated proteins upon dTAG treatment in synchronized cells in mitosis.

Protein	logFC	adj p-value
ANLN	1.067	0.0294
MCAM	1.074	0.0334
CENPF	1.127	0.0334
LAMB1	1.071	0.0334
TNS1	1.473	0.0357
BIRC5	1.293	0.0357
FAM64A	1.029	0.0357
HJURP	1.041	0.0405
SMTN	1.058	0.0442
CKAP2	1.185	0.0458
ARG2	1.059	0.0411
KIF20A	1.104	0.0484
CORO1A	1.118	0.0482
GTSE1	1.233	0.0494
LGMN	1.135	0.0494
KLF5	1.148	0.0494
SLC3A2	1.382	0.0482
ECM1	1.157	0.0494
AKAP5	1.129	0.0494
MYH15	1.260	0.0484

Table 4-2. Down regulated proteins upon dTAG treatment in synchronized cells in mitosis.

Protein	logFC	adj p-value
ATAD2	-1.410	0.028
HGFAC	-2.780	0.029
PLIN2	-1.405	0.036
SLBP	-1.354	0.049
FASN	-1.197	0.048
SAT2	-1.379	0.048

Concordance between FMF-04-159-2 compound effects and genetic modulation of CDK14 activity

In an attempt to further corroborate the effects of FMF-04-159-2 described in the previous chapter, we performed similar in the matched HCT116 cell line. dTAG CDK14 experiments in HCT116 cells were unsuccessful. Incomplete degradation was observed of the fusion protein, even at longer timepoints (Figure 4-10). Higher concentrations of dTAG did not improve degradation (Figure 4-10), and in both cases at most 70-75% degradation of the fusion protein was observed. This may be due to low expression of cereblon in these cell lines. However, dTAG molecules using a VHL-recruiting ligand rather than an iMiD to recruit cereblon were similarly unsuccessful.

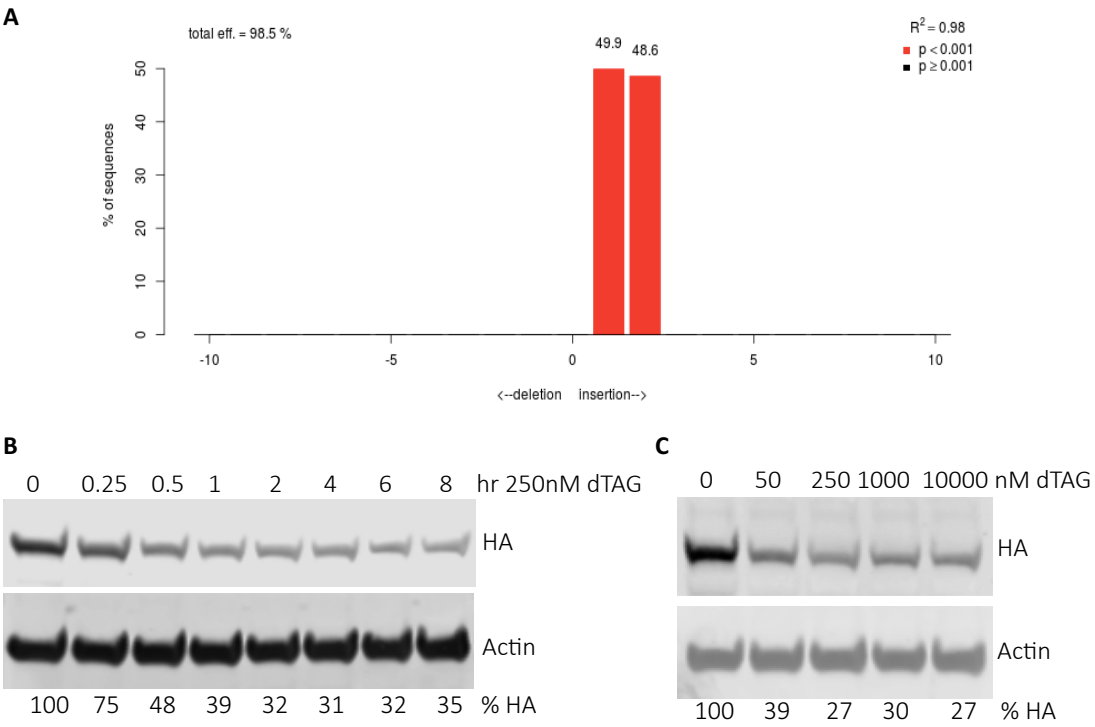

Figure 4-10. HCT116 CDK14 dTAG cells. (A) TIDE analysis (Brinkman et al., 2014) following genomic DNA PCR of edited clonal cell line. (B) Time-course of dTAG treatment using 250nM compound, followed by western blot analysis. (C) Concentration-course of dTAG treatment for 4 h, followed by western blot analysis.

CDK14 KO and WT paired clonal cell lines were also generated in the HCT116 background (Figure 3-8). In addition to their use in the characterization of FMF-04-159-2, CDK14 wild type, kinase-dead and cyclin binding-deficient variants were introduced back as rescues. There weren't any significant growth differences in the rescue cell lines at 72 h after plating (Figure 4-11). When assessing trans-well migration, there weren't clear CDK14 activity-dependent trends, similar to observations in the PATU-8988T cells. By western blot, the CDK14 KO line showed slightly higher expression of Snail and Slug, which repress E-cadherin, though E-cadherin was not dramatically decreased in the CDK14 KO line compared to WT (Figure 4-11).

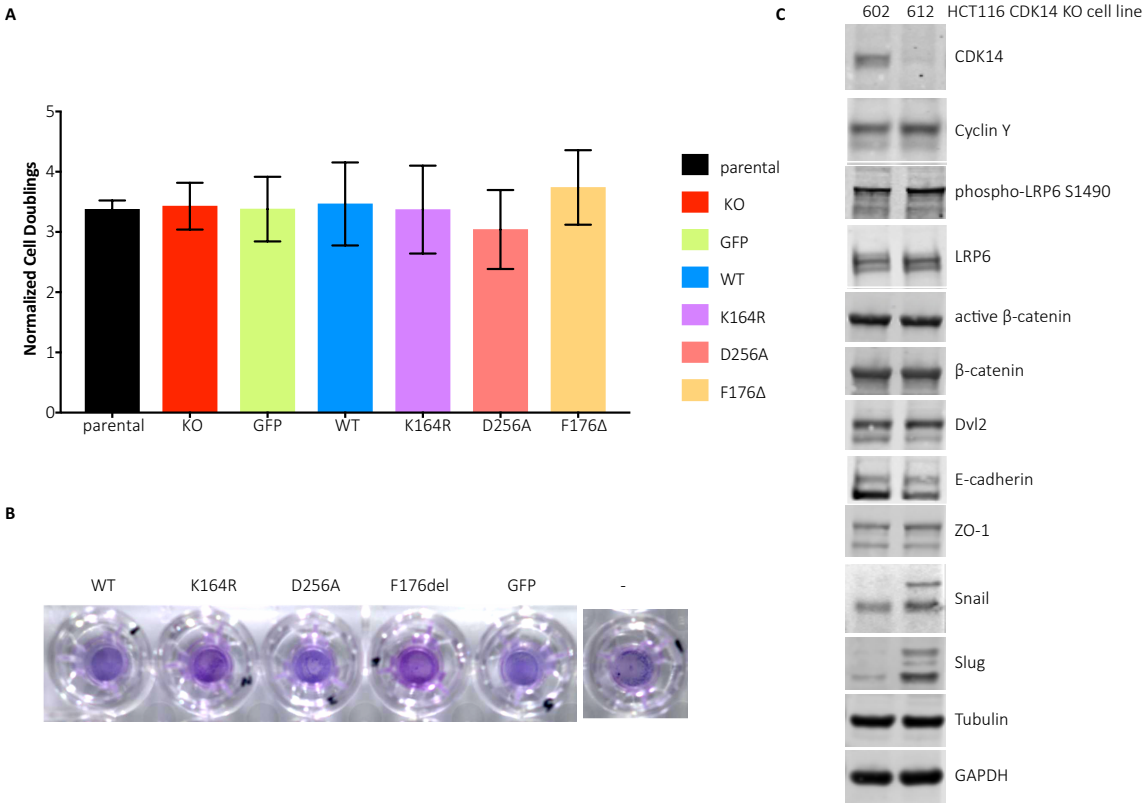

Figure 4-11. Growth and migration phenotypes of HCT116 CDK14 KO with rescues. (A) 72 h growth assay of CDK14 rescue cell lines, assessed using CellTiter-Glo. (B) 24 h trans-well migration assay of rescue cell lines. (C) Western blot for downstream Wnt signaling and EMT markers in CDK14 WT (602) and KO (612) paired CRISPR clonal cell lines.

There were no significant differences in basal expression of Wnt signaling markers in the HCT116 cell line (Figure 4-11). As shown previously, there were also no basal cell cycle differences in the WT versus KO lines (Figure 3-8). To further investigate cell cycle effects, and LRP6 phosphorylation during cell cycle progression, double thymidine synchronization was carried out in the CDK14 rescue lines. Compared to the GFP control and ATP binding-deficient K164R, the mitotic LRP6 S1490 peak was much more significant in the CDK14 WT rescue (Figure 4-12). These results are consistent with what was observed in the PATU-8988T cells and with FMF-04-159-2 treatment. The GFP only rescue in the CDK14 KO shows a slight peak in LRP6 S1490 phosphorylation in mitosis, consistent with previous results with the PATU-8988T rescues and the fact that there are possible compensatory mechanisms that could occur in CRISPR lines, or alternate kinases that could phosphorylate given the redundancy amongst the TAIRE kinases.

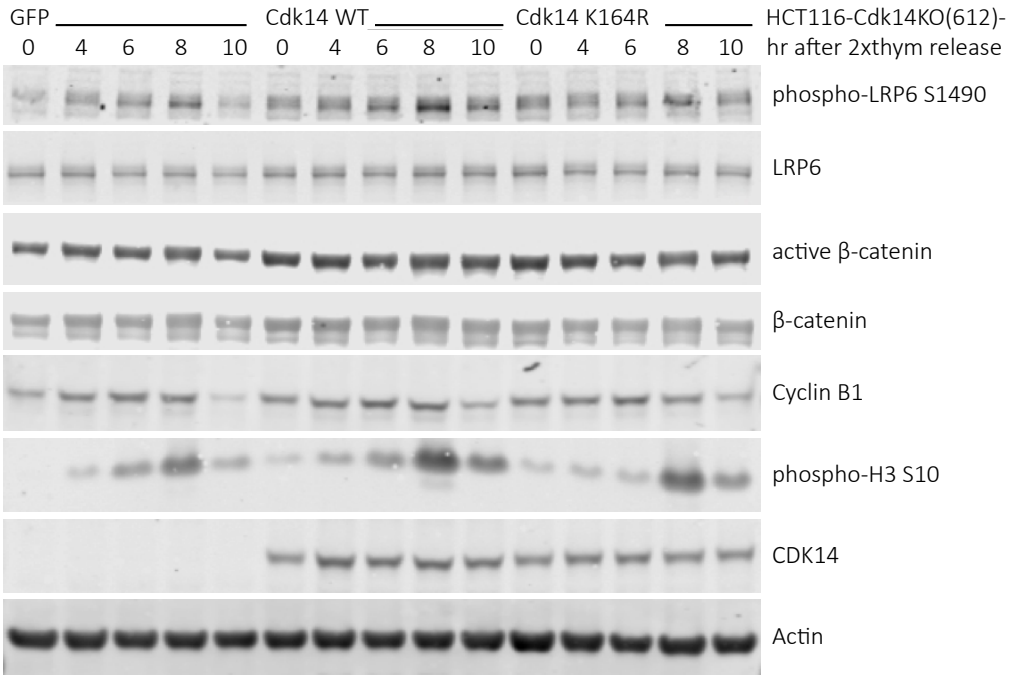

Figure 4-12. Cell cycle progression after double thymidine synchronization and release, monitored using western blotting.

Effects of the CDK14 inhibition were described previously in Chapter 3. As shown, the mild antiproliferative effects were not attributed to CDK14 targeting, consistent with the genetic studies in both pancreatic cancer lines and HCT116 cells. Rescue of CDK14 WT or C218S in CDK14 KO cells did not affect antiproliferative effects of CDK14 inhibitors in both the HCT116 and PATU-8988T cell backgrounds (Figure 4-13). Compound potency differed between the two cell lines, but there was consistency in the relative effects, as compound IC50s were nearly identical in the WT and C218S cells.

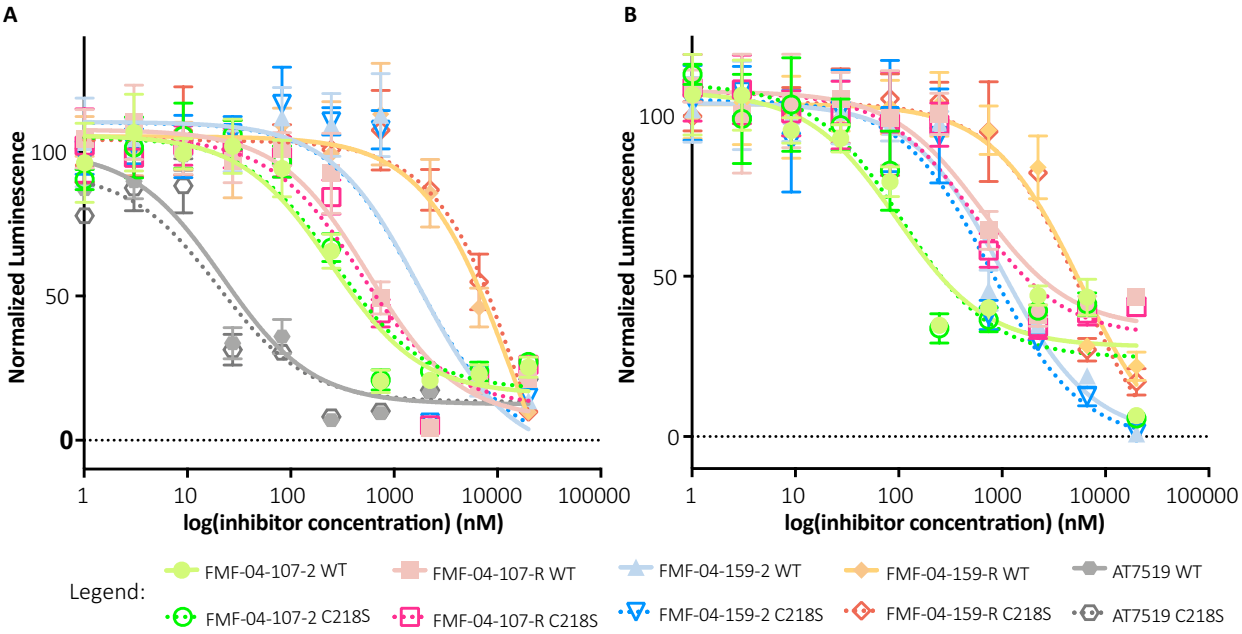

Figure 4-13. Anti-proliferative effects of CDK14 inhibitors in WT and C218S CDK14 rescues in HCT116 and PATU-8988T cells. (A) 72 h antiproliferation assay for CDK14 covalent inhibitors and their reversible pairs in HCT116 CDK14 KO rescues and (B) PATU-8988T CDK14 KO rescues.

Furthermore, mitotic LRP6 S1490 phosphorylation was decreased in double thymidine-synchronized PATU-8988T CDK14 KO cells rescued with CDK14 WT (Figure 4-14), consistent with the effects of FMF-04-159-2 characterized in HCT116 cells as previously described (Figure 3-7). An additional CDK14-targeting compound FMF-04-107-2, synthesized in the course of developing

FMF-04-159-2, was included alongside FMF-04-159-2. Both compounds reduced LRP6 phosphorylation after double thymidine synchronization, however in PATU-8988T CDK14 KO cells rescued with CDK14 C218 there was minimal impact on LRP6 phosphorylation upon compound treatment (Figure 4-14). This suggests that the effects on mitotic LRP6 S1490 phosphorylation from CDK14 inhibition primarily require covalent CDK14 engagement. However, non-covalent inhibition of the other TAIRE kinases may still impact the magnitude of the effect observed in the WT cells.

Conclusion

CDK14's role in promoting cancer cell growth, migration and EMT has been previously reported in a number of cancer cell lines, primarily using siRNA studies. To further investigate the specific role of CDK14 and its kinase activity and further complement the development of FMF-04-159-2, a covalent CDK14 inhibitor with pan-TAIRE selectivity, we applied and integrated multiple chemical and genetic tools, including CRISPR gene editing, the dTAG system for chemical-induced degradation, and rescue of knockout with CDK14 variants, to understand how pancreatic cancer cell lines respond to loss of CDK14 function.

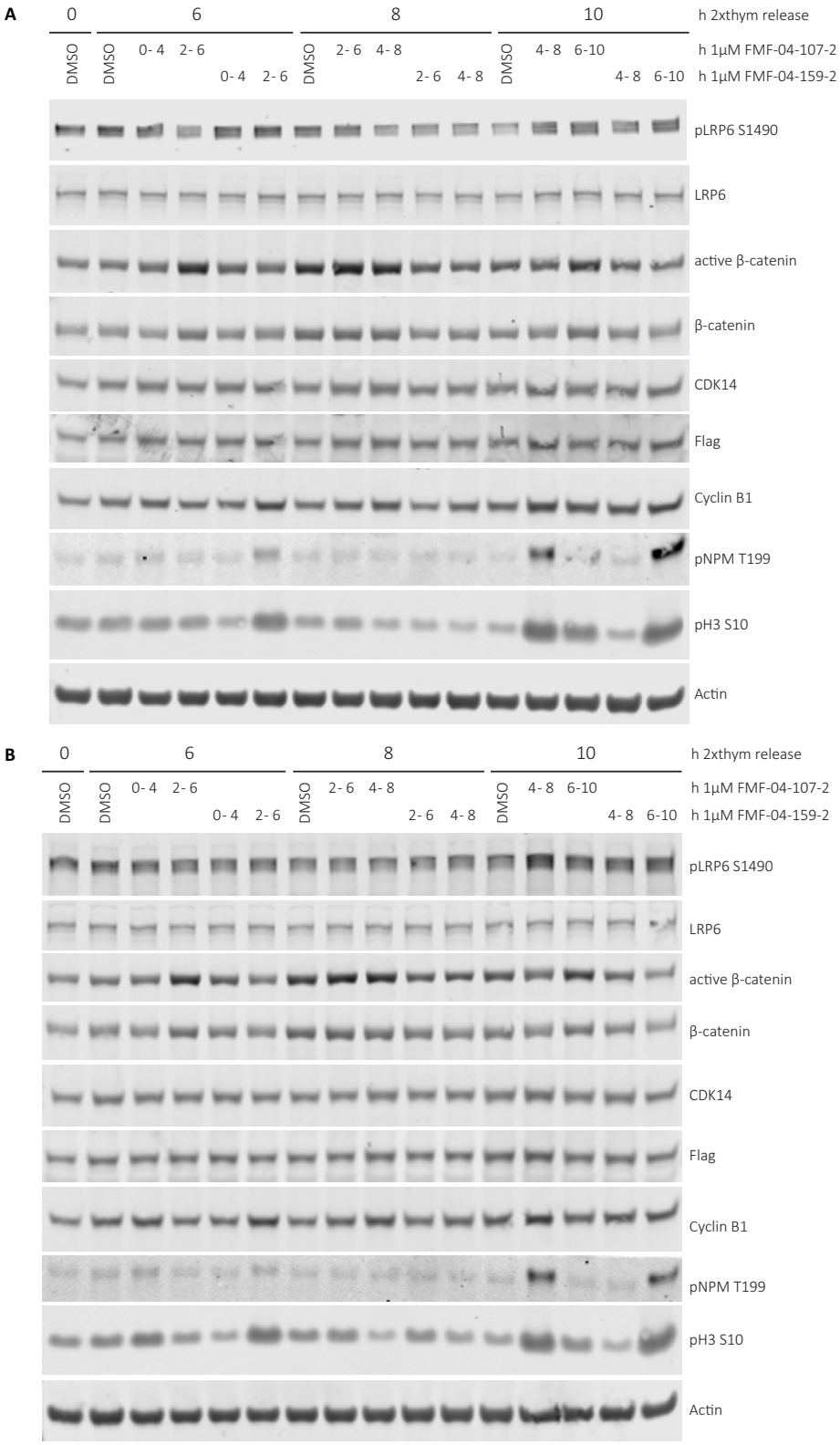

Figure 4-14. Effects of CDK14 inhibitors in WT and C218S CDK14 rescues in PATU-8988T cells. (A) Double thymidine synchronization and release, followed by treatment with FMF-04-107-2 or FMF-04-159-2 for 4 h windows in PATU-8988T CDK14 KO cells, rescued with CDK14 WT or with (B) CDK14 C218S.

Collectively, these efforts led to the conclusion that inhibition, depletion or genetic disruption of the kinase activity of CDK14 alone does not significantly impair the growth and migration of pancreatic cancer cell lines in any of the cell contexts assessed. Furthermore, there weren't any consistent or significant effects on growth or migration which were dependent on CDK14 kinase activity or cyclin binding in the pancreatic cancer cell lines evaluated. The effects were slightly magnified in ultra-low attachment (ULA) growth conditions, where functional CDK14 conferred a slight growth advantage in the PATU-8988T cells. This did not directly translate to clear effects on trans-well migration or on molecular expression of various EMT marker.

It is clear that CDK14 function depends on cellular context, as results differed even between the more epithelial versus mesenchymal pancreatic cancer cells tested. A decrease in the tight junction protein ZO-1 upon CDK14 overexpression was observed in the epithelial lines for only the wild type but not inactive variants, suggesting a requirement for CDK14 activity. The exception was in BxPC3 cells, where conflicting increases in ZO-1 and N-cadherin upon CDK14 overexpression were activity independent, suggesting the possibility of a protein scaffolding role for CDK14. In comparing these results to the activity in PATU-8988T cells, there weren't many similarities. No effects on ZO-1 were observed upon CDK14 perturbation. However, loss of Vimentin was observed in the PATU-8988T cells using both CRISPR/Cas9 and the dTAG system upon removal of CDK14 protein.

To truly understand the direct versus adaptive responses to loss of CDK14, we adopted a novel chemical-induced protein degradation strategy known as the dTAG system, which places CDK14 cellular levels under rapid chemical control. By introducing exogenous FKBP12F36V-

CDK14 into PATU-8988T cells before knockout of endogenous CDK14, we ensured that the cells never fully lost CDK14 expression until dTAG treatment. One important aspect of this strategy is to ensure that the FKBP12F36V-fusion protein behaves similarly to the endogenous protein. Although we were not able to directly test the kinase function of FKBP12F36V-CDK14 due to a lack of well-validated and specific CDK14 substrates, we did confirm that dTAG treatment in double thymidine synchronized cells abrogated mitotic LRP6 S1490 phosphorylation, a phenotype consistently observed across every orthogonal approach we employed to interrogate CDK14 function.

Many of the phenotypes observed in the PATU-8988T CDK14 dTAG cell line re-capitulated what was observed in the paired PATU-8988T CRISPR CDK14 KO and WT cell lines. The overall effects on cell cycle phase distribution as assessed by FACS PI staining was minimal upon CDK14 depletion, either by dTAG or by CRISPR knockout. The lack of mitosis-dependent LRP6 S1490 phosphorylation is consistent with reported literature (Davidson et al., 2009) and with observed effects of FMF-04-159-2 in HCT116 cells (Figure 3-7). Overall, there was a consistent dependence on functional CDK14 in order to see a cell cycle dependent peak in LRP6 S1490 phosphorylation, observed in the CRISPR knockout PATU-8988T lines, PATU-8988T CDK14 dTAG experiments, inhibitor treatment in PATU-8988T CDK14 KO cells rescued with CDK14 WT but not C218S, and CDK14 variant rescues in HCT116 cells. The novel chemical and chemical-genetic tools that were generated will be useful in future studies investigating CDK14-dependent biology.

Chapter 5: A Chemoproteomic Strategy for Direct and Proteome-wide Covalent Inhibitor Target-site Identification

Author Contributions

Christopher M. Browne performed the majority of the experiments, including all mass spectrometry-based experiments. Scott B. Ficarro provided critical expertise and advice on mass spectrometry and proteomics. Baishan Jiang and Tinghu Zhang synthesized all compounds. Zainab M. Doctor generated cell lines and performed biological experiments pertaining to compound characterization and phenotypic effects. Jared L. Johnson, Tomer M. Yaron, Charles J. Murphy and Lewis C. Cantley performed kinase motif analysis and provided biostatistical analysis for it. Joseph D. Card and Sindhu C. Sivakumaren performed target engagement assays. William M. Alexander provided programming expertise. Jarrod A. Marto and Nathanael S. Gray conceived the concept and research strategy of the project.

Introduction

Protein kinases govern many aspects of human physiology, and are associated and/or causatively linked to numerous human diseases. As a result, they are attractive targets for pharmacologic intervention, with most research efforts focused on developing reversible, small molecule kinase inhibitors. More recently, irreversible covalent inhibitors have emerged as compelling alternatives. These compounds permanently disable kinase activity, typically via covalent modification of a non-sequence conserved cysteine residue that lies in or near the ATP-binding pocket. The clinical potential for covalent kinase inhibitors (CKIs) is exemplified by the recent FDA approval of Ibrutinib, which targets BTK (Pan et al., 2007), and Afatinib, which targets EGFR (D. Li et al., 2008). In fact, there are some 200 human kinases which span major branches of the kinome phylogeny and harbor targetable, active site-proximal cysteines ('cys-kinases' (Q. Liu et al., 2013; J. Zhang et al., 2009)). We recently described a series of CKIs that selectively modify cysteine residues distal to the active site ('remote cysteines'), with THZ1 (Kwiatkowski et al., 2014) and THZ531 (T. Zhang et al., 2016) as the most advanced examples of this series. These results raise the intriguing possibility that cysteine-directed, selective CKIs may be developed for a much broader range of the human kinome than previously envisioned (J. Zhang et al., 2009).

Despite these promising developments, it remains difficult to predict cysteine reactivity, which represents a bottleneck in the rational design of CKIs (Z. Zhao, Liu, Bliven, Xie, & Bourne, 2017). More importantly, the potential for idiosyncratic toxicities caused by covalent modification of off-target cysteines drives skepticism for the broad use of irreversible inhibitors. Chemoproteomics, a subset of mass spectrometry (MS) experiments that combines the use of small molecules with the analytical power of proteomics, has been invaluable for interrogation of

CKIs and other probe classes. For example, recent chemoproteomic studies have sought to quantify the reactivity of endogenous cysteines across the proteome (Weerapana et al., 2010); these data reveal a range of highly reactive cysteine-thiols that represent potential off-target liabilities for CKIs, and highlight the need to include target-site analyses as part of covalent inhibitor development programs.

Tandem Orthogonal Activity-based Protein Profiling (TOP-ABPP, and the quantitative isoTOP-ABPP) is a well-established approach that employs alkyne-derivatized probes to enrich protein targets and identify likely sites of covalent modification (Weerapana, Speers, & Cravatt, 2007; Weerapana et al., 2010). An important limitation of this methodology noted by the authors, was the difficulty in obtaining site-level information when using irreversible pharmacologic inhibitors, i.e. chemically complex and target selective compounds (Weerapana et al., 2007). Thus, the current standard relies on small, non-selective cysteine probes as surrogates to profile the activity of cysteine-directed selective pharmacologic inhibitors (Abo & Weerapana, 2015; Backus et al., 2016; Bak, Pizzagalli, & Weerapana, 2017; Bar-Peled et al., 2017; Blewett et al., 2016; X. Deng et al., 2013; Quinti et al., 2017; C. Wang, Weerapana, Blewett, & Cravatt, 2014; Weerapana et al., 2010). This type of indirect, non-selective cysteine profiling does not formally confirm covalent ligand-target conjugation and may under sample low-abundance/-stoichiometry targets due to the stochastic nature of LC-MS/MS data acquisition. Recent modifications to the original approach address some of these issues by using affinity-tagged CKIs to identify off-targets and provide a more complete picture of potential toxicity liabilities (Lanning et al., 2014; Niessen et al., 2017). However, as reported this strategy

focused on target identification at the protein-level and therefore requires companion biochemical assays to determine the exact site and covalent nature of ligand engagement.

We recently demonstrated that cysteine-directed probes and covalent drugs share common gas-phase dissociation pathways (Ficarro et al., 2016). Pertinent to the limitations noted above, the predictable nature of these fragment ions can be used to improve peptide sequence assignment including the specific site of covalent modification. Here, we build on these results to establish a new chemoproteomic platform that leverages affinity-tagged analogs of pharmacologic CKIs for the biochemical enrichment of targets, along with tunable peptide fractionation and custom spectral processing to identify inhibitor target sites. Our new platform for Covalent Inhibitor Target-site Identification (CITe-Id) enables deeper coverage of cysteines modified by pharmacologic CKIs, while confirming covalent bond formation and providing dose-response data for inhibitor binding at each cysteine-thiol. As a powerful proof-of-concept, we used CITe-Id to identify multiple, unexpected off-targets of our cyclin-dependent kinase (CDK) inhibitor THZ1 (Kwiatkowski et al., 2014). These new targets included Cys-840 on Protein Kinase N3 (PKN3), an understudied AGC-type kinase linked to metastasis in aggressive prostate tumors (Leenders et al., 2004; Unsal-Kacmaz et al., 2012). Residue-level data from CITe-Id facilitated our development of JZ128 as a covalent inhibitor of PKN3. We used JZ128 as a tool compound to identify novel potential PKN3 substrates. Our work exemplifies the utility of CITe-Id to reveal new pharmacologically-addressable cysteines and accelerate development of selective, covalent inhibitors.

Developing and Optimizing CITe-Id (Covalent Inhibitor Target-site Identification)

Motivated by the growing clinical impact of CKIs, juxtaposed with key concerns related to potential toxicities as described above, we sought to develop CITe-Id as a robust chemoproteomic strategy that would go beyond protein-level identification of targets, and provide a residue-level direct readout of concentration-dependent covalent binding of a given CKI. We previously described specific gas-phase fragmentation pathways for peptides covalently modified by cysteine-directed, irreversible inhibitors and clinical drugs (Ficarro et al., 2016), including our recently described CDK7/12/13 inhibitor, THZ1 (Kwiatkowski et al., 2014) (Figure 5-1A (**1**)). Building on these insights, we first elaborated THZ1 with a desthiobiotin affinity handle (THZ1-DTB, Figure 5-1A (**2**)) and then used western blot to confirm concentration-dependent labeling and enrichment of CDK7 (Figure 5-2A). Beginning with a similar experiment using competition-format incubation (Figure 5-2A), we designed CITe-Id to readout dose-dependent binding of selective, pharmacologic inhibitors based specifically on the analysis of modified peptides (Figure 5-1B). We performed streptavidin pulldown after tryptic digestion of protein lysate to provide a highly enriched pool of THZ1-DTB labeled peptides for subsequent encoding with iTRAQ reagents, followed by multi-dimensional chromatography tailored for the hydrophobic nature of inhibitor-modified peptides and also providing wide flexibility for fractionation depth (Ficarro et al., 2011; F. Zhou et al., 2013; F. Zhou, Sikorski, Ficarro, Webber, & Marto, 2011). In addition, we extended our previous framework for identification of covalent inhibitor-modified peptides to account for the desthiobiotin affinity tag and linker, and confirmed improved sequence scores for ~85% of THZ1-DTB labeled sites (Ficarro et al., 2016).

Finally, we used peptide iTRAQ reporter ion intensities to calculate a competitive dose-response for inhibitor binding at individual cysteine residues.

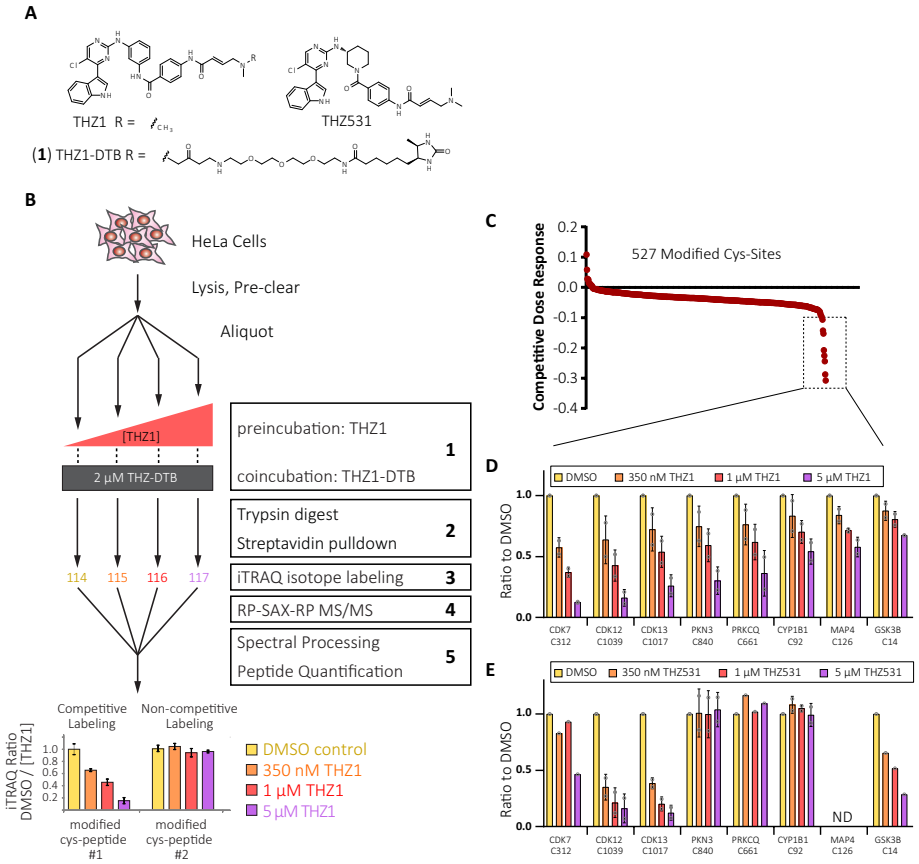

Figure 5-1. CITe-Id directly quantifies covalent probe binding with site-level resolution. (A) Structures of: THZ1 and tagged analog, previously described (Kwiatkowski et al., 2014); desthiobiotinylated analog (THZ1-DTB); and THZ531, previously described (T. Zhang et al., 2016). (B) Workflow of CITe-Id using THZ1/THZ1-DTB: 1) Cell lysates were treated with THZ1/THZ1-DTB in a competition format, 2) protease digestion was carried out before streptavidin enrichment to provide a highly enriched pool of CKI-labeled peptides, 3) samples were encoded with iTRAQ stable isotope reagents to enable mass spectrometry quantification of concentration-dependent binding at individual cysteine residues, 4) online, automated RP-SAX-RP chromatography (F. Zhou et al., 2013) was tailored for the increased hydrophobicity of labeled peptides and allowed for ready adjustment of fractionation depth, 5) pre-processing of MS/MS spectra following our previous framework (Ficarro et al., 2016) improved identification of cysteine residues covalently bound by THZ1-DTB. Competitive binding dose-response curves generated from iTRAQ reporter ions were used to distinguish concentration-dependent/-independent binding of CKIs. (C) THZ1-DTB-labeled cysteine sites rank ordered for competitive dose-response to THZ1. (D) Cysteine residues bound by THZ1-DTB in a concentration-dependent manner as indicated by a dose-response exceeding two standard deviations relative to the mean value of all 527 reproducibly labeled cysteine residues. (E) CITe-Id distinguishes the subset of THZ1 targets for their competitive dose-response to THZ531. CITe-Id analysis conducted as previous but THZ1 treatment was replaced with THZ531 followed by co-treatment with THZ1-DTB. For D and E, bars are the mean of the ratio of a condition from each biological replicate with standard deviation error bars and individual data points as grey circles.

Our CITe-Id analysis of THZ1/THZ1-DTB identified 527 unique cysteine residues which were covalently modified by THZ1-DTB, with good reproducibility across biological replicates (Figure 5-2B). Quantitative, competitive dose-response data from CITe-Id (Figure 5-1C) revealed that THZ1-DTB binding was independent of THZ1 concentration for a majority (>95%) of modified cysteine residues. These sites, which include highly abundant proteins such as glycolytic enzymes and tubulin, as well as many cysteines annotated as 'highly-reactive' (Weerapana et al., 2010), likely represent non-specific probe binding. Against this null-distribution we identified dose-dependent competitive binding of THZ1 to eight cysteine residues, including the known targets CDKs 7, 12, and 13 (Figure 5-1C, dashed box). In addition to these positive control data, we identified dose-dependent THZ1 competitive binding on several unexpected kinase targets, PKN3 at C840, protein kinase C theta (PRKCQ) at C661, and glycogen synthase kinase 3B (GSK3B) at C14 (Figure 5-1D). We next repeated CITe-Id, using THZ531, a THZ1 analog with reported selectivity for CDK12/13 over CDK7 (T. Zhang et al., 2016), as the competing, native inhibitor. These data recapitulated the known CDK selectivity profiles, and further demonstrate that THZ531 has little or no reactivity against the potential new targets of THZ1, PKN3, PRKCQ, or CYP1B1 while gaining some activity against GSK3B (Figure 5-1E). These results confirm the ability of CITe-Id to quantitatively distinguish the target landscape of structurally similar inhibitors.

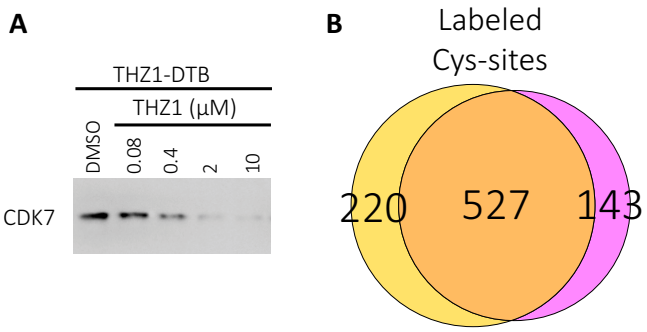

Figure 5-2. (A) HeLa S3 lysates were treated in a competition-format with increasing concentrations of THZ1 followed by co-treatment with THZ1-DTB, streptavidin pulldown and immunoblot for CDK7. (B) Venn diagram illustrating the overlap of THZ1-DTB-modified cysteine residues identified across replicate ClTe-Id experiments.

THZ1 inhibits PKN3 via covalent binding to C840

One of the kinases targeted by THZ1 was PKN3, a kinase that has been functionally linked to metastasis and tumor growth (Leenders et al., 2004; Unsal-Kacmaz et al., 2012), and is the target of a liposomal siRNA-based therapeutic currently in clinical trials (NCT00938574 (Schultheis et al., 2014)). Despite these data and clinical interest, PKN3 is understudied compared to other disease-associated kinases (Cerami et al., 2012; Gao et al., 2013; Nguyen et al., 2017), which motivated us to further investigate it as a THZ1 target. A comparison of structural data for CDK7 and PKN3 (Swiss-Model Q6P5Z2) revealed that C840 of PKN3 is positioned close to the kinase active site, similar to the 'remote cysteine' C312 of CDK7 targeted by THZ1 (Figure 5-3A). The targeted cysteines of CDK12 and PRKCQ are similarly positioned (Figure 5-4A). We therefore sought to validate PKN3 as a covalent target of THZ1 and explore the potential of developing selective tool compounds to study PKN3 biology. To confirm target engagement as well as the covalent nature of PKN3-THZ1 conjugate formation *in vivo*, we treated HeLa S3 cells with increasing concentrations of THZ1, using the reversible analog (THZ1-R

(Kwiatkowski et al., 2014)) as a negative control (Figure 5-3B). After cell lysis we incubated protein extracts with THZ1-DTB, followed by streptavidin pulldown and detection of bound proteins by western blot. As expected, THZ1 showed strong competition for CDK7, with similar reactivity profiles observed for CDK12/13 (probing for their obligate cyclin K binding partner as a proxy), as well as two new targets identified by CITe-Id, PKN3 and PRKCQ. The reversible analog THZ1-R competed poorly for binding to all targets.

We next sought to confirm that covalent modification of PKN3 by THZ1 inhibited enzyme activity. Using an *in vitro* kinase assay, we observed that THZ1 inhibited PKN3 in a fixed time-point format with an apparent IC50 of 72 nM, while the reversible analog was more than 50-fold less potent (Figure 5-3C and Figure 5-4B). We also confirmed that inhibition of PKN3 by THZ1 was time dependent, consistent with a covalent mechanism-of-action (Figure 5-3C and Figure 5-4C). A similar assay showed THZ1 to have weak potency against PRKCQ (Figure 5-4D). To demonstrate that C840 is essential for THZ1 binding to PKN3, we expressed tandem FLAG and HA-tagged wild type (WT) or C840S (CS) mutant PKN3 in a clonal PC3 cell line with CRISPR-Cas9-mediated deletion of endogenous PKN3 (PC3 PKN3 KO) (Figure 5-4E). PC3 is a prostate cancer cell line that has been used previously to investigate PKN3 biology (Leenders et al., 2004; H. Mukai et al., 2016). Lysates were treated with THZ1-DTB, followed by streptavidin pulldown or immunoprecipitation with HA antibody (Figure 5-3D). We found that the C840S mutation abrogated THZ1-DTB binding to PKN3. Collectively these data validate PKN3 as a new target of THZ1, and further demonstrate that pharmacologic activity is mediated by the covalent binding to a single cysteine (C840) on the kinase.

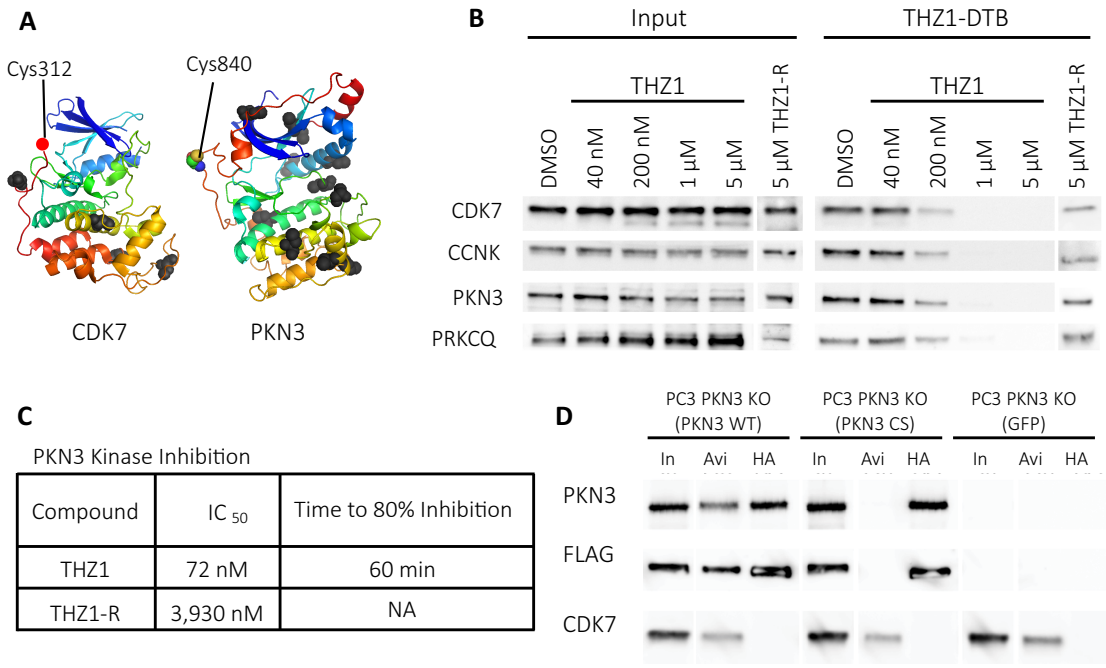

Figure 5-3. THZ1 inhibits PKN3 via specific targeting of C840. (A) Structures of CDK7 and PKN3 facing kinase active sites with cysteine labeling sites of THZ1-DTB highlighted as colored spheres. All other unlabeled cysteine residues are displayed as black spheres. For CDK7, structure for Cys-312 is unavailable, a red dot indicates its approximate location adjacent to the next closest visible residue (Asp-311) (CDK7: PDB 1UA2 (Lolli, Lowe, Brown, & Johnson, 2004), PKN3: Swiss-Model Q6P5Z2). (B) Live HeLa S3 cell treatments with THZ1 or reversible analog THZ1-R. Lysates treated with THZ1-DTB, followed by streptavidin pulldown and immunoblotting against THZ1 targets. CCNK is used as a proxy for CDK12/13. (C) Summary of PKN3 inhibition by THZ1 and THZ1-R. Middle column is IC50 values for 7-point dose-response kinase assay for PKN3. Right-most column is time-dependent kinase assays for PKN3 with fixed inhibitor concentration (1 µM). THZ1-R did not show time-dependent inhibition. See Figure 5-4B,C for enzyme assay curves. (D) C840 is essential for covalent labeling of PKN3. Dual FLAG-HA tagged PKN3 WT and PKN3 CS constructs were expressed in PC3 PKN3 KO cells. Lysates were treated with THZ1-DTB followed by streptavidin pulldown or HA immunoprecipitation and western blotting. In = 1% Input, Avi = Streptavidin pulldown, HA = HA pulldown. Blot lanes were rearranged for clarity.

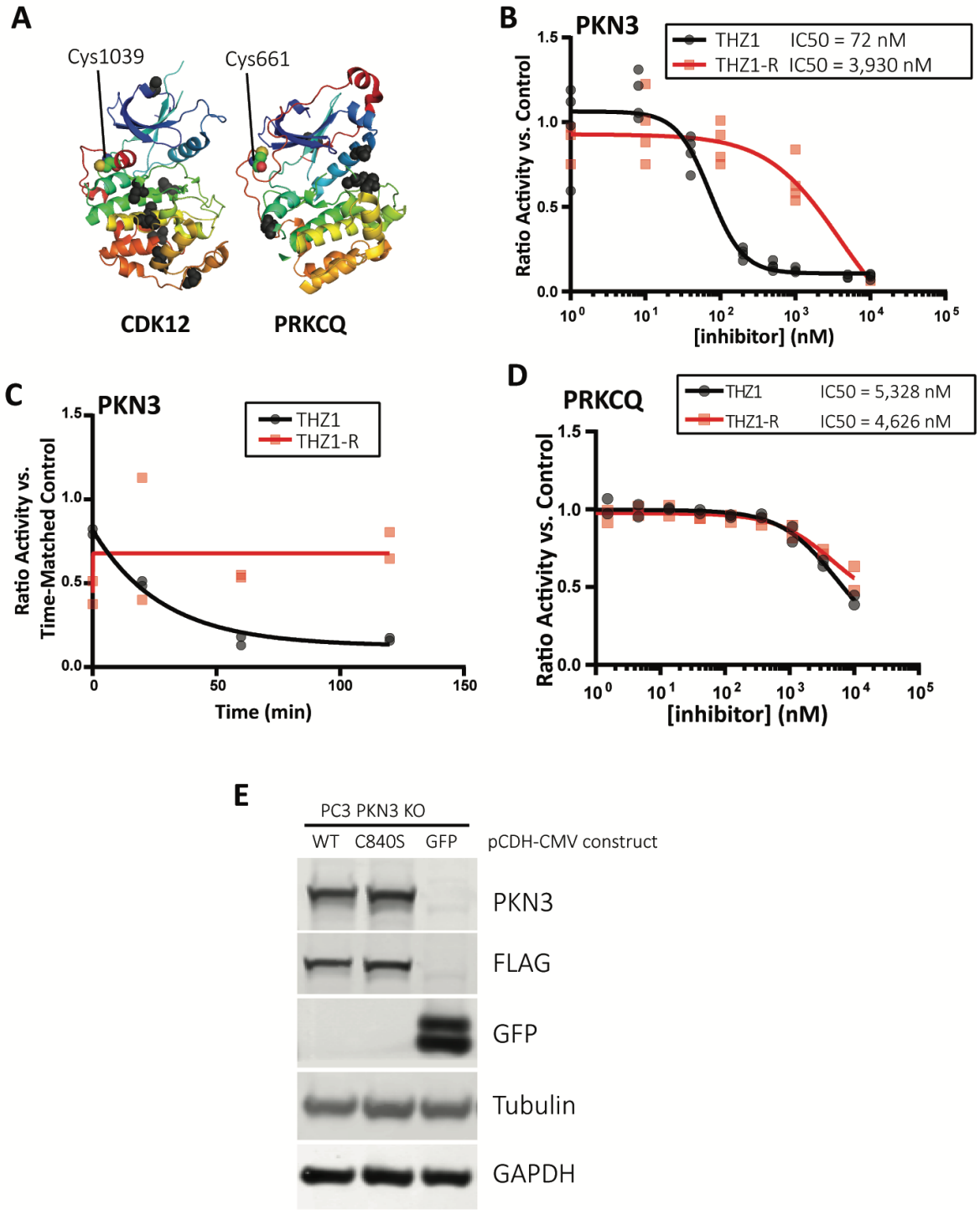

Figure 5-4. (A) Structures of CDK12 and PRKCQ facing kinase active sites with cysteine labeling sites of THZ1- DTB highlighted as colored spheres. All other unlabeled cysteine residues are displayed as black spheres. (CDK12: PDB 4NST (Bosken et al., 2014), PRKCQ: PDB 2JED). (B) In Vitro kinase assay for PKN3 inhibition. (C) In Vitro kinase assays performed as a time course for PKN3 inhibition. All time-points compared to time-matched DMSO control. (D) In Vitro kinase assays for inhibition of PRKCQ by THZ1 and THZ1-R. (E) Immunoblot of cell lysates from PC3 cells with CRISPR-CAS9 mediated PKN3 deletion expressing several FLAG-HA-tagged PKN3 rescue constructs.

Developing an Irreversible Inhibitor of PKN3

THZ1 exhibits good potency against PKN3, but is strongly cytotoxic due to its inhibition of the CDKs, and hence is limited as an inhibitor to study PKN3 biology. Nonetheless, our CITe-Id data suggested that the THZ-scaffold is a reasonable starting point to develop a selective, covalent inhibitor of PKN3. Towards this end we screened a small library of acrylamide-modified THZ-family compounds in our PKN3 kinase assay and compared these data to the activity of each compound against CDK7. Based on these results we identified JZ128 (**2**) as a potential selective inhibitor of PKN3 (Figure 5-5A). We also synthesized a desthiobiotin-tagged analog of JZ128 (JZ128-DTB, **3**) for subsequent CITe-Id analysis, as well as a non-covalent analog (JZ128-R, **4**), as a control. *In vitro* kinase assays against PKN3 revealed that JZ128 and the desthiobiotin-modified JZ128-DTB had similar IC50s of ca. 120 nM while the reversible analog was approximately 50-times less potent (Figure 5-5B and Figure 5-6B).

To confirm cellular target engagement, we treated PC3 cells with increasing concentrations of JZ128. After lysis we incubated protein extracts with JZ128-DTB or THZ1-DTB, followed by streptavidin pulldown and detection of bound proteins by western blot. As expected, JZ128 bound selectively to PKN3, with no activity against CDK7 or CDK12/13 (probing Cyclin K) (Figure 5-6C). We performed a similar experiment using the reversible analog (JZ128-R) and other PKN family members which lack an equivalently-positioned cysteine to C840 on PNK3 (Figure 5-6D). JZ128-R did not compete for PKN3, while neither PKN1 nor PKN2 was bound by JZ128-DTB. We also confirmed that JZ128 did not inhibit kinase activity of PKN1 or PNK2 (Figure 5-5C,D). To confirm C840 as the only site of JZ128 covalent modification, we again utilized tandem FLAG-HA tagged WT or C840S mutant PKN3 expressed in PC3 PKN3 KO cells. Lysates

were treated with JZ128-DTB, after which we performed streptavidin pulldown or immunoprecipitation with HA antibody (Figure 5-6E). This assay confirmed that C840 is required for JZ128-DTB binding to PKN3.

PKN3 has been functionally linked to cell migration (Leenders et al., 2004; H. Mukai et al., 2016; Unsal-Kacmaz et al., 2012). Based on these observations, we asked whether JZ128 could be used to recapitulate a PKN3-dependent phenotype. We first confirmed that JZ128 was not toxic to our set of PKN3 WT and mutant cell lines (Figure 5-5E). We then performed scratch assays in the presence of vehicle, JZ128, or JZ128-R using the cell lines described in Figure 5-3D. We observed that JZ128 significantly impaired wound healing in PKN3 WT cells but had no effect in cells that expressed the PKN3 C840S mutant (Figure 5-6F and Figure 5-7). Unexpectedly, PKN3 KO cells also exhibited impaired wound healing, indicating the potential for off-target JZ128 activity in the absence of PKN3. Collectively, our *in vitro* data and cell-based assays confirm PKN3 as a target of JZ128 and that the pharmacologic activity is predominantly mediated by covalent modification of a single cysteine (C840) on PKN3.

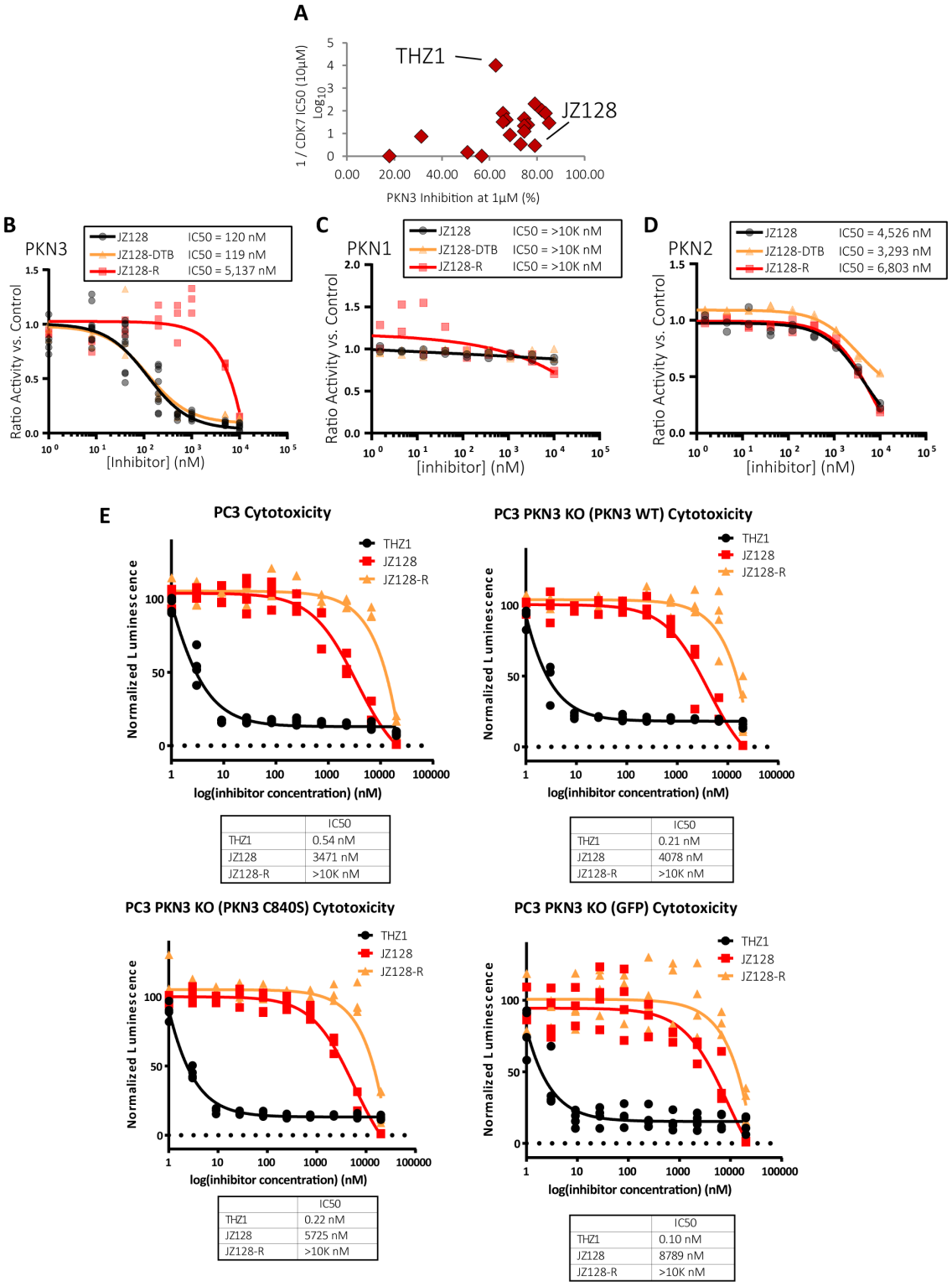

Figure 5-5. (A) Graph comparing CDK7 activity to PKN3 activity of screened THZ1 analogs. Vertical axis shows the log10 inverse of the IC50 of CDK7 inhibition, horizontal axis is the % inhibition of PKN3 for each compound at 1μM concentration. (B-D) In vitro kinase assays for PKN3, PKN1, and PKN2 inhibition respectively. (E) Results of CellTiter-Glo luminescent cell viability assays for PC3 rescue strains used in this study.

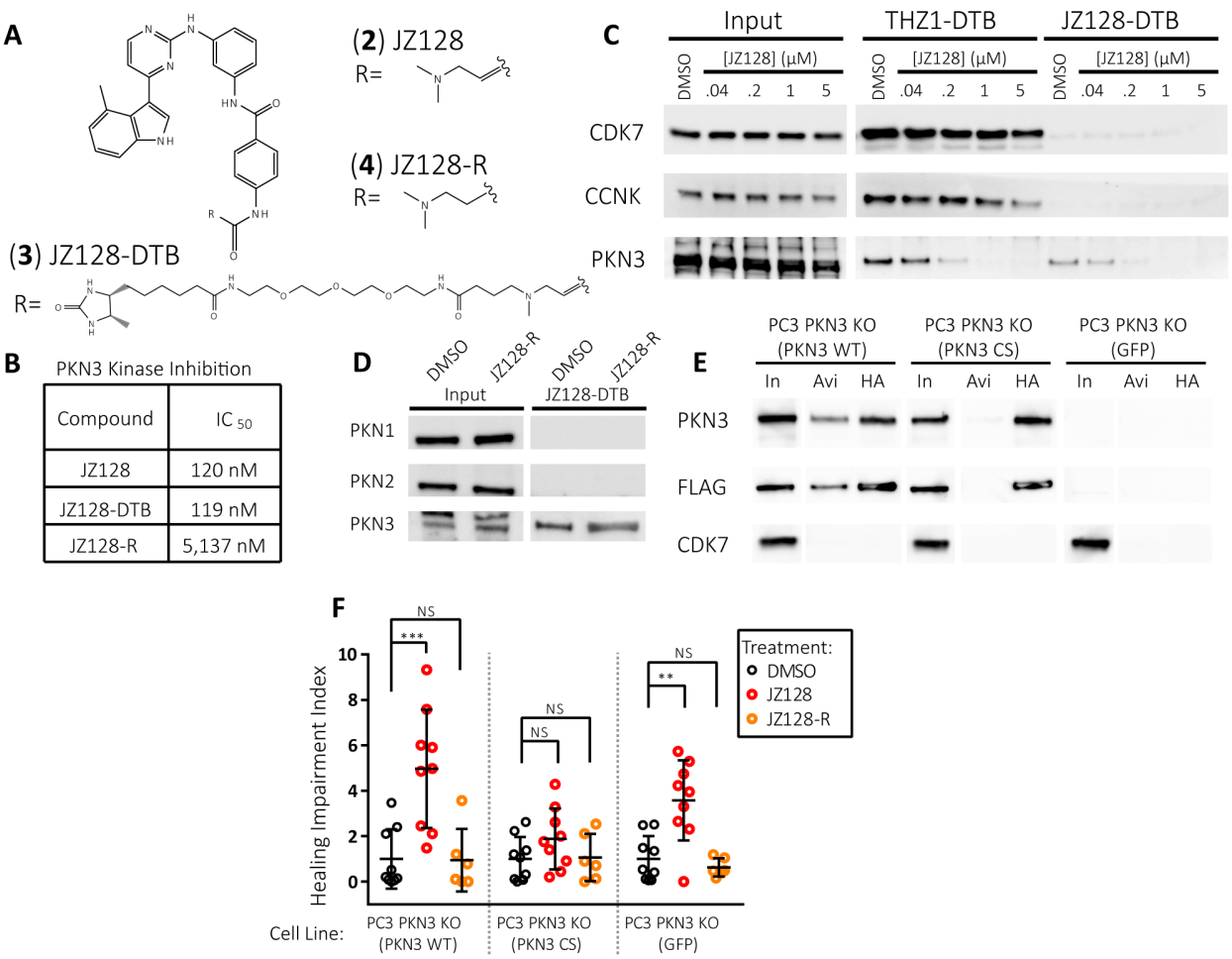

Figure 5-6. Identifying a selective inhibitor of PKN3. (A) Structures of JZ128 and related compounds. (B) Summary of results for *in vitro* kinase assays for PKN3. (C) Live PC3 cell treatments with JZ128. After lysis samples were treated with THZ1-DTB or JZ128-DTB, followed by streptavidin pulldown and western blot. CCNK was used as a proxy for CDK12/13. (D) Live PC3 cell treatments with JZ128-R. After lysis samples were treated with JZ128-DTB, followed by streptavidin pulldown and western blot. (E) Similar to Figure 2D, dual FLAG-HA tagged PKN3 WT and PKN3 C840S constructs were expressed in PC3 cells lacking endogenous PKN3. Lysates were treated with JZ128-DTB followed by streptavidin pulldown or HA immunoprecipitation and western blot. In = 1% Input, Avi = Streptavidin pulldown, HA = HA pulldown. Blot lanes were rearranged for clarity. (F) Confluent PC3 PKN3 KO cells expressing PKN3 rescue constructs were serum starved and treated with DMSO, JZ128, or reversible control. A wound was scored across the culture and monitored for 24 hr. Shown is the mean ratio of remaining wound area after 24 hr. normalized to the mean wound area of the DMSO condition for each cell line with individual replicate values shown as colored circles. See Figure 5-7 for representative raw images. p-values determined by unpaired 2-sided t-test. (n = 6-9 replicates) NS: p-value > 0.05, **: p-value = 0.0015, ***: p-value = <0.0009. Error bars show one standard deviation from the mean.

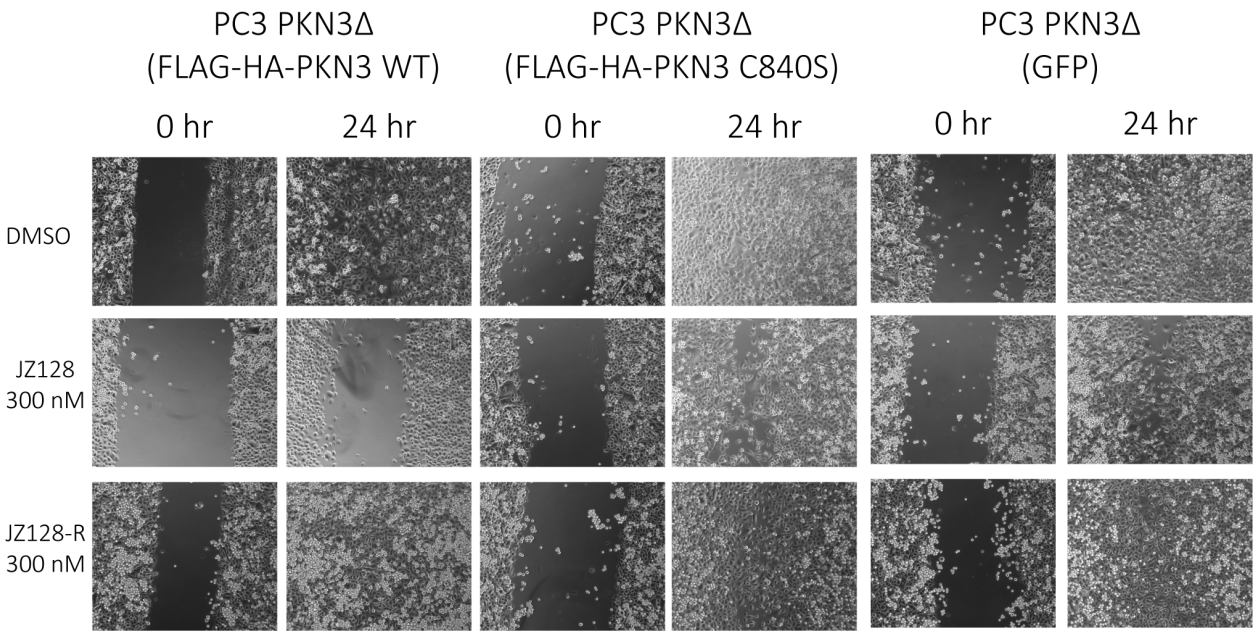

Figure 5-7. Representative images of PC3 cell wound healing assays taken 0 h or 24 h after wounding.

Next, we used CITe-Id in PC3 cells to assess the proteome-wide selectively of JZ128. Quantitative, dose-dependent competitive binding data for 686 reproducible JZ128-DTB-labeled cysteines confirmed C840 of PKN3 as the primary target, with slightly less potency against PIKFYVE and TNK1 (Figure 5-8A, left and Figure 5-8B). Twelve other sites showed significant competitive dose-response to JZ128, including the kinases SRC, RIPK2, and RIOK2 (Figure 5-9A). The JZ128-DTB labeling site for these kinases was positioned adjacent to the kinase active site (Figure 5-9B). *In vitro* kinase assays showed JZ128 to have a roughly 200 nM IC50 against SRC and RIPK2 (Figure 5-9C, D). While our CITe-Id profiling of JZ128 provided information on competitive dose-dependence of covalent bond formation at specific cysteine residues, these data do not necessarily correlate with inhibition of JZ128-labeled enzymes. We used the industry-standard KiNativ platform to interrogate JZ128 with respect to kinase inhibition (ActivX Biosciences, La Jolla, CA) (Patricelli et al., 2011; Patricelli et al., 2007). A Venn diagram in Figure 4A summarizes

our complementary data for JZ128 covalent binding (ClTe-Id) and kinase inhibition (KiNativ). In total 292 kinases were detected in PC3 cells, with only three showing greater than 50% inhibition at 1 μM JZ128 (Figure 5-8A, right). Two of these kinase targets (PIKFYVE and RIPK2) overlapped with ClTe-Id data, while a third (PIP4K2C) was identified only by KiNativ. In contrast, kinase targets including PKN3, TNK1, or RIOK2 were detected exclusively by CITe-Id. Further interrogation of these data revealed interesting anomalies. For example, CITe-Id identified SRC as being competitively bound at Cys280, proximal to the kinase active site. Our in vitro kinase assay demonstrated moderate activity of JZ128 for SRC (IC50 = 235nM), while KiNativ data suggested that JZ128 had little or no SRC-activity in vivo. RIPK2 was also enigmatic. CITe-Id reported competitive binding for JZ128 at multiple cysteines on RIPK2; each of these was outside the active site, but unresolved by available protein structures. Similarly, KiNativ data showed two lysines bound by the ActivX-ATP probe, but with different competition profiles. Our kinase assays for RIPK2 showed nearly equivalent potency for JZ128 and JZ128-R, while biochemical data indicated a substantial difference for RIPK2 engagement for JZ128 compared to its reversible analog (Figure 5-9F). These observations highlighted the complementary nature of CITe-Id and KiNativ, and also the importance of integrating multiple, orthogonal assays to fully validate the target landscape of small molecule inhibitors.

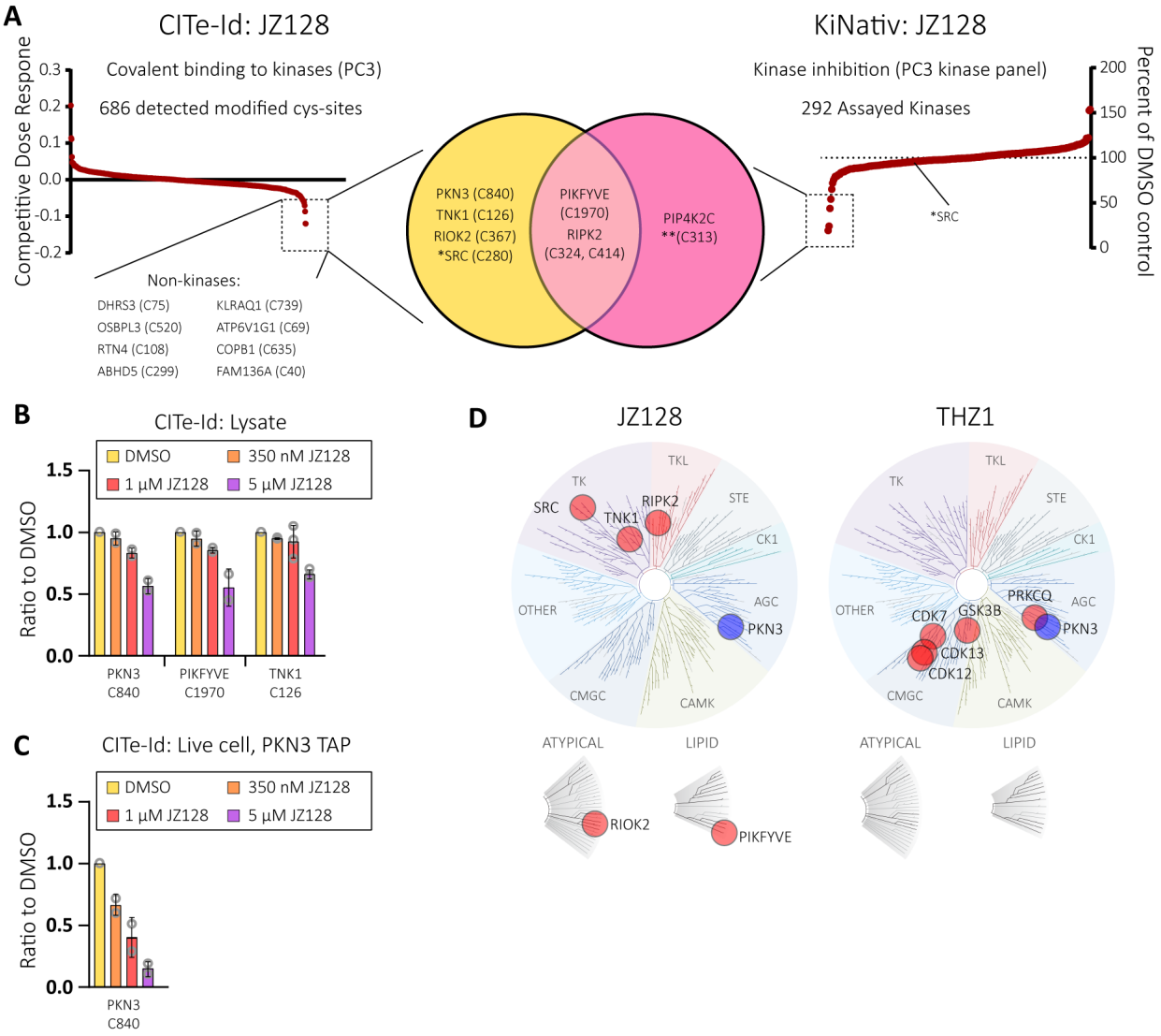

Figure 5-8. Selectivity Profiling of JZ128. (A) CITe-Id profiling compliments KiNativ profiling (Left) Replicate CITe-Id results for JZ128 and JZ128-DTB in PC3 lysates with JZ128-DTB-labeled cysteine sites rank ordered for competitive dose-response to JZ128. Dashed box indicates sites with a competitive dose response threshold two standard deviations relative to the mean value of the null. (Right) KiNativ results rank-ordered by kinase inhibition. Dashed box indicates kinases with >50% inhibition by JZ128 at 1 µM. (Middle) Venn diagram overlaying the kinase results for CITe-Id and KiNativ profiling. *SRC was competitively bound by JZ128-DTB (CITe-Id) but not enzymatically inhibited (KiNativ). **JZ128 labeling of PIP4K2C C313 was identified using non-tryptic protease digestion of the purified protein. All cysteine labeling sites were determined with CITe-Id except where noted for PIP4K2C. (B) CITe-Id data for kinase cysteines modified by JZ128-DTB with competitive dose responses (>3 std. dev. relative to the mean of the null). Bars represent the mean of the ratio of a condition from each biological replicate with standard deviation error bars and individual data points as grey circles. (C) Live PC3 cells expressing FLAG-HA-PKN WT were treated with JZ128. After lysis samples were treated with JZ128-DTB and FLAG-HA-PKN3 was enriched by tandem affinity purification. Bar plot shows competitive dose-response for the JZ128-DTB modified C840-containing PKN3 target peptide across two biological replicate experiments. (D) Dendrograms of the kinome depicting the covalent targets of JZ128 and THZ1 as identified by CITe-Id. Image generated using TREEspot™ Software Tool and reprinted with permission from KINOMEscan®, a division of DiscoveRx Corporation.

Figure 5-9. (A) Replicate CITe-Id results for JZ128 and JZ128-DTB in PC3 lysates. Cysteine residues bound by JZ128-DTB in a concentration-dependent manner as indicated by a dose-response exceeding two standard deviations relative to the median value of all 686 reproducibly labeled cysteine residues. (B) Structures of PIKFYVE, TNK1, and SRC facing kinase active sites with cysteine labeling sites of JZ128-DTB highlighted as colored spheres. All other unlabeled cysteine residues are displayed as black spheres. (PIKFYVE: Swiss-Model Q9Y1I7, TNK1: Swiss-Model Q13470, SRC: PDB 1FMK (Xu, Harrison, & Eck, 1997)). (C,D) In Vitro kinase assays for SRC and RIPK2 inhibition. (E) Live HEK 293T cell treatments with JZ128 or JZ128-R. Lysates treated with JZ128-DTB, followed by streptavidin pulldown and immunoblotting against PIP4K2A-C homologs or PIKFYVE. (F) Live PC3 cell treatments with JZ128 or JZ128-R. Lysates treated with JZ128-DTB, followed by streptavidin pulldown and immunoblotting against PKN3, PIKFYVE, or RIPK2.

Figure 5-9 (Continued).

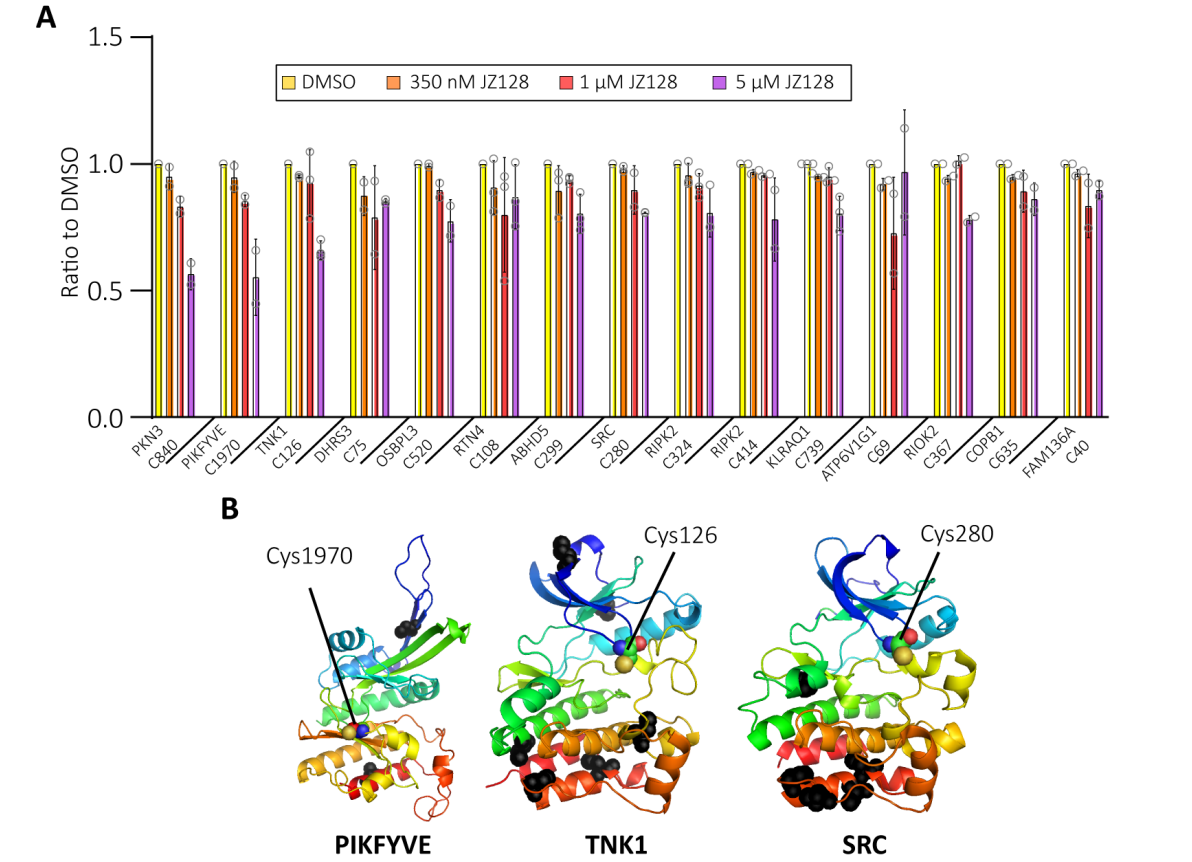

These data also provided clues for potential improvements in our CITe-Id platform. KiNativ detected PIP4K2C as a potential new off-target of JZ128, not reported by CITe-Id. We used cellular target engagement assays to confirm modest competitive binding of JZ128-DTB for PIP4K2C, in addition to its homologs PIP4K2A/B and PIKFYVE (Figure 5-9E, F). Closer inspection of PIP4K2C suggested C313 as the most likely JZ128 binding site. However, the tryptic peptide containing C313 comprised 65 amino acids, a size not likely amenable to LC-MS/MS. Importantly, our previous work demonstrated that generation of inhibitor-specific fragments during MS/MS was independent of peptide cleavage specificity (Ficarro et al., 2016). Pursuant to this observation we digested purified PIP4K2C-JZ128 conjugates with endoprotease GluC and readily identified the modified C313 peptide (Figure 5-10). These data suggested that use of a combination of proteolytic enzymes would provide increased target coverage for CITe-Id beyond use of trypsin alone. We also noted a significant difference in competitive dose-response for PKN3 as readout by CITe-Id (Figure 5-8B) and western blot target engagement (Figure 5-6C).

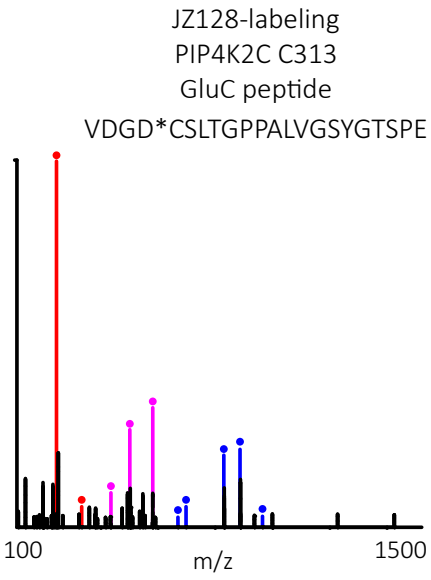

Figure 5-10. MS2 spectra of JZ128-labeled, GluC digested PIP4K2C peptide containing Cys-313. Red: y ions, blue: b ions, pink: JZ128 specific fragment ions.

To explore this discrepancy, we first used stable incorporation of labeled amino acids (SILAC) in a quantitative proteomic screen to confirm equivalent reactivity of JZ128 and its DTB-analog against cysteines in protein lysates. As further validation we used the same experimental design to test THZ1/THZ1-DTB (Figure 5-11). These analyses showed minimal reactivity differences between each pair of analogs for the majority of covalently modified cysteine sites. A second possible explanation was that JZ128 exhibits varying reactivity when incubated in protein lysates (CITe-Id, Figure 5-8B) versus live cells (WB target engagement, Figure 5-6C). To test this hypothesis, we treated live FLAG-HA-PKN3 WT PC3 cells with the same concentration range of JZ128 for 3hrs, lysed cells and incubated with JZ128-DTB as in CITe-Id, then purified tagged PKN3 using tandem affinity purification (Adelmant et al., 2012; Rozenblatt-Rosen et al., 2012), followed by iTRAQ labeling and LC-MS/MS. Dose-response for competitive JZ128-DTB binding was more robust in this targeted PKN3 analysis (Figure 5-8C). These data demonstrated the potential improvement afforded by incorporating live cell treatment into our CITe-Id workflow. These platform modifications notwithstanding, our cumulative data suggested that structurally related THZ1 and JZ128 each covalently modify and inhibit a limited set of kinases, with PKN3 as their only shared target (Figure 5-8D).

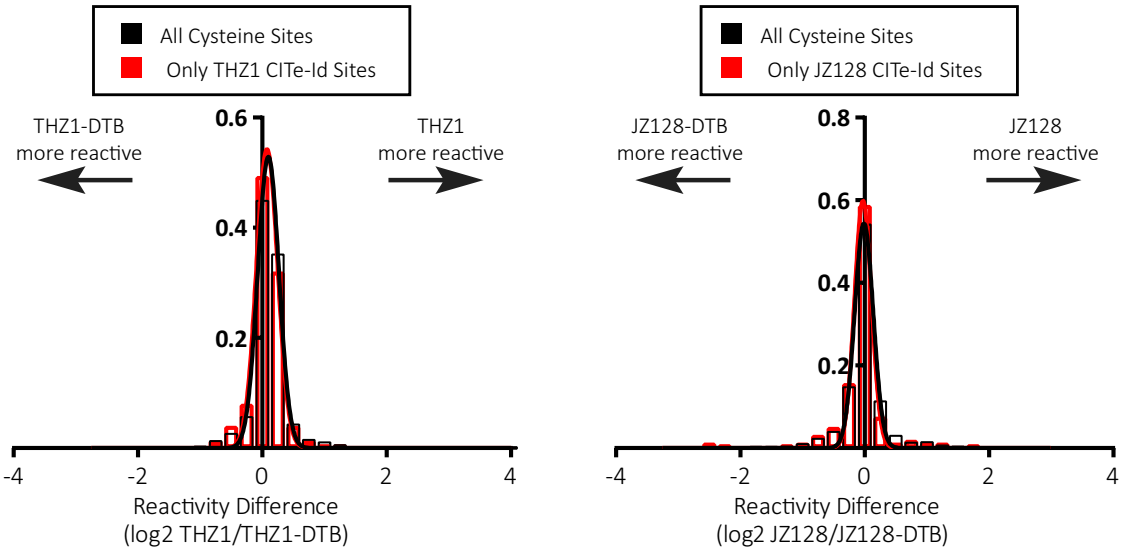

Figure 5-11. Comparison of untagged and desthiobiotin-tagged compound reactivity. Shown are overlaid density histograms of the reactivity between the untagged and tagged compounds used in this study for all cysteine sites detected (black) and only sites also found to be covalently modified in the compounds' respective CITe-Id experiments (red). Both the bins and a 9 nonlinear regression for the data are included. Arrows indicate direction of higher reactivity for each compound. THZ1/THZ1- DTB comparison: all sites N = 1,177, CITe-Id sites N = 75; JZ128/JZ128-DTB comparison: all sites N = 854, CITe-Id sites N = 160.

Identification of Potential PKN3 Substrates Using JZ128 and THZ1

Mechanistic studies place PKN3 downstream of phosphoinositide 3-kinase (PI3K), and have suggested that biochemical complex formation between RhoC, PKN3, and PDK1 may lead to PDK1-dependent activation of PKN3 (Unsal-Kacmaz et al., 2012). Previous studies using mouse models and siRNA knock down demonstrated a role for PKN3 in cell migration, invasiveness, and increased metastatic potential of prostate cancer cells (Leenders et al., 2004; H. Mukai et al., 2016), as well as the dynamics of adherens junctions (Mopert et al., 2012). Interestingly, unlike PKN1 and PKN2 that are ubiquitously expressed, PKN3 is tissue specific (Oishi et al., 1999). Data from various cancer genomics studies suggest that PKN3 is amplified and/or over-expressed in some solid tumors (Cerami et al., 2012; Gao et al., 2013; Nguyen et al., 2017; Oishi et al., 1999). However, the substrates and downstream effectors of PKN3 are unknown.

We therefore focused on using JZ128 and THZ1 as tool compounds to identify potential PKN3 substrates and get additional insights into PKN3 function. We utilized our set of PC3 cells in a combined quantitative, chemical, and genetic phosphoproteomic analysis (Figure 5-12A). We incorporated cells expressing the mutant CS PKN3 to control for covalent on-target effects of JZ128, as well as treatment with JZ128-R as a control for potential off-target, non-covalent effects of the inhibitor. We further reasoned that combined use of JZ128 and THZ1 would reduce false-positives, as these probes share PKN3 as their only common target. In total, we reproducibly quantified 14,700 phosphorylation sites across 3,136 proteins for two biological replicates. We used phosphopeptides enriched from untreated PC3 cells to establish reporter ion variance as a function of intensity (Breitwieser et al., 2011; Y. Zhang et al., 2010). Based on this error model we identified 91 discrete phosphorylation sites which exhibited a regulation pattern consistent with a PKN3 substrate under the different conditions tested in our phosphoproteomic analysis (Figure 5-12B). We next sought to prioritize this set based on similarity with a PKN3 phosphorylation motif. We used recombinant PKN3 with our expanded, randomized peptide library (Singel et al., 2014) to generate a putative PKN3 motif consisting of Leu-X-Arg-X-Pro-*Ser-Phe-Arg-X-X (Figure 5-12C). These data further refine a previously reported PKN3 motif (F. Liu et al., 2013; Uehara et al., 2017), placing stronger emphasis on proline at the -1 and arginine at the +2 positions, with reduced dependence on positions -5, -4, -2, +3, and +4. We scored each of the 91 phosphorylation sites based on sequence-similarity with our PKN3 motif in addition to an estimate of the likelihood of a motif-match for PKN3 compared to a larger set of 191 kinase motifs determined using our peptide library approach (unpublished data). This analysis highlighted 25 phosphorylation sites as putative direct substrates, including a potential

site of autophosphorylation (S544) on PKN3 (Figure 5-12D). Consistent with reported functional roles for PKN3 (Mopert et al., 2012) these putative substrates are enriched for proteins involved in cellular junction related GO terms: cadherin binding (Odds ratio = 23; p_{adj} <0.001) and cell adhesion molecule binding (Odds ratio = 15; p_{adj} = 0.021) (Berriz, Beaver, Cenik, Tasan, & Roth, 2009). As a first step in validating these data, we obtained synthetic peptides encompassing the phosphorylation site and surrounding motif and used them as substrates for *in vitro* PKN3 kinase assays. Our analysis confirmed the original peptide sequence and phosphorylation site assignment (Figure 5-13A), and furthermore that PKN3 phosphorylated 100% and 50% of motif-serine residues on LAD1 (S375) and EXOC2 (S432), respectively. Pretreatment with either THZ1 or JZ128 partially blocked PKN3-mediated phosphorylation of these sites (Figure 5-12E). We also tested EGFR (S1064) but failed to detect PKN3-mediated phosphorylation. While we validated the EGFR phosphopeptide assignment identified in our screen (Figure 5-13B), we noted that the neighboring residues comprised a lower-score sequence for a potential PKN3 motif, compared to LAD1 or EXOC2. Although subject to further validation, these results illustrate a powerful use of our covalent inhibitors to identify promising, candidate PKN3 substrates.

Discussion

Although historically eschewed by drug development programs, irreversible inhibitors are now gaining momentum (Bauer, 2015). We and others have used structure-guided synthesis to develop selective CKIs which inhibit kinase activity through covalent modification of non-conserved, active-site cysteine residues (Q. Liu et al., 2013). We recently extended this paradigm to achieve selective inhibition by targeting 'remote' cysteine residues (Kwiatkowski et al., 2014;

T. Zhang et al., 2016). Encouragingly these results suggest that the landscape of drug targets amenable to selective covalent inhibition via cysteine reactivity may be significantly larger than previously predicted (Q. Liu et al., 2013). However, our inability to predict potential off-target reactivity represents a major liability for development of covalent drugs. Therefore, design, development, and characterization of covalent inhibitors must be considered in the context of the entire proteome (Weerapana et al., 2010).

Activity based protein profiling, exemplified by TOP-ABPP has provided valuable insight for the cellular activity of a variety of small molecules (Backus et al., 2016; Bar-Peled et al., 2017; Blewett et al., 2016; X. Deng et al., 2013; Quinti et al., 2017; Weerapana et al., 2010). However, in the specific case of CKIs, these techniques typically rely on the use of promiscuous cysteine probes as surrogate readouts for the reactivity of selective inhibitors (Backus et al., 2016; Blewett et al., 2016; X. Deng et al., 2013; Quinti et al., 2017; C. Wang et al., 2014; Weerapana et al., 2007; Weerapana et al., 2010). In contrast, our CITe-Id platform repurposes selective CKIs as affinity reagents to directly enrich protein targets. Moreover, incorporation of our new knowledge of gas-phase fragmentation behavior characteristic of covalent probe-peptide adducts (Ficarro et al., 2016) enables us to focus exclusively on CKI-modified peptides. With CITe-Id we circumvent the difficult task of exhaustively profiling a large set of cysteine residues bound by a biologically irrelevant ABPP probe in order to identify the modest set of residues which are bound by a selective inhibitor. Importantly, CITe-Id data provide direct evidence of covalent mechanism-of-action, while the incorporation of multiplexed isotope labels provides a readout of competitive dose-response at each CKI-modified cysteine-thiol.

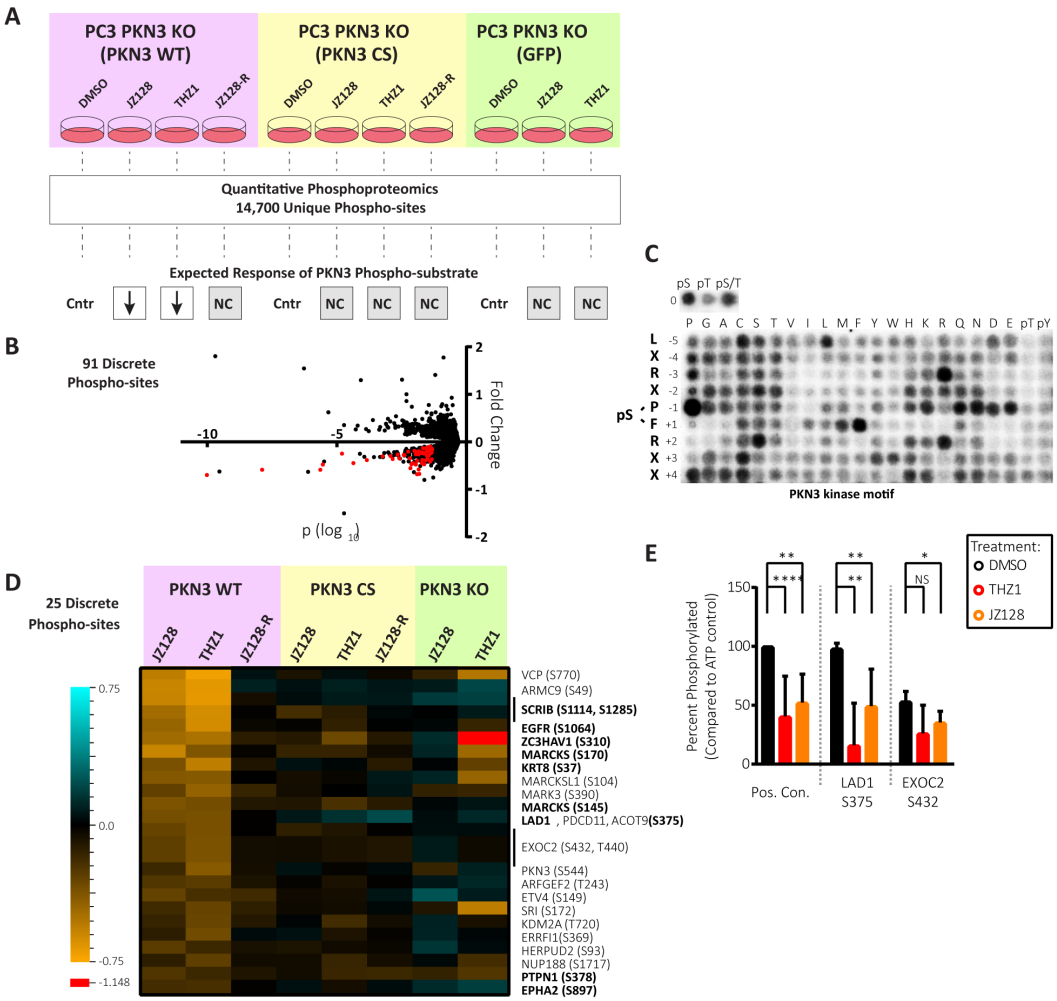

Figure 5-12. Phosphoproteomic discovery of potential PKN3 substrates. (A) Illustration of genetic and chemical controls, experimental workflow, and the expected response of a direct PKN3 phosphorylation substrate under the conditions tested. Each experimental treatment was compared to its matched DMSO control (Cntr). Only the JZ128 and THZ1 treatments in the WT PKN3 background were expected to mediate reduced phosphorylation (down arrows). All other treatment conditions were expected to show no change (NC). 91 phospho-sites fit these criteria. (B) Representative volcano plot showing the fold change and $\log_{10}$ p-value of 14,700 reproducibly quantified phosphorylation sites. The p-values were determined by use of a variance model as previously described (Breitwieser et al., 2011; Y. Zhang et al., 2010). Data for the PKN3 WT JZ128 treatment vs. PKN3 WT DMSO treatment is shown. Red dots comprise the 91 phosphorylation sites that met all criteria in A for potential direct substrates of PKN3. (C) PKN3 motif derived from analysis of randomized peptide library. (D) Heat map of fold change values for the 25 phosphorylation sites meeting all criteria for potential direct substrates of PKN3. The single red cell (value = -1.148) in the heatmap is outside the range of the legend. (E) PKN3 *in vitro* phosphorylation of synthetic peptides which exhibited reduced phospho-serine levels in PKN3 WT cells treated with JZ128/THZ1, and closely matched our predicted PKN3 motif. Bar graphs show percent phosphorylation of each site compared to no ATP control conditions across four replicate experiments. Positive control is the same synthetic peptide used for *in vitro* kinase assays with PKN3. THZ1 and JZ128 treatments were at 1 µM for 30 min prior to starting the assay. (N = 4-10 replicates) NS: p-value > 0.05, *: p-value < 0.05, **: p-value < 0.001, ****: p-value = <0.0001.

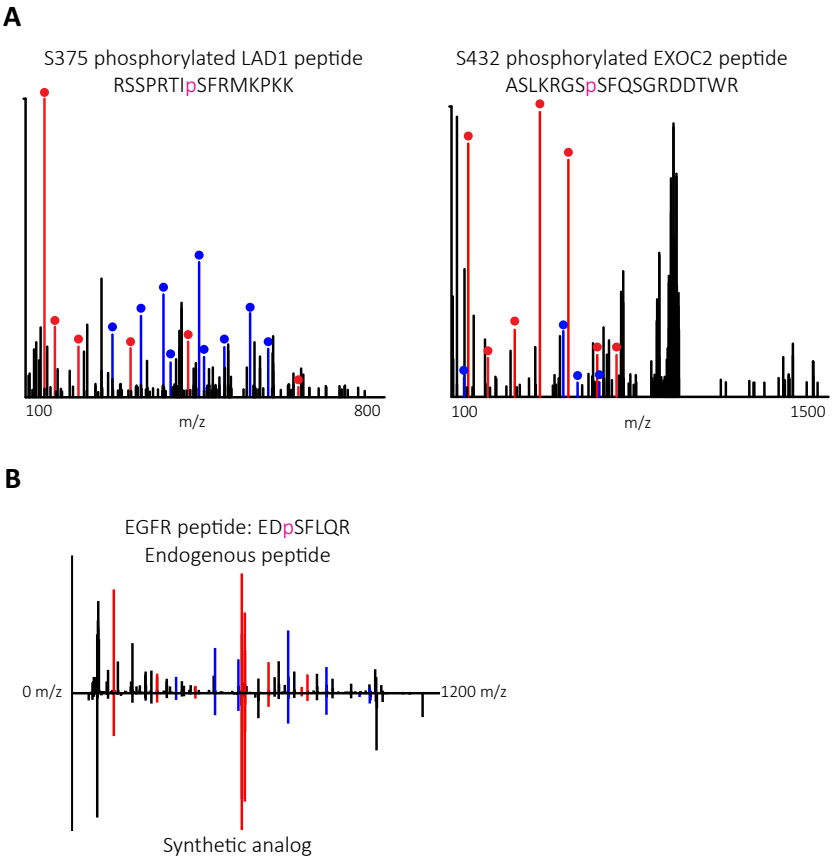

Figure 5-13. Peptide sequence and phosphosite validation. (A) MS/MS spectra for the LAD1 S375 and EXOC2 S432 peptides phosphorylated in vitro by PKN3. y-type ions are colored red and b-type ions are colored blue. (B) MS/MS spectra for EGFR phosphopeptide observed in phosphoproteomic experiment (top) and the synthetic peptide analog (bottom). y-type ions are colored red and b-type ions are colored blue. Pink lower case 'p' indicates phosphorylation on the subsequent serine residue.

In the work described here, we used CITe-Id to profile THZ1 reactivity, and discovered PKN3 as a new selectively-bound THZ1 target. PKN3 is a downstream effector of activated phosphoinositide-3-kinase (PI3K) that mediates metastatic transformation and growth (Leenders et al., 2004), tumor angiogenesis (H. Mukai et al., 2016), as well as bone resorption (Uehara et al., 2017). A siRNA based therapeutic strategy against PKN3 has been in clinical trials for advanced solid tumors and as a combination treatment for advanced or metastatic pancreatic cancer ((Schultheis et al., 2014), and NCT01808638), highlighting its relevance as a disease target. However, the biology of PKN3 is understudied, nominating it as a bona fide member of

the ‘dark-kinome’ (Nguyen et al., 2017). These data, in addition to the lack of commercial assays for this kinase, motivated us to explore PKN3 further. Using THZ1 as a starting scaffold we confirmed JZ128 as a ~100 nM covalent inhibitor for PKN3 with good selectivity over CDK7, 12, and 13. In addition, JZ128 exhibited improved cellular toxicity profiles compared to THZ1, enabling its use in cell-based assays to interrogate PKN3 function. We used CRISPR-engineered prostate cancer-derived PC3 cells to confirm an on-target phenotype for PKN3 WT versus the C840S mutant in a wound healing assay. These results were confounded by re-appearance of wound healing defects in matched cells depleted of *PKN3*. It is difficult to predict the myriad effects of genetic depletion and how they may activate compensatory pathways. It would be interesting for future studies to investigate possible genetic links between PKN3 and the off-targets of JZ128 such as RIPK2 or PIKFYVE, which both play key roles in cellular pathways related to wound healing (Adams, Valchanova, & Munz, 2010; Haugsten, Oppelt, & Wesche, 2013; Oppelt et al., 2014; Singel et al., 2014; S. Wu, Kanda, Nakamoto, Imazeki, & Yokosuka, 2012). Pending in-depth exploration of *PKN3* genetic dependencies, we recommend the PKN3 C840S mutant as the most suitable negative control for pharmacologic studies of JZ128. It also is important to note that installation of the affinity handle may disrupt the kinetics of ligand binding. For the work herein, we attached desthiobiotin to the dimethylaminomethyl (DMAM) moiety of THZ1 and JZ128, respectively. While the DMAM functionality is not formally required for implementation of CITe-Id, we found it a convenient, solvent-exposed anchor point. Ongoing work in our group suggests CITe-Id is compatible with numerous warhead chemistries including unsubstituted acrylamides, haloacetamides, haloketones, and halotetrahydroacridines (unpublished data). For new covalent probe architectures, western blot target engagement

assays can be used to confirm expected competitive binding behavior for new DTB-analogs against known kinase targets. Additionally, when using a new covalent warhead, initial database searches of CITe-Id data should include the possibility for covalent modification on other amino acid side chains.

We used KiNativ to corroborate our CITe-Id results for JZ128; both platforms identified several off-targets, including PIKFYVE, TNK1, RIPK2, RIOK2, and SRC. Consistent with our experience with other kinome profiling services, KiNativ provided no data for PKN3, the primary target of JZ128 as revealed by CITe-Id. KiNativ did uniquely identify PIP4K2C as an off-target. In this case we confirmed that use of an alternative protease enabled identification of the JZ128-modified cysteine residue. In fact, consistent with our previous work (Ficarro et al., 2016), it should be straightforward to incorporate multiple enzymes to improve the 'proteomic reach' of CITe-Id. In addition, our analysis of enriched FLAG-HA-PKN3 from live cells treated with JZ128, then further processed with our CITe-Id workflow, better replicated our competition-format target engagement western blot assays. These results provide another promising avenue for further improvement to our CITe-Id platform.

Intrigued that our data apparently represent the first report of a targetable cysteine on PKN3, we performed a meta-analysis based on a compendium of cysteine residues included in eight different TOP-ABPP studies which used broad-reactivity iodoacetamide-alkyne probes (Abo & Weerapana, 2015; Backus et al., 2016; Bak et al., 2017; Bar-Peled et al., 2017; Blewett et al., 2016; X. Deng et al., 2013; Quinti et al., 2017; Weerapana et al., 2010) (Figure 5-14, yellow). In total, these TOP-ABPP data captured approximately 14,000 cysteines. Interestingly, 28% of cysteines covalently labeled by THZ1 or JZ128 are not represented in the TOP-ABPP catalog. But

strikingly, 12 of the 22 CITe-Id derived cysteine thiols labeled in a concentration-dependent manner were identified exclusively by CITe-Id, including C840 on PKN3 (Figure 5-14). Taken together, these data highlight the power of CITe-Id to uncover new, pharmacologically-addressable regions of the cellular cysteineome.

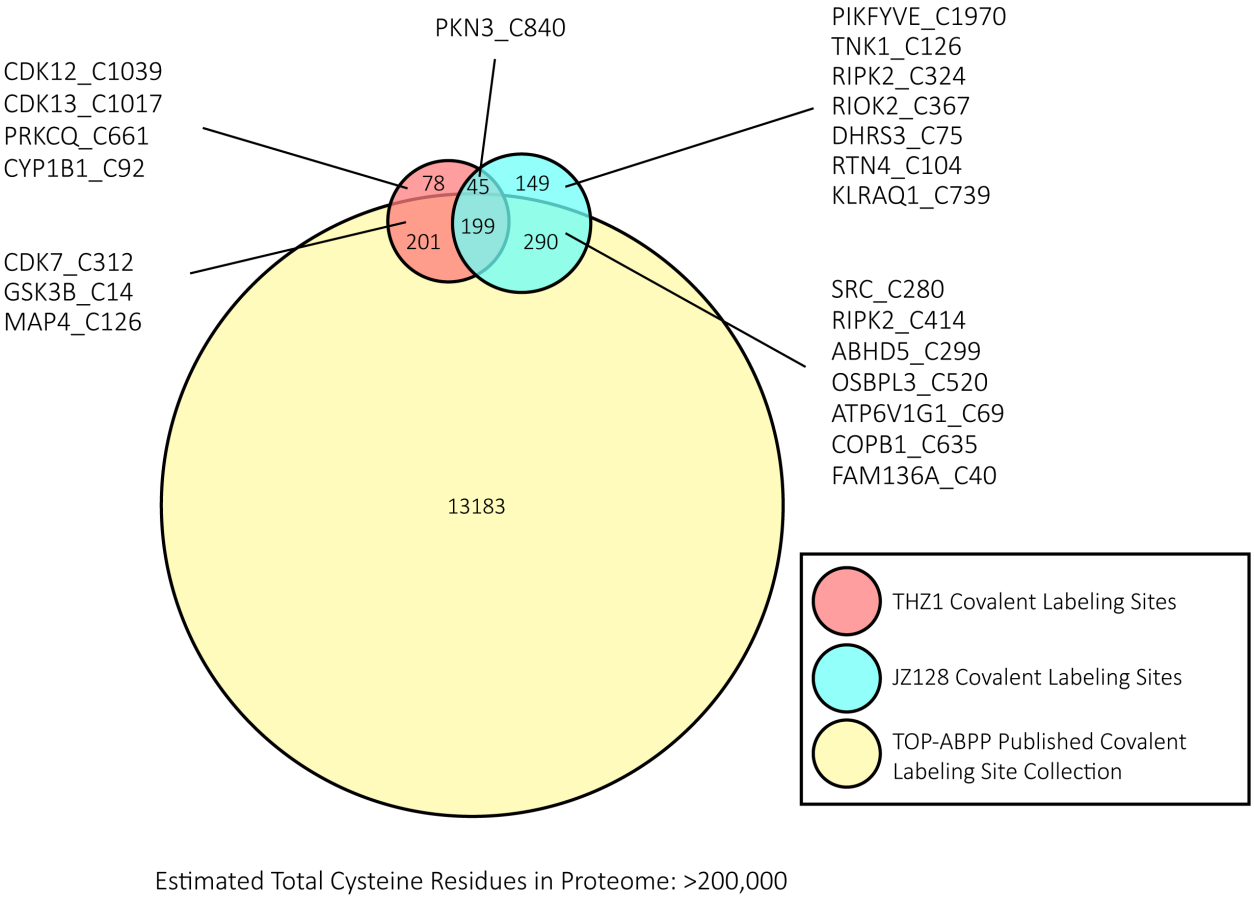

Figure 5-14. Venn diagram of reported cysteine labeling sites for THZ1, JZ128, and 8 seminal TOP-ABPP site-level publications. Data represents the union of reported cysteine labeling sites. The 22 dose-dependent targets of THZ1 and JZ128 identified by CITe-Id are listed individually, along with the modified cysteine residue. Twelve of these 22 sites are unique to CITe-Id.

Our CITe-Id data streamlined development of JZ128 as a new, first-in-class inhibitor of PKN3. In an initial interrogation of PKN3 cellular activity, we used JZ128 in a quantitative phosphoproteomic analysis to identify PKN3 substrates. Numerous chemical and genetic

controls along with a refined prediction of a PKN3 kinase motif provided stringent criteria for identification of potential phosphorylation substrates. *In vitro* phosphorylation assays confirmed PKN3 activity on S375 of LAD1 and to a lesser extent S432 of EXOC2. LAD1 is an attractive candidate for future functional validation given its well-established role in cell junctions (Marinkovich, Taylor, Keene, Burgeson, & Zone, 1996). In addition to LAD1 and consistent with reports of PKN3's functional role in normal physiology and tumor metastases (Leenders et al., 2004; Mopert et al., 2012), our set of 25 putative substrates is enriched for proteins involved in adherens junctions, including SCRIB, EGFR, ZC3HAV1, MARCKS, KRT8, PTPN1, and EPHA2. Collectively, our data provide important leads for future mechanistic studies to interrogate the role of PKN3 in cellular junctions as well as the metastatic potential of solid tumors.

It should be noted that binding data from CITe-Id is not directly analogous to inhibition of enzymatic activity, with CITe-Id supplementing but not replacing traditional enzyme-activity assays. Overall, CITe-Id is a complementary methodology that fits well within an irreversible inhibitor development program as it offers information valuable for understanding the precise mechanism of action as well as proteome-wide, covalent off-target effects.

Taken together, CITe-Id represents a conceptually novel strategy for rapid and accurate proteome-wide identification of covalently-modified sites targeted by irreversible inhibitors. We expect that CITe-Id profiling will enable rapid irreversible inhibitor screening to inform medicinal chemistry optimization efforts as well as mechanistic studies of these inhibitors and their off-target effects. As illustrated by our PKN3 work, CITe-Id analysis can accelerate discovery of novel selective inhibitors and functional characterization, especially in the context of the understudied kinome.

Chapter 6: Discovery and Characterization of Potent and Selective PIN1 Inhibitors Targeted to an Active Site Cysteine

Author Contributions

Benika J. Pinch, a graduate student in the Gray lab, designed and synthesized all compounds, performed the experiments, interpreted the data. Zainab M. Doctor generated cell lines as well as all constructs used, performed the GFP dropout experiment, performed data analysis for cell cycle and RNAseq experiments, and helped with biological experiment design. Christopher M. Browne performed the mass spectrometry experiments under the guidance of Jarrod Marto. Shingo Kozono and Xiaolan Lian performed the biochemical characterization of the inhibitors. Daniel Zaidman, Dina Daitchman and Nir London provided computational docking support. Li Tan provided input in the initial compound designs. Yujin Chun performed yeast complementation growth assays. Zoe C. Yeoh, Nicholas E. Vangos, Ezekiel A. Geffken and Hyuk-Soo Seo performed the protein expression and crystallography experiments, H.S.S and Sirano Dhe-Paganon analyzed the crystallography data. Kun Ping Lu and Xiao Zhou helped supervise the project and provided experimental support and advice. Nathanael S. Gray conceived of and supervised the project.

Introduction

Proline-directed phosphorylation controls numerous cellular processes, including cell cycle regulation, transcription, and cell differentiation. Deregulation of such signaling networks is a hallmark of cell transformation and oncogenesis. Proline (Pro) is unique among the amino acids in that its imidic peptide bond can populate either the *cis* or the *trans* conformation (Z. Lu & Hunter, 2014). The intrinsic isomerization rate of proline-containing motifs is slow relative to biological signaling processes, requiring catalysis by peptidyl prolyl isomerases (PPIases). Three families of PPIases have been identified, including the cyclophilins (Cyp), FK506 binding proteins (FKBPs), and parvulins. Cyp and FKBP proteins isomerize peptidyl prolyl bonds adjacent to a serine or threonine residue (Ser/Thr-Pro) and bind the immunosuppressant drugs, Cyclosporin A and FK506. PIN1 belongs to the parvulin family and is the only known isomerase specific to phosphorylated Ser/Thr-Pro motifs (K. P. Lu & Zhou, 2007; E. S. Yeh & Means, 2007).

PIN1 acts in tandem with Pro-directed kinases and phosphatases to control the activity of their common targets. Examples of kinases and phosphatases that act on Ser/Thr-Pro motifs include the cyclin-dependent protein kinases (CDKs), glycogen synthase kinase 3β (GSK3β), mitogen-activated protein kinases (MAPKs), and protein phosphatase 2 (PP2A) (K. P. Lu et al., 2007; X. Z. Zhou & Lu, 2016). These enzymes act in a conformationally specific manner, often catalyzing phosphorylation or dephosphorylation only when their substrates' peptidyl prolyl bond is in the *trans* conformation (Weiwad, Küllertz, Schutkowski, & Fischer, 2000; E. S. Yeh & Means, 2007). This makes PIN1 a critical regulator of proline-directed phosphorylation signaling networks by modulating the access of kinases and phosphatases to their respective substrates,

leading to changes in phosphorylation status, protein-protein interactions, stability, and/or localization (Liou, Zhou, & Lu, 2011).

PIN1 is frequently overexpressed in cancer, including pancreatic ductal adenocarcinoma (PDAC), and PIN1 overexpression correlates with poor prognosis (Liang et al., 2019). Furthermore, PIN1 is a key effector in Ras signaling in that PIN1 ablation prevents MMTV-Ras - driven mouse mammary gland carcinoma (G. Wulf et al., 2004). While mutations in *KRAS* are observed in 90-95% of PDAC cases (Zeitouni, Pylayeva-Gupta, Der, & Bryant, 2016), it has historically proven extremely difficult to develop small molecule inhibitors of mutant Ras, spurring an effort to target proteins that enable Ras-mediated transformation, such as PIN1. Notably, while the yeast homolog of PIN1 (Ess1) is essential (Hanes, 2014), PIN1-null mice have no obvious defects (Liou et al., 2002) suggesting that PIN1 inhibition could reduce tumorigenic potential with limited toxicity.

Several PIN1 inhibitors have been described to date, including juglone, all-trans retinoic acid (ATRA) (Wei et al., 2015), arsenic trioxide (ATO) (Kozono et al., 2018), KPT-6566 (Campaner et al., 2017), and (S)-2 (Ieda et al., 2019). However, these reported compounds lack the potency and/or selectivity to accurately assess PIN1-mediated phenotypes (Moore & Potter, 2013). Notably, while available PIN1 inhibitors demonstrate potent single-agent cellular cytotoxicity, PIN1 is not a statistically significant cancer dependency in genome-wide RNAi and CRISPR-Cas9 screens conducted across hundreds of cancer cell lines in 2D-adherent monolayer cell culture (Cancer Dependency Map, Broad Institute) – thus highlighting a contradiction in our understanding of PIN1 biology. A selective PIN1 inhibitor is needed in order to better understand PIN1's role in oncogenesis, which may not manifest in traditional cell viability assays.

Targeted covalent inhibitors allow for improved potency and selectivity, and prolonged duration of action (Q. Liu et al., 2013; Mah, Thomas, & Shafer, 2014). Oxidation of the conserved cysteine residue in the PIN1 active site, Cys113, eliminates its isomerase activity (C. H. Chen et al., 2015), suggesting that covalent binders would irreversibly inhibit PIN1's cellular function. Also, previously reported inhibitors juglone, KPT-6566, and (S)-2, provide precedent for targeting PIN1 covalently.

We report the rational design of covalent peptides based on the high affinity but cell impenetrant substrate mimetic inhibitor, pintide (pTide) (Y. Zhang et al., 2007). Through biochemical, cellular, and structural experiments, we demonstrate that the resulting lead compound, BJP-06-005-3, is potent, cell permeable, and highly selective. In a chemoproteomic study using Covalent Inhibitor Target Site Identification (ClTe-Id), described in the previous chapter, dose-dependent labeling of BJP-06-005-3 identified PIN1 Cys113 as the only individual cysteine target, highlighting the pronounced selectivity of BJP-06-005-3 for PIN1. We also characterized the global effects of covalent PIN1 inhibition on transcription by performing RNA sequencing at 4 and 24 hours after compound treatment.

To complement our inhibitor characterization efforts, we utilized the chemical genetic degradation tag (dTAG) strategy (Nabet et al., 2018) to achieve rapid and targeted PIN1 degradation through the generation of $FKBP12^{F36V}$-PIN1, $PIN1^{-/-}$ PATU-8988T cells. We show that PIN1 cooperates with $KRAS^{G12V}$ to promote tumorigenesis in PDAC using ultra-low adherent (ULA) spheroid suspension models, and that treatment with BJP-06-005-3 or targeted degradation of $FKBP12^{F36V}$-PIN1 diminishes the viability of human PDAC cell lines over time. In addition, we used CRISPR/Cas9 GFP-dropout screens to further validate the dependence of these cell lines on PIN1.

Structure-Based Design and Optimization of PIN1 Inhibitors

To develop a PIN1-targeted chemical probe, we modified the substrate mimetic peptide, pTide (Ac-Phe-D-pThr-Pip-Nal-Gln-NH2; K_i = 20 nM), which is a potent PIN1 inhibitor that cannot enter cells (Y. Zhang et al., 2007). We sought to replace the phosphate of pTide with a less polar and therefore more cell permeable moiety, while compensating for the resulting loss in potency via a covalent bond to Cys113. Based on the co-crystal structure of pTide bound to the PIN1 PPIase active site (PDB 2ITK), the N-terminus provided the best access to Cys113 and therefore served as the attachment site for a cysteine-targeting warhead (Figure 6-1A). We chose an α-chloroacetamide electrophile as the reactive warhead because a proteome-wide screen to quantify cysteine reactivity identified several α-chloroacetamide-containing fragments as covalent PIN1 binders (Backus et al., 2016). An α-chloroacetamide is also featured in the covalent PIN1 binder, KPT-6566 (Campaner et al., 2017).

Given precedent that a carboxylate can successfully replace a phosphate in PIN1 inhibitors (Guo et al., 2014), we initially substituted the phospho-Thr of pTide with a carboxylic acid. While an aspartic acid-containing derivative (BJP-02-038-2) was incapable of binding PIN1, the extra methylene of a glutamic acid enabled interaction with the phosphate binding pocket, giving a 2 μM PIN1 binder (BJP-02-041-2), as determined in a competitive fluorescence polarization (FP) assay. Replacing the glutamine of BJP-02-041-2 with an arginine residue improved potency by 12-fold (BJP-02-118-2). We obtained a co-crystal structure of BJP-02-118-2 bound to PIN1, which revealed a charge-charge interaction with Glu135 (Figure 6-2B). We further improved potency by substituting the arginine with its biological precursor, citrulline

(BJP-02-188-2), and by replacing the naphthylalanine with tryptophan, bringing the K_i down to 30 nM (BJP-03-098-3) (Figure 6-1B).

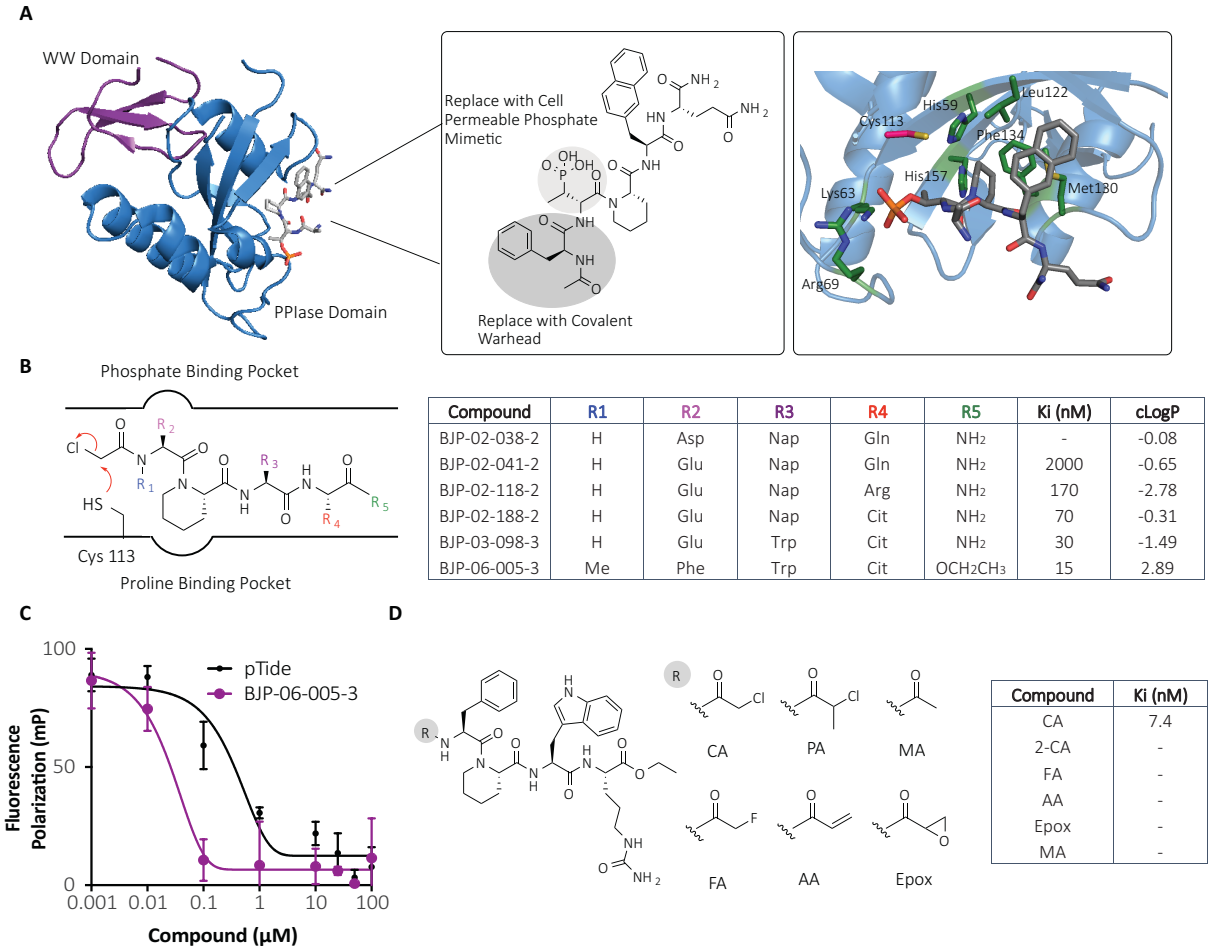

Compound	R1	R2	R3	R4	R5	Ki (nM)	cLogP
BJP-02-038-2	H	Asp	Nap	Gln	NH_2	-	-0.08
BJP-02-041-2	H	Glu	Nap	Gln	NH_2	2000	-0.65
BJP-02-118-2	H	Glu	Nap	Arg	NH_2	170	-2.78
BJP-02-188-2	H	Glu	Nap	Cit	NH_2	70	-0.31
BJP-03-098-3	H	Glu	Trp	Cit	NH_2	30	-1.49
BJP-06-005-3	Me	Phe	Trp	Cit	OCH_2CH_3	15	2.89

Compound	Ki (nM)
CA	7.4
2-CA	-
FA	-
AA	-
Epox	-
MA	-

Figure 6-1. Structure-guided modification of the high affinity substrate mimetic inhibitor, pTide, to yield optimized PIN1 binders. (A) Structure of pTide (gray) bound to the PIN1 (PPIase domain in blue, WW domain in purple) and plan for pTide modification to achieve covalency and cell permeability; key residues for binding are indicated in green, with Cys113 highlighted in magenta (B) Schematic representation of PIN1 PPIase active site and table of synthesized derivatives, their Ki values (measured via fluorescence polarization (FP) assay after a 12 h incubation of the inhibitor and recombinant full-length PIN1 protein), and cLogP values (determined using ChemDraw). (C) Potency of BJP-06-005-3 (Ki = 15 nM) versus pTide in the FP assay after a 12 h incubation of compound and recombinant human full-length PIN1 protein (D) Chemical structures of synthesized derivatives with alternate electrophiles. Alpha-chloracetamide (CA), 2-chloropropionamide (PA), alpha-fluoroacetamide (FA), acrylamide (AA), epoxide (Epox). Unreactive negative control methylacetamide (MA). Corresponding table of FP assay results of compounds with alternate electrophiles after a 12 h incubation of the inhibitor and recombinant full-length PIN1.

Despite successfully replacing the phosphate with a carboxylate, the resulting inhibitors had negative cLogP values and therefore low lipophilicity, which is known to govern passive

membrane permeability (Figure 6-1B, Figure 6-2D). We next sought to increase compound lipophilicity by capping the C-terminus with an ethyl ester, methylating the N-terminal nitrogen to eliminate a hydrogen bond donor, and replacing the glutamic acid with a phenyalanine (Phe) residue to give BJP-06-005-3 (Figure 6-1B). With a K_i of 15 nM (FP assay), BJP-06-005-3 is a more potent PIN1 binder than pTide (Figure 6-1C). We hypothesized that the surprising affinity of this Phe-containing derivative might be explained by a cation-pi interaction between the Phe benzene and Arg68 or Arg69 in the phosphate-binding pocket. Cation-pi interactions can enhance binding energies by 2-5 kcal/mol and are common between arginines and aromatic sidechains (Gallivan & Dougherty, 1999).

We next explored whether alternate thiol-targeting electrophiles might be tolerated by substituting the alpha-chloroacetamide with either an acrylamide (AA), alpha-fluoroacetamide (FA), epoxide (Epox), or 2-chloropropionamide (PA). For these studies, we used a derivative of BJP-06-005-3 lacking the methylated N-terminal nitrogen (CA; K_i = 7.4 nM) so as to enhance the reactivity of the series. As a control, we also synthesized the unreactive *N*-methylacetamide (MA) (Figure 6-1, Figure 6-3A, B). None of the compounds featuring alternate electrophiles were capable of binding to PIN1, highlighting that the α-chloroacetamide is necessary to achieve covalency in this scaffold (Figure 6-1D). Similarly, an analogue of BJP-06-005-3 in which the α-chloroacetamide was replaced with an unreactive *N*-methylacetamide (BJP-R, Figure 6-2C) lost all binding to PIN1, indicative of a covalent binding mechanism. This also highlights that, despite optimizing the noncovalent interactions with the PPIase active site, the binding of BJP-06-005-3 is primarily driven by its covalency. While pTide features a D-phos.Thr residue, the covalent

binding of BJP-06-005-3 flips the preferred stereochemistry at that position such that a D-Phe substitution (BJP-06-121-3) completely eliminates PIN1 binding (Figure 6-2D).

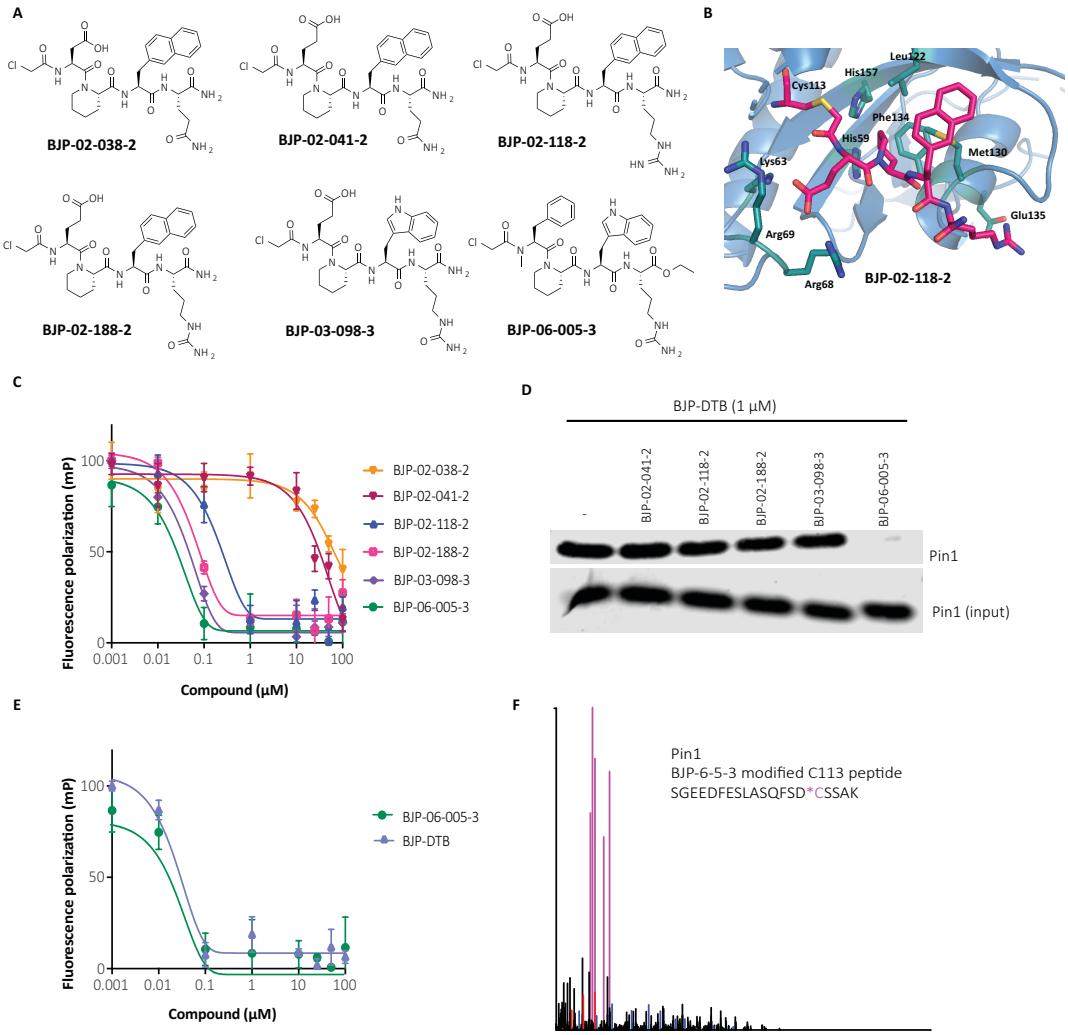

Figure 6-2. (A) Chemical structures of the peptides that informed the structure-activity relationship (SAR) progression and identification of lead inhibitor, BJP-06-005-3. (B) Co-crystal structure of BJP-02-118-2 (magenta) bound to PIN1 (blue) with key binding residues highlighted in green (PDB 6033), (C) BJP-06-005-3 is biochemically more potent than any of the preceding peptide derivatives. Fluorescence Polarization data for compounds shown in panel (a) after a 12 h incubation of compound and recombinant human full-length PIN1 protein. (D) Live cell competition experiment demonstrating that, of the compounds shown in panel (a), BJP-06-005-3 was the only compound to achieve cell permeability. PATU-8988T cells were treated with 10 μM of the indicated compounds for 5 hours, followed by cell lysis, incubation with BJP-DTB for 1 hour, avidin pulldown, and immunoblot analysis. (E) BJP-DTB and BJP-06-005-3 demonstrate equivalent biochemical potency for PIN1. Fluorescence Polarization data for BJP-DTB and BJP-06-005-3 after a 12 h incubation of compound and recombinant human full-length PIN1 protein. (F) MS/MS spectrum of PIN1 Cys113 labeled with BJP-06-005-3.

In summary, by making a series of structure-guided modifications to pTide, we identified BJP-06-005-3 as a high affinity PIN1 binder with a cLogP (2.89) within the average range for an oral drug (Hopkins, Keseru, Leeson, Rees, & Reynolds, 2014). The covalent binding mode ultimately allowed us to replace the phosphate of pTide with a Phe in BJP-06-005-3, achieving potency without compensating lipophilicity.

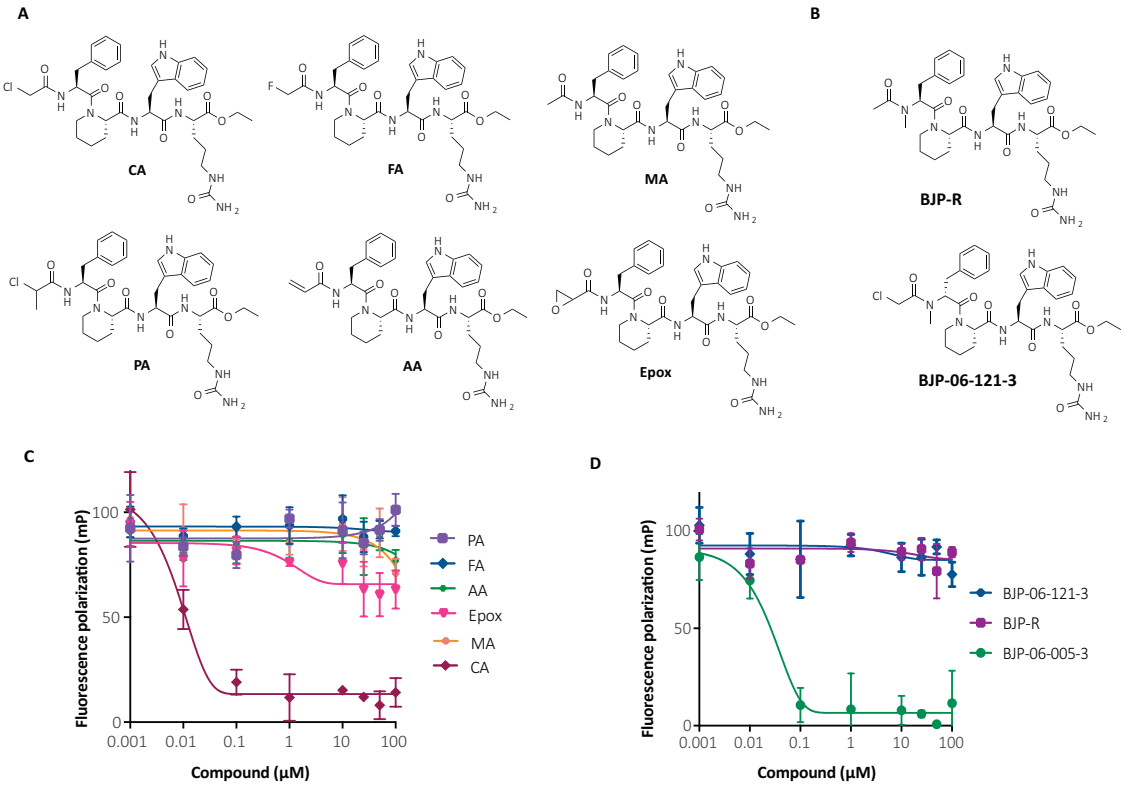

Figure 6-3. (A) Chemical structures of compounds synthesized with alternate electrophilic warheads. (B) Chemical structures of the reversible negative control, BJP-R, and the inactive stereoisomer, BJP-06-121-3. (C) Only the α-chloroacetamide warhead (CA) enables binding to PIN1. Fluorescence Polarization data for compounds shown in panel (a) after a 12 h incubation of compound and recombinant human full-length PIN1 protein. (D) Negative controls, BJP-R and BJP-06-121-3, do not bind PIN1. Fluorescence Polarization data for compounds shown in panel (b) after a 12 h incubation of compound and recombinant human full-length PIN1 protein.

BJP-06-005-3 is a Potent and Covalent PIN1 Inhibitor, Targeted to Cys113

We next performed a flow-chart of assays (Figure 6-4A) to evaluate the potency and binding mode of BJP-06-005-3 (Figure 6-4B). Having established that BJP-06-005-3 was a potent

PIN1 binder using a competitive FP assay (Figure 6-1C), we next assessed the ability of BJP-06-005-3 to inhibit PIN1 enzymatic activity using a chymotrypsin-coupled peptidyl-prolyl isomerization assay (PPIase assay). In this spectrophotometric assay, the peptidic substrate (Succ-Ala-p.Ser-Pro-Phe-pNA) is only cleaved by chymotrypsin when the peptidyl-prolyl bond is in the *trans* conformation, such that compounds that inhibit the rate of *cis* to *trans* isomerization will decrease the fluorescent output (Figure 6-4A) (Wei et al., 2015). BJP-06-005-3 potently diminished PIN1 catalytic activity with an IC_{50} of 48 nM, indicating that BJP-06-005-3 is a high-affinity PIN1 inhibitor (Figure 6-4B).

To assess the covalency of BJP-06-005-3, recombinant full-length human PIN1 protein was analyzed by intact mass spectrometry following incubation with BJP-06-005-3 or DMSO. BJP-06-005-3 showed 100% covalent labeling of PIN1 as indicated by a 702 da increase in the molecular weight of PIN1, corresponding to modification by BJP-06-005-3 upon loss of its chlorine via a nucleophilic substitution reaction (Figure 6-4D). Trypsin digest confirmed the site of covalent modification as Cys113 (Figure 6-2).

To evaluate the binding mode of BJP-06-005-3, we next sought to obtain a co-crystal structure of BJP-06-005-3 bound to the full-length PIN1 protein. Unfortunately, BJP-06-005-3 precipitated out of the crystallization buffer, which was unsurprising given the hydrophobicity of this scaffold. To address this, we synthesized a more hydrophilic derivative of BJP-06-005-3 featuring a C-terminal amide, rather than a C-terminal ethyl ester (BJP-07-017-3; Figure 6-4B). BJP-07-017-3 thus maintained the key binding modalities of BJP-06-005-3, but with lower lipophilicity and improved solubility in aqueous buffers.

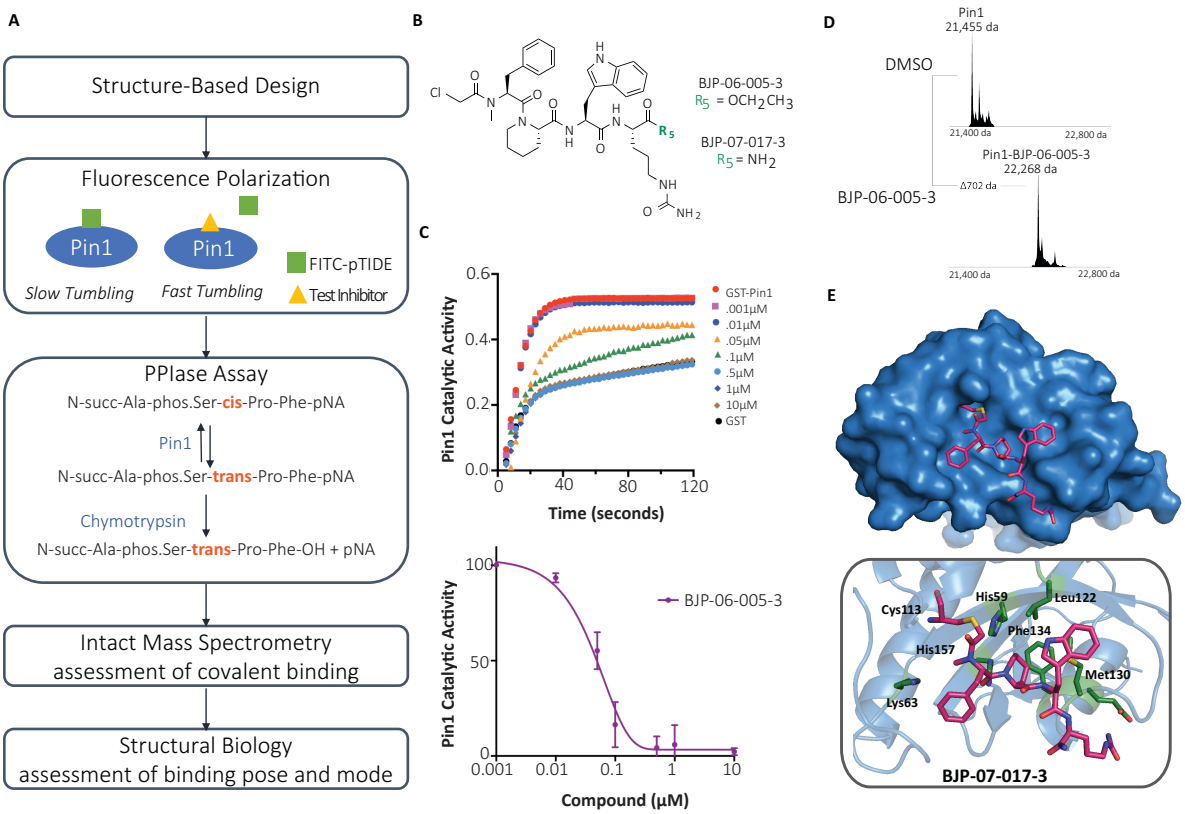

Figure 6-4. Biochemical and Structural Characterization of BJP-06-005-3. (A) Flow-chart of assays used to guide compound optimization and characterization. Abbreviations: FITC = fluorescein isothiocyanate, succ = succinyl, pNA = para-nitroaniline, phos. = phosphorylated. (B) Chemical structure of BJP-06-005-3 and derivative used for crystallography, BJP-07-017-3. (C) Potency of BJP-06-005-3 (Ki = 15 nM) versus pTide in the FP assay after a 12 h incubation of compound and recombinant human full-length PIN1 protein. (D) PPIase assay results for BJP-06-005-3 (IC50 = 48 nM) following a 12 h incubation of BJP-06-005-3 and recombinant human full-length PIN1 protein. (E) Intact mass spectrometry of PIN1 after incubation with DMSO or BJP-06-005-3 for 1 h. A MW increase of 702 Da is evident in the compound-treated sample. (F) 1.6 A co-crystal structure of BJP-06-005-3 (magenta) bound to PIN1 (blue) with key binding residues highlighted in green.

We obtained a 1.6 A high-resolution co-crystal structure of BJP-07-017-3 bound to the full-length PIN1 protein. This structure showed electron density with excellent covalency to Cys113 (Figure 6-4D). The structure confirmed that the pipecolinic acid of BJP-07-017-3 acts as a proline mimetic, making hydrophobic contacts with Leu122, Met130, Phe134, His59, and His157 in the prolyl-binding pocket. Given that both Arg68 and Arg69 were disordered in this structure, we were unable to conclude whether the Phe of BJP-07-017-3 is engaged in a cation-pi interaction, as per our original hypothesis. The Cit residue of BJP-07-017-3 is engaged in

hydrogen bonds to the backbone amide of Met130 and Glu135, and the Trp of BJP-07-017-3 is interacting with the sidechain of Met130 in a methionine-aromatic motif (Valley et al., 2012).

Collectively, this biochemical and structural data confirmed that BJP-06-005-3 is a potent and covalent PIN1 inhibitor. We next sought to evaluate its selectivity and cellular target engagement.

BJP-06-005-3 engages PIN1 in cell lysates and is selective to PIN1 Cys113

To evaluate the engagement of PIN1 in cell lysates, we synthesized a derivative of BJP-06-005-3 featuring a desthiobiotin (DTB) affinity handle (BJP-DTB), which retained high affinity for PIN1, with a K_i of 15 nM (Figure 6-2E, Figure 6-5A). This probe exhibited potent (1 μM) and rapid (1 h incubation of probe and lysate) pull down of PIN1 from PATU-8988T cell lysates (Figure 6-5B and 3C). Pre-incubation with BJP-06-005-3 selectively outcompeted the binding of BJP-DTB to PIN1 in PATU-8988T cell lysates (Figure 6-5D).

We next employed BJP-DTB to assess the selectivity of BJP-06-005-3 using Covalent Inhibitor Target Site Identification (CITe-Id), described in the previous chapter, which quantifies the proteome-wide binding of covalent inhibitors to individual cysteine residues. In this competition assay, HEK293 lysates were preincubated with increasing concentrations of BJP-06-005-3, followed by co-incubation with BJP-DTB (Figure 6-5C). Across the proteome, out of 604 sites reproducibly labeled by BJP-DTB in two replicate experiments, PIN1 Cys113 was the only cysteine that exhibited concentration-dependent binding to BJP-06-005-3 (Figure 6-5F). The pronounced selectivity of BJP-06-005-3 towards PIN1 affirmed its utility as a chemical probe with which to study PIN1 biology.

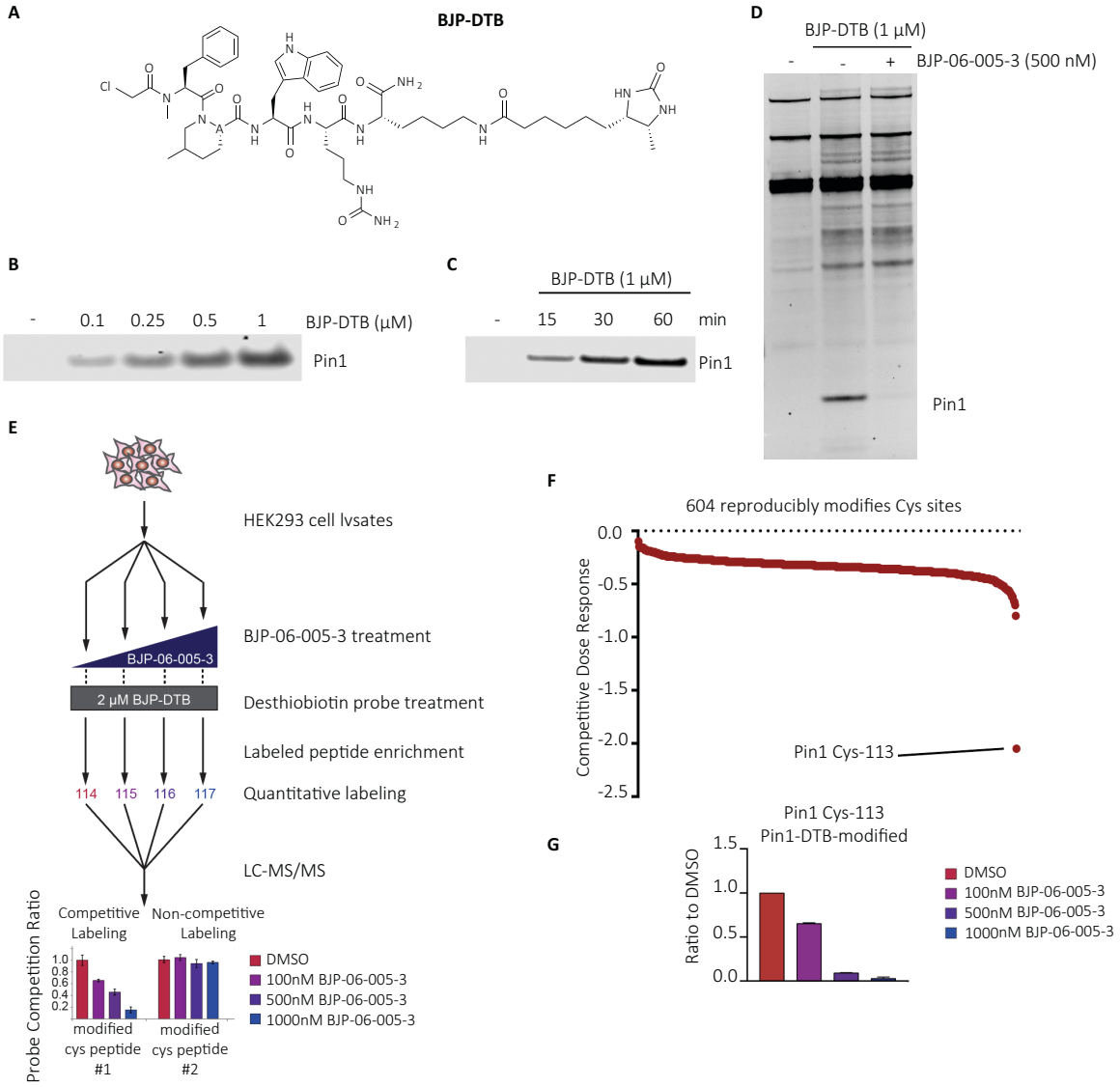

Figure 6-5. BJP-06-005-3 shows pronounced selectivity for PIN1 Cys113. (A) Chemical structure of desthiobiotin (DTB)-labeled scaffold (BJP-DTB). (B) Pull Down of PIN1 from PATU-8988T lysate with the indicated concentrations of BJP-DTB after a 1 h incubation. (C) Pull down of PIN1 from PATU-8988T lysate with 1 μM of BJP-DTB following incubation in lysate at the indicated time points. (D) Covalent labeling of purified PIN1 protein using BJP-DTB, with or without competition using the parent compound. (E) Workflow of Covalent Inhibitor Target Site Identification (CITe-Id) in HEK293 cell lysates incubated with DMSO, 100 nM, 500 nM, or 1000 nM of BJP-06-005-3, followed by co-incubation with 2 μM BJP-DTB. (F) Out of 604 cysteine sites reproducibly modified by BJP-DTB in two replicate experiments, PIN1 Cys113 was the only identified cysteine that was modified by BJP-06-005-3 in a dose-dependent manner.

PIN1 Cooperates with KRAS^{G12V} to Induce Cellular Transformation and PIN1 Knockout Causes Cell Viability Defects in Pancreatic Ductal Adenocarcinoma (PDAC)

Before evaluating the biological phenotypes of BJP-06-005-3 in PDAC, we first sought to characterize the role of PIN1 in PDAC cell growth using genetic strategies. Given reports that transformed human mammary epithelial cells (HMLE-Ras) that overexpress PIN1 result in a higher incidence of tumors in nude mice (Luo et al., 2014), we tested whether PIN1 could cooperate with mutant *KRAS* to drive cell transformation. To evaluate the effects of PIN1 overexpression on transformation, we infected non-transformed NIH/3T3 cells with either doxycycline (Dox)-inducible PIN1, or FKBP12^{F36V}-HA-KRAS^{G12V} and Dox-inducible PIN1, and then confirmed that Dox treatment for 48 hours increased PIN1 levels (Figure 6-6A). We have previously demonstrated that FKBP12^{F36V}-HA-KRAS^{G12V} is a functional oncoprotein and leads to characteristic changes in growth, morphology, and signaling upon transduction of NIH/3T3 cells (Nabet et al., 2018). We assessed the ability of these cell lines to proliferate in ultra-low adherent (ULA) 3D-spheroid suspensions, a high-throughput version of the traditional soft-agar assay to assess cellular transformation (Rotem et al., 2015). Compared to the parental NIH/3T3 cells, PIN1 overexpression alone led to a modest increase in proliferation, whereas PIN1 overexpression in the context of FKBP12^{F36V}-KRAS^{G12V} expression led to a significant and pronounced increase in proliferation (Figure 6-6B). The same trend was true in 2D-monolayer cell culture, though the phenotype was more modest (Figure 6-6C). Previous studies have demonstrated that 3D-spheroid systems may best predict the magnitude of *in vivo* response, as compared to 2D-adherent monolayers (Janes et al., 2018). These results demonstrate that PIN1

overexpression is mildly transformative by itself and cooperates with activated RAS to magnify cell transformation.

To assess the consequences of PIN1 loss on viability in PDAC cell lines, we performed a long-term competition-based CRISPR/Cas9 GFP dropout assay (Shi et al., 2015) in Cas9-expressing PATU-8988T cells (Figure 6-6D). We employed eight individual GFP-tagged sgRNAs targeting *PIN1*, which were confirmed to induce Cas9-mediated knockout of PIN1 (Figure 6-7). Monitoring the GFP signal over time enabled evaluation of the prolonged consequences of PIN1 loss. PIN1 KO led to mild and time-dependent defects in PDAC cell growth rate (Figure 6-6E). To confirm this observation, we isolated single cell PIN1 KO clones from PATU-8988T cells and compared the basal growth rate of a clone lacking PIN1 (C2) to a clone that maintained expression of endogenous PIN1 (C1) as a control (Figure 6-6F). The PIN1 KO clone exhibited a significantly slower growth rate ($p<0.0001$), as compared to the parental PATU-8988T cells and the control clone expressing WT PIN1 (Figure 6-6G).

These results indicate that PIN1 overexpression drives cell proliferation in $KRAS^{G12V}$-expressing cell lines, and PIN1 loss causes viability defects in PATU-8988T cells, thereby highlighting PDAC as a relevant model system in which to characterize our lead PIN1 inhibitor, BJP-06-005-3.

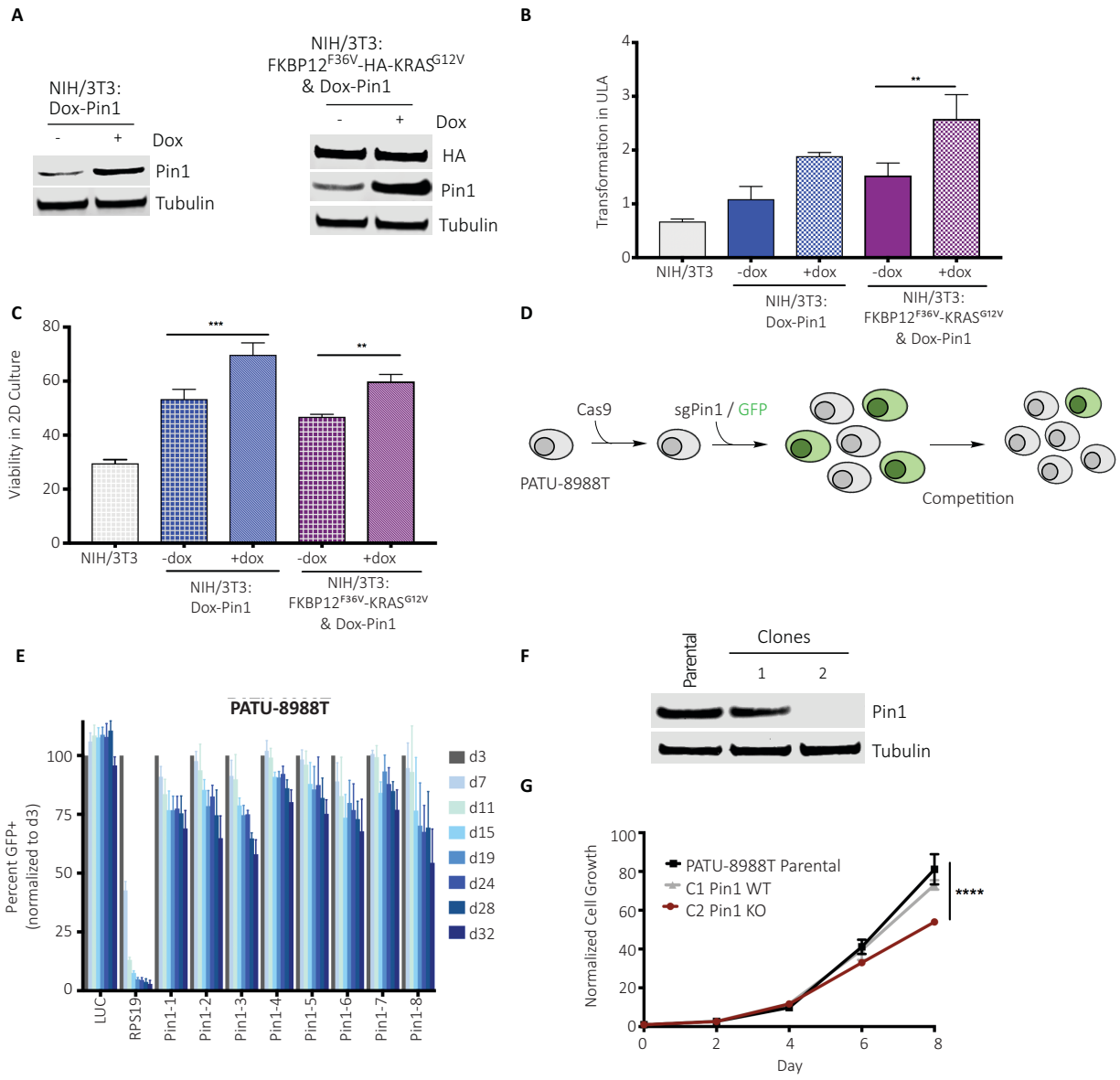

Figure 6-6. PIN1 Cooperates with KRAS^{G12V} to Drive Cellular Transformation in NIH/3T3 cells and PIN1 Loss Leads to Viability Defects in Human PDAC Cell Lines. (A) Immunoblot analysis of NIH/3T3 cells expressing Dox-inducible PIN1 or FKBP12^{F36V}-HA-KRAS^{G12V} and Dox-inducible PIN1 after 48 h treatment with 100 ng/mL dox. (B) Day 0-normalized proliferation of parental NIH/3T3 cells, or NIH/3T3 cells expressing dox-inducible PIN1 or FKBP12^{F36V}-HA-KRAS^{G12V} and Dox-inducible PIN1 (as in panel a) treated with 100 ng/mL dox for 120 hrs. Cells were cultured as either ultra-low adherent 3D-spheroid suspensions, ** $p < 0.01$ by two-way ANOVA, or in (C) 2D-monolayer cell culture. (D) Schematic representation of competition-based CRISPR/Cas9 knockout assay. (E) GFP+ (sgRNA+) population percentage is depicted at the indicated days following lentiviral transduction in Cas9-expressing PATU-8988T cells. (F) Immunoblot analysis of two PATU-8988T clones generated using CRISPR/Cas9. One clone maintains expression of WT PIN1 (C1), while one clone shows PIN1 KO (C2). (G) Day 0-normalized growth rate of PATU-8988T CRISPR/Cas9 clones depicted in panel (f) and parental PATU-8988T cells out to 8 days, with readings taken every 2 days. **** $p < 0.0001$ by two-way ANOVA.

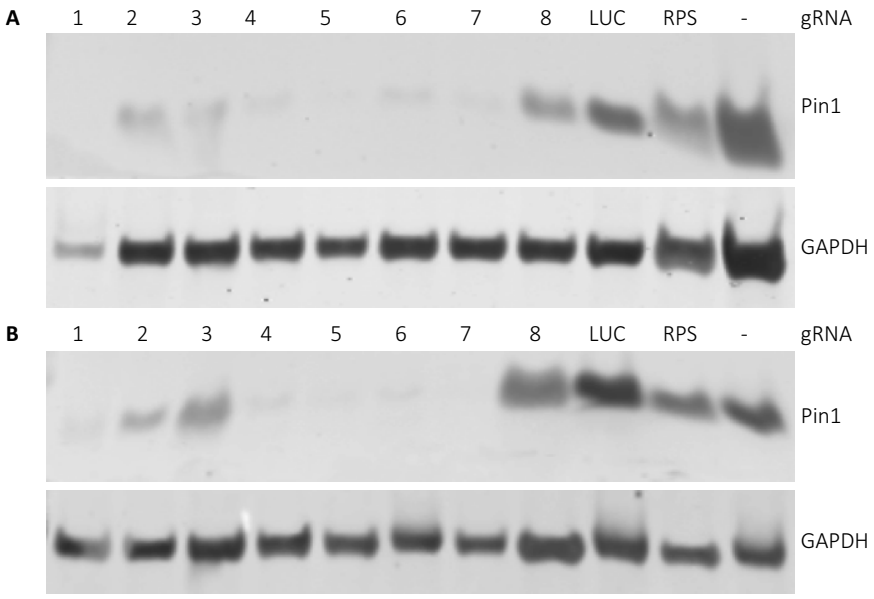

C

Guide	Sequence of gRNA
Pin1-1	AGTCACGGCGGCCCTCGTCC
Pin1-2	AGGACGAGGGCCGCCGTGAC
Pin1-3	CAGTGGTGGCAAAAACGGGC
Pin1-4	CATCACTAACGCCAGCCAGT
Pin1-5	TGAAGCACAGCCAGTCACGG
Pin1-6	GAAGATCACCCGGACCAAGG
Pin1-7	GATCTTCTGGATGTAGCCTG
Pin1-8	CCCCGTCCGCAGCGCAAACG
LUC	CCCGGCGCCATTCTATCCGC
RPS19	GTAGAACCAGTTCTCATCGT

Figure 6-7. (A) Validation of sgRNAs used in the CRISPR-Cas9 GFP dropout experiment in Cas9-expressing PATU-8988T cells. Cells were infected with 1-8 sgRNAs targeting PIN1 or controls for 48 hours and then PIN1 protein levels were assessed by immunoblot analysis. (B) Sequences of sgRNAs used in the CRISPR-Cas9 GFP dropout experiment.

BJP-06-005-3 Engages Cellular PIN1 and Causes PIN1 Degradation

To assess the permeability and cellular target engagement of BJP-06-005-3 in PDAC cell lines, we performed a live cell competition assay using BJP-DTB (Figure 6-8A). Following 5 hour treatment in PATU-8988T cells, BJP-06-005-3 exhibited dose-dependent competition with BJP-DTB for binding to PIN1, while the corresponding reversible negative control, BJP-R, did not show competition (Figure 6-8B). Complete engagement of PIN1 by BJP-06-005-3 was evident within 4

hours in PATU-8988T cells and was maintained for 48 hours (Figure 6-8C, Figure 6-9B). The recovery evident at 72 hours indicates that compound replenishment is necessary for assays requiring greater than 48 hours of treatment, likely due to hydrolysis of the peptide (Figure 6-9A-C).

Covalent inhibitors can induce degradation of their target proteins, often by causing structural rearrangement (Long, Gollapalli, & Hedstrom, 2012). PIN1 is frequently degraded following inhibitor binding, as previously demonstrated with ATRA (Wei et al., 2015), ATO (Kozono et al., 2018), and KPT-6566 (Campaner et al., 2017). Similarly, BJP-06-005-3 caused partial degradation of PIN1 following a 48 hour treatment in two independent PDAC cell lines, PATU-8988T and PATU-8902 (Figure 6-8D). Notably, in addition to causing incomplete PIN1 degradation, binding of BJP-06-005-3 to PIN1 caused a slight upward shift in the PIN1 protein band by Western blot, indicative of the molecular weight increase when the relatively small PIN1 protein (18 kDa) is labeled by a large inhibitor (BJP-06-005-3, MW 738) (Figure 6-8D). BJP-06-005-3 also reduced PIN1 protein half-life in PATU-8988T cells, as determined in a cycloheximide (CHX) chase experiment (Figure 6-8E). This demonstrates that PIN1 is destabilized upon the covalent binding of BJP-06-005-3. Taken together, these findings affirmed that BJP-06-005-3 is cell penetrant and engages PIN1 in PDAC cell lines.

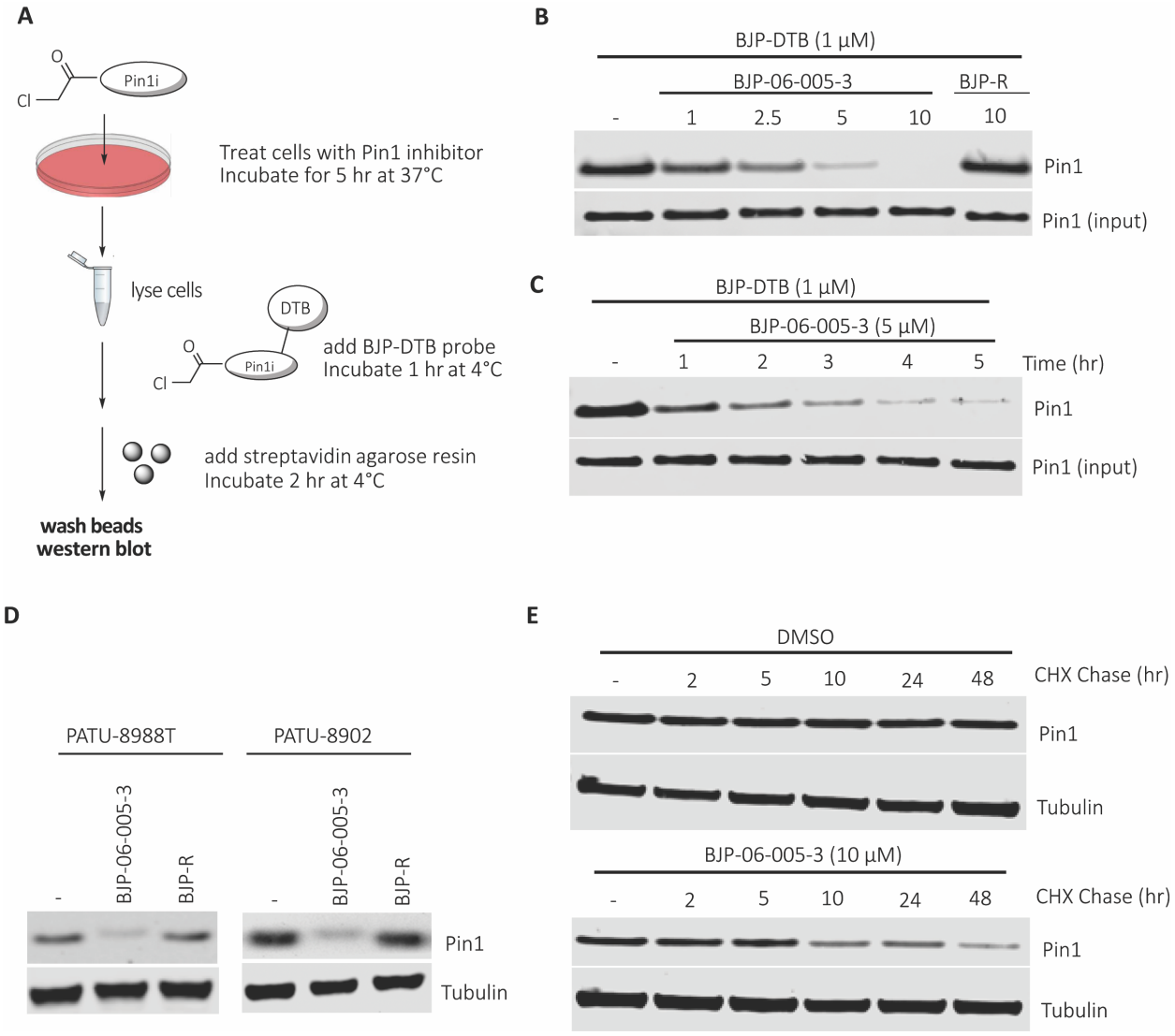

Figure 6-8. BJP-06-005-3 Binds and Degrades Cellular PIN1. (A) Schematic representation of live cell competition pulldown experiment to assess cellular target engagement. (B) PATU-8988T cells treated in a competition format with the indicated concentrations of BJP-06-005-3 or BJP-R for 5 h, followed by cell lysis, incubation with BJP-DTB for 1 h, avidin pulldown, and immunoblot analysis. (C) PATU-8988T cells treated with 5 μM BJP-06-005-3 for the indicated times, followed by cell lysis, incubation with BJP-DTB for 1 h, avidin pulldown, and immunoblot analysis. (D) Immunoblotting of the indicated proteins in PATU-8988T or PATU-8902 cells treated with 10 μM BJP-06-005-3 or BJP-R for 48 hrs. (E) PATU-8988T cells treated with DMSO, 10 μM BJP-06-005-3, or 10 μM BJP-R for 24 h, followed by cycloheximide (CHX) chase for the indicated times. (F) Immunoblotting of the basal expression levels of the indicated proteins in PATU-8988T CRISPR/Cas9 clones. (G) Immunoblotting of the indicated proteins after treatment with 10 μM BJP-06-005-3 for the indicated times.

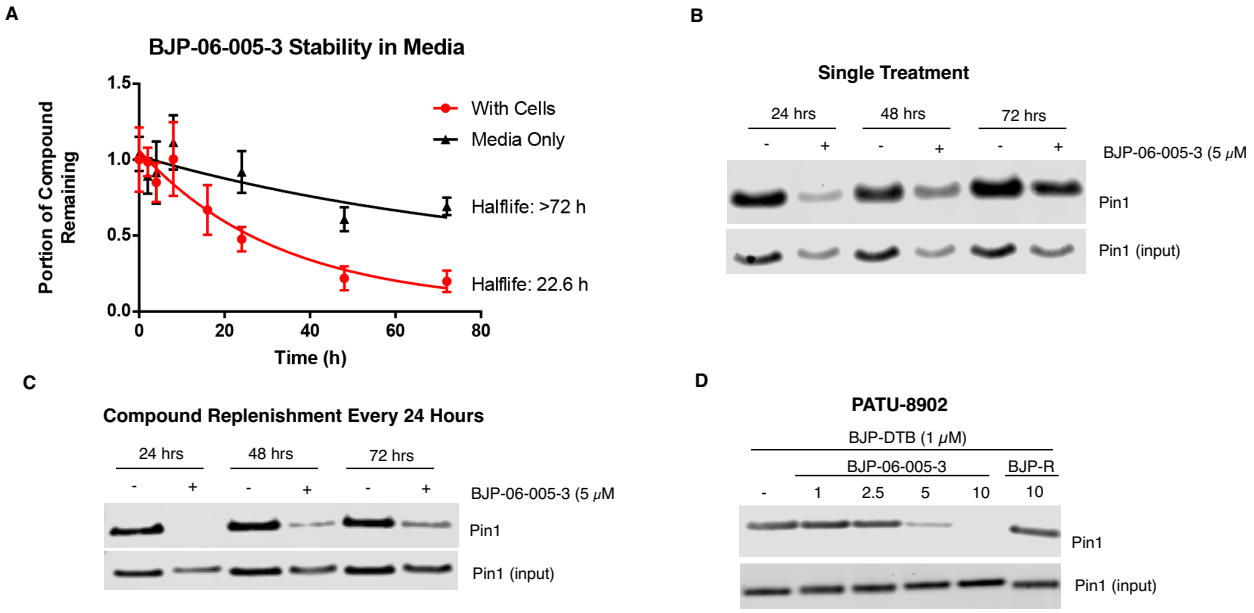

Figure 6-9. (A) BJP-06-005-3 is stable in media (half-life > 72 hours) but is unstable in media containing cells (half-life = 22.6 hours). PATU-8988T cells were treated with BJP-06-005-3 (10 μM) and the media off of the cells was collected at 2, 4, 8, 10, 24, 48, and 72 hours and subject to MS/MS analysis (red curve). In parallel, pure media (DMEM with 20% FBS/5% penn/strep) was incubated with BJP-06-005-3 (10 μM) for 2, 4, 8, 10, 24, 48, and 72 hours and subject to MS/MS analysis (black curve). (B) After a single treatment, BJP-06-005-3 loses engagement of PIN1 by 72 hours. PATU-8988T cells treated with 5 μM BJP-06-005-3 for the indicated times, followed by cell lysis, incubation with BJP-DTB for 1 h at 4°C, streptavidin pulldown, and immunoblot analysis. (C) By replenishing compound in media every 24 hours, PIN1 engagement can be maintained out to 72 hours. PATU-8988T cells were treated with 5 μM BJP-06-005-3, and every 24 hours the media was aspirated and replaced with fresh media/BJP-06-005-3. At the indicated time points, the cells were lysed, incubated with BJP-DTB for 1 h at 4°C, then subject to avidin pulldown, and immunoblot analysis. (D) BJP-06-005-3 engages PIN1 in PATU-8902 cells, while the negative control BJP-R does not engage PIN1. PATU-8902 cells were treated with the indicated concentrations of BJP-06-005-3 or BJP-R for 5 hours, followed by cell lysis, incubation with BJP-DTB for 1 h at 4°C, avidin pulldown, and immunoblot analysis.

BJP-06-005-3 Induces PIN1-Mediated Antiproliferative Effects in Human PDAC Cell Lines

Having validated cellular target engagement, we next assessed whether treatment with BJP-06-005-3 affected cell viability in PDAC cell lines. In agreement with results from the CRISPR/Cas9 GFP dropout assay (Figure 6-6E), prolonged treatment with BJP-06-005-3 diminished cell viability in PATU-8988T cells, which was completely rescued upon treatment with the reversible negative control, BJP-R (Figure 6-10A). To ensure that PIN1 inhibition was

maintained for the duration of this experiment, we replenished BJP-06-005-3 in media every 48 hours. To assess whether this antiproliferative phenotype was PIN1-mediated, we compared the effects of BJP-06-005-3 treatment in a PATU-8988T clone expressing wild-type (WT) PIN1 (C1), and a PIN1 KO clone (C2). BJP-06-005-3 treatment led to a dose-dependent decrease in cell growth over time in the WT PIN1-expressing cell line, which was completely rescued in the corresponding PIN1 KO cells (Figure 6-10B).

To further assess whether the antiproliferative phenotype of BJP-06-005-3 was on-target, we infected the PIN1 KO PATU-8988T cells (C2) with Dox-inducible PIN1 and confirmed that treatment with Dox for 48 hours induced PIN1 expression (Figure 6-10C). In the absence of Dox, the Dox-inducible PIN1 KO PATU-8988T cells were resistant to BJP-06-005-3 treatment, while in the presence of Dox, the cells were re-sensitized to BJP-06-005-3, providing further confirmation that the viability effects were PIN1-mediated (Figure 6-10D). To assess whether this phenotype was generalizable to other PDAC cell lines, we repeated the experiment in PATU-8902 cells, in which BJP-06-005-3 treatment similarly reduced cell growth in a dose-dependent manner, with complete rescue evident upon treatment with the negative control, BJP-R (Figure 6-10E).

We then directly compared the antiproliferative effects of BJP-06-005-3 in monolayer (2D-adherent) and 3D ULA suspension spheroids after a 4-day treatment. In PATU-8988T cells, BJP-06-005-3 treatment caused a mild decrease in proliferation in 2D cell culture, which was more pronounced in ULA suspensions. This phenotype was rescued in the corresponding PIN1 KO cells (Figure 6-10F). Taken together, these data indicate that PIN1 inhibition has only very mild effects on cell proliferation in PDAC cell lines at short time points (Figure 6-11A-B), with

antiproliferative phenotypes becoming more pronounced after prolonged treatments, or in 3D cell culture.

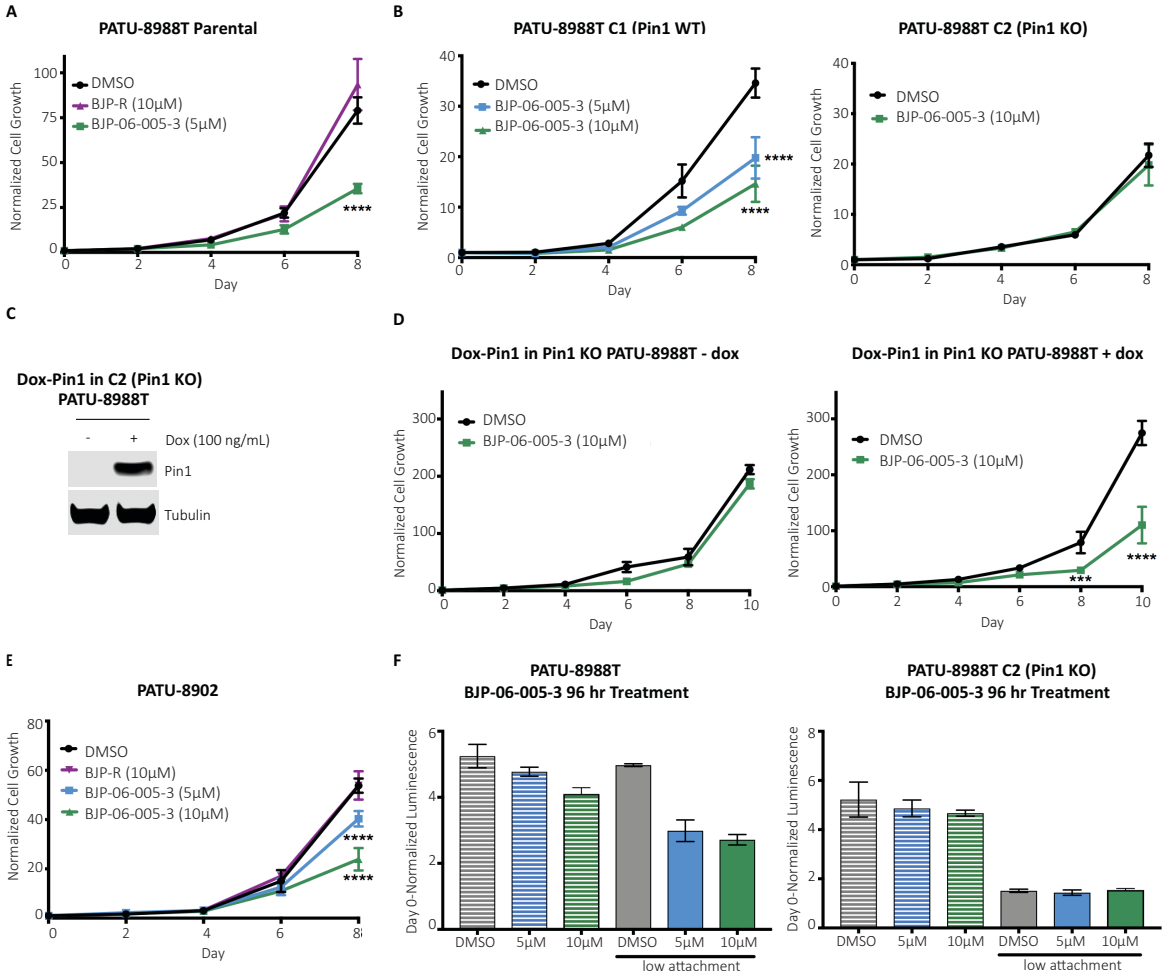

Figure 6-10. BJP-06-005-3 Impacts Cells Viability in PDAC Cell Lines in a PIN1-Mediated Manner. (A) Growth curves of PATU-8988T cells treated with DMSO or the indicated concentrations of BJP-06-005-3 or negative control, BJP-R. Readings taken every 2 days out to 8 days. (B) Growth curves of PATU-8988T CRISPR/Cas9 clones that maintain expression of WT PIN1 (C1) or a PIN1 KO clone (C2). Cells were treated with DMSO or the indicated concentrations of BJP-06-005-3, with readings taken every 2 days out to 8 days. (C) Immunoblot analysis of PIN1 KO PATU-8988T cells infected with Dox-inducible PIN1, and treated with 100 ng/mL doxycycline (Dox) for 48 h. (D) Growth curves of Dox-inducible PIN1, PIN1$^{-/-}$ PATU-8988T cells treated with DMSO or the indicated concentrations of BJP-06-005-3, in the presence (100 ng/mL) or absence of Dox, with readings taken every 2 days out to 10 days. (E) Growth curves of BxPC-3 cells treated with DMSO or the indicated concentrations of BJP-06-005-3, with readings taken every 2 days out to 8 days. (F) PATU-8988T cells were cultured as ultra-low adherent 3D-spheroid suspensions and treated with DMSO, 5 or 10 μM BJP-06-005-3 for 4 days, with compound re-treatment on day 2.

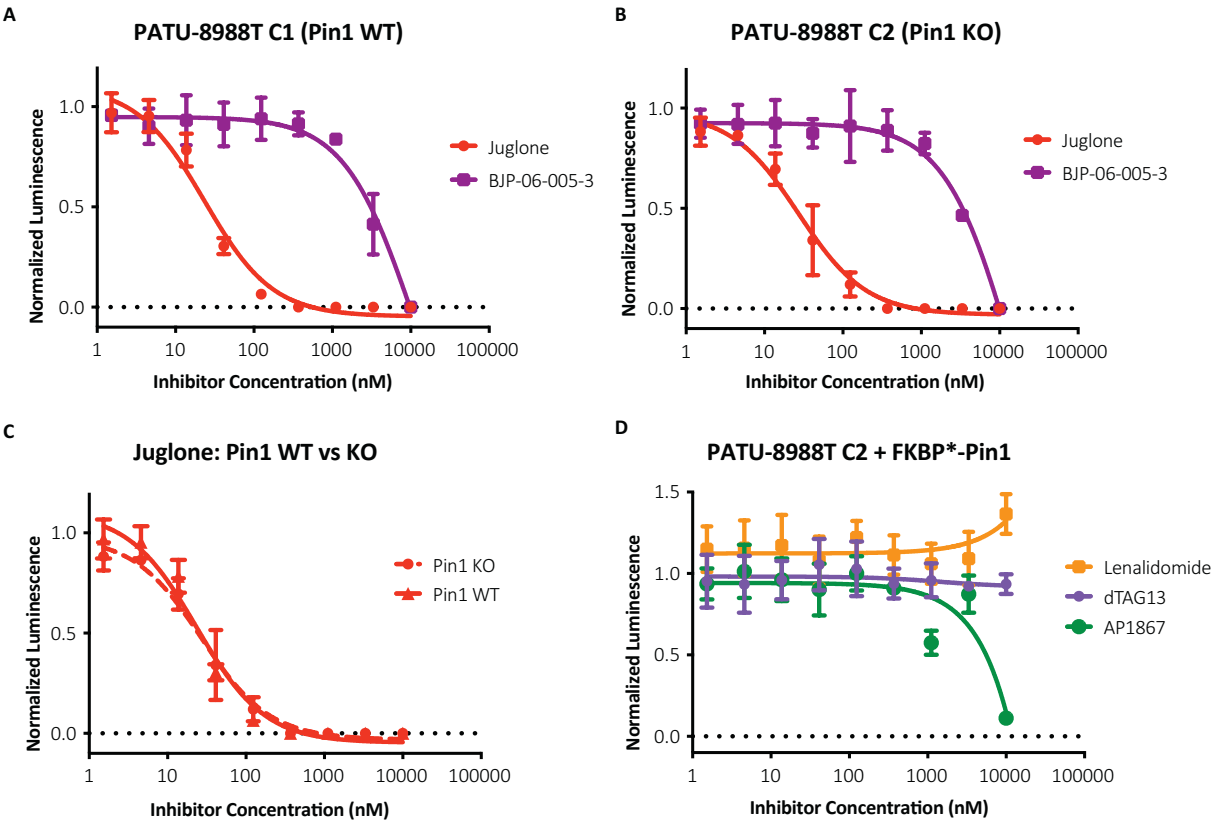

Figure 6-11. (A) PATU-8988T cells that express WT PIN1 (left) or with PIN1 knockout (right) were treated with Juglone or BJP-06-005-3 for 4 days, with media and compound replaced every 24 hours to ensure continual engagement of PIN1. Viability was assessed by CellTiter-Glo. (C) Juglone graphs from (a) and (b) superimposed. The potent antiproliferative effects of juglone are not PIN1-mediated given that there is no rescue in the PIN1 KO PATU-8988T cells. (D) PIN1 KO PATU-8988T cells (C2) expressing FKBP^{F36V}-PIN1 were treated with dTAG13, lenalidomide or AP1867 (as controls) for 4 days. Viability was assessed by CellTiter-Glo.

Degradation of FKBP^{F36V}-tagged PIN1 in PATU-8988T Cells

To complement the characterization of BJP-06-005-3 in PDAC, we employed our recently described chemical-genetic strategy known as the degradation tag (dTAG) system to induce rapid and specific PIN1 degradation (Nabet et al., 2018). To implement the dTAG system, we exogenously expressed PIN1 as an N-terminally tagged FKBP12^{F36V} chimera (FKBP12^{F36V}-HA-PIN1) in PATU-8988T PIN1 KO cells, C2 (Figure 6-6F, Figure 6-12A). We optimized the viral titer in order to match the expression level of FKBP12^{F36V}-PIN1 to the expression of PIN1 in parental PATU-

8988T cells (Figure 6-12C). Treatment with a bivalent small molecule degrader, dTAG-13 (Figure 6-12B), consisting of AP1867 connected to thalidomide via a short alkyl linker, resulted in rapid and potent degradation of FKBP12^{F36V}-tagged PIN1 (Figure 6-12D). Maximal degradation was achieved at 100-500 nM treatment, with protein visible by 1 μM treatment, consistent with the "hook effect" observed for small molecule degraders, in which at high concentrations, each end of the molecule saturates its respective binding sites, preventing formation of the ternary complex required for degradation (Winter et al., 2015).

We found that degradation of FKBP12^{F36V}-PIN1 occurred rapidly, with complete degradation achieved by 4 hours (Figure 6-10E). Degradation could be rescued upon pretreatment with carfilzomib (proteasome inhibitor) or MLN4924 (Nedd8 activating enzyme inhibitor), confirming that the mechanism of degradation requires engagement of the ubiquitin-proteasome system and cullin-RING E3 ligases (Figure 6-12F).

Consistent with the slower basal growth rate of PIN1 KO PATU-8988T cells (Figure 6-6G), introduction of FKBP12^{F36V}-PIN1 into C2 PIN1 KO cells restored the basal growth rate to parental levels (Figure 6-12G), suggesting that the fusion protein was functional. To further assess the activity of FKBP12^{F36V}-PIN1, we performed complementation experiments in Saccharomyces cerevisiae, in which the PIN1 homolog *ESS1* is an essential gene. Overexpression of PIN1 or FKBP12^{F36V}-PIN1 successfully supported growth of the *ESS1* deletion strain, and immunoblotting confirming expression of the intact fusion protein (Figure 6-13). Furthermore, we demonstrated that FKBP12^{F36V}-PIN1 could be pulled down by BJP-DTB, and that this binding could be outcompeted upon a 5 hour pre-treatment with BJP-06-005-3 (10 μM) (Figure 6-10H). This indicates that the active site of the FKBP12^{F36V}-tagged PIN1 resembles that of the native PIN1

protein, allowing for inhibitor binding and inactivation. Furthermore, while C2 PIN1 KO cells were resistant to BJP-06-005-3 treatment (Figure 6-10B, Figure 6-11A), treatment with BJP-06-005-3 in C2 PIN1 KO cells expressing FKBP12^{F36V}-PIN1 resulted in significant and time-dependent antiproliferative effects (Figure 6-12I), providing further indication that the FKBP12^{F36V}-PIN1 chimera maintains the function of native PIN1 protein. Similar to BJP-06-005-3, 3 day treatment with dTAG13 in 2D growth conditions did not result in any antiproliferative effects (Figure 6-11C).

Mirroring the phenotype of BJP-06-005-3 treatment, FKBP12^{F36V}-PIN1 degradation via dTAG13 treatment resulted in impaired cell proliferation after 6-8 days (Figure 6-12J). This phenotype was apparent upon treatment with either 100 nM or 500 nM dTAG13, but was rescued at 1 μM dTAG13, consistent with the appearance of the hook effect and the resulting stabilization of the FKBP12^{F36V}-PIN1 chimera. The consistency observed between dTAG13 and BJP-06-005-3 treatment lends validity to the fact that this time-dependent growth phenotype is PIN1-mediated.

Cellular Consequences of PIN1 Inhibition by BJP-06-005-3

Given that the growth rate of the PATU-8988T PIN1 KO clone C2 was significantly decreased compared to the control clone C1, we wished to further characterize the underlying cause for this at the molecular level. Phosho-CDK1Tyr15 was increased in C2 compared to C1, with total CDK1 remaining the same (Figure 6-14A). To further validate that this effect was PIN1-specific, we used the PIN1 dTAG cell line described above, and demonstrated that dTAG treatment for 5 hours resulted in an increase in phospho-CDK1 Tyr15 only at concentrations at

which FKBP^{F36V}-PIN1 was degraded (Figure 6-14B). We next verified that PIN1 inhibition using BJP-06-005-3 resulted in increased phospho-CDK1 Tyr15 in PATU-8988T C1 cells with intact PIN1, but not in C2 PIN1 KO cells (Figure 6-14C,D).

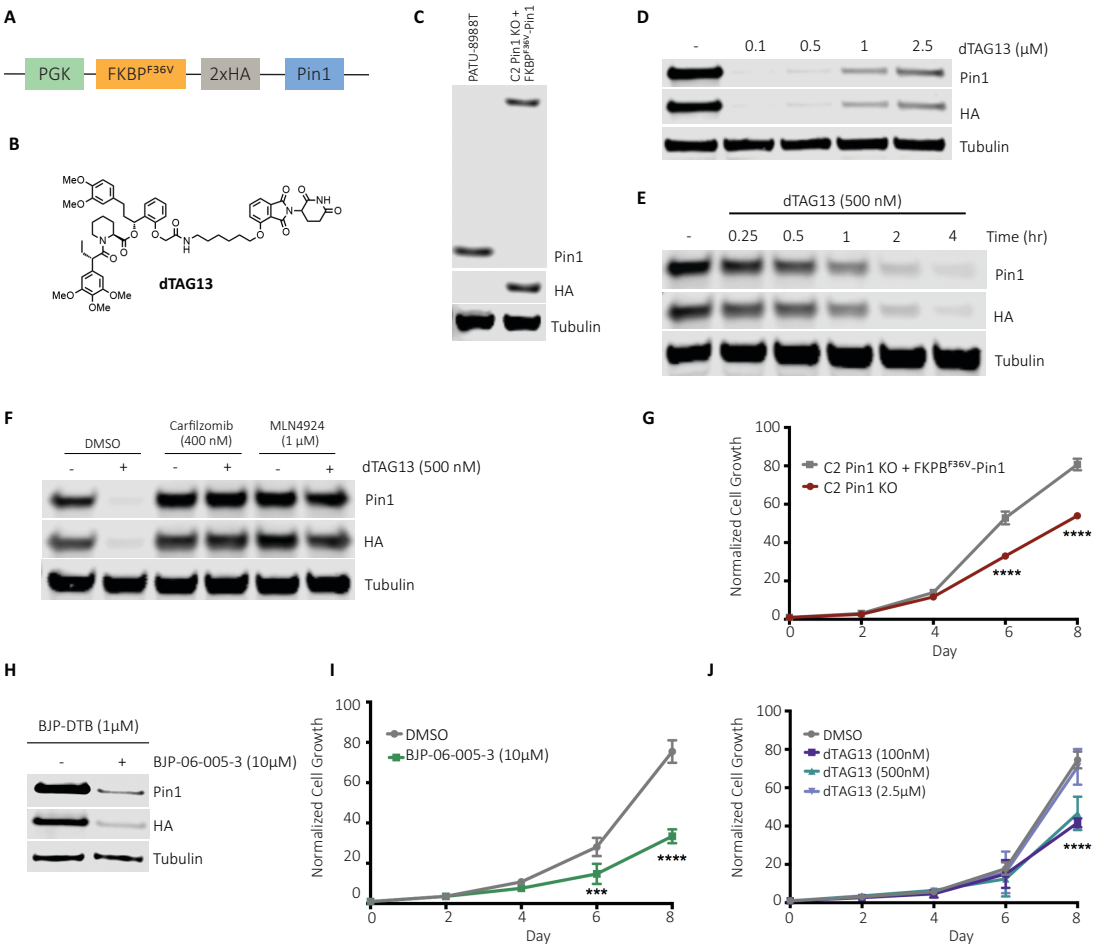

Figure 6-12. Rapid Degradation of FKBP12^{F36V}-PIN1 in PATU-8988T cells mimics the effects of BJP-06-005-3 treatment. (A) Schematic depiction of the lentiviral expression strategy. (B) Chemical structure of the bivalent degrader molecule, dTAG13. (C) Immunoblot analysis of PATU-8988T parental cells versus PATU-8988T PIN1 KO cells (C2) expressing FKBP^{F36V}-PIN1 (= FKBP*-PIN1). (D) Immunoblot analysis of PATU-8988T C2 PIN1 KO cells expressing FKBPF^{36V}-PIN1 treated with the indicated concentrations of dTAG13 for 5 hours. (E) Immunoblot analysis of PATU-8988T C2 PIN1 KO cells expressing FKBPF^{36V}-PIN1 treated with 500 nM of dTAG13 for the indicated time points. (F) Immunoblot analysis of PATU-8988T C2 PIN1 KO cells expressing FKBPF^{36V}-PIN1 pre-treated for 2 hours with DMSO, Carfilzomib (400 nM) or MLN4924 (1 μM), followed by a 5 h co-treatment with dTAG13 (500 nM). (G) Day 0-normalized growth rate of PATU-8988T C2 PIN1 KO versus PATU-8988T C2 PIN1 KO cells expressing FKBP^{F36V}-PIN1 out to 8 days, with readings taken every 2 days. **** $p < 0.0001$. (H) Live cell competition experiment in PATU-8988T C2 PIN1 KO cells expressing FKBP^{F36V}-PIN1. Cells were treated with either DMSO or BJP-06-005-3 (10 μM) for 5 hours, followed by cell lysis, incubation with BJP-DTB (1 μM) for 1 hour, avidin pulldown, and immunoblot analysis. (I) Day 0-normalized growth rate of PATU-8988T C2 PIN1 KO cells expressing FKBP^{F36V}-PIN1 out to 8 days, with readings taken every 2 days and compound/media replaced every 2 days, treated with BJP-06-005-3 (10 μM) or (J) dTAG13 (100 nM, 500 nM). **** $p < 0.0001$.

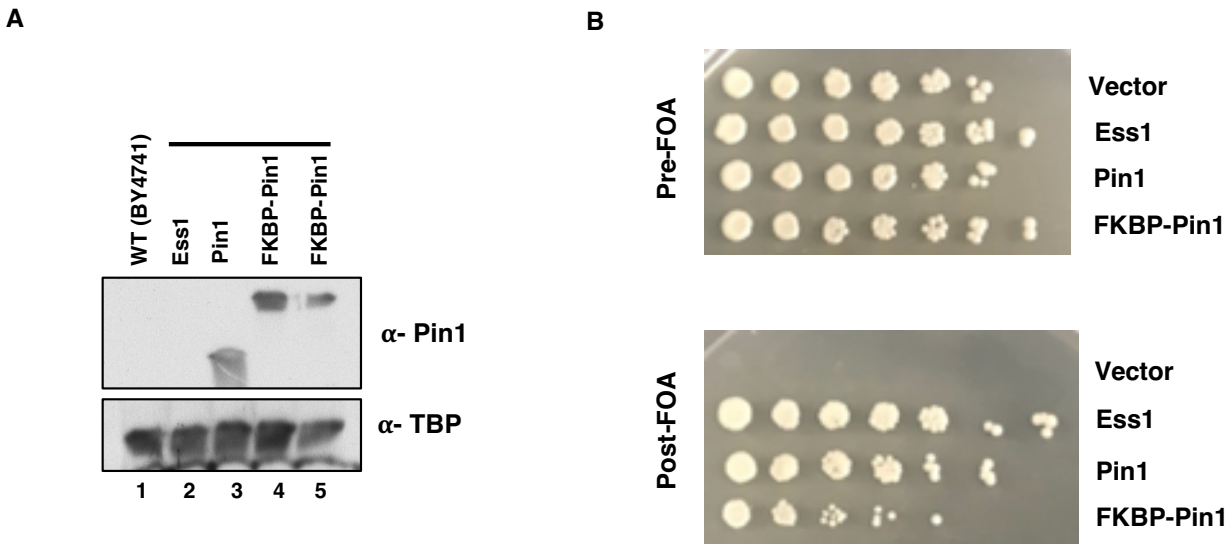

Figure 6-13. (A) Expression of PIN1 and FKBP^{F36V}-PIN1 were tested by immunoblotting with anti-PIN1 antibody. Lane 1 shows yeast strain BY4741 with wild-type *ESS1* in the chromosome. Lanes 2-5 are derivatives of YXW-3 (X. Wu et al., 2000), in which the chromosomal *ESS1* deletion is complemented by plasmids expressing yeast Ess1, human PIN1, or two isolates of the FKBP-PIN1 fusion. (B) Growth assay showing that PIN1 and FKBP-PIN1 complement an *ESS1* deletion. Yeast strain YSB1026 (based on YXW-3, but with covering plasmid pRS426-PIN1) was transformed with *HIS3*-marked plasmids expressing Ess1, PIN1, or FKBP-PIN1, or the vector alone. Cell growth was tested before (upper panel) and after selection (bottom panel) on media containing 5-fluoro-orotic acid (FOA), which selects against the *URA3* marker on the pRS426-PIN1 plasmid. Cells were spotted onto plates using a series of 3-fold dilutions, from left to right.

Given these concordant effects on phospho-CDK1 Tyr15, a critical regulatory site for mitotic entry, we went on to characterize the effects of PIN1 disruption on the cell cycle. Treatment with BJP-06-005-3 did not result in significant effects on cell cycle after 24 hours (Figure 6-14E). Though not significant, a slight decrease in the percentage of S phase cells was observed with BJP-06-005-3 compared to DMSO but not with the negative control BJP-06-115-3. Similarly, in the dTAG system, a 24 h treatment with dTAG13 did not result in significant cell cycle effects (Figure 6-14F).

Figure 6-14. Cell cycle and transcriptional consequences of PIN1 inhibition. (A) Immunoblot analysis of the indicated proteins in PATU-8988T clones C1 (PIN1 WT) and C2 (PIN1 KO). (B) dTAG13 treatment for 5 h at the indicated concentrations in PATU-8988T C2 with $FKBP12^{F36V}$-PIN1. (C) Immunoblot analysis following treatment with BJP-06-005-3 at the indicated concentrations for 5 h in PATU-8988T C1 (PIN1 WT) and (D) C2 (PIN1 KO). (E) 24 h treatment of PATU-8988T cells with the indicated compounds, followed by FACS PI analysis. (F) 24 h treatment of PATU-8988T C2 with $FKBP12^{F36V}$-PIN1 with DMSO or dTAG13, followed by FACS PI analysis. (G) Transcriptome-wide effect of BJP-06-005-3, showing differential effects relative to BJP-R treatment at 4 hours after treatment and (H) 24 h after treatment.

Figure 6-14 (Continued).

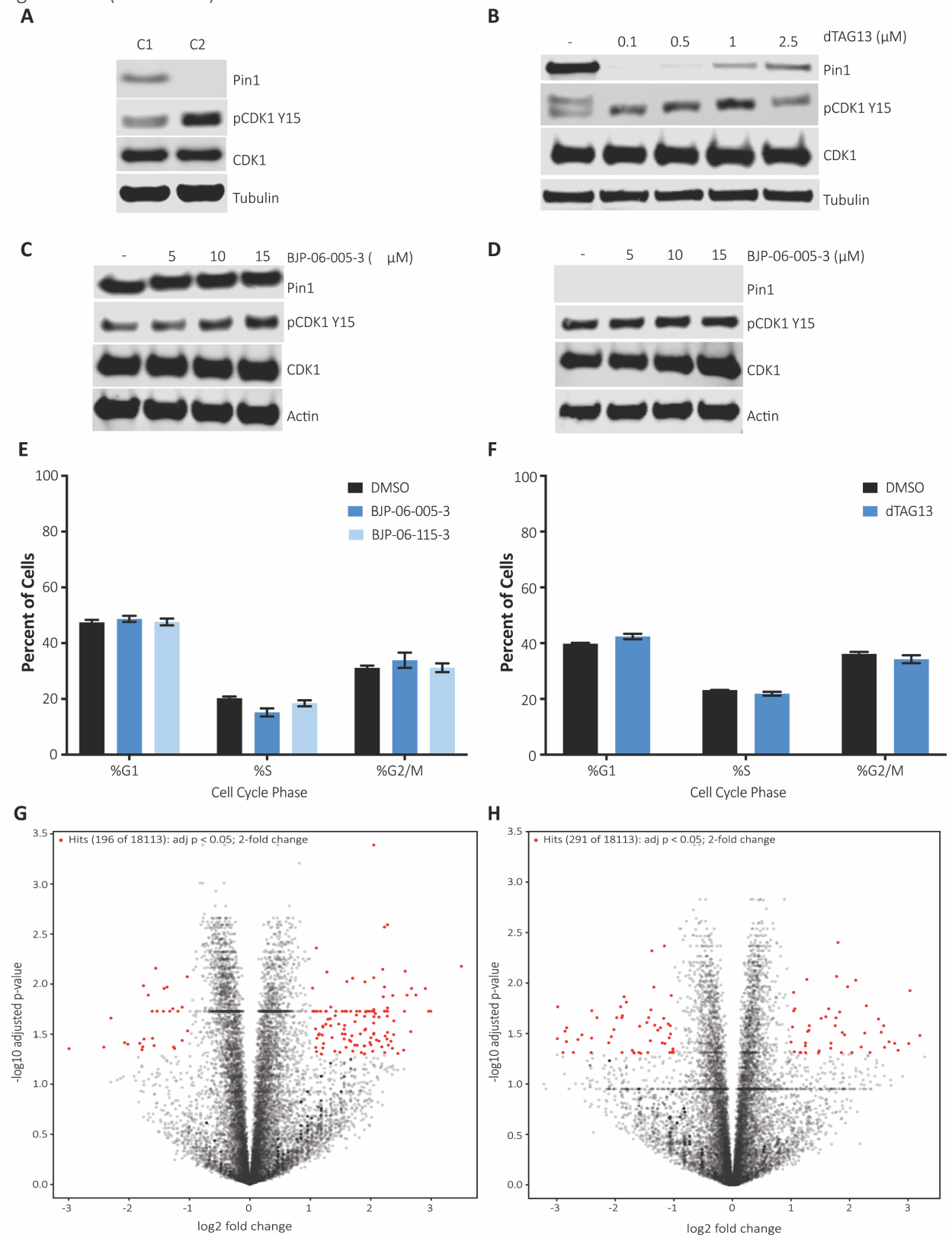

To characterize the impact of PIN1 inhibition on global transcription, we performed RNA-sequencing in PATU-8988T cells at two timepoints, using both BJP-06-005-3 with the negative control BJP-R as a control. 18113 genes were detected with non-zero expression. At 4 hours after treatment, differential expression of 196 genes was observed (log2 fold change > 1, adjusted p-value < .05) with BJP-06-005-3, normalizing for effects of BJP-R (Figure 6-14G). At 24 hours after treatment, 291 genes were differentially expressed (Figure 6-14H). The sets of differentially expressed genes at both timepoints were relatively distinct, with only four genes overlapping between both sets: C20orf152, DHR5, LOC100507299 and TEDDM1. Modest effects on gene expression were seen with BJP-R treatment relative to DMSO (Figure 6-15), possibly due to non-covalent binding to other targets; thus, controlling for BJP-R in addition to a DMSO comparison was important for elucidating effects on transcription that were dependent on covalent PIN1 inhibition. Treatment with BJP-06-005-3 did not have significant effects on any well-known signaling pathways at the timepoints investigated. In particular, PIN1 has been reported to regulate transcription through myc and NFκB (Farrell et al., 2013; Helander et al., 2015; A. Ryo et al., 2003). Signatures of myc-regulated gene expression were not significantly enriched in the differentially expressed genes at either timepoint. At 24 hours after compound treatment, up-regulated genes were enriched for NFκB activation, IRAK1 pathway activation, recruitment/activation of the IKK complex, and p38 MAPK activation. The transcriptional consequences of PIN1 covalent inhibition require further study.

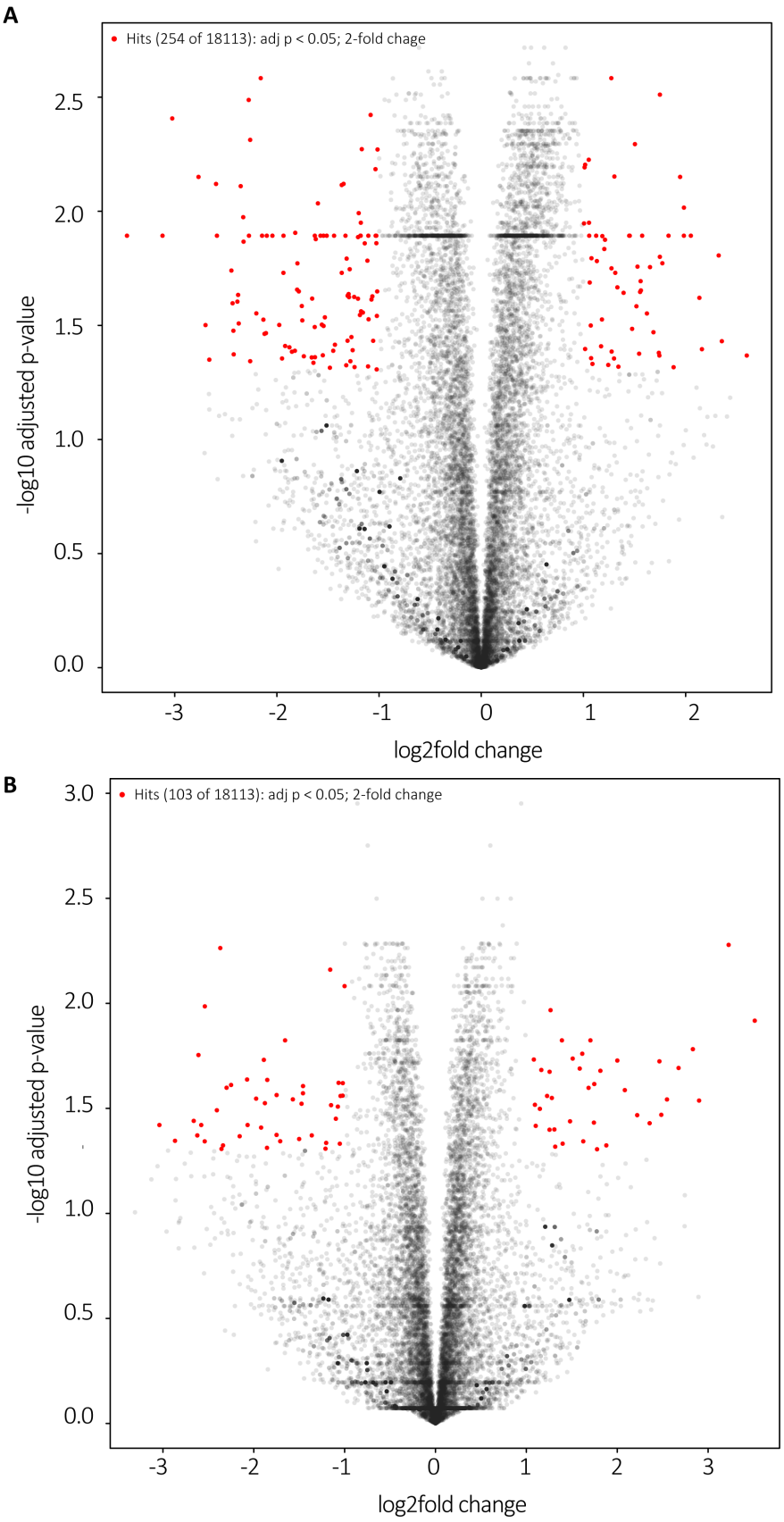

Figure 6-15. (A) RNA-sequencing differential expression upon treatment with BJP-06-115-3 for 4 h or (B) 24 h.

Discussion

Despite decades of research highlighting PIN1 as an important driver of oncogenesis, the development of selective PIN1 inhibitors has proven challenging. Achieving potency generally requires anionic compounds that can interact with the basic phosphate binding pocket in the PIN1 active site, which imposes severe cell permeability challenges. For instance, a series of carboxylate-containing benzimidazoles developed by Pfizer using a structure-based design approach show potent PIN1 binding but were not cell permeable, requiring a liposomal formulation for efficient delivery (Guo et al., 2014; Russo Spena et al., 2018). On the other hand, cell penetrant PIN1 inhibitors are highly non-selective. Numerous studies feature the natural product, juglone, which has various known off targets, including RNA Polymerase II (Chao, Greenleaf, & Price, 2001), and which shows identical cell viability effects in PIN1 WT and KO cells (Figure 6-11). More recently identified PIN1 inhibitors include ATRA (Wei et al., 2015), which degrades cellular PIN1 but also targets the retinoic acid receptors, and KPT-6566 (Campaner et al., 2017), a potent and covalent PIN1 modifier that releases a quinone-mimetic substructure after PIN1 binding that then engages a host of other proteins to induce an oxidative stress response. This dual mechanism of action allows for impressive anti-cancer efficacy but obscures purely PIN1-mediated phenotypes.

This study describes the first selective, covalent PIN1 inhibitor (BJP-06-005-3), suitable for a comprehensive investigation of PIN1 biology in cells. The covalency of this series enabled the replacement of the phospho-Thr of pTide with a Phe, greatly increasing hydrophobicity and cell permeability. The selectivity of BJP-06-005-3 is currently unparalleled, with PIN1 Cys113 being the only labeled cysteine proteome-wide.

We found PIN1 inhibition to be largely non-toxic after traditional 4-day treatments in 2D-adherent monolayer cell culture, which aligns with results from the Cancer Dependency Map, showing that PIN1 is not a significant dependency in any cancer cell line tested. This result was validated using the dTAG system, in which dTAG13 treatment and subsequent FKBP12^{F36V}-PIN1 degradation did not affect cell growth at short time points in 2D-cell culture, highlighting that BJP-06-005-3's negligible cytotoxicity could not be explained by differences in PIN1 inhibition versus PIN1 degradation. Given the critical role of proline-directed phosphorylation in cell signaling networks, this general lack of cytotoxicity is surprising and may be explained by upregulation of another PPIase that can perhaps compensate for PIN1 function, though this remains to be explored.

PIN1 loss in the context of ULA 3D-spheroid suspensions gave rise to more pronounced antiproliferative phenotypes, demonstrating that adherent monolayer cell cultures may underestimate PIN1 dependency. PIN1 inhibition also caused antiproliferative phenotypes in PDAC cell lines in 2D-cell culture after prolonged treatments (6-8 days), indicating that growth defects from PIN1 become more pronounced over time. To further validate this finding, we used CRISPR-based competitive growth assays to characterize the long-term effects of PIN1 loss out to 32 days and saw a moderate dependence for growth on PIN1 that became more pronounced at longer time points. However, this growth effect was extremely mild in comparison to that of the essential gene, RPS19. We hypothesize that this time-dependent cytotoxicity could be explained by minor defects in cell cycle progression, which accumulate over time giving rise to exponential effects on cell viability. It is thus unsurprising that cell cycle effects were not observed after 24

hours with either PIN1 inhibition or dTAG13 treatment, despite the observed increase in phosphor-CDK1 Tyr15 with PIN1 disruption in both systems.

PIN1 covalent inhibition differentially impacted transcription of specific transcripts at 4 and 24 hours, but did not appear to exert pathway-level effects on transcription. It is also possible that the timescale at which PIN1 impacts transcription through regulation of factors such as c-myc and NFκB was not captured at the timepoints investigated.

Collectively, this study suggests that PIN1 inhibition may prove a viable strategy in PDAC and highlights that 3D cell culture models and prolonged treatments best predict PIN1 dependency. Future efforts to cyclize and/or depeptidize BJP-06-005-3 could allow for improvements in its cell permeability and stability. Also, future studies to identify synthetic lethal interactions may point to suitable drug combinations to enhance therapeutic efficacy. PIN1 is implicated in various diseases, including Alzheimer's disease, breast cancer, prostate cancer, hepatocellular carcinoma, and asthma. We envision that BJP-06-005-3 and future analogs thereof will allow for biological exploration and target validation in such systems to further our understanding of PIN1-mediated phenotypes.

Chapter 7: Conclusion

The challenges of understudied proteins and need for novel cancer targets

There is a reluctance in biology to study the unknown. It is often easier to validate existing hypotheses or delve further into the mechanisms of a described pathway than to discover novel protein functions (Edwards et al., 2011). Though due in part to funding biases towards the research of well-studied targets and pathways, this is also due to missing biologic, genetic and chemical resources to aid the study of understudied proteins. Initiatives such as the NIH illuminating the druggable genome aim to close this knowledge gap (Oprea et al., 2018).

Targeted cancer therapeutics work by exploiting genetic vulnerabilities specific to tumor cells, ideally while minimizing effects on normal cells. Though there have been several advances in FDA approvals for targeted therapy, resistance is seen in a vast majority of patients shortly after treatment. However, opportunities remain to expand the reach of targeted therapy. As discussed previously there have been several definitions of the 'druggable genome', but regardless of the definition the numbers of putative therapeutic targets far exceed the number of proteins that are currently targeted by existing drugs (Rask-Andersen, Almen, & Schioth, 2011). Treatment options for a variety of cancers remain limited and the productivity of existing drug development pipelines has been declining despite increased biomedical research, partly because current drug discovery efforts are mainly focusing on previously validated proteins and protein families, leaving a significant proportion of the proteome un-targeted by cancer drugs (Rask-Andersen et al., 2011).

Candidates for targeted therapy must be extensively characterized and validated in preclinical studies before development of a targeted therapy could be initiated. Investigating understudied proteins thus provides the opportunity to furthering understanding of protein

function in cellular networks, and potentially uncover novel candidates for targeted therapy based on better understanding of a target's role in normal cellular states as well as human disease.

Leveraging covalent inhibitors as chemical tools for the study of CDK14, PKN3 and PIN1

Covalent inhibitors, which irreversibly react with nucleophilic moieties such as cysteine thiols in and around the protein active site, have several advantages compared to their reversible counterparts. We leveraged these advantages in the previously described studies in order to develop tool compounds in order to interrogate and clarify the function of three understudied proteins. Using structure guided design and structure-activity relationships, we were able to achieve relative selectivity through covalent targeting of CDK14 Cys218 from a starting scaffold (AT7519) with multiple CDK targets, retaining non-covalent activity only towards the TAIRE family CDKs. Addressing one of the major concerns of using covalent inhibitors, namely irreversible off-target protein modification, we developed CITe-Id to quantify dose-dependent binding of covalent inhibitors to cysteine thiols across the proteome. As an exemplar of the utility of CITe-Id, we identified a novel addressable cystine, PKN3 Cys840, as an off-target of the CDK7/12/13 inhibitor THZ1, and quickly developed JZ128 as a selective covalent inhibitor of PKN3. Finally, we used the improved potency afforded by covalent targeting of PIN1 Cys113 to develop a highly selective cell-penetrant PIN1 inhibitor. We were able to take advantage of Cys113 targeting and pharmacologically validate the specificity of the biological effects we observed using the paired reversible inhibitor as well as through mutation of the reactive cysteine residue.

Clarifications to functions of CDK14, PKN3 and PIN1

Through the use of the developed covalent inhibitors, we were able to further investigate the functions of CDK14, PKN3 and PIN1, particularly in the setting of cancer. CDK14, PKN3 and PIN1 have all been reported to promote oncogenic growth and cell migration in a number of cancer types, mostly through genetic studies, and in the case of PIN1, through the use of inhibitors poorly characterized as PIN1-specific probes (Moore & Potter, 2013). The development of FMF-04-159-2 for covalent inhibition of CDK14 (with reversible activity towards the TAIRE CDKs), of JZ128 for covalent inhibition of PKN3 and BJP-06-005-3 for covalent inhibition of PIN1 represent novel chemical tools which will have broader utility in future studies of each of these proteins beyond the work presented here.

The dTAG system (Nabet et al., 2018) for rapid and specific chemical-induced targeted degradation was beneficial in complementing inhibitor studies of CDK14 and PIN1. Due to residual off-target activity of FMF-04-159-2 towards CDK2, use of this chemical genetic approach allowed for specific disruption of CDK14. Consistent effects on mitotic LRP6 phosphorylation were observed. Effects of CDK14 disruption on markers of EMT varied across the panel of epithelial and mesenchymal pancreatic cancer cell lines. Further use of genetic variants of CDK14 which mimic disruption of CDK14 kinase activity did not further clarify the observed effects, though the cyclin binding-deficient variant of CDK14 most consistently limited the expression of pro-EMT markers.

Extensive PIN1 literature has cited it as a master regulator of numerous oncogenic signaling pathways and transcription factors, making it an attractive therapeutic candidate (Cheng & Tse, 2018). The mild growth effects of BJP-06-005-3, only evident after eight days of

continuous treatment of cells in 2D culture conditions, were thus somewhat unexpected. Genetic studies involving CRISPR knockout and cysteine to serine mutation as well as use of the reversible inhibitor as a chemical control all further validated that the observed growth effects were on-target. Targeted degradation of PIN1 using the dTAG system showed further concordance with the observed mild growth phenotype. Further characterization of the cellular consequences of covalent PIN1 inhibition beyond the cell cycle and transcriptome-wide effects presented here is necessary to understand which phenotypes are truly PIN1 dependent. In particular, proteomics and phosphoproteomics studies using the acute degradation afforded by the dTAG system could provide insights that complement parallel studies using the inhibitor.

Examining the substrates of kinases can reveal insights into their cellular function. Knowledge about targets for kinases is unequally distributed: just 20% of kinases are responsible for the phosphorylation of 87% of currently annotated substrates (Needham, Parker, Burykin, James, & Humphrey, 2019). Considering that around 80% of kinases have less than 20 substrates, and 30% have not yet been assigned a single substrate, the actual distribution is likely different than currently reported. Moreover, more than 95% of identified human phosphorylation sites have no known kinase or biological function assigned (Needham et al., 2019).

For CDK14 and PKN3, we utilized the covalent inhibitors we developed to perform unbiased phosphoproteomics experiments to characterize the downstream consequences of inhibiting kinase activity. Using JZ128 in combination with PKN3 Cys840Ser mutant or PKN3 knockout lines led to PKN3-dependent reduction in phospho-sites related to adherens junctions, consistent with reported phenotypic roles from the few PKN3 studies which have been

conducted. These phospho-sites merit further follow-up as to whether they are direct PKN3 substrates or are downstream consequences of kinase inhibition. The use of FMF-04-159-2 with washout conditions in combination with prioritizing peptides matching the phospho-motif we determined for CDK14 and the TAIRE kinases compared to that of CDK2/CDK3 resulted in a set of candidate phospho-sites involved in cell cycle and mitotic regulation associated with FMF-04-159-2 treatment. CDK14 direct substrates beyond LRP6 have not been previously described, and these prioritized sites represent putative CDK14 direct substrates. A major challenge for phosphoproteomics also lies in interrogating and understanding the functional consequences of modified sites (Needham et al., 2019). To this end, follow-up studies to the presented experiments are required for both PKN3 and CDK14.

Despite recent clinical successes for irreversible drugs, potential toxicities mediated by unpredictable modification of off-target cysteines represents a major hurdle for expansion of covalent drug programs (Chaikuad et al., 2018). CITe-Id has the potential to impact the development of covalent kinase inhibitors through better understanding of the target profile, as was exemplified by its use to profile our PIN1 inhibitor. Understanding the proteome-wide binding profile of covalent inhibitors can therefore significantly accelerate the development of clinical kinase inhibitors and validate the specificity of covalent chemical probes.

Summary

Leveraging the advantages of covalent inhibitors allowed us to access two understudied kinases and a proline isomerase whose study, albeit extensive, has been complicated by the use of non-specific compounds as chemical probes. The development of FMF-04-159-2 for covalent

inhibition of CDK14 (with reversible activity towards the TAIRE CDKs), of JZ128 for covalent inhibition of PKN3 and BJP-06-005-3 for covalent inhibition of PIN1 represent novel chemical tools which will have broader utility in future studies of each of these proteins beyond the work presented here. CITe-Id provides a powerful complement to current platforms to characterize the selectivity of covalent inhibitors at the site-level, identify new, pharmacologically-addressable cysteine-thiols, and inform structure-based drug design programs. Thee utilization of genetic and chemical genetic strategies complementary to covalent inhibitors, including CRISPR knockout, rescues with genetic variants and induced targeted degradation using dTAG provide a framework for approaching preclinical target validation.

Appendix

Methods

CDK14 Projects

Experimental Models

HCT116 cells (adult male) were grown in McCoy's 5A media (Life Technologies) and HEK293 cells (fetal), MDA-MB-231 (adult female), HepG2 (adolescent male) and PATU-8988T (adult female) were grown in Dulbecco's Modified Eagle's Medium (Invitrogen). All base media was supplemented with 10% FBS (Sigma) and 100U/mL Penicillin-Streptomycin (Gibco). All cells were cultured at 37°C in a humidified chamber in the presence of 5% CO_2. Cell lines were purchased from ATCC, with the exception of PATU-8988T cells, which were purchased from DSMZ. All cell lines were tested for mycoplasma on a monthly basis.

Pull Down / Cellular Target Engagement Protocol

HEK293 cells overexpressing a CDK14-flag fusion protein were treated with candidate compounds for 4 hours. Cells were washed with PBS, harvested and lysed in Pierce IP buffer with protease and phosphatase inhibitors (Roche). Lysates were clarified by centrifugation, then incubated with 1uM biotin-FMF-03-198 (or 1uM biotin-ATP mimetic) overnight at 4 °C. To enhance pulldown, lysates were incubated at room temperature for an additional 2 hours. Lysates were then incubated with streptavidin agarose (Thermo Fisher #20349) for 2 hours at 4 °C. Agarose beads were washed 3 times with Pierce IP buffer, then boiled in 2x LDS + 10% β–mercaptoethanol at 95 °C for 5 minutes. Proteins of interest engaged by the biotinylated compound were then assessed using western blotting.

For washout pull downs, medium containing inhibitors was removed after 4-hour compound treatment to effectively 'wash out' the compound. Cells were washed 1x with PBS, 1x

with media. Fresh media was replaced, and cells were allowed to grow in the absence of inhibitor. Cells were then harvested at indicated times after washout (usually 2 hours unless otherwise noted) for lysis and subsequent pull down, as described above.

Antiproliferation Assay Protocol

HCT116 cells were plated in 384-well plates at 750 cells/well in 50ul fresh media and were treated the next day with 0.1 µl compounds in four-fold dilution series using the Janus pinner. Cells were incubated with compounds for 72 hours in 37 °C 5% CO2. Anti-proliferative effects of these compounds were then assessed using Cell Titer Glo (Promega # G7571) according to manufacturer protocol by measuring luminescence using an Envision plate-reader. All proliferation assays were performed in biological quadruplicate. IC_{50} values were determined using a non-linear regression curve fit in GraphPad Prism 6. N=4 biological replicates were used for each treatment condition.

In vitro Kinase Assays

LanthaScreen Eu kinase binding assays were conducted for CDK14/CycY as performed in the commercial assay service by Life Technologies, but included a 30 minute pre-incubation step of the kinase and Eu-labelled anti-GST antibody with candidate compounds to facilitate covalent bond formation. CDK14/CycY protein was purchased from Life Technologies.

For some compounds, LanthaScreen Eu kinase binding assays were conducted for CDK14/CycY at Life Technologies. LanthaScreen Eu kinase binding assays were conducted for CDK16/CycY at Life Technologies. Z'LYTE kinase assays were conducted for CDK2/CycA at Life Technologies using Km ATP concentrations. CDK14 ^{33}P kinase assays were performed by Reaction Biology Corp.

For RB phosphorylation, assayed using phospho-specific antibodies, CDK14/CycY (Life Technologies # PV6382) was used to phosphorylate truncated RB protein (Signal Chem # R05-55G-50). Reaction was allowed to proceed with 500uM ATP at 30 °C for 15 minutes. The reaction was stopped by addition of 2X LDS + 10% β–mercaptoethanol followed by incubation at 95 °C for 5 minutes. Western blotting was performed as described above, with the indicated phospho-specific RB antibodies (Cell Signaling) used to assess phosphorylation.

Intact Mass Spectrometry Analysis

Un-tagged CDK14 (amino acids 124-169) was expressed and purified using baculovirus. This recombinant CDK14 protein was incubated with DMSO or a 10-fold molar excess of FMF-03-198-2 or FMF-04-159-2 at room temperature for 2 hours in buffer (50 mM HEPES, 150 mM NaCl, 10% Glycerol, 2 mM TCEP, pH 7.5). Reacted protein (5 µg) was desalted on a self packed column (500 µm I.D. packed with 4 cm POROS 50R2, Applied Biosystems, Framingham, MA), eluted with a ballistic HPLC gradient (0-100% B in 1 minute; A=0.1 M acetic acid in water; B=0.1 M acetic acid in acetonitrile), and introduced to an LTQ ion trap mass spectrometer via electrospray ionization. The mass spectrometer collected profile data over *m/z* 300-2000. Mass spectra were deconvoluted using MagTran 1.03b2 (Z. Zhang & Marshall, 1998).

Nano-LC/MS analysis of labeled CDK14

Protein labeled as described above was denatured with rapigest (0.1% final concentration), reduced (10 mM DTT, 56 °C, 30 minutes), alkylated (22.5 mM IAA, RT, dark), and digested with chymotrypsin overnight at 37 °C. Digests were acidified with 10% TFA, incubated at 37 °C for 30 minutes, and centrifuged at 13,000 rpm for 10 minutes at 4 °C to remove rapigest by-products. Supernatant was then desalted by C18 and peptides dried by vacuum centrifugation. Dried

peptides were resuspended in 50% acetonitrile with 1% formic acid, 100 mM ammonium acetate and analyzed by CE-MS using a ZipChip CE system and autosampler (908 Devices, Boston, MA) interfaced to a QExactive HF mass spectrometer (ThermoFisher Scientific). Peptides were loaded for 30 seconds and CE separation performed at 500 V/cm on an HR chip for 10 minutes with a background electrolyte consisting of 1% formic acid in 50% acetonitrile. Pressure assist was utilized and started at 1 minute. The mass spectrometer was operated in data dependent mode and subjected the 5 most abundant ions in each MS scan (60k resolution, 1E6 target, lock mass enabled) to MS/MS (15k resolution, 2E5 target, 100 ms max inject time). Dynamic exclusion was enabled with a repeat count of 1 and an exclusion time of 6 seconds. MS/MS data was extracted to .mgf using mulitplierz (Alexander, Ficarro, Adelmant, & Marto, 2017; Askenazi, Parikh, & Marto, 2009) and searched against a custom database containing the sequence of CDK14 using Mascot version 2.2. Search parameters specified fixed carbamidomethylation of cysteine, and variable oxidation (methionine) and variable FMF-03-198-2 or FMF-04-159-2 modification (cysteine). Precursor mass tolerance was set to 10 ppm and product ion tolerance was 25 mmu. Peptide sequence confirmation was performed using mzStudio (Ficarro, Alexander, & Marto, 2017).

Cell Line Generation

HEK293 cells were transfected with pCMV-CDK14-myc/DDK (Origene # RC224426) using the Neon electroporation system according to manufacturer's protocol (Life Technologies). The C218S CDK14 was generated using QuikChange (Agilent) according to manufacturer's protocol, using the following primers:

fwd: GTGCACACTGATTTATCTCAGTACATGGAC

rev: GTCCATGTACTGAGATAAATCAGTGTGCAC

Sequence verification was performed using the following primer: GAAGAAGAAGGGACAC

Cloning was performed using NEB 10-beta cells (NEB # C3019I).

HCT116 CDK14 knockout cell lines were generated by cloning CDK14-targeting sgRNAs into the BbsI site of pX458 (Addgene # 48138). The genomic sequence complementary to the CDK14-directed guide RNA that was cloned into pX458 and used in the genome editing experiments is: TCATGACATCATCCATACCA.

Cloning was performed using NEB Stable cells (NEB #C3040I). Single cells expressing GFP 48 hours after transfection using the Neon electroporation system (Life Technologies) were sorted into 96 well plates using FACS. Clones were verified both by western blotting and genomic DNA PCR of the edited region. CDK14 was cloned into the XbaI/NotI sites of the pCDH-CMV-MCS vector backbone (System Biosciences # CD510B-1). CDK14-flag wild type or C218S was re-introduced to the HCT116 CDK14 knockout cells using lentiviral infection.

KiNativ Live Cell Profiling Protocol

HCT116 cells were plated in fresh media in 15cm plates and treated for 4 hours with candidate compounds. For washout conditions, compound-containing media was removed from cells, and cells were washed 1x with PBS and 1x with media before fresh media was replaced. Cells were incubated for an additional 2 hours after washout. To harvest cells, plates were washed 1x with cold PBS, then collected by scraping and centrifugation. Cell pellets were snap-frozen in liquid nitrogen. The remainder of the KiNativ profiling experiment was performed by ActivX Biosciences (La Jolla, CA).

Fluorescence-Activated Cell Sorting Analysis (FACS) for Cell Cycle Analysis

Cells were plated and treated the next day with the indicated compounds for 24 hours. Cells were trypsinized, washed once in phosphate-buffered saline (PBS), and fixed overnight with 80% ethanol in PBS at −20°C. Cells were washed three times with PBS. Cells were stained in PBS containing 0.1% Triton X-100, 25 µg/mL propidium iodide (PI, Molecular Probes), and 0.2 mg/mL RNase A (Sigma) overnight at 4 °C. Cells were filtered through a 0.2um filter prior to data acquisition on a BD LSR II. Data were analyzed using FlowJo. N=3 biological replicates were used for each treatment condition.

Inhibitor Treatment and Western Blotting Experiments

HCT116 cells were plated and treated for 6 hours or 4 hours followed by compound washout for 2 hours with indicated compounds at 1uM. Cells were dissociated using trypsin, washed with PBS and lysed in RIPA buffer + protease and phosphatase inhibitor (Roche) + nuclear (Pierce). Samples were normalized and prepped in 4x LDS + 10% β-mercaptoethanol and boiled for 5 minutes at 95 °C. Lysates were probed for specified proteins by western blotting using the Bolt system (Life Technologies).

NanoBRET Live Cell Target Engagement

HCT116 cells were transiently transfected with luciferase fusion-expressing CDK constructs and a Cyclin Y carrier (plasmids courtesy of Promega). Cells were treated with compound and an ATP-mimetic Tracer 20-24 hours later and assayed 4 hours after treatment using the Intracellular TE Nano-Glo kit according to manufacturer protocol (Promega #N2160). N=3 biological replicates were used for each treatment condition.

Immunohistochemistry for Phalloidin Staining

HCT116 cells with CDK14 wild type or KO (CRISPR-generated clonal lines) were plated in 6 well plates with a single coverslip in each well, and treated the next day with DMSO or FMF-04-159-2 for 24 h. Cells were washed once with PBS, fixed with 4% formaldehyde in PBS for 15 minutes at room temperature, then washed three times with PBS. Cells were incubated in the dark at room temperature for 1 hour with Phalloidin-488 (Santa Cruz # sc-363791) according to manufacturer instructions. Cells were washed three times with PBS, then coverslips were mounted on slides with ProLong Gold Antifade Reagent with DAPI (Cell Signaling # 8961) and cured in the dark at room temperature overnight before storage at 4°C. Slides were imaged using a Zeiss Axiostar microscope using a 20X objective, and images were captured using a Zeiss Axiocam and ZENlite software. N=3 biological replicates were used for each treatment condition.

Double Thymidine Synchronization with Compound Treatment

100,000 cells per well were plated in a 6-well tissue culture-treated plate. The next day, cells were treated with 2mM thymidine final concentration (from 100mM stock) for 18 h. Cells were washed 2x with media, and fresh media was replaced. After 8 h, cells were treated again with 2mM thymidine as before for 16 h. Cells were released by washing 2x with media, and fresh media was replaced. Cells were treated with 1uM FMF-04-159-2 for 4 h time periods, and were either harvested, or where indicated, compound was washed out by washing cells 2x with media and replacing with fresh media, and cells were incubated further for 2 h. Cells were harvested at the indicated timepoint using trypsin, and western blot was performed as described above.

Peptide Library Assay for Phospho-motif Identification

Assay was performed as described previously (Hutti et al., 2004). The spot densities from the dot array were quantified and normalized by each row. These values were used to score the amino

acid sequence surrounding the serine or threonine of each identified phospho-peptide, by summing the corresponded dots of each substrate. Two outputs were generated: Raw scores and relative rankings. In the relative rankings, CDK14/16 score was ranked in comparison to 189 other serine/threonine kinase substrate motif scores (Johnson J.L. et al., unpublished). CDK16/Cyclin Y (cat # PV6379) was purchased from Life Technologies, CDK14/Cyclin Y (cat # P15-10G-05) and CDK18/Cyclin Y (cat # P11-10G-05) were purchased from SignalChem. CDK2/Cyclin E1 (cat # C29-18G-10) and CDK3/Cyclin E1 (cat # C30-10G-10) were also purchased from SignalChem.

Proteomics and Phospho-proteomics Cell Lysis, Protein Digest and TMT Labeling

Cells were lysed by homogenization (QIAshredder) in lysis buffer (2% SDS, 150 mM NaCl, 50 mM Tris pH 7.4). Lysates were reduced with 5 mM DTT, alkylated with 15 mM iodoacetamide for 30 minutes in the dark, alkylation reactions quenched with 50 mM freshly prepared DTT and proteins precipitated by methanol/chloroform precipitation. Digests were carried out in 200 mM EPPS pH 8.5 in presence of 2% acetonitrile (v/v) with LysC (Wako, 2mg/ml, used 1:75) for 3 hours at room temperature and after subsequent addition of trypsin (Promega #V5111, stock 1:75) over night at 37°C.

Missed cleavage rate was assayed from a small aliquot by mass spectrometry. For whole proteome analysis, digests containing approximately 60 µg of peptide material were directly labeled with TMT reagents (Thermo Fisher Scientific). Labeling efficiency and TMT ratios were assayed by mass spectrometry, while labeling reactions were stored at -80°C. After quenching of TMT labeling reactions with hydroxylamine, TMT labeling reactions were mixed, solvent evaporated to near completion and TMT labeled peptides purified and desalted by acidic

reversed phase C_{18} chromatography. Peptides were then fractionated by alkaline reversed phase chromatography into 96 fractions and combined into 12 samples. Before mass spectrometric analysis, peptides were desalted over Stage Tips (Rappsilber, Ishihama, & Mann, 2003).

Proteomics and Phospho-proteomics Phosphopeptide Enrichment

Phosphopeptides were enriched from digested material containing approximately 4 mg of peptide material per sample by Fe-NTA chromatography (Thermo Fisher Scientific #A32992). After TMT labeling, phosphopeptides were subjected to alkaline reverse fractionation by a linear acetonitrile gradient into 96 fractions and combined into 24 samples. TMT labeled, fractionated phosphopeptides were desalted over StageTips (Rappsilber et al., 2003) prior to mass spectrometry analysis.

Proteomics and Phospho-proteomics Mass Spectrometry Analysis

Data were collected by a MultiNotch MS^3 TMT method (McAlister et al., 2014) using an Orbitrap Lumos mass spectrometer (Thermo Fisher Scientific) coupled to a Proxeon EASY-nLC 1200 liquid chromatography (LC) system (Thermo Fisher Scientific). The 100 µm inner diameter capillary column used was packed with C_{18} resin (SepPax Technologies Inc. 1.8 µm). Peptides of each fraction were separated over 3 h acidic acetonitrile gradients by LC prior to mass spectrometry (MS) injection. The first scan of the sequence was an MS^1 spectrum (Orbitrap analysis; resolution 120,000; mass range 400−1400 Th). MS^2 analysis followed collision-induced dissociation (CID, CE=35) with a maximum ion injection time of 150 ms (350 ms for phosphopeptides) and an isolation window of 0.7 Da. In order to obtain quantitative information, MS^3 precursors were fragmented by high-energy collision-induced dissociation (HCD) and analyzed in the Orbitrap at a resolution of 50,000 at 200 Th.

For phosphopeptides, MS^2 spectra were recorded with an isolation window of 0.5 Da and multistage activation (MSA) with a neutral loss of 97.9763 Da. In the MS^3 for charge states of 2 and 3, an isolation window of 1.2 m/z and for charge states 4-6 an isolation window of 0.8 m/z was chosen. MS^3 injection time for phosphopeptides was 350 ms at a resolution of 50,000. Further details on LC and MS parameters and settings used were described recently (Paulo, O'Connell, & Gygi, 2016).

Peptides were searched with a SEQUEST-based in-house software against a human database with a target decoy database strategy and a false discovery rate (FDR) of 2% set for peptide-spectrum matches following filtering by linear discriminant analysis (LDA) and a final collapsed protein-level FDR of 2%. Quantitative information on peptides was derived from MS^3 scans. Quant tables were generated requiring an MS^2 isolation specificity of >65% for each peptide and a sum of TMT s/n of >150 over all channels for any given peptide and exported to Excel and further processed therein. To quantify the confidence assignment of phosphorylation sites, a modified version of the Ascore algorithm was used. For confident site localization, Ascore values of >13 ($p <= 0.05$) were required (Huttlin et al., 2010). Details of the TMT intensity quantification method and further search parameters applied were described recently (Paulo et al., 2016).

<u>In Vitro Phosphorylation of Synthetic Peptides followed by MS/MS</u>

Recombinant CDK14/Cyclin Y (Life Technologies) was preincubated with or without 1 µM FMF-04-159-2 for 1 h at 37 °C. The kinase was then reacted with synthetic peptides (100:1 substrate to enzyme ratio) in kinase buffer (50 mM Tris pH 7.5, 150 mM NaCl, 5% glycerol, 1 mM TCEP, 20 mM MgCl2, 1 mM ATP) for 18 h at 37 °C. Reactions were desalted and analyzed using a ZipChip

(908 Devices, Cambridge MA) capillary electrophoresis source on a Q Exactive HF mass spectrometer using a 10 min run method as described previously (Ficarro et al., 2016). MS/MS spectra of synthetic phosphopeptides were annotated using mzStudio (Ficarro et al., 2017). Spectra were searched with Mascot using no enzyme specificity against a forward and reverse human proteome database.

Chemistry Synthetic Schemes

Scheme 1

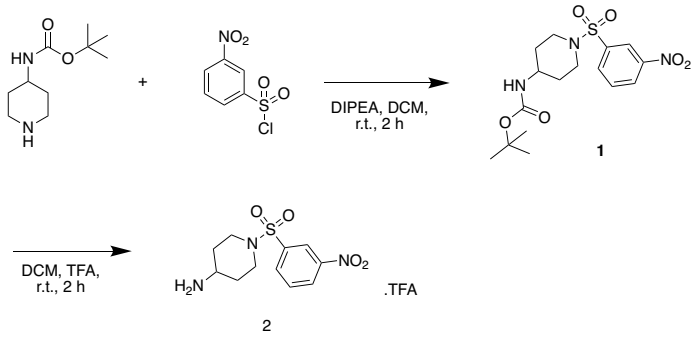

Scheme 2

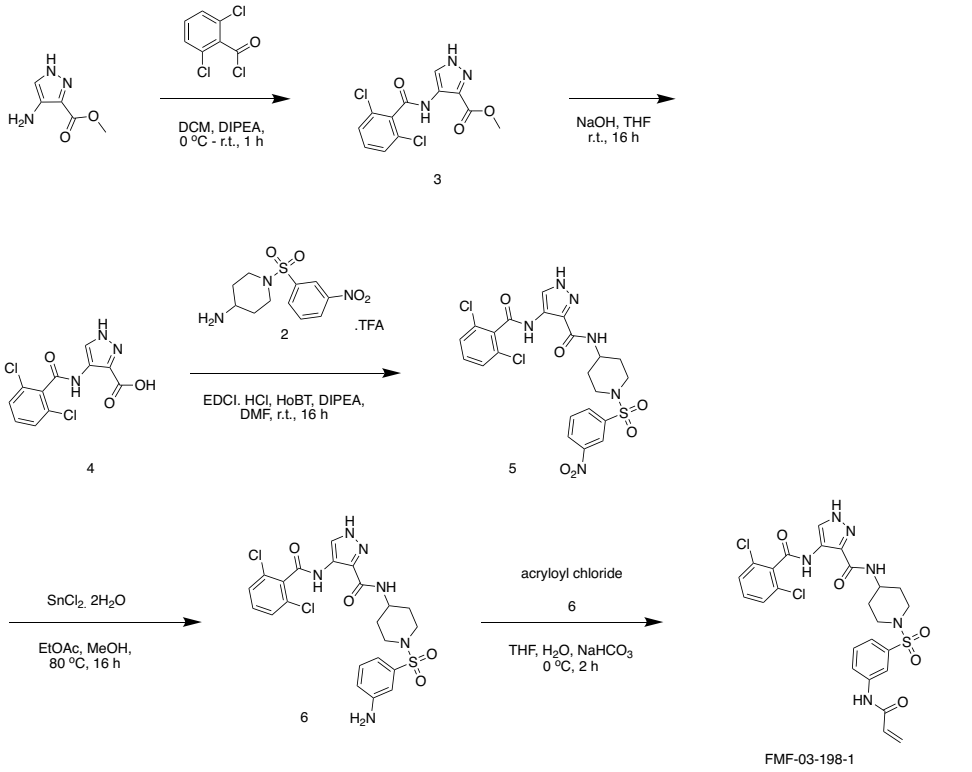

Scheme 3

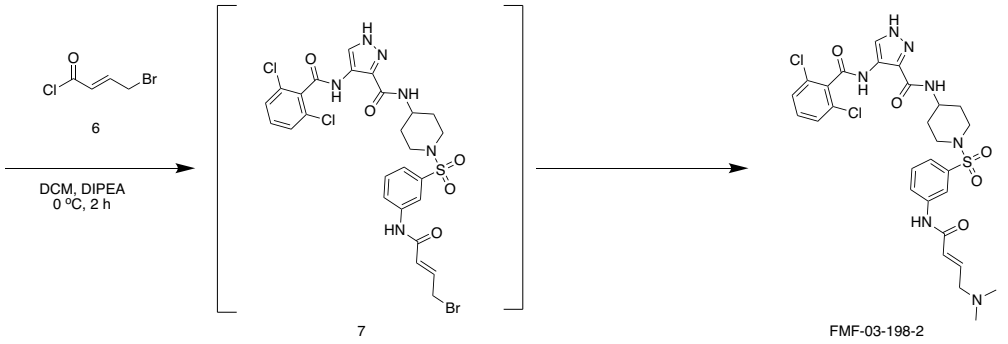

General Chemistry Methods

Unless otherwise noted, reagents and solvents were obtained from commercial suppliers and were used without further purification. ^{1}H NMR spectra were recorded on 500 MHz Bruker Avance III spectrometer, and chemical shifts are reported in parts per million (ppm, δ) downfield from tetramethylsilane (TMS). Coupling constants (J) are reported in Hz. Spin multiplicities are described as s (singlet), br (broad singlet), d (doublet), t (triplet), q (quartet), and m (multiplet). Mass spectra were obtained on a Waters Acquity UPLC. Preparative HPLC was performed on a Waters Sunfire C18 column (19 mm × 50 mm, 5 μM) using a gradient of 15–95% methanol in water containing 0.05% trifluoroacetic acid (TFA) over 22 min (28 min run time) at a flow rate of 20 mL/min. Assayed compounds were isolated and tested as TFA salts. Purities of assayed compounds were in all cases greater than 95%, as determined by reverse-phase HPLC analysis. Schemes and method similar to those described here were used for all analogs described in Chapter 2.

CDK14 Variant Cloning

CDK14 variants were generated using QuikChange II (Agilent) mutagenesis according to manufacturer protocol. QuikChange was performed on CDK14, which was previously cloned into

the XbaI/NotI sites of the pCDH-CMV-MCS vector backbone (System Biosciences # CD510B-1). The following primers were used:

D256A fwd: GAG TTA AAG CTG GCA GCT TTC GGT CTT GCA AGA GC

D256A rev: GCT CTT GCA AGA CCG AAA GCT GCC AGC TTT AAC TC

K164R fwd: GTTGGTAGCTCTGAGGGTGATCAGGCTGC

K164R rev: GCAGCCTGATCACCCTCAGAGCTACCAAC

F176Δ fwd: GAAGGGACACCTACAGCTATCAGGGAAGGC

F176Δ rev: GCCTTCCCTGATAGCTGTAGGTGTCCCTTC

Trans-well migration assay

Cells were serum-starved for 24 hours prior to assay by aspirating complete growth media, washing twice, and replacing with serum-free media. The transwell plate (Corning, 6.5mm with 8µm pore size) was equilibrated by adding 600 µl complete media containing 15% FBS. Serum-starved cells were trypsinized, quenched with complete media, washed twice with serum-free media then counted. 100,000 cells were plated in upper chamber in 100µl serum-free media and incubated for 48 h under typical culture conditions described above. Migration was assessed by removing the inserts and performing crystal violet staining before imaging.

Additional Antibodies

All western blots shown in Chapter 4 were performed using antibodies from Cell Signaling Technologies, other than CDK14 and Cyclin Y.

PKN3 Project

Antibodies and Reagents

Antibodies were obtained from the following sources: α-PKN3 (Novus Biologicals, Littleton, CO), α-CDK7 (Cell Signaling Technologies, Danvers, MA), α-CCNK (Bethyl Laboratories, Montgomery, TX), PRKCQ (Thermo Fisher Scientific), α-FLAG (Sigma), α-PKN1 (Invitrogen, Carlsbad, CA), α-PKN2 (Cell Signaling), α-LIMK1 (Cell Signaling), α-PIP4K2A (Cell Signaling), α-PIP4K2B (Cell Signaling), α-PIP4K2C (Sigma), α-PIKFYVE (Millipore), α-RIPK2 (Novus Biologicals). Sources for supplies and reagents are as follows: Activated Thiol Sepharose 4B beads (GE Healthcare, Piscataway, NJ); Sep-pak tC18 100 mg 96-well plate (tC18; Waters, Milford, MA); SOLA C18 plate (SOLA C18; Thermo Fisher Scientific, Waltham, MA); Ni:NTA magnetic agarose beads (Qiagen, Valencia, CA); Ammonium bicarbonate (AMBIC; Sigma, St. Louis, MO); Triethylammonium bicarbonate buffer (TEAB; Sigma), Ethanol (EtOH; Sigma); Acetonitrile (Macron, Avantor Performance Materials, Center Valley, PA); tris(2-carboxyethyl)phosphine (TCEP; Sigma); *S*-Methyl methanethiosulfonate (MMTS; Sigma); DL-Dithiothreitol (Sigma); Iodoacetamide (IAA; Sigma); Trifluoroacetic Acid (TFA; Pierce, Rockford, IL); formic acid (FA; Sigma). High-Capacity Streptavidin Resin (streptavidin resin; Pierce). Kinase substrate library (Anaspec). Streptavidin-conjugated membranes (Promega). Synthetic peptides were produced by use of Fmoc chemistry and purified by reversed phase HPLC. THZ1, THZ1-R, and THZ531 were synthesized as described (Kwiatkowski et al., 2014; T. Zhang et al., 2016).

Chemical Synthesis

All solvents and reagents were used as obtained. For verification of chemical structures, 1H NMR spectra were recorded with a Varian Inova 500 NMR spectrometer and referenced to dimethylsulfoxide. Chemical shifts are expressed in ppm. Mass spectra were measured with Waters Micromass ZQ using an ESI source coupled to a Waters 2525 HPLC system operating in

reverse mode with a Waters Sunfire C18 5 µm, 4.6 mm x 50 mm column. Purification of compounds was performed with either a Teledyne ISCO CombiFlash Rf system or a Waters Micromass ZQ preparative system. The purity was analyzed on an above-mentioned Waters LC-MS Symmetry (C18 column,4.6 mm x 50 mm, 5 µM) using a gradient of 5-95% methanol in water containing 0.035% trifluoroacetic acid (TFA). Detailed synthetic schemes and characterization data are available elsewhere (Kwiatkowski et al., 2014; T. Zhang et al., 2016).

Cell Culture and Cloning

All cell culture was performed using standard techniques. HeLa S3 and HEK 293T cells were cultured in DMEM with 10% FBS, PC3 cells were cultured in RPMI1640 with 10% FBS. Cells were collected using a scraper. The cells were centrifuged at 300g and washed twice with PBS before cell pellets were frozen at -80^{o}C. Full length PKN3 cDNA with a N-terminal FLAG-HA tag was cloned into the pUC57 vector (GenScript USA, Piscataway, NJ). At the same time, a point mutation was introduced at position 2886 (local sequence: ggccacacagggt) from a→t to generate the C840S mutant PKN3. Both PKN3 constructs were excised from pUC57 with EcoRI and XhoI and inserted into a pCDH-CMV backbone.

Target Engagement Pulldown Assays

HeLa S3 or PC3 cells were treated with increasing concentrations of either DMSO, THZ1, THZ1-R, JZ128, or JZ128-R for 4 h. Cells were harvested by scraping and washed twice with PBS before lysis with NP-40 lysis buffer (50 mM Tris pH 7.5, 150 mM NaCl, 1 mM EDTA, 10% v/v glycerol, 0.5% v/v NP-40, protease inhibitors). Protein content was measured by BCA. Samples were treated with 2 µM of either THZ1-DTB or JZ128-DTB for 18 hr. at 4^{o}C. Streptavidin resin was added and incubated for 1 hr. at room temperature. The beads were washed three times with

NP-40 lysis buffer. Bound protein was eluted by adding SDS-PAGE loading buffer and boiling for 5 min before western blotting. 1% of sample input was used for loading controls.

Kinase Assays

Kinase assays for PKN3 were performed using the synthetic peptide GGGGPKGPGRRGRRRTSSFAEGG as substrate (Falk et al., 2014). Assay conditions were 26 mM Tris pH 7.5, 0.002% CHAPS, 5.2 mM $MgCl_2$, 2.3 mM DTT, 25 ng PKN3, 20 µM substrate, 68 µM ATP, 1 µCi ATP [γ-^{32}P]. Enzyme was pre-incubated with compounds for 30 min before adding ATP and reacting for 30 min at room temperature. Reaction was stopped with TCA and spotted in 96 well phosphocellulose plates (Millipore). Wells were washed seven times with 150 mM phosphoric acid, once with 95% isopropanol, and dried before scintillation counting. For the time-course PKN3 kinase assay in Figure 2E, all compound treatments were at 1 µM and preincubation times were from 0 to 120 min. Kinase assays for PRKCQ, CDK7, LIMK1, PKN1, and PKN2 were performed using SelectScreen (Invitrogen) in a 10-dose titration format.

For *in vitro* validation of PKN3 substrates, the following changes were made to the above methodology: candidate substrate synthetic peptides were used at 4 µM concentration, ATP was used at 1 mM concentration, and ATP [γ-^{32}P] was omitted. Reactions were performed for 1 hour at 37^{o}C and stopped by adding acetic acid to 1% FC. 10 pmol of each substrate peptide was desalted and mixed with α-cyano-4-hydroxycinnamic acid matrix and analyzed on a 4800 MALDI TOF/TOF (AB SCIEX). Unphosphorylated peptide signal was compared to a control reaction lacking ATP using label free quantitation to indirectly determine the percentage of phosphopeptide conversion. Synthetic peptide sequences: LAD1 S375, RSSPRTI<u>S</u>FRMKPKK; EXOC2 S432, ASLKRGS<u>S</u>FQSGRDDTWR; EGFR S1064, NGLQSCPIKED<u>S</u>FLQRYSSDPT.

PKN3 Rescue Pulldowns

PKN3 constructs were transiently expressed in HEK 293T cells. Cells were harvested and lysed with NP-40 lysis buffer as above. Lysates were initially probed for FLAG signal via western blotting to determine construct expression in each cell line. Input lysates for subsequent pulldowns and immunoprecipitations was normalized for construct expression with empty vector input equal to highest input used. Lysates were split in four: two were treated with THZ1-DTB or JZ128-DTB for 18 hr. at 4^{o}C, two were treated with DMSO under the same conditions. One probe treated and one DMSO treated sample received streptavidin pulldowns as in target engagement pulldowns above. The remaining two samples were immunoprecipitated with α-HA-agarose resin (Sigma) for 2 hr. at room temperature. Resin was washed and bound proteins eluted as for the streptavidin pulldowns. Samples were then analyzed with western blotting.

Antiproliferation Assays

PC3 cells were plated in 384-well plates at 750 cells/well in 50ul fresh media (RPMI + 15% FBS + 1% Penn/Strep) and treated with 0.1 µl candidate compounds in ten point four-fold dilution series using the JANUS (Perkin Elmer). Cells were incubated with compounds for 72 hours in 37 °C 5% CO_2. Anti-proliferative effects of these compounds were assessed 72 hours after compound addition using Cell Titer Glo (Promega cat# G7571) as described in product manual by luminescence measurements using an Envision platereader. All proliferation assays were performed in biological quadruplicate. IC50 values were determined using a non-linear regression curve fit in GraphPad Prism 7.

Wound Healing Assays

PC3 cells were seeded in 24-well plates (1×10^5 cells/well) and grown to confluency. The media was replaced with serum-free media for 12 hours to stop cell division. Wounds were made across the well with a P10 pipette tip and cells washed with PBS before replacing with fresh serum-free media containing the indicated compounds at 300 nM. Images of wound were then captured over two days with a Zeiss Axiostar microscope. Wound area was quantified using ImageJ.

PKN3 Phospho Motif Identification

To determine the substrate motif of PKN3, *in vitro* kinase assays were performed with recombinant PKN3 on the peptide substrate library in the presence of ATP[γ-^{32}P]. These reactions were carried out in Kinase Assay Buffer I (SignalChem) at 30^{o}C for 90 minutes. The peptides, which are biotinylated at their C-termini, were blotted onto streptavidin-conjugated membranes and imaged with a Typhoon FLA 7000 phosphorimager. Detailed information of the protocol is provided elsewhere (Turk, Hutti, & Cantley, 2006). The spot densities from the blot array were quantified and normalized by each row. These values were used to score the amino acid sequence surrounding each identified phospho-site

Isotopic Reporter Labeling

For ClTe-Id experiments, iTRAQ labeling was performed after streptavidin pulldown. Samples were resuspended in 30% 0.5M TEAB, 70% EtOH. The iTRAQ reagent was added to each corresponding sample. After incubation at room temperature for 1 hr, the samples were combined and acidified before vacuum drying. For phosphoproteomics experiments, TMT labeling was performed prior to phosphopeptide enrichment. Samples were resuspended in 50

mM TEAB. ACN was added to each TMT reagent and then mixed with each corresponding sample. After incubation at room temperature for 1 hr., the samples were combined and acidified prior to a final desalting step on a SOLA C18 plate.

Phosphoproteome Analysis

Qiagen Ni:NTA magnetic agarose beads stored as a 5% suspension in 30% ethanol were used for phosphopeptide enrichment. The magnetic beads were prepared by rinsing three times with water and then incubating in 100 mM EDTA pH 8 for 30 minutes. Next, the beads were rinsed three times with water and incubated in 10 mM $FeCl_3$ for 30 minutes. Prior to incubation with the sample peptides, the bead pellet was rinsed three times with water and once with 80% ACN, 0.1% TFA and finally resuspended with 80% ACN, 0.1% TFA. Reduced, alkylated, desalted, tryptic peptides were TMT-labeled, pooled, and dried prior to phosphopeptide enrichment. Peptides were reconstituted in 80% ACN, 0.1% TFA and incubated with the Fe-activated magnetic agarose NTA bead suspension for 30 minutes. After incubation, the supernatant was retained and the bead pellet was washed three times with 80% ACN, 0.1% TFA. The bead pellet was eluted with 1.4 % ammonia by weight, 3 mM EDTA and water before being vacuum dried. Phosphopeptides were analyzed using our RP-SAX-RP chromatography platform. Detailed descriptions of the multidimensional chromatography system are provided elsewhere (Ficarro et al., 2011; F. Zhou et al., 2013; F. Zhou et al., 2011). Peptides were automatically fractionated across first and second dimension high-pH reversed phase and high-pH strong anion exchange chromatographic stages. Peptides were gradient eluted from the third dimension (low-pH RP) into a Q-Exactive HF mass spectrometer (ThermoFisher Scientific) using a 4 hour organic gradient (5-30% B in 4 hr., A = 0.1% FA, B = acetonitrile with 0.1% FA). The electrospray voltage was set at 3.2 kV. A top-15

data-dependent method was used for precursor selection and MS/MS. A normalized collision energy of 37 eV was used. Data processing of phosphopeptide MS/MS spectra is described below.

Processing of Mass Spectrometry Data

Native .RAW data files from the Q-Exactive HF mass spectrometer were processed using our multiplierz Python-based framework (Alexander et al., 2017; Askenazi et al., 2009; Parikh et al., 2009) to generate .mgf files for input to Mascot (Matrix Science). For CITe-Id experiments with THZ1-DTB and JZ128-DTB labeled peptides, MS/MS spectra were processed to account for inhibitor-specific fragmentation behavior as described previously (Ficarro et al., 2016). Peptide precursor masses were recalibrated on a per-scan basis by correcting all m/z values based on accurate mass recorded for the $Si(CH_3)_2O_6$ peak in each spectrum. All data were searched against a forward-reverse human database assembled from the NCBI Refseq database. For de-isotoped HCD spectra, the precursor mass tolerance was set to 10 ppm and the MS/MS fragment ion tolerance was set to 25 mmu. Search parameters included trypsin specificity, with a maximum of two missed cleavages, fixed carbamidomethylation of Cys (+57 Da), variable oxidation on Met (+16 Da with -64 Da neutral loss possible). Depending on the experiment, fixed TMT 6-plex labeling on Lys and peptide N-termini (+229 Da), fixed iTRAQ 4-plex labeling on Lys and N-termini (+144 Da), variable phosphorylation on Ser, Thr and Tyr (+80 Da, allowing neutral loss of 98 Da), variable THZ1-DTB labeling of Cys (+993 Da, allowing neutral loss of 993 Da), variable JZ128-DTB labeling of Cys (+987 Da, allowing neutral loss of 987 Da). Reported peptide sequences were filtered based on a 1% FDR.

Phosphopeptide validation

Synthetic phosphopeptides were TMT labeled and desalted with batch mode C18 cleanup as above. They were then analyzed on a Q Exactive HF mass spectrometer using a 20 min organic gradient as described above. MS/MS spectra of Endogenous and synthetic phosphopeptides were annotated using mzStudio (Ficarro et al., 2017).

CITe-Id

HeLa S3 or PC3 cell pellets were lysed with NP-40 lysis buffer as above. After lysate clearance centrifugation, protein concentration was determined by BCA. Samples were precleared with streptavidin resin for 1 hr. at 4°C. After centrifugation, the supernatant was split in four and pretreated with DMSO or increasing concentrations of inhibitor (THZ1, THZ531, JZ128) and incubated at room-temperature for 1 hr. 2 μM of desthiobiotin-tagged analog (THZ1-DTB, THZ1-DTB, JZ128-DTB respectively) was added to all samples and incubated at 4°C for 18 h. Urea was added to 8 M final concentration followed by cleanup using Zeba™ desalting columns. Samples were diluted to 4 M urea with pH 8 lysis buffer and reduced with 10 mM DTT for 30 min at 56°C. Samples were then alkylated with 20 mM IAA for 30 min at RT. Samples were further diluted to 2 M urea before trypsin digestion at 37°C overnight. Streptavidin resin was added to the samples and incubated at RT for 1 h. The beads were sequentially washed with lysis buffer three times, PBS three times, and water two times. Peptides were eluted with four sequential incubations of 50% acetonitrile (MeCN), 0.1% trifluoroacetic acid (TFA) for 3 min at RT. Eluted peptides were concentrated by vacuum centrifugation and resuspended in 0.1% TFA before batch mode C18 cleanup as described previously (Adelmant GO). Samples were vacuum dried before iTRAQ labeling as described above. Peptides were cleaned using the SP3 paramagnetic bead methodology (Hughes et al., 2014). Briefly, dual-Speed Bead Carboxylate Beads (GE Healthcare)

were added to peptides reconstituted in 95% MeCN and allowed to bind for 10 min at RT. Beads were washed with MeCN before peptides eluted in 100 mM Ambic, 2% DMSO and vacuum dried. Samples were reconstituted in 5% DMSO, 100 mM ammonium formate for RP-SAX-RP LC-MS/MS as described above. LC gradients were 5%-60% B for 90 min. Data was processed as above with spectral processing to account for inhibitor-specific fragmentation pathways and searching with variable modifications to cysteine for the respective probe used in each experiment. Normalized reporter ion signal for labeled cysteine residues from multiple PSMs was summed and a ratio was generated for each reporter channel by comparing it to the DMSO-treated control channel. Inhibitor concentrations and ratios were used to generate a trendline for each labeled site with the slope being the competitive dose response for the cysteine site.

Targeted live cell PKN3 CITe-Id using TAP-MS

PC3 cells with CRISPR mediated gene depletion of PKN3 with rescue by FLAG-HA-PKN3 WT expression were treated with JZ128 for 3 hours. Cells were lysed and treated with 2 µM JZ128-DTB at 4°C overnight. Tandem affinity purification of PKN3 was performed as previously described (Adelmant et al., 2012; Rozenblatt-Rosen et al., 2012). Purified proteins were trypsin digested, iTRAQ labeled, and analyzed by LC-MS/MS as described for CITe-Id. Reporter signal for the JZ128-DTB modified C840-containing PKN3 peptide was normalized to total signal for unmodified PKN3 peptides in the experiment.

SILAC analysis of compound reactivity

Lysates were made of SILAC incorporated HeLa S3 cell pellets. Heavy incorporated lysates were treated with a single compound (e.g. THZ1) at 4°C overnight and light lysates similarly treated with DMSO. The two samples were pooled, trypsin digested, and cysteine peptides enriched

using activated thiol resin (GE Healthcare). After LC-MS/MS, each cysteine peptide was quantified based on its reactivity compared to DMSO control. A log-2 fold-change reactivity difference was then determined for cysteine peptides in common between each untagged and tagged compound-pair. Density histograms were plotted for both the entire set of cysteine sites as well as the subset of cysteine sites also detected as inhibitor-modified in the respective CITe-Id experiments for each compound-pair. Density histograms were generated using Prism.

Data Availability

All raw mass spectrometry data has been uploaded to MassIVE (*https://massive.ucsd.edu/)*.

PIN1 Project

Fluorescence Polarization Binding Assay

Binding affinity to Pin1 was determined using a fluorescence polarization assay to assess competition with an N-terminal fluorescein-labeled peptide (Bth-D-phos.Thr-Pip-Nal), which was synthesized by a peptide synthesis company. The indicated concentrations of candidate compound were pre-incubated for 12 hours at 4°C with a solution containing 250 nM glutathione *S*-transferase (GST)-Pin1, 5 nM of fluorescein-labeled peptide probe, 10 µg/ml bovine serum albumin, 0.01% Tween-20 and 1 mM DTT in a buffer of 10 mM HEPES, 10 mM NaCl and 1% glycerol (pH 7.4). Measurements of FP and FA were made in black 384-well plates (Corning) using an EnVision reader. K_i values obtained from the FP assay results were derived from the Kenakin K_i equation: Kenakin K_i = (Lb)(EC_{50})(K_d)/(Lo)(Ro) + Lb(Ro–Lo + Lb–K_d), where K_d [M]: K_d of the probe, EC_{50} [M]: obtained from FP assay, total tracer Lo [M]: probe concentration

in FP, bound tracer Lb [M]: 85% of probe concentration binds to target protein, total receptor Ro [M]: Pin1 concentration in the FP assay, as described (Sittampalam et al., 2004).

PPIase Isomerase Inhibition Assay

Inhibition of Pin1 isomerase activity was determined using the chymotrypsin-coupled PPIase assay, using GST-Pin1 and Suc-Ala-pSer-Pro-Phe-pNA peptide substrate (50 mM), as described previously (Yaffe et al., 1997). GST-Pin1 was pre-incubated with the indicated concentrations of compound for 12 hours at 4°C in buffer containing 35 mM HEPES (pH 7.8), 0.2 mM DTT, and 0.1 mg/mL BSA. Immediately before the assay was started, chymotrypsin (final concentration of 6 mg/mL), followed by the peptide substrate (Suc-Ala-pSer-Pro-Phe-pNA peptide substrate, final concentration 50 mM) was added. The K_i value obtained from the PPIase assay was derived from the Cheng–Prusoff equation, $K_i = IC_{50}/ (1 + S/K_m)$, where K_m is the Michaelis constant for the used substrate, S is the initial concentration of the substrate in the assay, and IC_{50} is the half-minimal inhibitory concentration of the inhibitor.

Covalent Labeling by Intact Mass Spectrometry

5 µg of purified Pin1 protein in 50 µL of 20 mM HEPES pH 7.5 and 75 mM NaCl was incubated with 5 µM of respective Pin1 inhibitors for 0-3 hr. A Shimadzu XR HPLC was used to inject the entire sample onto a self-packed reverse-phase column (1/32 in outer diameter × 500 µm inner diameter, 5 cm of POROS 50R2 resin). After desalting, protein was eluted with an HPLC gradient (0%–100% B in 4 min, A = 0.2 M acetic acid in water, B = 0.2 M acetic acid in acetonitrile, flow rate = 10 µl/min) into an LTQ XL mass spectrometer (Thermo Fisher Scientific, San Jose, CA, USA). LTQ XL MS spectra were acquired in centroid mode using the electron multipliers for ion

detection. Mass spectra were deconvoluted using MagTran1.03b2 software (Z. Zhang & Marshall, 1998).

Cell Culture and Reagents

All cell lines were purchased from American Type Cell Collection (ATCC). They were routinely tested for the absence of Mycoplasma infection. PATU-8988T, PATU-8902, and HEK293 cells were cultured in Dulbecco's modified Eagle's medium (DMEM) supplemented with 10% fetal bovine serum (FBS, Sigma) and 1% penicillin/streptomycin. NIH/3T3 cells were cultured in DMEM supplemented with 10% fetal calf serum (FCS, Vendor) and 1% penicillin/streptomycin. All cell lines were cultured at 37°C in a humidified chamber. Antibodies used against various proteins were as follows: Pin1 (1:1,000, Cell Signaling cat #3722), a-Tubulin (1:1000, Cell Signaling cat #3873S), phoshpo-cdc2 (Tyr15) (1:1000, Cell Signaling cat# 4539S), HA-Tag (1:1000, Cell Signaling cat# 3724S).

Establishment of Pin1 KO cell lines using CRISPR/Cas9

Pin1-targeting guides were annealed into the BbsI restriction site of the pX458 plasmid (Addgene cat# 48138). The gRNA sequence used was: CAGTGGTGGCAAAAACGGGC. Cells were transfected using the Neon Transfection System (Life Technologies) according to manufacturer guidelines, and GFP+ cells were sorted using fluorescence-activated cell sorting (FACS) using a J AriaII SORP UV machine (BD). Single cell clones were isolated from the bulk-sorted population using limiting dilution plating in a 96-well plate. Once clones were isolated, they were verified for Pin1 knockout by western blotting and by genomic DNA PCR using the following primers: forward: GAGCCTGTGGCACATGGTG, reverse: CAGGGTCAGGTCATGCACTG, sequencing: CTGGCTTCTGGCTGTG, and sequenced were analyzed using TiDe (https://tide.nki.nl/).

Generation of stable cell lines

The dox-inducible Pin1 construct was generated by using GATEWAY cloning to insert the Pin1 coding sequence from a pDONR221-Pin1 donor vector construct into the pCW57.1 plasmid (Addgene cat# 41393). To generate lentivirus, HEK293FT cells were co-transfected with the packaging vector, envelope, and various lentivirus-expressing constructs using Lipofectamine 2000 (Thermo Fisher cat# 11668027). The virus-containing supernatant was harvested and filtered. Cells were infected with virus supplemented with 8 μg/mL of polybrene, and stable cell lines were selected and maintained with 2 μg/mL puromycin beginning two days after infection.

Immunoblotting

Whole cell lysates for immunoblotting were prepared by pelleting cells from each cell line at 4°C (300 g) for 5 minutes. The resulting cell pellets were washed 1x with ice-cold 1x PBS and then resuspended in the indicated cell lysis buffer. Lysates were clarified at 14,000 rpm for 15 minutes at 4°C prior to quantification by BCA assay (Pierce, cat #23225). Whole cell lysates were loaded into Bolt 4-12% Bis-Tris Gels (Thermo Fisher, cat#NW04120BOX) and separated by electrophoreses at 95 V for 1.5 hours. The gels were transferred to a nitrocellulose membrane using the iBlot Gel Transfer at P3 for 6 minutes (Thermo Fisher, cat # IB23001) and then blocked for 1 hour at room temperature in Odyssey blocking buffer (LICOR Biosciences, cat# 927-50010). Membranes were probed using antibodies against the relevant proteins at 4°C overnight in 20% Odyssey Blocking Buffer in 1x TBST. Membranes were then washed three times with 1x TBST (at least 5 minutes per wash) followed by incubation with the IRDye goat anti-mouse (LICOR, cat # 926-32210) or goat anti-rabbit (LICOR, cat # 926-32211) secondary antibody (diluted 1:10,000) in 20% Odyssey Blocking Buffer in 1x TBST for 1 hour at room temperature. After three washes with

1x TBST (at least 5 minutes per wash), the immunoblots were visualized using the ODYSSEY Infrared Imaging System (LICOR).

Lysate Pull Down with BJP-DTB (desthiobiotin)

Cells were lysed in 50 mM Hepes, pH 7.4, 1 mM EDTA, 10% glycerol, 1 mM TCEP, 150 mM NaCl, 1 mM EDTA, 0.5% NP-40, and protease inhibitor tablet (Roche cat# 4693159001). After clarifying, lysates were incubated with the indicated concentration of BJP-DTB for 1 hour (unless noted otherwise) at 4°C, using 500 μg of protein per sample. Lysates were then incubated with streptavidin agarose resin (Thermo scientific, cat. #20349) for 1.5 hours at 4°C. Beads were washed four times with 500 μL of washing buffer (50 mM Hepes, pH7.5, 10 mM NaCl, 1 mM EDTA, 10 % glycerol), then pelleted by centrifugation and dried. The beads were boiled for 5 minutes at 95°C in 2x LDS + 10% β-mercaptoethanol. Proteins of interest were then assessed via western blotting.

Cellular Target Engagement – Competition with BJP-DTB (desthiobiotin)

PATU-8988T cells were plated in 10 cm plates with 2.5 million cells per plate in 6 mL of media. The day after plating, cells were treated with the indicated concentrations of candidate inhibitor for the indicated time points. The cells were then washed two times with cold PBS (1 mL per 10 cm plate) and collected by scraping with a cell scraper. Cells were lysed in 50 mM HEPES, pH 7.4, 1 mM EDTA, 10% glycerol, 1 mM TCEP, 150 mM NaCl, 1 mM EDTA, 0.5% NP-40, and protease inhibitor tablet (Roche) – using 210 μL of cell lysis buffer per 10 cm plate of cells. After clarifying, 5 μL of each lysate sample was combined with 5 μL of 2x LDS + 10% β-mercaptoethanol, boiled for 5 minutes, and set aside for the input loading control. Then, 200 μL of each lysate sample was

incubated with 1 µM of BJP-DTB for 1 hour at 4°C and processed as in the "lysate pull down with BJP-DTB" (above).

Pin1 Stability Assays

PATU-8988T cells were plated in 6 well plates at a density of 50,000 cells per well in 2 mL media. The day after plating, cells were treated with either DMSO, BJP-06-005-3, or BJP-R for 24 hours. The media was then aspirated and replaced with fresh media containing cycloheximide (100 µg/mL) to block new protein synthesis. Cells were harvested at the indicated time points by washing two times with ice-cold 1x PBS, and then lysing in the plate with 100 µL of RIPA lysis buffer per well (Sigma, cat# R0278) supplemented with protease and phosphatase inhibitor tablets (Roche cat#4906845001).

Cell Viability Assays: Growth Over Time in 2D-Adherent Monolayer Cell Culture

Cells were plated at a density of 100 cells per well in 100 µL media in a 96 well white clear bottom plate (Corning cat# 3903), with at least one plate per time point (Day 0, 2, 4, 6, 8). Cells were treated the day after plating with the indicated concentrations of DMSO, BJP-06-005-3, BJP-R, or dTAG13. Every 48 hours, the media was aspirated and replaced with fresh media, and the compounds or DMSO were retreated. When the indicated time points had been reached, cell viability was evaluated using the CellTiter-Glo Luminescent Cell Viability Assay (Promega cat# G7570) according to the manufacturer's standards.

Inhibitor Effects on Pin1 Downstream Signaling and Pin1 Degradation

Cells were plated in 6 well plates at a density of 100,000 cells per well in 2 mL media. The day after plating, cells were treated with DMSO or the indicated concentrations of BJP-06-005-3, BJP-R, or dTAG13. Cells were harvested at the indicated time points by washing two times with ice-

cold 1x PBS, and then lysing in the plate with 100 µL of RIPA lysis buffer per well (Sigma, cat# R0278) supplemented with protease and phosphatase inhibitor tablets (Roche cat#4906845001).

Ultra-Low Adherent (ULA) GILA Assay

Cells were plated in clear, round bottom 96 well plates (Corning cat# 07201680) at a density of 1,000 cells per well in 100 µL media. After plating, cells were spun at 300 g for 5 minutes to encourage spheroid formation. The day after plating, cells were treated with DMSO, or the indicated concentrations of BJP-06-005-3, BJP-R, dTAG13, or Dox. 48 hours after the initial treatment, cells were re-treated with the indicated concentrations of BJP-06-005-3, BJP-R, dTAG13, or Dox. 96 hours after the initial treatment, cell viability was evaluated using CellTiter-Glo (Promega cat# G7570). To normalize for differences in plating density between cell lines, a duplicate Day 0 plate of cells was plated at the beginning of the experiment and exposed using CellTiter-Glo (Promega cat# G7570) the day after plating. The final absorbance was then divided by the average zero timepoint reading for each cell line to normalize for starting cell numbers. For direct comparisons to growth in 2D-adherent monolayer cell culture, plating conditions and treatments were performed identically as described for the GILA assay, but cells were plated in flat bottom 96 well plates (Corning cat# 3903) instead of round bottom plates.

Protein expression and purification

A construct of full-length human PIN1 in a pET28 vector was overexpressed in E. coli BL21 (DE3) in LB medium in the presence of 50 mg/ml of kanamycin. Cells were grown at 37°C to an OD of 0.8, cooled to 17°C, induced with 500 µM isopropyl-1-thio-D-galactopyranoside, incubated overnight at 17°C, collected by centrifugation, and stored at -80°C. Cell pellets were sonicated in buffer A (50 mM HEPES 7.5, 300 mM NaCl, 10% glycerol, 10 mM Imidazole, and 3 mM BME) and

the resulting lysate was centrifuged at 30,000 xg for 40 min. Ni-NTA beads (Qiagen) were mixed with lysate supernatant for 30 min and washed with buffer A. Beads were transferred to an FPLC-compatible column and the bound protein was washed with 15% buffer B (50 mM hepes 7.5, 300 mM NaCl, 10% glycerol, 300 mM Imidazole, and 3 mM BME) and eluted with 100% buffer B. Thrombin was added to the eluted protein and incubated at 4°C overnight. The sample was concentrated and passed through a Superdex 200 10/300 column (GE helathcare) in a buffer containing 20 mM hepes7.5, 150 mM NaCl, 5% glycerol, 3mM DTT, and 1mM TCEP. Fractions were pooled, concentrated to approximately 37 mg/ml and frozen at -80°C.

Crystallization: BJP-02-118-2

Apo protein at a final concentration of 1mM was crystallized by sitting-drop (200nL+200nL) vapor diffusion at 20°C in the following crystallization buffer: 3M NH4SO4, 100mM BisTris-pH7.0, 1% PEG400, and 1mM DTT. A volume of 200nL of 1mM BJP-02-118-2 was added directly to crystals for soaking at 20°C for 16hrs. Crystals were transferred briefly into crystallization buffer containing 25% glycerol prior to flash-freezing in liquid nitrogen.

Crystallization: BJP-07-017-3

Apo protein at a final concentration of 1mM was crystallized by sitting-drop (200nL+200nL) vapor diffusion at 20°C in the following crystallization buffer: 3M NH4SO4, 100mM BisTris-pH7.0, 1% PEG400, and 1mM DTT. A volume of 1ul of 100mM BJP-07-017-3 was mixed with 25ul mother liquor, and 2ul of that solution was added to crystal drops. Crystallization wells were resealed, plates were incubated at 20dc for 2hrs, and crystals were cryoprotected/harvested as usual.

Crystallization: Data collection and structure determination

Diffraction data from complex crystals were collected at beamline 24ID-C/E of the NE-CAT at the Advanced Photon Source at the Argonne National Laboratory. Data sets were integrated and scaled using XDS (Kabsch, 2010). Structures were solved by molecular replacement using the program Phaser (McCoy et al., 2007) and the search model PDB entry 1PIN. Iterative manual model building and refinement using Phenix (P. D. Adams et al., 2010) and Coot (Emsley & Cowtan, 2004) led to models with excellent statistics.

CiTe-ID Selectivity Assessment

HEK 293 cell pellets were lysed with NP-40 lysis buffer (50 mM Tris pH 7.5, 150 mM NaCl, 1 mM EDTA, 10% v/v glycerol, 0.5% v/v NP-40, protease inhibitors). After lysate clearance centrifugation, protein concentration was determined by BCA. Samples were precleared with avidin resin for 1 hr. at 4°C. After centrifugation, the supernatant was split in four and pretreated with DMSO or increasing concentrations of BJP-06-005-3 (100 nM, 1 µM, 2.5 µM) and incubated at room-temperature for 3 hr. 2 µM of the desthiobiotin-tagged analog (BJP-05-171-3) was added to all samples and incubated at 4°C for 18 h. Urea was added to 8 M final concentration followed by cleanup using Zeba™ desalting columns. Samples were diluted to 4 M urea with pH 8 lysis buffer and reduced with 10 mM DTT for 30 min at 56°C. Samples were then alkylated with 20 mM IAA for 30 min at RT. Samples were further diluted to 2 M urea before trypsin digestion at 37°C overnight. Avidin resin was added to the samples and incubated at RT for 1 h. The beads were sequentially washed with lysis buffer three times, PBS three times, and water two times. Peptides were eluted with four sequential incubations of 50% acetonitrile (MeCN), 0.1% trifluoroacetic acid (TFA) for 3 min at RT. Eluted peptides were concentrated by vacuum centrifugation and resuspended in 0.1% TFA before batch mode C18 cleanup, as described

previously (Adelmant GO). Samples were vacuum dried and resuspended in 30% 0.5M TEAB, 70% EtOH. iTRAQ stable isotope labeling reagent was added to each corresponding sample. After incubation at room temperature for 1 hr, the samples were combined and acidified before vacuum drying. Samples were reconstituted in 0.1% TFA and desalted using a SOLA desalting plate before vacuum drying. Samples were reconstituted in 25% MeCN, 0.1% TFA and batch mode SCX cleaned, as described previously (Adelmant GO). Samples were vacuum dried and reconstituted in 5% DMSO, 100 mM ammonium formate for 3D RP-SAX-RP LC-MS/MS (F. Zhou et al., 2013). Peptides were separated across eleven fractions using a 90 min 5%-60% MeCN gradient on a Q-Exactive HF mass spectrometer. For data processing, Native .RAW data files from the mass spectrometer were processed using the multiplierz Python-based framework (Parikh et al., 2009) to generate .mgf files for input to Mascot (Matrix Science). MS/MS spectra were processed to remove peaks corresponding to inhibitor fragmentation, as described previously (Ficarro et al., 2016). The following inhibitor fragment ion associated m/z values were removed from each spectrum: 110.07, 134.096, 140.07, 147.11, 159.09, 170.06, 197.127, 199.07, 208.08, 234.06, 236.074, 266.19, 280.202, 284.14, 297.23, 315.18, 325.22, 342.25, 344.17, 353.22, 412.233, 438.21, 439.3, 447.27, 455.24, 456.33, 464.3, 465.28, 472.27, 482.307, 499.334, 607.37, 625.38, 642.407, 651.361, 668.389, 685.413, 718.44, 736.45, 753.476, 762.43, 779.456, 796.482. Peptide precursor masses were recalibrated on a per-scan basis by correcting all m/z values based on accurate mass recorded for the $Si(CH_3)_2O_6$ peak in each spectrum. All data was searched against a forward-reverse human database assembled from the NCBI Refseq database. For de-isotoped HCD spectra, the precursor mass tolerance was set to 10 ppm and the MS/MS fragment ion tolerance was set to 25 mmu. Search parameters included trypsin specificity, with a

maximum of two missed cleavages, fixed carbamidomethylation of Cys (+57 Da), variable oxidation on Met (+16 Da with -64 Da neutral loss possible), variable deamidation on Asn and Gln (+1 Da), fixed iTRAQ 4-plex labeling on Lys and N-termini (+144 Da), variable BJP-05-171-3 labeling of Cys (+997 Da, with -997 Da neutral loss possible). Reported peptide sequences were filtered based on a 1% false discovery rate. Normalized reporter ion signal for labeled cysteine residues from multiple PSMs was summed and a ratio was generated for each reporter channel by comparing it to the DMSO-treated control channel. Inhibitor concentrations and ratios were used to generate a trendline for each labeled site with the slope being the competitive dose response for the cysteine site.

Yeast experiments

To test complementation of yeast Ess1, strain YSB1026 was transformed with HIS3-marked plasmids expressing yeast Ess1, human Pin1, the FKBP-Pin1 fusion, or the non-expressing HIS3 vector. Transformants were grown at 30˚C overnight in synthetic complete media lacking histidine. After normalizing cell density to ensure that equal numbers of cells were spotted, four-fold serial dilutions were spotted onto the appropriate selective plates. Plates containing 5-fluoro-orotic acid (5FOA) were used to select against pRS426-Pin1, carrying the wild-type Pin1 on a URA3 plasmid. Plates were incubated for three days at 30˚C. Although only one set is shown, four biological replicates gave the identical results. To ensure that the FKBP-Pin1 fusion protein was expressed and intact, whole cell extracts were made by glass bead lysis. Fifty micrograms of protein from each strain was separate by standard SDS-PAGE, blotted to nitrocellulose membrane, and probed with antibodies against Pin1.

Yeast strains:

YXW-3: MATa, ura3-1, leu2-3,112, trp1-1, his3-11,15, ade2-1, can1-100, ess1Δ::TRP1 (pRS413-Ess1)

YSB1026: MATa, ura3-1, leu2-3,112, trp1-1, his3-11,15, ade2-1, can1-100, ess1Δ::TRP1 (pRS426-Pin1)

Plasmids:

pTPI-Pin1

pTPI-FKBP^{F36V}-Pin1

pRS413-Ess1

pRS426-Ess1

References

Abo, M., & Weerapana, E. (2015). A Caged Electrophilic Probe for Global Analysis of Cysteine Reactivity in Living Cells. *J Am Chem Soc, 137*(22), 7087-7090. doi:10.1021/jacs.5b04350

Adams, P. D., Afonine, P. V., Bunkoczi, G., Chen, V. B., Davis, I. W., Echols, N., . . . Zwart, P. H. (2010). PHENIX: a comprehensive Python-based system for macromolecular structure solution. *Acta Crystallogr D Biol Crystallogr, 66*(Pt 2), 213-221. doi:10.1107/S0907444909052925

Adams, S., Valchanova, R. S., & Munz, B. (2010). RIP2: a novel player in the regulation of keratinocyte proliferation and cutaneous wound repair? *Exp Cell Res, 316*(5), 728-736. doi:10.1016/j.yexcr.2009.12.001

Adelmant, G., Calkins, A. S., Garg, B. K., Card, J. D., Askenazi, M., Miron, A., . . . Lazaro, J. B. (2012). DNA ends alter the molecular composition and localization of Ku multicomponent complexes. *Mol Cell Proteomics, 11*(8), 411-421. doi:10.1074/mcp.M111.013581

Adelmant GO, C. J., Ficarro SB, Sikorski TW, Zhang Y, Marto JA. Affinity and Chemical Enrichment for Mass Spectrometry-Based Proteomics Analyses. In L. A. Ivanov AR (Ed.), *Sample Preparation in Biological Mass Spectrometry*. New York: Springer.

Aleku, M., Schulz, P., Keil, O., Santel, A., Schaeper, U., Dieckhoff, B., . . . Kaufmann, J. (2008). Atu027, a liposomal small interfering RNA formulation targeting protein kinase N3, inhibits cancer progression. *Cancer Res, 68*(23), 9788-9798. doi:10.1158/0008-5472.CAN-08-2428

Alexander, W. M., Ficarro, S. B., Adelmant, G., & Marto, J. A. (2017). multiplierz v2.0: A Python-based ecosystem for shared access and analysis of native mass spectrometry data. *Proteomics, 17*(15-16). doi:10.1002/pmic.201700091

Ali, F., Hindley, C., McDowell, G., Deibler, R., Jones, A., Kirschner, M., . . . Philpott, A. (2011). Cell cycle-regulated multi-site phosphorylation of Neurogenin 2 coordinates cell cycling with differentiation during neurogenesis. *Development, 138*(19), 4267-4277. doi:10.1242/dev.067900

Anderson, J. C., Willey, C. D., Mehta, A., Welaya, K., Chen, D., Duarte, C. W., . . . Sonpavde, G. (2015). High Throughput Kinomic Profiling of Human Clear Cell Renal Cell Carcinoma Identifies Kinase Activity Dependent Molecular Subtypes. *PLoS One, 10*(9), e0139267. doi:10.1371/journal.pone.0139267

Andreeff, M., Stone, R., Michaeli, J., Young, C. W., Tong, W. P., Sogoloff, H., . . . Marks, P. A. (1992). Hexamethylene bisacetamide in myelodysplastic syndrome and acute myelogenous leukemia: a phase II clinical trial with a differentiation-inducing agent. *Blood, 80*(10), 2604-2609.

Ang, X. L., & Harper, J. W. (2004). Interwoven ubiquitination oscillators and control of cell cycle transitions. *Sci STKE, 2004*(242), pe31. doi:10.1126/stke.2422004pe31

Asghar, U., Witkiewicz, A. K., Turner, N. C., & Knudsen, E. S. (2015). The history and future of targeting cyclin-dependent kinases in cancer therapy. *Nat Rev Drug Discov, 14*(2), 130-146. doi:10.1038/nrd4504

Ashburner, M., Ball, C. A., Blake, J. A., Botstein, D., Butler, H., Cherry, J. M., . . . Sherlock, G. (2000). Gene ontology: tool for the unification of biology. The Gene Ontology Consortium. *Nat Genet, 25*(1), 25-29. doi:10.1038/75556

Askenazi, M., Parikh, J. R., & Marto, J. A. (2009). mzAPI: a new strategy for efficiently sharing mass spectrometry data. *Nat Methods, 6*(4), 240-241. doi:10.1038/nmeth0409-240

Avendaño, C., & Menéndez, J. C. (2008). Drugs That Inhibit Signalling Pathways for Tumor Cell Growth and Proliferation *Medicinal Chemistry of Anticancer Drugs* (pp. 251-305). Amsterdam: Elsevier.

Backus, K. M., Correia, B. E., Lum, K. M., Forli, S., Horning, B. D., Gonzalez-Paez, G. E., . . . Cravatt, B. F. (2016). Proteome-wide covalent ligand discovery in native biological systems. *Nature, 534*(7608), 570-574. doi:10.1038/nature18002

Bak, D. W., Pizzagalli, M. D., & Weerapana, E. (2017). Identifying Functional Cysteine Residues in the Mitochondria. *ACS Chem Biol, 12*(4), 947-957. doi:10.1021/acschembio.6b01074

Bar-Peled, L., Kemper, E. K., Suciu, R. M., Vinogradova, E. V., Backus, K. M., Horning, B. D., . . . Cravatt, B. F. (2017). Chemical Proteomics Identifies Druggable Vulnerabilities in a Genetically Defined Cancer. *Cell, 171*(3), 696-709 e623. doi:10.1016/j.cell.2017.08.051

Bauer, R. A. (2015). Covalent inhibitors in drug discovery: from accidental discoveries to avoided liabilities and designed therapies. *Drug Discov Today, 20*(9), 1061-1073. doi:10.1016/j.drudis.2015.05.005

Berriz, G. F., Beaver, J. E., Cenik, C., Tasan, M., & Roth, F. P. (2009). Next generation software for functional trend analysis. *Bioinformatics, 25*(22), 3043-3044. doi:10.1093/bioinformatics/btp498

Bhullar, K. S., Lagaron, N. O., McGowan, E. M., Parmar, I., Jha, A., Hubbard, B. P., & Rupasinghe, H. P. V. (2018). Kinase-targeted cancer therapies: progress, challenges and future directions. *Mol Cancer, 17*(1), 48. doi:10.1186/s12943-018-0804-2

Bishop, A. C., Kung, C.-y., Shah, K., Witucki, L., Shokat, K. M., & Liu, Y. (1999). Generation of Monospecific Nanomolar Tyrosine Kinase Inhibitors via a Chemical Genetic Approach. *Journal of the American Chemical Society, 121*(4), 627-631. doi:10.1021/ja983267v

Bishop, A. C., Ubersax, J. A., Petsch, D. T., Matheos, D. P., Gray, N. S., Blethrow, J., . . . Shokat, K. M. (2000). A chemical switch for inhibitor-sensitive alleles of any protein kinase. *Nature, 407*(6802), 395-401. doi:10.1038/35030148

Blagg, J., & Workman, P. (2017). Choose and Use Your Chemical Probe Wisely to Explore Cancer Biology. *Cancer Cell, 32*(1), 9-25. doi:10.1016/j.ccell.2017.06.005

Blewett, M. M., Xie, J., Zaro, B. W., Backus, K. M., Altman, A., Teijaro, J. R., & Cravatt, B. F. (2016). Chemical proteomic map of dimethyl fumarate-sensitive cysteines in primary human T cells. *Sci Signal, 9*(445), rs10. doi:10.1126/scisignal.aaf7694

Bosken, C. A., Farnung, L., Hintermair, C., Merzel Schachter, M., Vogel-Bachmayr, K., Blazek, D., . . . Geyer, M. (2014). The structure and substrate specificity of human Cdk12/Cyclin K. *Nat Commun, 5*, 3505. doi:10.1038/ncomms4505

Breitwieser, F. P., Muller, A., Dayon, L., Kocher, T., Hainard, A., Pichler, P., . . . Colinge, J. (2011). General statistical modeling of data from protein relative expression isobaric tags. *J Proteome Res, 10*(6), 2758-2766. doi:10.1021/pr1012784

Brinkman, E. K., Chen, T., Amendola, M., & van Steensel, B. (2014). Easy quantitative assessment of genome editing by sequence trace decomposition. *Nucleic Acids Res, 42*(22), e168. doi:10.1093/nar/gku936

Buratowski, S. (2003). The CTD code. *Nat Struct Biol, 10*(9), 679-680. doi:10.1038/nsb0903-679

Campaner, E., Rustighi, A., Zannini, A., Cristiani, A., Piazza, S., Ciani, Y., . . . Del Sal, G. (2017). A covalent PIN1 inhibitor selectively targets cancer cells by a dual mechanism of action. *Nat Commun, 8*, 15772. doi:10.1038/ncomms15772

Castagna, M., Takai, Y., Kaibuchi, K., Sano, K., Kikkawa, U., & Nishizuka, Y. (1982). Direct activation of calcium-activated, phospholipid-dependent protein kinase by tumor-promoting phorbol esters. *J Biol Chem, 257*(13), 7847-7851.

Cerami, E., Gao, J., Dogrusoz, U., Gross, B. E., Sumer, S. O., Aksoy, B. A., . . . Schultz, N. (2012). The cBio cancer genomics portal: an open platform for exploring multidimensional cancer genomics data. *Cancer Discov, 2*(5), 401-404. doi:10.1158/2159-8290.CD-12-0095

Chaikuad, A., Koch, P., Laufer, S. A., & Knapp, S. (2018). The Cysteinome of Protein Kinases as a Target in Drug Development. *Angew Chem Int Ed Engl, 57*(16), 4372-4385. doi:10.1002/anie.201707875

Chao, S. H., Greenleaf, A. L., & Price, D. H. (2001). Juglone, an inhibitor of the peptidyl-prolyl isomerase Pin1, also directly blocks transcription. *Nucleic Acids Res, 29*(3), 767-773.

Chen, C. H., Li, W., Sultana, R., You, M. H., Kondo, A., Shahpasand, K., . . . Lu, K. P. (2015). Pin1 cysteine-113 oxidation inhibits its catalytic activity and cellular function in Alzheimer's disease. *Neurobiol Dis, 76*, 13-23. doi:10.1016/j.nbd.2014.12.027

Chen, M., Mao, A., Xu, M., Weng, Q., Mao, J., & Ji, J. (2019). CRISPR-Cas9 for cancer therapy: Opportunities and challenges. *Cancer Lett, 447*, 48-55. doi:10.1016/j.canlet.2019.01.017

Cheng, C. W., & Tse, E. (2018). PIN1 in Cell Cycle Control and Cancer. *Front Pharmacol, 9*, 1367. doi:10.3389/fphar.2018.01367

Cingöz, O., & Goff, S. P. (2018). Cyclin-dependent kinase activity is required for type I interferon production. *Proceedings of the National Academy of Sciences, 115*(13), E2950-E2959. doi:10.1073/pnas.1720431115

Clackson, T., Yang, W., Rozamus, L. W., Hatada, M., Amara, J. F., Rollins, C. T., . . . Holt, D. A. (1998). Redesigning an FKBP-ligand interface to generate chemical dimerizers with novel specificity. *Proc Natl Acad Sci U S A, 95*(18), 10437-10442. doi:10.1073/pnas.95.18.10437

Cohen, P. (2002). Protein kinases--the major drug targets of the twenty-first century? *Nat Rev Drug Discov, 1*(4), 309-315. doi:10.1038/nrd773

Coqueret, O. (2002). Linking cyclins to transcriptional control. *Gene, 299*(1-2), 35-55.

Dai, J., Xu, L., Hu, X., Han, G., Jiang, H., Sun, H., . . . Tang, X. (2018). Long noncoding RNA OIP5-AS1 accelerates CDK14 expression to promote osteosarcoma tumorigenesis via targeting miR-223. *Biomed Pharmacother, 106*, 1441-1447. doi:10.1016/j.biopha.2018.07.109

Davidson, G., & Niehrs, C. (2010). Emerging links between CDK cell cycle regulators and Wnt signaling. *Trends Cell Biol, 20*(8), 453-460. doi:10.1016/j.tcb.2010.05.002

Davidson, G., Shen, J., Huang, Y. L., Su, Y., Karaulanov, E., Bartscherer, K., . . . Niehrs, C. (2009). Cell cycle control of wnt receptor activation. *Dev Cell, 17*(6), 788-799. doi:10.1016/j.devcel.2009.11.006

Davis, M. I., Hunt, J. P., Herrgard, S., Ciceri, P., Wodicka, L. M., Pallares, G., . . . Zarrinkar, P. P. (2011). Comprehensive analysis of kinase inhibitor selectivity. *Nat Biotechnol, 29*(11), 1046-1051. doi:10.1038/nbt.1990

Deng, J., Wang, E. S., Jenkins, R. W., Li, S., Dries, R., Yates, K., . . . Wong, K. K. (2018). CDK4/6 Inhibition Augments Antitumor Immunity by Enhancing T-cell Activation. *Cancer Discov, 8*(2), 216-233. doi:10.1158/2159-8290.CD-17-0915

Deng, X., Weerapana, E., Ulanovskaya, O., Sun, F., Liang, H., Ji, Q., . . . He, C. (2013). Proteome-wide quantification and characterization of oxidation-sensitive cysteines in pathogenic bacteria. *Cell Host Microbe, 13*(3), 358-370. doi:10.1016/j.chom.2013.02.004

Dimova, D., & Bajorath, J. (2017). Assessing Scaffold Diversity of Kinase Inhibitors Using Alternative Scaffold Concepts and Estimating the Scaffold Hopping Potential for Different Kinases. *Molecules, 22*(5). doi:10.3390/molecules22050730

Dong, L., Marakovits, J., Hou, X., Guo, C., Greasley, S., Dagostino, E., . . . Murray, B. W. (2010). Structure-based design of novel human Pin1 inhibitors (II). *Bioorg Med Chem Lett, 20*(7), 2210-2214. doi:10.1016/j.bmcl.2010.02.033

Du, B., Zhang, P., Tan, Z., & Xu, J. (2017). MiR-1202 suppresses hepatocellular carcinoma cells migration and invasion by targeting cyclin dependent kinase 14. *Biomed Pharmacother, 96*, 1246-1252. doi:10.1016/j.biopha.2017.11.090

Dungo, R. T., & Keating, G. M. (2013). Afatinib: first global approval. *Drugs, 73*(13), 1503-1515. doi:10.1007/s40265-013-0111-6

Duong-Ly, K. C., & Peterson, J. R. (2013). The human kinome and kinase inhibition. *Curr Protoc Pharmacol, Chapter 2*, Unit2 9. doi:10.1002/0471141755.ph0209s60

Eckerdt, F., Yuan, J., Saxena, K., Martin, B., Kappel, S., Lindenau, C., . . . Strebhardt, K. (2005). Polo-like kinase 1-mediated phosphorylation stabilizes Pin1 by inhibiting its ubiquitination in human cells. *J Biol Chem, 280*(44), 36575-36583. doi:10.1074/jbc.M504548200

Edwards, A. M., Isserlin, R., Bader, G. D., Frye, S. V., Willson, T. M., & Yu, F. H. (2011). Too many roads not taken. *Nature, 470*(7333), 163-165. doi:10.1038/470163a

Emsley, P., & Cowtan, K. (2004). Coot: model-building tools for molecular graphics. *Acta Crystallogr D Biol Crystallogr, 60*(Pt 12 Pt 1), 2126-2132. doi:10.1107/S0907444904019158

Engel, B. E., Cress, W. D., & Santiago-Cardona, P. G. (2015). The Retinoblastoma Protein: A Master Tumor Suppressor Acts as a Link between Cell Cycle and Cell Adhesion. *Cell Health Cytoskelet, 7*, 1-10. doi:10.2147/CHC.S28079

Erb, M. A., Scott, T. G., Li, B. E., Xie, H., Paulk, J., Seo, H. S., . . . Bradner, J. E. (2017). Transcription control by the ENL YEATS domain in acute leukaemia. *Nature, 543*(7644), 270-274. doi:10.1038/nature21688

Espinoza, I., & Miele, L. (2013). Deadly crosstalk: Notch signaling at the intersection of EMT and cancer stem cells. *Cancer Lett, 341*(1), 41-45. doi:10.1016/j.canlet.2013.08.027

Evans, T., Rosenthal, E. T., Youngblom, J., Distel, D., & Hunt, T. (1983). Cyclin: a protein specified by maternal mRNA in sea urchin eggs that is destroyed at each cleavage division. *Cell, 33*(2), 389-396.

Fabregat, A., Jupe, S., Matthews, L., Sidiropoulos, K., Gillespie, M., Garapati, P., . . . D'Eustachio, P. (2018). The Reactome Pathway Knowledgebase. *Nucleic Acids Res, 46*(D1), D649-D655. doi:10.1093/nar/gkx1132

Falk, M. D., Liu, W., Bolanos, B., Unsal-Kacmaz, K., Klippel, A., Grant, S., . . . Timofeevski, S. (2014). Enzyme kinetics and distinct modulation of the protein kinase N family of kinases by lipid activators and small molecule inhibitors. *Biosci Rep, 34*(2). doi:10.1042/BSR20140010

Fan, S., Zhao, C., Zhang, L., Dai, S., Ren, J., Zhang, X., . . . Tao, T. (2015). Knockdown of PFTK1 Inhibits the Migration of Glioma Cells. *J Mol Neurosci, 57*(2), 257-264. doi:10.1007/s12031-015-0600-z

Farrell, A. S., Pelz, C., Wang, X., Daniel, C. J., Wang, Z., Su, Y., . . . Sears, R. C. (2013). Pin1 regulates the dynamics of c-Myc DNA binding to facilitate target gene regulation and oncogenesis. *Mol Cell Biol, 33*(15), 2930-2949. doi:10.1128/MCB.01455-12

Fedorov, O., Muller, S., & Knapp, S. (2010). The (un)targeted cancer kinome. *Nat Chem Biol, 6*(3), 166-169. doi:10.1038/nchembio.297

Ferguson, F. M., & Gray, N. S. (2018). Kinase inhibitors: the road ahead. *Nat Rev Drug Discov, 17*(5), 353-377. doi:10.1038/nrd.2018.21

Ficarro, S. B., Alexander, W. M., & Marto, J. A. (2017). mzStudio: A Dynamic Digital Canvas for User-Driven Interrogation of Mass Spectrometry Data. *Proteomes, 5*(3). doi:10.3390/proteomes5030020

Ficarro, S. B., Browne, C. M., Card, J. D., Alexander, W. M., Zhang, T., Park, E., . . . Marto, J. A. (2016). Leveraging Gas-Phase Fragmentation Pathways for Improved Identification and Selective Detection of Targets Modified by Covalent Probes. *Anal Chem, 88*(24), 12248-12254. doi:10.1021/acs.analchem.6b03394

Ficarro, S. B., Zhang, Y., Carrasco-Alfonso, M. J., Garg, B., Adelmant, G., Webber, J. T., . . . Marto, J. A. (2011). Online nanoflow multidimensional fractionation for high efficiency phosphopeptide analysis. *Mol Cell Proteomics, 10*(11), O111 011064. doi:10.1074/mcp.O111.011064

Finn, R. S., Dering, J., Conklin, D., Kalous, O., Cohen, D. J., Desai, A. J., . . . Slamon, D. J. (2009). PD 0332991, a selective cyclin D kinase 4/6 inhibitor, preferentially inhibits proliferation of luminal estrogen receptor-positive human breast cancer cell lines in vitro. *Breast Cancer Res, 11*(5), R77. doi:10.1186/bcr2419

Fischer, P. M., & Lane, D. P. (2000). Inhibitors of cyclin-dependent kinases as anti-cancer therapeutics. *Current medicinal chemistry, 7*(12), 1213-1245.

Fleuren, E. D., Zhang, L., Wu, J., & Daly, R. J. (2016). The kinome 'at large' in cancer. *Nat Rev Cancer, 16*(2), 83-98. doi:10.1038/nrc.2015.18

Fruman, D. A., Meyers, R. E., & Cantley, L. C. (1998). Phosphoinositide kinases. *Annu Rev Biochem, 67*(1), 481-507. doi:10.1146/annurev.biochem.67.1.481

Fry, D. W., Bridges, A. J., Denny, W. A., Doherty, A., Greis, K. D., Hicks, J. L., . . . Dobrusin, E. M. (1998). Specific, irreversible inactivation of the epidermal growth factor receptor and erbB2, by a new class of tyrosine kinase inhibitor. *Proc Natl Acad Sci U S A, 95*(20), 12022-12027.

Galbraith, M. D., Bender, H., & Espinosa, J. M. (2019). Therapeutic targeting of transcriptional cyclin-dependent kinases. *Transcription, 10*(2), 118-136. doi:10.1080/21541264.2018.1539615

Gallivan, J. P., & Dougherty, D. A. (1999). Cation-pi interactions in structural biology. *Proc Natl Acad Sci U S A, 96*(17), 9459-9464.

Gao, J., Aksoy, B. A., Dogrusoz, U., Dresdner, G., Gross, B., Sumer, S. O., . . . Schultz, N. (2013). Integrative analysis of complex cancer genomics and clinical profiles using the cBioPortal. *Sci Signal, 6*(269), pl1. doi:10.1126/scisignal.2004088

Garbaccio, R. M., & Parmee, E. R. (2016). The Impact of Chemical Probes in Drug Discovery: A Pharmaceutical Industry Perspective. *Cell Chem Biol, 23*(1), 10-17. doi:10.1016/j.chembiol.2015.11.011

Glotzer, M. (1995). Cell cycle. The only way out of mitosis. *Curr Biol, 5*(9), 970-972.

Goel, S., DeCristo, M. J., Watt, A. C., BrinJones, H., Sceneay, J., Li, B. B., . . . Zhao, J. J. (2017). CDK4/6 inhibition triggers anti-tumour immunity. *Nature, 548*(7668), 471-475. doi:10.1038/nature23465

Gopinathan, L., Ratnacaram, C. K., & Kaldis, P. (2011). Established and novel Cdk/cyclin complexes regulating the cell cycle and development. *Results Probl Cell Differ, 53*, 365-389. doi:10.1007/978-3-642-19065-0_16

Gu, X., Wang, Y., Wang, H., Ni, Q., Zhang, C., Zhu, J., . . . Yang, S. (2015). Upregulated PFTK1 promotes tumor cell proliferation, migration, and invasion in breast cancer. *Med Oncol, 32*(7), 195. doi:10.1007/s12032-015-0641-8

Gu, Z., Hou, Z., Zheng, L., Wang, X., Wu, L., & Zhang, C. (2018). Long noncoding RNA LINC00858 promotes osteosarcoma through regulating miR-139-CDK14 axis. *Biochem Biophys Res Commun, 503*(2), 1134-1140. doi:10.1016/j.bbrc.2018.06.131

Gujral, T. S., Peshkin, L., & Kirschner, M. W. (2014). Exploiting polypharmacology for drug target deconvolution. *Proc Natl Acad Sci U S A, 111*(13), 5048-5053. doi:10.1073/pnas.1403080111

Guo, C., Hou, X., Dong, L., Marakovits, J., Greasley, S., Dagostino, E., . . . Murray, B. W. (2014). Structure-based design of novel human Pin1 inhibitors (III): optimizing affinity beyond the phosphate recognition pocket. *Bioorg Med Chem Lett, 24*(17), 4187-4191. doi:10.1016/j.bmcl.2014.07.044

Hanahan, D., & Weinberg, R. A. (2000). The hallmarks of cancer. *Cell, 100*(1), 57-70.

Hanahan, D., & Weinberg, R. A. (2011). Hallmarks of cancer: the next generation. *Cell, 144*(5), 646-674. doi:10.1016/j.cell.2011.02.013

Hanes, S. D. (2014). The Ess1 prolyl isomerase: traffic cop of the RNA polymerase II transcription cycle. *Biochim Biophys Acta, 1839*(4), 316-333. doi:10.1016/j.bbagrm.2014.02.001

Haugsten, E. M., Oppelt, A., & Wesche, J. (2013). Phosphatidylinositol 5-phosphate is a second messenger important for cell migration. *Commun Integr Biol, 6*(5), e25446. doi:10.4161/cib.25446

Helander, S., Montecchio, M., Pilstal, R., Su, Y., Kuruvilla, J., Elven, M., . . . Sunnerhagen, M. (2015). Pre-Anchoring of Pin1 to Unphosphorylated c-Myc in a Fuzzy Complex Regulates c-Myc Activity. *Structure, 23*(12), 2267-2279. doi:10.1016/j.str.2015.10.010

Hennig, L., Christner, C., Kipping, M., Schelbert, B., Rucknagel, K. P., Grabley, S., . . . Fischer, G. (1998). Selective inactivation of parvulin-like peptidyl-prolyl cis/trans isomerases by juglone. *Biochemistry, 37*(17), 5953-5960. doi:10.1021/bi973162p

Hidaka, H., Inagaki, M., Kawamoto, S., & Sasaki, Y. (2002). Isoquinolinesulfonamides, novel and potent inhibitors of cyclic nucleotide-dependent protein kinase and protein kinase C. *Biochemistry, 23*(21), 5036-5041. doi:10.1021/bi00316a032

Hopkins, A. L., & Groom, C. R. (2002). The druggable genome. *Nat Rev Drug Discov, 1*(9), 727-730. doi:10.1038/nrd892

Hopkins, A. L., Keseru, G. M., Leeson, P. D., Rees, D. C., & Reynolds, C. H. (2014). The role of ligand efficiency metrics in drug discovery. *Nat Rev Drug Discov, 13*(2), 105-121. doi:10.1038/nrd4163

Huang, H. T., Seo, H. S., Zhang, T., Wang, Y., Jiang, B., Li, Q., . . . Gray, N. S. (2017). MELK is not necessary for the proliferation of basal-like breast cancer cells. *Elife, 6*. doi:10.7554/eLife.26693

Huang, L. C., Ross, K. E., Baffi, T. R., Drabkin, H., Kochut, K. J., Ruan, Z., . . . Kannan, N. (2018). Integrative annotation and knowledge discovery of kinase post-translational modifications and cancer-associated mutations through federated protein ontologies and resources. *Sci Rep, 8*(1), 6518. doi:10.1038/s41598-018-24457-1

Hughes, C. S., Foehr, S., Garfield, D. A., Furlong, E. E., Steinmetz, L. M., & Krijgsveld, J. (2014). Ultrasensitive proteome analysis using paramagnetic bead technology. *Mol Syst Biol, 10*, 757. doi:10.15252/msb.20145625

Hunter, T. (1998). Prolyl isomerases and nuclear function. *Cell, 92*(2), 141-143.

Hutti, J. E., Jarrell, E. T., Chang, J. D., Abbott, D. W., Storz, P., Toker, A., . . . Turk, B. E. (2004). A rapid method for determining protein kinase phosphorylation specificity. *Nat Methods, 1*(1), 27-29. doi:10.1038/nmeth708

Huttlin, E. L., Jedrychowski, M. P., Elias, J. E., Goswami, T., Rad, R., Beausoleil, S. A., . . . Gygi, S. P. (2010). A tissue-specific atlas of mouse protein phosphorylation and expression. *Cell, 143*(7), 1174-1189. doi:10.1016/j.cell.2010.12.001

Hydbring, P., Malumbres, M., & Sicinski, P. (2016). Non-canonical functions of cell cycle cyclins and cyclin-dependent kinases. *Nat Rev Mol Cell Biol, 17*(5), 280-292. doi:10.1038/nrm.2016.27

Ieda, N., Itoh, K., Inoue, Y., Izumiya, Y., Kawaguchi, M., Miyata, N., & Nakagawa, H. (2019). An irreversible inhibitor of peptidyl-prolyl cis/trans isomerase Pin1 and evaluation of cytotoxicity. *Bioorg Med Chem Lett, 29*(3), 353-356. doi:10.1016/j.bmcl.2018.12.044

Ira, G., Pellicioli, A., Balijja, A., Wang, X., Fiorani, S., Carotenuto, W., . . . Foiani, M. (2004). DNA end resection, homologous recombination and DNA damage checkpoint activation require CDK1. *Nature, 431*(7011), 1011-1017. doi:10.1038/nature02964

Jackson, A. L., Bartz, S. R., Schelter, J., Kobayashi, S. V., Burchard, J., Mao, M., . . . Linsley, P. S. (2003). Expression profiling reveals off-target gene regulation by RNAi. *Nat Biotechnol, 21*(6), 635-637. doi:10.1038/nbt831

Janes, M. R., Zhang, J., Li, L. S., Hansen, R., Peters, U., Guo, X., . . . Liu, Y. (2018). Targeting KRAS Mutant Cancers with a Covalent G12C-Specific Inhibitor. *Cell, 172*(3), 578-589 e517. doi:10.1016/j.cell.2018.01.006

Jarolim, S., Ayer, A., Pillay, B., Gee, A. C., Phrakaysone, A., Perrone, G. G., . . . Dawes, I. W. (2013). Saccharomyces cerevisiae genes involved in survival of heat shock. *G3 (Bethesda), 3*(12), 2321-2333. doi:10.1534/g3.113.007971

Ji, Q., Xu, X., Li, L., Goodman, S. B., Bi, W., Xu, M., . . . Wang, Y. (2017). miR-216a inhibits osteosarcoma cell proliferation, invasion and metastasis by targeting CDK14. *Cell Death Dis, 8*(10), e3103. doi:10.1038/cddis.2017.499

Jiang, M., Gao, Y., Yang, T., Zhu, X., & Chen, J. (2009). Cyclin Y, a novel membrane-associated cyclin, interacts with PFTK1. *FEBS Lett, 583*(13), 2171-2178. doi:10.1016/j.febslet.2009.06.010

Jin, B., Jin, H., Wu, H. B., Xu, J. J., & Li, B. (2018). Long non-coding RNA SNHG15 promotes CDK14 expression via miR-486 to accelerate non-small cell lung cancer cells progression and metastasis. *J Cell Physiol, 233*(9), 7164-7172. doi:10.1002/jcp.26543

Johannessen, L., Sundberg, T. B., O'Connell, D. J., Kolde, R., Berstler, J., Billings, K. J., . . . Xavier, R. J. (2017). Small-molecule studies identify CDK8 as a regulator of IL-10 in myeloid cells. *Nat Chem Biol, 13*(10), 1102-1108. doi:10.1038/nchembio.2458

Johnson, L. N., Lowe, E. D., Noble, M. E., & Owen, D. J. (1998). The Eleventh Datta Lecture. The structural basis for substrate recognition and control by protein kinases. *FEBS Lett, 430*(1-2), 1-11.

Kabsch, W. (2010). Integration, scaling, space-group assignment and post-refinement. *Acta Crystallogr D Biol Crystallogr, 66*(Pt 2), 133-144. doi:10.1107/S0907444909047374

Kalluri, R., & Neilson, E. G. (2003). Epithelial-mesenchymal transition and its implications for fibrosis. *J Clin Invest, 112*(12), 1776-1784. doi:10.1172/JCI20530

Kalluri, R., & Weinberg, R. A. (2009). The basics of epithelial-mesenchymal transition. *J Clin Invest, 119*(6), 1420-1428. doi:10.1172/JCI39104

Kasten, M., & Giordano, A. (2001). Cdk10, a Cdc2-related kinase, associates with the Ets2 transcription factor and modulates its transactivation activity. *Oncogene, 20*(15), 1832-1838. doi:10.1038/sj.onc.1204295

Kim, H.-J. J., & Bae, S.-C. C. (2011). Histone deacetylase inhibitors: molecular mechanisms of action and clinical trials as anti-cancer drugs. *American journal of translational research, 3*(2), 166-179.

Kim, K., Lu, Z., & Hay, E. D. (2002). Direct evidence for a role of beta-catenin/LEF-1 signaling pathway in induction of EMT. *Cell Biol Int, 26*(5), 463-476.

Klaeger, S., Gohlke, B., Perrin, J., Gupta, V., Heinzlmeir, S., Helm, D., . . . Kuster, B. (2016). Chemical Proteomics Reveals Ferrochelatase as a Common Off-target of Kinase Inhibitors. *ACS Chem Biol, 11*(5), 1245-1254. doi:10.1021/acschembio.5b01063

Klaeger, S., Heinzlmeir, S., Wilhelm, M., Polzer, H., Vick, B., Koenig, P. A., . . . Kuster, B. (2017). The target landscape of clinical kinase drugs. *Science, 358*(6367). doi:10.1126/science.aan4368

Kleinman, H. K., & Martin, G. R. (2005). Matrigel: basement membrane matrix with biological activity. *Semin Cancer Biol, 15*(5), 378-386. doi:10.1016/j.semcancer.2005.05.004

Knapp, S., Arruda, P., Blagg, J., Burley, S., Drewry, D. H., Edwards, A., . . . Zuercher, W. J. (2013). A public-private partnership to unlock the untargeted kinome. *Nat Chem Biol, 9*(1), 3-6. doi:10.1038/nchembio.1113

Knudsen, E. S., & Witkiewicz, A. K. (2017). The Strange Case of CDK4/6 Inhibitors: Mechanisms, Resistance, and Combination Strategies. *Trends Cancer, 3*(1), 39-55. doi:10.1016/j.trecan.2016.11.006

Kollmann, K., Heller, G., Schneckenleithner, C., Warsch, W., Scheicher, R., Ott, R. G., . . . Sexl, V. (2013). A kinase-independent function of CDK6 links the cell cycle to tumor angiogenesis. *Cancer Cell, 24*(2), 167-181. doi:10.1016/j.ccr.2013.07.012

Kozono, S., Lin, Y. M., Seo, H. S., Pinch, B., Lian, X., Qiu, C., . . . Zhou, X. Z. (2018). Arsenic targets Pin1 and cooperates with retinoic acid to inhibit cancer-driving pathways and tumor-initiating cells. *Nat Commun, 9*(1), 3069. doi:10.1038/s41467-018-05402-2

Kubinyi, H. (2003). Drug research: myths, hype and reality. *Nat Rev Drug Discov, 2*(8), 665-668. doi:10.1038/nrd1156

Kumar, R., Gururaj, A. E., & Barnes, C. J. (2006). p21-activated kinases in cancer. *Nat Rev Cancer, 6*(6), 459-471. doi:10.1038/nrc1892

Kwiatkowski, N., Zhang, T., Rahl, P. B., Abraham, B. J., Reddy, J., Ficarro, S. B., . . . Gray, N. S. (2014). Targeting transcription regulation in cancer with a covalent CDK7 inhibitor. *Nature, 511*(7511), 616-620. doi:10.1038/nature13393

Kwong, L. N., Costello, J. C., Liu, H., Jiang, S., Helms, T. L., Langsdorf, A. E., . . . Chin, L. (2012). Oncogenic NRAS signaling differentially regulates survival and proliferation in melanoma. *Nat Med, 18*(10), 1503-1510. doi:10.1038/nm.2941

Lai, A. C., & Crews, C. M. (2017). Induced protein degradation: an emerging drug discovery paradigm. *Nat Rev Drug Discov, 16*(2), 101-114. doi:10.1038/nrd.2016.211

Lam, P. B., Burga, L. N., Wu, B. P., Hofstatter, E. W., Lu, K. P., & Wulf, G. M. (2008). Prolyl isomerase Pin1 is highly expressed in Her2-positive breast cancer and regulates erbB2 protein stability. *Mol Cancer, 7*, 91. doi:10.1186/1476-4598-7-91

Lanning, B. R., Whitby, L. R., Dix, M. M., Douhan, J., Gilbert, A. M., Hett, E. C., . . . Cravatt, B. F. (2014). A road map to evaluate the proteome-wide selectivity of covalent kinase inhibitors. *Nat Chem Biol, 10*(9), 760-767. doi:10.1038/nchembio.1582

Laplante, M., & Sabatini, D. M. (2012). mTOR signaling in growth control and disease. *Cell, 149*(2), 274-293. doi:10.1016/j.cell.2012.03.017

Larochelle, S., Merrick, K. A., Terret, M. E., Wohlbold, L., Barboza, N. M., Zhang, C., . . . Fisher, R. P. (2007). Requirements for Cdk7 in the assembly of Cdk1/cyclin B and activation of Cdk2 revealed by chemical genetics in human cells. *Mol Cell, 25*(6), 839-850. doi:10.1016/j.molcel.2007.02.003

Lawson, C. D., & Ridley, A. J. (2018). Rho GTPase signaling complexes in cell migration and invasion. *J Cell Biol, 217*(2), 447-457. doi:10.1083/jcb.201612069

Lee, M. S., Helms, T. L., Feng, N., Gay, J., Chang, Q. E., Tian, F., . . . Kopetz, S. (2016). Efficacy of the combination of MEK and CDK4/6 inhibitors in vitro and in vivo in KRAS mutant colorectal cancer models. *Oncotarget, 7*(26), 39595-39608. doi:10.18632/oncotarget.9153

Lee, T. H., Chen, C. H., Suizu, F., Huang, P., Schiene-Fischer, C., Daum, S., . . . Lu, K. P. (2011). Death-associated protein kinase 1 phosphorylates Pin1 and inhibits its prolyl isomerase activity and cellular function. *Mol Cell, 42*(2), 147-159. doi:10.1016/j.molcel.2011.03.005

Leenders, F., Mopert, K., Schmiedeknecht, A., Santel, A., Czauderna, F., Aleku, M., . . . Klippel, A. (2004). PKN3 is required for malignant prostate cell growth downstream of activated PI 3-kinase. *EMBO J, 23*(16), 3303-3313. doi:10.1038/sj.emboj.7600345

Lemmon, M. A., & Schlessinger, J. (2010). Cell signaling by receptor tyrosine kinases. *Cell, 141*(7), 1117-1134. doi:10.1016/j.cell.2010.06.011

Leproult, E., Barluenga, S., Moras, D., Wurtz, J. M., & Winssinger, N. (2011). Cysteine mapping in conformationally distinct kinase nucleotide binding sites: application to the design of selective covalent inhibitors. *J Med Chem, 54*(5), 1347-1355. doi:10.1021/jm101396q

Lera, R. F., & Burkard, M. E. (2012). The final link: tapping the power of chemical genetics to connect the molecular and biologic functions of mitotic protein kinases. *Molecules, 17*(10), 12172-12186. doi:10.3390/molecules171012172

Leung, W. K., Ching, A. K., Chan, A. W., Poon, T. C., Mian, H., Wong, A. S., . . . Wong, N. (2011). A novel interplay between oncogenic PFTK1 protein kinase and tumor suppressor TAGLN2 in the control of liver cancer cell motility. *Oncogene, 30*(44), 4464-4475. doi:10.1038/onc.2011.161

Leung, W. K., Ching, A. K., & Wong, N. (2011). Phosphorylation of Caldesmon by PFTAIRE1 kinase promotes actin binding and formation of stress fibers. *Mol Cell Biochem, 350*(1-2), 201-206. doi:10.1007/s11010-010-0699-8

Li, D., Ambrogio, L., Shimamura, T., Kubo, S., Takahashi, M., Chirieac, L. R., . . . Wong, K. K. (2008). BIBW2992, an irreversible EGFR/HER2 inhibitor highly effective in preclinical lung cancer models. *Oncogene, 27*(34), 4702-4711. doi:10.1038/onc.2008.109

Li, J., Kim, S. G., & Blenis, J. (2014). Rapamycin: one drug, many effects. *Cell Metab, 19*(3), 373-379. doi:10.1016/j.cmet.2014.01.001

Li, J., Shao, W., & Feng, H. (2019). MiR-542-3p, a microRNA targeting CDK14, suppresses cell proliferation, invasiveness, and tumorigenesis of epithelial ovarian cancer. *Biomed Pharmacother, 110*, 850-856. doi:10.1016/j.biopha.2018.11.104

Li, L., Wang, J., Hou, J., Wu, Z., Zhuang, Y., Lu, M., . . . Zhang, W. (2012). Cdk1 interplays with Oct4 to repress differentiation of embryonic stem cells into trophectoderm. *FEBS Lett, 586*(23), 4100-4107. doi:10.1016/j.febslet.2012.10.030

Li, Q., Zhou, L., Wang, M., Wang, N., Li, C., Wang, J., & Qi, L. (2018). MicroRNA-613 impedes the proliferation and invasion of glioma cells by targeting cyclin-dependent kinase 14. *Biomed Pharmacother, 98*, 636-642. doi:10.1016/j.biopha.2017.12.044

Li, S., Song, W., Jiang, M., Zeng, L., Zhu, X., & Chen, J. (2014). Phosphorylation of cyclin Y by CDK14 induces its ubiquitination and degradation. *FEBS Lett, 588*(11), 1989-1996. doi:10.1016/j.febslet.2014.04.019

Liang, C., Shi, S., Liu, M., Qin, Y., Meng, Q., Hua, J., . . . Yu, X. (2019). PIN1 Maintains Redox Balance via the c-Myc/NRF2 Axis to Counteract Kras-Induced Mitochondrial Respiratory Injury in Pancreatic Cancer Cells. *Cancer Res, 79*(1), 133-145. doi:10.1158/0008-5472.CAN-18-1968

Lim, S., & Kaldis, P. (2013). Cdks, cyclins and CKIs: roles beyond cell cycle regulation. *Development, 140*(15), 3079-3093. doi:10.1242/dev.091744

Liou, Y. C., Ryo, A., Huang, H. K., Lu, P. J., Bronson, R., Fujimori, F., . . . Lu, K. P. (2002). Loss of Pin1 function in the mouse causes phenotypes resembling cyclin D1-null phenotypes. *Proc Natl Acad Sci U S A, 99*(3), 1335-1340. doi:10.1073/pnas.032404099

Liou, Y. C., Zhou, X. Z., & Lu, K. P. (2011). Prolyl isomerase Pin1 as a molecular switch to determine the fate of phosphoproteins. *Trends Biochem Sci, 36*(10), 501-514. doi:10.1016/j.tibs.2011.07.001

Liu, F., Zhang, X., Weisberg, E., Chen, S., Hur, W., Wu, H., . . . Gray, N. S. (2013). Discovery of a selective irreversible BMX inhibitor for prostate cancer. *ACS Chem Biol, 8*(7), 1423-1428. doi:10.1021/cb4000629

Liu, J., Farmer, J. D., Lane, W. S., Friedman, J., Weissman, I., & Schreiber, S. L. (1991). Calcineurin is a common target of cyclophilin-cyclosporin A and FKBP-FK506 complexes. *Cell, 66*(4), 807-815.

Liu, Q., Sabnis, Y., Zhao, Z., Zhang, T., Buhrlage, S. J., Jones, L. H., & Gray, N. S. (2013). Developing irreversible inhibitors of the protein kinase cysteinome. *Chem Biol, 20*(2), 146-159. doi:10.1016/j.chembiol.2012.12.006

Liu, Y., Shah, K., Yang, F., Witucki, L., & Shokat, K. M. (1998). Engineering Src family protein kinases with unnatural nucleotide specificity. *Chem Biol, 5*(2), 91-101.

Loewith, R., & Hall, M. N. (2011). Target of rapamycin (TOR) in nutrient signaling and growth control. *Genetics, 189*(4), 1177-1201. doi:10.1534/genetics.111.133363

Lolli, G., Lowe, E. D., Brown, N. R., & Johnson, L. N. (2004). The crystal structure of human CDK7 and its protein recognition properties. *Structure, 12*(11), 2067-2079. doi:10.1016/j.str.2004.08.013

Long, M. J., Gollapalli, D. R., & Hedstrom, L. (2012). Inhibitor mediated protein degradation. *Chem Biol, 19*(5), 629-637. doi:10.1016/j.chembiol.2012.04.008

Lu, K. P., Finn, G., Lee, T. H., & Nicholson, L. K. (2007). Prolyl cis-trans isomerization as a molecular timer. *Nat Chem Biol, 3*(10), 619-629. doi:10.1038/nchembio.2007.35

Lu, K. P., Hanes, S. D., & Hunter, T. (1996). A human peptidyl-prolyl isomerase essential for regulation of mitosis. *Nature, 380*(6574), 544-547. doi:10.1038/380544a0

Lu, K. P., & Zhou, X. Z. (2007). The prolyl isomerase PIN1: a pivotal new twist in phosphorylation signalling and disease. *Nat Rev Mol Cell Biol, 8*(11), 904-916. doi:10.1038/nrm2261

Lu, Z., & Hunter, T. (2014). Prolyl isomerase Pin1 in cancer. *Cell Res, 24*(9), 1033-1049. doi:10.1038/cr.2014.109

Lundberg, A. S., & Weinberg, R. A. (1998). Functional inactivation of the retinoblastoma protein requires sequential modification by at least two distinct cyclin-cdk complexes. *Mol Cell Biol, 18*(2), 753-761.

Luo, M. L., Gong, C., Chen, C. H., Lee, D. Y., Hu, H., Huang, P., . . . Lu, K. P. (2014). Prolyl isomerase Pin1 acts downstream of miR200c to promote cancer stem-like cell traits in breast cancer. *Cancer Res, 74*(13), 3603-3616. doi:10.1158/0008-5472.CAN-13-2785

MacDonald, B. T., & He, X. (2012). Frizzled and LRP5/6 receptors for Wnt/beta-catenin signaling. *Cold Spring Harb Perspect Biol, 4*(12). doi:10.1101/cshperspect.a007880

Mah, R., Thomas, J. R., & Shafer, C. M. (2014). Drug discovery considerations in the development of covalent inhibitors. *Bioorg Med Chem Lett, 24*(1), 33-39. doi:10.1016/j.bmcl.2013.10.003

Malumbres, M. (2014). Cyclin-dependent kinases. *Genome Biol, 15*(6), 122.

Manning, G., Whyte, D. B., Martinez, R., Hunter, T., & Sudarsanam, S. (2002). The protein kinase complement of the human genome. *Science, 298*(5600), 1912-1934. doi:10.1126/science.1075762

Mao, Y., Jia, Y., Zhu, H., Wang, W., Jin, Q., Huang, F., . . . Li, X. (2017). High expression of PFTK1 in cancer cells predicts poor prognosis in colorectal cancer. *Mol Med Rep, 16*(1), 224-230. doi:10.3892/mmr.2017.6560

Marinkovich, M. P., Taylor, T. B., Keene, D. R., Burgeson, R. E., & Zone, J. J. (1996). LAD-1, the linear IgA bullous dermatosis autoantigen, is a novel 120-kDa anchoring filament protein synthesized by epidermal cells. *J Invest Dermatol, 106*(4), 734-738.

Marks, P. A., & Breslow, R. (2007). Dimethyl sulfoxide to vorinostat: development of this histone deacetylase inhibitor as an anticancer drug. *Nat Biotechnol, 25*(1), 84-90. doi:10.1038/nbt1272

Marks, P. A., & Dokmanovic, M. (2005). Histone deacetylase inhibitors: discovery and development as anticancer agents. *Expert Opin Investig Drugs, 14*(12), 1497-1511. doi:10.1517/13543784.14.12.1497

Marks, P. A., & Rifkind, R. A. (1978). Erythroleukemic differentiation. *Annu Rev Biochem, 47*, 419-448. doi:10.1146/annurev.bi.47.070178.002223

McAlister, G. C., Nusinow, D. P., Jedrychowski, M. P., Wuhr, M., Huttlin, E. L., Erickson, B. K., . . . Gygi, S. P. (2014). MultiNotch MS3 enables accurate, sensitive, and multiplexed detection of differential expression across cancer cell line proteomes. *Anal Chem, 86*(14), 7150-7158. doi:10.1021/ac502040v

McCarthy, B. A., Yancopoulos, S., Tipping, M., Yan, X. J., Wang, X. P., Bennett, F., . . . Chiorazzi, N. (2015). A seven-gene expression panel distinguishing clonal expansions of pre-leukemic and

chronic lymphocytic leukemia B cells from normal B lymphocytes. *Immunol Res, 63*(1-3), 90-100. doi:10.1007/s12026-015-8688-3

McCoy, A. J., Grosse-Kunstleve, R. W., Adams, P. D., Winn, M. D., Storoni, L. C., & Read, R. J. (2007). Phaser crystallographic software. *J Appl Crystallogr, 40*(Pt 4), 658-674. doi:10.1107/S0021889807021206

McDonald, E. R., 3rd, de Weck, A., Schlabach, M. R., Billy, E., Mavrakis, K. J., Hoffman, G. R., . . . Sellers, W. R. (2017). Project DRIVE: A Compendium of Cancer Dependencies and Synthetic Lethal Relationships Uncovered by Large-Scale, Deep RNAi Screening. *Cell, 170*(3), 577-592 e510. doi:10.1016/j.cell.2017.07.005

Medici, D., Hay, E. D., & Olsen, B. R. (2008). Snail and Slug promote epithelial-mesenchymal transition through beta-catenin-T-cell factor-4-dependent expression of transforming growth factor-beta3. *Mol Biol Cell, 19*(11), 4875-4887. doi:10.1091/mbc.E08-05-0506

Mikolcevic, P., Rainer, J., & Geley, S. (2012). Orphan kinases turn eccentric: a new class of cyclin Y-activated, membrane-targeted CDKs. *Cell Cycle, 11*(20), 3758-3768. doi:10.4161/cc.21592

Milstein, S., Nguyen, M., Meyers, R., & de Fougerolles, A. (2013). Measuring RNAi knockdown using qPCR. *Methods Enzymol, 533*, 57-77. doi:10.1016/B978-0-12-420067-8.00006-4

Min, S. H., Lau, A. W., Lee, T. H., Inuzuka, H., Wei, S., Huang, P., . . . Lu, K. P. (2012). Negative regulation of the stability and tumor suppressor function of Fbw7 by the Pin1 prolyl isomerase. *Mol Cell, 46*(6), 771-783. doi:10.1016/j.molcel.2012.04.012

Miyagaki, H., Yamasaki, M., Miyata, H., Takahashi, T., Kurokawa, Y., Nakajima, K., . . . Doki, Y. (2012). Overexpression of PFTK1 predicts resistance to chemotherapy in patients with oesophageal squamous cell carcinoma. *Br J Cancer, 106*(5), 947-954. doi:10.1038/bjc.2012.35

Moore, J. D., & Potter, A. (2013). Pin1 inhibitors: Pitfalls, progress and cellular pharmacology. *Bioorg Med Chem Lett, 23*(15), 4283-4291. doi:10.1016/j.bmcl.2013.05.088

Mopert, K., Loffler, K., Roder, N., Kaufmann, J., & Santel, A. (2012). Depletion of protein kinase N3 (PKN3) impairs actin and adherens junctions dynamics and attenuates endothelial cell activation. *Eur J Cell Biol, 91*(9), 694-705. doi:10.1016/j.ejcb.2012.03.010

Morales, F., & Giordano, A. (2016). Overview of CDK9 as a target in cancer research. *Cell Cycle, 15*(4), 519-527. doi:10.1080/15384101.2016.1138186

Morgan, D. O. (1997). Cyclin-dependent kinases: engines, clocks, and microprocessors. *Annu Rev Cell Dev Biol, 13*, 261-291. doi:10.1146/annurev.cellbio.13.1.261

Mukai, H. (2003). The structure and function of PKN, a protein kinase having a catalytic domain homologous to that of PKC. *Journal of biochemistry, 133*(1), 17-27.

Mukai, H., Muramatsu, A., Mashud, R., Kubouchi, K., Tsujimoto, S., Hongu, T., . . . Sugiura, R. (2016). PKN3 is the major regulator of angiogenesis and tumor metastasis in mice. *Sci Rep, 6*, 18979. doi:10.1038/srep18979

Murray, A. W., Solomon, M. J., & Kirschner, M. W. (1989). The role of cyclin synthesis and degradation in the control of maturation promoting factor activity. *Nature, 339*(6222), 280-286. doi:10.1038/339280a0

Nabet, B., Roberts, J. M., Buckley, D. L., Paulk, J., Dastjerdi, S., Yang, A., . . . Bradner, J. E. (2018). The dTAG system for immediate and target-specific protein degradation. *Nat Chem Biol, 14*(5), 431-441. doi:10.1038/s41589-018-0021-8

Needham, E. J., Parker, B. L., Burykin, T., James, D. E., & Humphrey, S. J. (2019). Illuminating the dark phosphoproteome. *Sci Signal, 12*(565). doi:10.1126/scisignal.aau8645

Nguyen, D. T., Mathias, S., Bologa, C., Brunak, S., Fernandez, N., Gaulton, A., . . . Guha, R. (2017). Pharos: Collating protein information to shed light on the druggable genome. *Nucleic Acids Res, 45*(D1), D995-D1002. doi:10.1093/nar/gkw1072

Niehrs, C., & Acebron, S. P. (2012). Mitotic and mitogenic Wnt signalling. *EMBO J, 31*(12), 2705-2713. doi:10.1038/emboj.2012.124

Niehrs, C., & Shen, J. (2010). Regulation of Lrp6 phosphorylation. *Cell Mol Life Sci, 67*(15), 2551-2562. doi:10.1007/s00018-010-0329-3

Niessen, S., Dix, M. M., Barbas, S., Potter, Z. E., Lu, S., Brodsky, O., . . . Cravatt, B. F. (2017). Proteome-wide Map of Targets of T790M-EGFR-Directed Covalent Inhibitors. *Cell Chem Biol, 24*(11), 1388-1400 e1387. doi:10.1016/j.chembiol.2017.08.017

Novellasdemunt, L., Antas, P., & Li, V. S. (2015). Targeting Wnt signaling in colorectal cancer. A Review in the Theme: Cell Signaling: Proteins, Pathways and Mechanisms. *Am J Physiol Cell Physiol, 309*(8), C511-521. doi:10.1152/ajpcell.00117.2015

Oishi, K., Mukai, H., Shibata, H., Takahashi, M., & Ona, Y. (1999). Identification and characterization of PKNbeta, a novel isoform of protein kinase PKN: expression and arachidonic acid dependency are different from those of PKNalpha. *Biochem Biophys Res Commun, 261*(3), 808-814. doi:10.1006/bbrc.1999.1116

Oliver, A. W., Knapp, S., & Pearl, L. H. (2007). Activation segment exchange: a common mechanism of kinase autophosphorylation? *Trends Biochem Sci, 32*(8), 351-356. doi:10.1016/j.tibs.2007.06.004

Olson, C. M., Jiang, B., Erb, M. A., Liang, Y., Doctor, Z. M., Zhang, Z., . . . Gray, N. S. (2018). Pharmacological perturbation of CDK9 using selective CDK9 inhibition or degradation. *Nat Chem Biol, 14*(2), 163-170. doi:10.1038/nchembio.2538

Opoku-Temeng, C., Dayal, N., Hernandez, D. E., Naganna, N., & Sintim, H. O. (2018). Tetrahydro-3H-pyrazolo[4,3-a]phenanthridine-based CDK inhibitor. *Chem Commun (Camb), 54*(36), 4521-4524. doi:10.1039/c8cc01154k

Oppelt, A., Haugsten, E. M., Zech, T., Danielsen, H. E., Sveen, A., Lobert, V. H., . . . Wesche, J. (2014). PIKfyve, MTMR3 and their product PtdIns5P regulate cancer cell migration and invasion through activation of Rac1. *Biochem J, 461*(3), 383-390. doi:10.1042/BJ20140132

Oprea, T. I., Bologa, C. G., Brunak, S., Campbell, A., Gan, G. N., Gaulton, A., . . . Zahoranszky-Kohalmi, G. (2018). Unexplored therapeutic opportunities in the human genome. *Nat Rev Drug Discov, 17*(5), 317-332. doi:10.1038/nrd.2018.14

Ou-Yang, J., Huang, L. H., & Sun, X. X. (2017). Cyclin-Dependent Kinase 14 Promotes Cell Proliferation, Migration and Invasion in Ovarian Cancer by Inhibiting Wnt Signaling Pathway. *Gynecol Obstet Invest, 82*(3), 230-239. doi:10.1159/000447632

Pan, Z., Scheerens, H., Li, S. J., Schultz, B. E., Sprengeler, P. A., Burrill, L. C., . . . Palmer, J. T. (2007). Discovery of selective irreversible inhibitors for Bruton's tyrosine kinase. *ChemMedChem, 2*(1), 58-61. doi:10.1002/cmdc.200600221

Pang, E. Y., Bai, A. H., To, K. F., Sy, S. M., Wong, N. L., Lai, P. B., . . . Wong, N. (2007). Identification of PFTAIRE protein kinase 1, a novel cell division cycle-2 related gene, in the motile phenotype of hepatocellular carcinoma cells. *Hepatology, 46*(2), 436-445. doi:10.1002/hep.21691

Parikh, J. R., Askenazi, M., Ficarro, S. B., Cashorali, T., Webber, J. T., Blank, N. C., . . . Marto, J. A. (2009). multiplierz: an extensible API based desktop environment for proteomics data analysis. *BMC Bioinformatics, 10*, 364. doi:10.1186/1471-2105-10-364

Patnaik, A., Rosen, L. S., Tolaney, S. M., Tolcher, A. W., Goldman, J. W., Gandhi, L., . . . Shapiro, G. I. (2016). Efficacy and Safety of Abemaciclib, an Inhibitor of CDK4 and CDK6, for Patients with Breast Cancer, Non-Small Cell Lung Cancer, and Other Solid Tumors. *Cancer Discov, 6*(7), 740-753. doi:10.1158/2159-8290.CD-16-0095

Patricelli, M. P., Nomanbhoy, T. K., Wu, J., Brown, H., Zhou, D., Zhang, J., . . . Kozarich, J. W. (2011). In situ kinase profiling reveals functionally relevant properties of native kinases. *Chem Biol, 18*(6), 699-710. doi:10.1016/j.chembiol.2011.04.011

Patricelli, M. P., Szardenings, A. K., Liyanage, M., Nomanbhoy, T. K., Wu, M., Weissig, H., . . . Kozarich, J. W. (2007). Functional interrogation of the kinome using nucleotide acyl phosphates. *Biochemistry, 46*(2), 350-358. doi:10.1021/bi062142x

Paulo, J. A., O'Connell, J. D., & Gygi, S. P. (2016). A Triple Knockout (TKO) Proteomics Standard for Diagnosing Ion Interference in Isobaric Labeling Experiments. *J Am Soc Mass Spectrom, 27*(10), 1620-1625. doi:10.1007/s13361-016-1434-9

Paulovich, A. G., Toczyski, D. P., & Hartwell, L. H. (1997). When Checkpoints Fail. *Cell, 88*(3), 315-321. doi:10.1016/s0092-8674(00)81870-x

Pelish, H. E., Liau, B. B., Nitulescu, I. I., Tangpeerachaikul, A., Poss, Z. C., Da Silva, D. H., . . . Shair, M. D. (2015). Mediator kinase inhibition further activates super-enhancer-associated genes in AML. *Nature, 526*(7572), 273-276. doi:10.1038/nature14904

Perez-Riverol, Y., Csordas, A., Bai, J., Bernal-Llinares, M., Hewapathirana, S., Kundu, D. J., . . . Vizcaino, J. A. (2019). The PRIDE database and related tools and resources in 2019: improving support for quantification data. *Nucleic Acids Res, 47*(D1), D442-D450. doi:10.1093/nar/gky1106

Phadke, M., Remsing Rix, L. L., Smalley, I., Bryant, A. T., Luo, Y., Lawrence, H. R., . . . Smalley, K. S. M. (2018). Dabrafenib inhibits the growth of BRAF-WT cancers through CDK16 and NEK9 inhibition. *Mol Oncol, 12*(1), 74-88. doi:10.1002/1878-0261.12152

Polakis, P. (2012). Wnt signaling in cancer. *Cold Spring Harb Perspect Biol, 4*(5). doi:10.1101/cshperspect.a008052

Potashman, M. H., & Duggan, M. E. (2009). Covalent modifiers: an orthogonal approach to drug design. *J Med Chem, 52*(5), 1231-1246. doi:10.1021/jm8008597

Quinti, L., Dayalan Naidu, S., Trager, U., Chen, X., Kegel-Gleason, K., Lleres, D., . . . Kazantsev, A. G. (2017). KEAP1-modifying small molecule reveals muted NRF2 signaling responses in neural stem cells from Huntington's disease patients. *Proc Natl Acad Sci U S A, 114*(23), E4676-E4685. doi:10.1073/pnas.1614943114

Rajbhandari, P., Schalper, K. A., Solodin, N. M., Ellison-Zelski, S. J., Ping Lu, K., Rimm, D. L., & Alarid, E. T. (2014). Pin1 modulates ERalpha levels in breast cancer through inhibition of phosphorylation-dependent ubiquitination and degradation. *Oncogene, 33*(11), 1438-1447. doi:10.1038/onc.2013.78

Rakhit, R., Navarro, R., & Wandless, T. J. (2014). Chemical biology strategies for posttranslational control of protein function. *Chem Biol, 21*(9), 1238-1252. doi:10.1016/j.chembiol.2014.08.011

Rao, D. D., Vorhies, J. S., Senzer, N., & Nemunaitis, J. (2009). siRNA vs. shRNA: similarities and differences. *Adv Drug Deliv Rev, 61*(9), 746-759. doi:10.1016/j.addr.2009.04.004

Rappsilber, J., Ishihama, Y., & Mann, M. (2003). Stop and go extraction tips for matrix-assisted laser desorption/ionization, nanoelectrospray, and LC/MS sample pretreatment in proteomics. *Anal Chem, 75*(3), 663-670.

Rask-Andersen, M., Almen, M. S., & Schioth, H. B. (2011). Trends in the exploitation of novel drug targets. *Nat Rev Drug Discov, 10*(8), 579-590. doi:10.1038/nrd3478

Rask-Andersen, M., Masuram, S., & Schioth, H. B. (2014). The druggable genome: Evaluation of drug targets in clinical trials suggests major shifts in molecular class and indication. *Annu Rev Pharmacol Toxicol, 54*, 9-26. doi:10.1146/annurev-pharmtox-011613-135943

Reed, S. I. (2006). The ubiquitin-proteasome pathway in cell cycle control. *Results Probl Cell Differ, 42*, 147-181.

Richon, V. M., Ramsay, R. G., Rifkind, R. A., & Marks, P. A. (1989). Modulation of the c-myb, c-myc and p53 mRNA and protein levels during induced murine erythroleukemia cell differentiation. *Oncogene, 4*(2), 165-173.

Rodgers, G., Austin, C., Anderson, J., Pawlyk, A., Colvis, C., Margolis, R., & Baker, J. (2018). Glimmers in illuminating the druggable genome. *Nat Rev Drug Discov, 17*(5), 301-302. doi:10.1038/nrd.2017.252

Rotem, A., Janzer, A., Izar, B., Ji, Z., Doench, J. G., Garraway, L. A., & Struhl, K. (2015). Alternative to the soft-agar assay that permits high-throughput drug and genetic screens for cellular transformation. *Proc Natl Acad Sci U S A, 112*(18), 5708-5713. doi:10.1073/pnas.1505979112

Rozenblatt-Rosen, O., Deo, R. C., Padi, M., Adelmant, G., Calderwood, M. A., Rolland, T., . . . Vidal, M. (2012). Interpreting cancer genomes using systematic host network perturbations by tumour virus proteins. *Nature, 487*(7408), 491-495. doi:10.1038/nature11288

Russo Spena, C., De Stefano, L., Palazzolo, S., Salis, B., Granchi, C., Minutolo, F., . . . Rizzolio, F. (2018). Liposomal delivery of a Pin1 inhibitor complexed with cyclodextrins as new therapy for high-grade serous ovarian cancer. *J Control Release, 281*, 1-10. doi:10.1016/j.jconrel.2018.04.055

Rustighi, A., Tiberi, L., Soldano, A., Napoli, M., Nuciforo, P., Rosato, A., . . . Del Sal, G. (2009). The prolyl-isomerase Pin1 is a Notch1 target that enhances Notch1 activation in cancer. *Nat Cell Biol, 11*(2), 133-142. doi:10.1038/ncb1822

Rustighi, A., Zannini, A., Tiberi, L., Sommaggio, R., Piazza, S., Sorrentino, G., . . . Del Sal, G. (2014). Prolyl-isomerase Pin1 controls normal and cancer stem cells of the breast. *EMBO Mol Med, 6*(1), 99-119. doi:10.1002/emmm.201302909

Ryo, A., Liou, Y.-C. C., Wulf, G., Nakamura, M., Lee, S. W., & Lu, K. P. (2002). PIN1 is an E2F target gene essential for Neu/Ras-induced transformation of mammary epithelial cells. *Molecular and cellular biology, 22*(15), 5281-5295.

Ryo, A., Nakamura, M., Wulf, G., Liou, Y. C., & Lu, K. P. (2001). Pin1 regulates turnover and subcellular localization of beta-catenin by inhibiting its interaction with APC. *Nat Cell Biol, 3*(9), 793-801. doi:10.1038/ncb0901-793

Ryo, A., Suizu, F., Yoshida, Y., Perrem, K., Liou, Y. C., Wulf, G., . . . Lu, K. P. (2003). Regulation of NF-kappaB signaling by Pin1-dependent prolyl isomerization and ubiquitin-mediated proteolysis of p65/RelA. *Mol Cell, 12*(6), 1413-1426.

Santos, R., Ursu, O., Gaulton, A., Bento, A. P., Donadi, R. S., Bologa, C. G., . . . Overington, J. P. (2017). A comprehensive map of molecular drug targets. *Nat Rev Drug Discov, 16*(1), 19-34. doi:10.1038/nrd.2016.230

Schlessinger, K., Hall, A., & Tolwinski, N. (2009). Wnt signaling pathways meet Rho GTPases. *Genes Dev, 23*(3), 265-277. doi:10.1101/gad.1760809

Schmitz, M. L., & Kracht, M. (2016). Cyclin-Dependent Kinases as Coregulators of Inflammatory Gene Expression. *Trends Pharmacol Sci, 37*(2), 101-113. doi:10.1016/j.tips.2015.10.004

Schreiber, S. L. (1991). Chemistry and biology of the immunophilins and their immunosuppressive ligands. *Science (New York, N.Y.), 251*(4991), 283-287.

Schultheis, B., Strumberg, D., Santel, A., Vank, C., Gebhardt, F., Keil, O., . . . Drevs, J. (2014). First-in-human phase I study of the liposomal RNA interference therapeutic Atu027 in patients with advanced solid tumors. *J Clin Oncol, 32*(36), 4141-4148. doi:10.1200/JCO.2013.55.0376

Schwartz, P. A., Kuzmic, P., Solowiej, J., Bergqvist, S., Bolanos, B., Almaden, C., . . . Murray, B. W. (2014). Covalent EGFR inhibitor analysis reveals importance of reversible interactions to potency and mechanisms of drug resistance. *Proc Natl Acad Sci U S A, 111*(1), 173-178. doi:10.1073/pnas.1313733111

Shannon, D. A., & Weerapana, E. (2015). Covalent protein modification: the current landscape of residue-specific electrophiles. *Curr Opin Chem Biol, 24*, 18-26. doi:10.1016/j.cbpa.2014.10.021

Sheng, N., Xie, Z., Wang, C., Bai, G., Zhang, K., Zhu, Q., . . . Jing, N. (2010). Retinoic acid regulates bone morphogenic protein signal duration by promoting the degradation of phosphorylated Smad1. *Proc Natl Acad Sci U S A, 107*(44), 18886-18891. doi:10.1073/pnas.1009244107

Shi, J., Wang, E., Milazzo, J. P., Wang, Z., Kinney, J. B., & Vakoc, C. R. (2015). Discovery of cancer drug targets by CRISPR-Cas9 screening of protein domains. *Nat Biotechnol, 33*(6), 661-667. doi:10.1038/nbt.3235

Shu, F., Lv, S., Qin, Y., Ma, X., Wang, X., Peng, X., . . . Wu, J. (2007). Functional characterization of human PFTK1 as a cyclin-dependent kinase. *Proc Natl Acad Sci U S A, 104*(22), 9248-9253. doi:10.1073/pnas.0703327104

Singel, S. M., Batten, K., Cornelius, C., Jia, G., Fasciani, G., Barron, S. L., . . . Shay, J. W. (2014). Receptor-interacting protein kinase 2 promotes triple-negative breast cancer cell migration and invasion via activation of nuclear factor-kappaB and c-Jun N-terminal kinase pathways. *Breast Cancer Res, 16*(2), R28. doi:10.1186/bcr3629

Sittampalam, G. S., Coussens, N. P., Brimacombe, K., Grossman, A., Arkin, M., Auld, D., . . . Xu, X. (2004). Assay Guidance Manual. *Eli Lilly & Company and the National Center for Advancing Translational Sciences*.

Skaar, J. R., & Pagano, M. (2009). Control of cell growth by the SCF and APC/C ubiquitin ligases. *Curr Opin Cell Biol, 21*(6), 816-824. doi:10.1016/j.ceb.2009.08.004

Song, A., Wang, Q., Goebl, M. G., & Harrington, M. A. (1998). Phosphorylation of nuclear MyoD is required for its rapid degradation. *Molecular and cellular biology, 18*(9), 4994-4999.

Squires, M. S., Feltell, R. E., Wallis, N. G., Lewis, E. J., Smith, D. M., Cross, D. M., . . . Thompson, N. T. (2009). Biological characterization of AT7519, a small-molecule inhibitor of cyclin-dependent kinases, in human tumor cell lines. *Mol Cancer Ther, 8*(2), 324-332. doi:10.1158/1535-7163.MCT-08-0890

Stewart, Z. A., & Pietenpol, J. A. (2001). p53 Signaling and cell cycle checkpoints. *Chem Res Toxicol, 14*(3), 243-263. doi:10.1021/tx000199t

Stewart, Z. A., Westfall, M. D., & Pietenpol, J. A. (2003). Cell-cycle dysregulation and anticancer therapy. *Trends Pharmacol Sci, 24*(3), 139-145. doi:10.1016/S0165-6147(03)00026-9

Suizu, F., Ryo, A., Wulf, G., Lim, J., & Lu, K. P. (2006). Pin1 regulates centrosome duplication, and its overexpression induces centrosome amplification, chromosome instability, and oncogenesis. *Mol Cell Biol, 26*(4), 1463-1479. doi:10.1128/MCB.26.4.1463-1479.2006

Sun, T., Co, N. N., & Wong, N. (2014). PFTK1 interacts with cyclin Y to activate non-canonical Wnt signaling in hepatocellular carcinoma. *Biochem Biophys Res Commun, 449*(1), 163-168. doi:10.1016/j.bbrc.2014.05.002

Sun, Y., Zhu, Q., Yang, W., Shan, Y., Yu, Z., Zhang, Q., & Wu, H. (2019). LncRNA H19/miR-194/PFTK1 axis modulates the cell proliferation and migration of pancreatic cancer. *J Cell Biochem, 120*(3), 3874-3886. doi:10.1002/jcb.27669

Surade, S., & Blundell, T. L. (2012). Structural biology and drug discovery of difficult targets: the limits of ligandability. *Chem Biol, 19*(1), 42-50. doi:10.1016/j.chembiol.2011.12.013

Taylor, S. S., & Kornev, A. P. (2011). Protein kinases: evolution of dynamic regulatory proteins. *Trends Biochem Sci, 36*(2), 65-77. doi:10.1016/j.tibs.2010.09.006

Thiery, J. P. (2002). Epithelial-mesenchymal transitions in tumour progression. *Nat Rev Cancer, 2*(6), 442-454. doi:10.1038/nrc822

Tse, J. C., & Kalluri, R. (2007). Mechanisms of metastasis: epithelial-to-mesenchymal transition and contribution of tumor microenvironment. *J Cell Biochem, 101*(4), 816-829. doi:10.1002/jcb.21215

Tsherniak, A., Vazquez, F., Montgomery, P. G., Weir, B. A., Kryukov, G., Cowley, G. S., . . . Hahn, W. C. (2017). Defining a Cancer Dependency Map. *Cell, 170*(3), 564-576 e516. doi:10.1016/j.cell.2017.06.010

Tu, J., Zhao, Z., Xu, M., Chen, M., Weng, Q., Wang, J., & Ji, J. (2019). LINC00707 contributes to hepatocellular carcinoma progression via sponging miR-206 to increase CDK14. *J Cell Physiol, 234*(7), 10615-10624. doi:10.1002/jcp.27737

Turk, B. E., Hutti, J. E., & Cantley, L. C. (2006). Determining protein kinase substrate specificity by parallel solution-phase assay of large numbers of peptide substrates. *Nat Protoc, 1*(1), 375-379. doi:10.1038/nprot.2006.57

Uehara, S., Udagawa, N., Mukai, H., Ishihara, A., Maeda, K., Yamashita, T., . . . Kobayashi, Y. (2017). Protein kinase N3 promotes bone resorption by osteoclasts in response to Wnt5a-Ror2 signaling. *Sci Signal, 10*(494). doi:10.1126/scisignal.aan0023

Unsal-Kacmaz, K., Ragunathan, S., Rosfjord, E., Dann, S., Upeslacis, E., Grillo, M., . . . Klippel, A. (2012). The interaction of PKN3 with RhoC promotes malignant growth. *Mol Oncol, 6*(3), 284-298. doi:10.1016/j.molonc.2011.12.001

Urich, R., Grimaldi, R., Luksch, T., Frearson, J. A., Brenk, R., & Wyatt, P. G. (2014). The design and synthesis of potent and selective inhibitors of Trypanosoma brucei glycogen synthase kinase 3 for the treatment of human african trypanosomiasis. *J Med Chem, 57*(18), 7536-7549. doi:10.1021/jm500239b

Valley, C. C., Cembran, A., Perlmutter, J. D., Lewis, A. K., Labello, N. P., Gao, J., & Sachs, J. N. (2012). The methionine-aromatic motif plays a unique role in stabilizing protein structure. *J Biol Chem, 287*(42), 34979-34991. doi:10.1074/jbc.M112.374504

Verdecia, M. A., Bowman, M. E., Lu, K. P., Hunter, T., & Noel, J. P. (2000). Structural basis for phosphoserine-proline recognition by group IV WW domains. *Nat Struct Biol, 7*(8), 639-643. doi:10.1038/77929

Vora, S. R., Juric, D., Kim, N., Mino-Kenudson, M., Huynh, T., Costa, C., . . . Engelman, J. A. (2014). CDK 4/6 inhibitors sensitize PIK3CA mutant breast cancer to PI3K inhibitors. *Cancer Cell, 26*(1), 136-149. doi:10.1016/j.ccr.2014.05.020

Wang, B., Zou, A., Ma, L., Chen, X., Wang, L., Zeng, X., & Tan, T. (2017). miR-455 inhibits breast cancer cell proliferation through targeting CDK14. *Eur J Pharmacol, 807*, 138-143. doi:10.1016/j.ejphar.2017.03.016

Wang, C., Weerapana, E., Blewett, M. M., & Cravatt, B. F. (2014). A chemoproteomic platform to quantitatively map targets of lipid-derived electrophiles. *Nat Methods, 11*(1), 79-85. doi:10.1038/nmeth.2759

Wang, Q., Ma, J., Lu, Y., Zhang, S., Huang, J., Chen, J., . . . Xu, S. (2017). CDK20 interacts with KEAP1 to activate NRF2 and promotes radiochemoresistance in lung cancer cells. *Oncogene, 36*(37), 5321-5330. doi:10.1038/onc.2017.161

Wang, X., Jia, Y., Fei, C., Song, X., & Li, L. (2016). Activation/Proliferation-associated Protein 2 (Caprin-2) Positively Regulates CDK14/Cyclin Y-mediated Lipoprotein Receptor-related Protein 5 and 6 (LRP5/6) Constitutive Phosphorylation. *J Biol Chem, 291*(51), 26427-26434. doi:10.1074/jbc.M116.744607

Wang, Y. (2009). Wnt/Planar cell polarity signaling: a new paradigm for cancer therapy. *Mol Cancer Ther, 8*(8), 2103-2109. doi:10.1158/1535-7163.MCT-09-0282

Ward, N. E., & O'Brian, C. A. (1992). Kinetic analysis of protein kinase C inhibition by staurosporine: evidence that inhibition entails inhibitor binding at a conserved region of the catalytic domain but not …. *Molecular pharmacology*.

Weerapana, E., Speers, A. E., & Cravatt, B. F. (2007). Tandem orthogonal proteolysis-activity-based protein profiling (TOP-ABPP)--a general method for mapping sites of probe modification in proteomes. *Nat Protoc, 2*(6), 1414-1425. doi:10.1038/nprot.2007.194

Weerapana, E., Wang, C., Simon, G. M., Richter, F., Khare, S., Dillon, M. B., . . . Cravatt, B. F. (2010). Quantitative reactivity profiling predicts functional cysteines in proteomes. *Nature, 468*(7325), 790-795. doi:10.1038/nature09472

Wei, S., Kozono, S., Kats, L., Nechama, M., Li, W., Guarnerio, J., . . . Lu, K. P. (2015). Active Pin1 is a key target of all-trans retinoic acid in acute promyelocytic leukemia and breast cancer. *Nat Med, 21*(5), 457-466. doi:10.1038/nm.3839

Weiwad, M., Küllertz, G., Schutkowski, M., & Fischer, G. (2000). Evidence that the substrate backbone conformation is critical to phosphorylation by p42 MAP kinase. *FEBS letters, 478*(1-2), 39-42.

White, M. F., Shoelson, S. E., Keutmann, H., & Kahn, C. R. (1988). A cascade of tyrosine autophosphorylation in the beta-subunit activates the phosphotransferase of the insulin receptor. *J Biol Chem, 263*(6), 2969-2980.

Whittaker, S. R., Mallinger, A., Workman, P., & Clarke, P. A. (2017). Inhibitors of cyclin-dependent kinases as cancer therapeutics. *Pharmacol Ther, 173*, 83-105. doi:10.1016/j.pharmthera.2017.02.008

Wildemann, D., Erdmann, F., Alvarez, B. H., Stoller, G., Zhou, X. Z., Fanghanel, J., . . . Fischer, G. (2006). Nanomolar inhibitors of the peptidyl prolyl cis/trans isomerase Pin1 from combinatorial peptide libraries. *J Med Chem, 49*(7), 2147-2150. doi:10.1021/jm060036n

Winter, G. E., Buckley, D. L., Paulk, J., Roberts, J. M., Souza, A., Dhe-Paganon, S., & Bradner, J. E. (2015). DRUG DEVELOPMENT. Phthalimide conjugation as a strategy for in vivo target protein degradation. *Science, 348*(6241), 1376-1381. doi:10.1126/science.aab1433

Wohlbold, L., Larochelle, S., Liao, J. C., Livshits, G., Singer, J., Shokat, K. M., & Fisher, R. P. (2006). The cyclin-dependent kinase (CDK) family member PNQALRE/CCRK supports cell proliferation but has no intrinsic CDK-activating kinase (CAK) activity. *Cell Cycle, 5*(5), 546-554. doi:10.4161/cc.5.5.2541

Workman, P., & Collins, I. (2010). Probing the probes: fitness factors for small molecule tools. *Chem Biol, 17*(6), 561-577. doi:10.1016/j.chembiol.2010.05.013

Wu, P., Nielsen, T. E., & Clausen, M. H. (2015). FDA-approved small-molecule kinase inhibitors. *Trends Pharmacol Sci, 36*(7), 422-439. doi:10.1016/j.tips.2015.04.005

Wu, S., Kanda, T., Nakamoto, S., Imazeki, F., & Yokosuka, O. (2012). Knockdown of receptor-interacting serine/threonine protein kinase-2 (RIPK2) affects EMT-associated gene expression in human hepatoma cells. *Anticancer Res, 32*(9), 3775-3783.

Wu, X., Wilcox, C. B., & G., D.-. (2000). The Ess1 prolyl isomerase is linked to chromatin remodeling complexes and the general transcription machinery. *EMBO*.

Wulf, G., Garg, P., Liou, Y. C., Iglehart, D., & Lu, K. P. (2004). Modeling breast cancer in vivo and ex vivo reveals an essential role of Pin1 in tumorigenesis. *EMBO J, 23*(16), 3397-3407. doi:10.1038/sj.emboj.7600323

Wulf, G. M., Ryo, A., Wulf, G. G., Lee, S. W., Niu, T., Petkova, V., & Lu, K. P. (2001). Pin1 is overexpressed in breast cancer and cooperates with Ras signaling in increasing the transcriptional activity of c-Jun towards cyclin D1. *EMBO J, 20*(13), 3459-3472. doi:10.1093/emboj/20.13.3459

Wyatt, P. G., Woodhead, A. J., Berdini, V., Boulstridge, J. A., Carr, M. G., Cross, D. M., . . . Woolford, A. J. (2008). Identification of N-(4-piperidinyl)-4-(2,6-dichlorobenzoylamino)-1H-pyrazole-3-carboxamide (AT7519), a novel cyclin dependent kinase inhibitor using fragment-based X-ray crystallography and structure based drug design. *J Med Chem, 51*(16), 4986-4999. doi:10.1021/jm800382h

Xi, M., Chen, T., Wu, C., Gao, X., Wu, Y., Luo, X., . . . Sun, H. (2019). CDK8 as a therapeutic target for cancers and recent developments in discovery of CDK8 inhibitors. *Eur J Med Chem, 164*, 77-91. doi:10.1016/j.ejmech.2018.11.076

Xu, W., Harrison, S. C., & Eck, M. J. (1997). Three-dimensional structure of the tyrosine kinase c-Src. *Nature, 385*(6617), 595-602. doi:10.1038/385595a0

Yaffe, M. B., Schutkowski, M., Shen, M., Zhou, X. Z., Stukenberg, P. T., Rahfeld, J. U., . . . Lu, K. P. (1997). Sequence-specific and phosphorylation-dependent proline isomerization: a potential mitotic regulatory mechanism. *Science, 278*(5345), 1957-1960.

Yan, T. H., Qiu, C., Sun, J., & Li, W. H. (2018). MiR-877-5p suppresses cell growth, migration and invasion by targeting cyclin dependent kinase 14 and predicts prognosis in hepatocellular carcinoma. *Eur Rev Med Pharmacol Sci, 22*(10), 3038-3046. doi:10.26355/eurrev_201805_15061

Yanagi, T., & Matsuzawa, S. (2015). PCTAIRE1/PCTK1/CDK16: a new oncotarget? *Cell Cycle, 14*(4), 463-464. doi:10.1080/15384101.2015.1006539

Yanagi, T., Tachikawa, K., Wilkie-Grantham, R., Hishiki, A., Nagai, K., Toyonaga, E., . . . Matsuzawa, S. (2016). Lipid Nanoparticle-mediated siRNA Transfer Against PCTAIRE1/PCTK1/Cdk16 Inhibits In Vivo Cancer Growth. *Mol Ther Nucleic Acids, 5*(6), e327. doi:10.1038/mtna.2016.40

Yang, J., & Weinberg, R. A. (2008). Epithelial-mesenchymal transition: at the crossroads of development and tumor metastasis. *Dev Cell, 14*(6), 818-829. doi:10.1016/j.devcel.2008.05.009

Yang, J., Zhu, H., Jin, Y., & Song, Y. (2018). MiR-431 inhibits cell proliferation and induces cell apoptosis by targeting CDK14 in pancreatic cancer. *Eur Rev Med Pharmacol Sci, 22*(14), 4493-4499. doi:10.26355/eurrev_201807_15503

Yang, L., Zhu, J., Huang, H., Yang, Q., Cai, J., Wang, Q., . . . Wang, Y. (2015). PFTK1 Promotes Gastric Cancer Progression by Regulating Proliferation, Migration and Invasion. *PLoS One, 10*(10), e0140451. doi:10.1371/journal.pone.0140451

Yang, T., & Chen, J. Y. (2001). Identification and cellular localization of human PFTAIRE1. *Gene, 267*(2), 165-172.

Yeh, E., Cunningham, M., Arnold, H., Chasse, D., Monteith, T., Ivaldi, G., . . . Sears, R. (2004). A signalling pathway controlling c-Myc degradation that impacts oncogenic transformation of human cells. *Nat Cell Biol, 6*(4), 308-318. doi:10.1038/ncb1110

Yeh, E. S., & Means, A. R. (2007). PIN1, the cell cycle and cancer. *Nat Rev Cancer, 7*(5), 381-388. doi:10.1038/nrc2107

Yoshida, M., Kijima, M., Akita, M., & Beppu, T. (1990). Potent and specific inhibition of mammalian histone deacetylase both in vivo and in vitro by trichostatin A. *The Journal of biological chemistry, 265*(28), 17174-17179.

Yoshida, M., Nomura, S., & Beppu, T. (1987). Effects of trichostatins on differentiation of murine erythroleukemia cells. *Cancer Res, 47*(14), 3688-3691.

Zeisberg, M., & Neilson, E. G. (2009). Biomarkers for epithelial-mesenchymal transitions. *J Clin Invest, 119*(6), 1429-1437. doi:10.1172/JCI36183

Zeitouni, D., Pylayeva-Gupta, Y., Der, C. J., & Bryant, K. L. (2016). KRAS Mutant Pancreatic Cancer: No Lone Path to an Effective Treatment. *Cancers (Basel), 8*(4). doi:10.3390/cancers8040045

Zeng, M., Lu, J., Li, L., Feru, F., Quan, C., Gero, T. W., . . . Gray, N. S. (2017). Potent and Selective Covalent Quinazoline Inhibitors of KRAS G12C. *Cell Chem Biol, 24*(8), 1005-1016 e1003. doi:10.1016/j.chembiol.2017.06.017

Zhang, J., Yang, P. L., & Gray, N. S. (2009). Targeting cancer with small molecule kinase inhibitors. *Nat Rev Cancer, 9*(1), 28-39. doi:10.1038/nrc2559

Zhang, T., Inesta-Vaquera, F., Niepel, M., Zhang, J., Ficarro, S. B., Machleidt, T., . . . Gray, N. S. (2012). Discovery of potent and selective covalent inhibitors of JNK. *Chem Biol, 19*(1), 140-154. doi:10.1016/j.chembiol.2011.11.010

Zhang, T., Kwiatkowski, N., Olson, C. M., Dixon-Clarke, S. E., Abraham, B. J., Greifenberg, A. K., . . . Gray, N. S. (2016). Covalent targeting of remote cysteine residues to develop CDK12 and CDK13 inhibitors. *Nat Chem Biol, 12*(10), 876-884. doi:10.1038/nchembio.2166

Zhang, W., Liu, R., Tang, C., Xi, Q., Lu, S., Chen, W., . . . Deng, Y. (2016). PFTK1 regulates cell proliferation, migration and invasion in epithelial ovarian cancer. *Int J Biol Macromol, 85*, 405-416. doi:10.1016/j.ijbiomac.2016.01.009

Zhang, Y., Askenazi, M., Jiang, J., Luckey, C. J., Griffin, J. D., & Marto, J. A. (2010). A robust error model for iTRAQ quantification reveals divergent signaling between oncogenic FLT3 mutants in acute myeloid leukemia. *Mol Cell Proteomics, 9*(5), 780-790. doi:10.1074/mcp.M900452-MCP200

Zhang, Y., Daum, S., Wildemann, D., Zhou, X. Z., Verdecia, M. A., Bowman, M. E., . . . Noel, J. P. (2007). Structural basis for high-affinity peptide inhibition of human Pin1. *ACS Chem Biol, 2*(5), 320-328. doi:10.1021/cb7000044

Zhang, Z., & Marshall, A. G. (1998). A universal algorithm for fast and automated charge state deconvolution of electrospray mass-to-charge ratio spectra. *J Am Soc Mass Spectrom, 9*(3), 225-233. doi:10.1016/S1044-0305(97)00284-5

Zhao, S., & Etzkorn, F. A. (2007). A phosphorylated prodrug for the inhibition of Pin1. *Bioorg Med Chem Lett, 17*(23), 6615-6618. doi:10.1016/j.bmcl.2007.09.073

Zhao, Z., & Bourne, P. E. (2018). Progress with covalent small-molecule kinase inhibitors. *Drug Discov Today, 23*(3), 727-735. doi:10.1016/j.drudis.2018.01.035

Zhao, Z., Liu, Q., Bliven, S., Xie, L., & Bourne, P. E. (2017). Determining Cysteines Available for Covalent Inhibition Across the Human Kinome. *J Med Chem, 60*(7), 2879-2889. doi:10.1021/acs.jmedchem.6b01815

Zheng, L., Hu, N., & Zhou, X. (2019). TCF3-activated LINC00152 exerts oncogenic role in osteosarcoma through regulating miR-1182/CDK14 axis. *Pathol Res Pract, 215*(2), 373-380. doi:10.1016/j.prp.2018.12.031

Zheng, L., & Lee, W. H. (2001). The retinoblastoma gene: a prototypic and multifunctional tumor suppressor. *Exp Cell Res, 264*(1), 2-18. doi:10.1006/excr.2000.5129

Zheng, L., Zhou, Z., & He, Z. (2015). Knockdown of PFTK1 inhibits tumor cell proliferation, invasion and epithelial-to-mesenchymal transition in pancreatic cancer. *Int J Clin Exp Pathol, 8*(11), 14005-14012.

Zhou, F., Lu, Y., Ficarro, S. B., Adelmant, G., Jiang, W., Luckey, C. J., & Marto, J. A. (2013). Genome-scale proteome quantification by DEEP SEQ mass spectrometry. *Nat Commun, 4*, 2171. doi:10.1038/ncomms3171

Zhou, F., Sikorski, T. W., Ficarro, S. B., Webber, J. T., & Marto, J. A. (2011). Online nanoflow reversed phase-strong anion exchange-reversed phase liquid chromatography-tandem mass spectrometry platform for efficient and in-depth proteome sequence analysis of complex organisms. *Anal Chem, 83*(18), 6996-7005. doi:10.1021/ac200639v

Zhou, X. Z., & Lu, K. P. (2016). The isomerase PIN1 controls numerous cancer-driving pathways and is a unique drug target. *Nat Rev Cancer, 16*(7), 463-478. doi:10.1038/nrc.2016.49

Zhou, Y., Rideout, W. M., 3rd, Bressel, A., Yalavarthi, S., Zi, T., Potz, D., . . . Heyer, J. (2014). Spontaneous genomic alterations in a chimeric model of colorectal cancer enable metastasis and guide effective combinatorial therapy. *PLoS One, 9*(8), e105886. doi:10.1371/journal.pone.0105886

Zhu, J., Liu, C., Liu, F., Wang, Y., & Zhu, M. (2016). Knockdown of PFTAIRE Protein Kinase 1 (PFTK1) Inhibits Proliferation, Invasion, and EMT in Colon Cancer Cells. *Oncol Res, 24*(3), 137-144. doi:10.3727/096504016X14611963142218

Zilfou, J. T., & Lowe, S. W. (2009). Tumor suppressive functions of p53. *Cold Spring Harb Perspect Biol, 1*(5), a001883. doi:10.1101/cshperspect.a001883

Page left intentionally blank.